

# **Safety in Mines Research Advisory Committee**

## **Final Project Report**

# **Fundamental aspects of the integration of seismic monitoring with numerical modelling**

**A J Mendecki, J A L Napier,  
A Ilchev and E Sellers**

**Research agency : ISS International Limited  
CSIR, Miningtek**

**Project number : GAP 603**

**Project duration : January 1999 – March 2001**

**Report date : June 2001**

**Document number : GAP603-REP-020**

## Executive summary

### Introduction

Numerical modelling of rock-mass response to underground excavations is of vital importance for the decision-making process in designing and running a mine. Likewise, seismic monitoring with state-of-the-art local seismic systems is indispensable as a means for quantifying hazard and as an indicator for potential instabilities in the rock-mass due to mining activities, geological structures and other hazard-enhancing factors. The concept of integrating observational data with mining-oriented numerical modelling has emerged as the next logical step in the development of more reliable computer-based methods for treating the problems of rock-mass stability, damage evolution and the on-set of sudden material failure.

The most important feature of an integrated numerical model is the ability to take real data, as provided by a seismic monitoring system, and to use this data as an additional input for solving a forward problem about the evolution of the physical state of the modelled rock-mass.

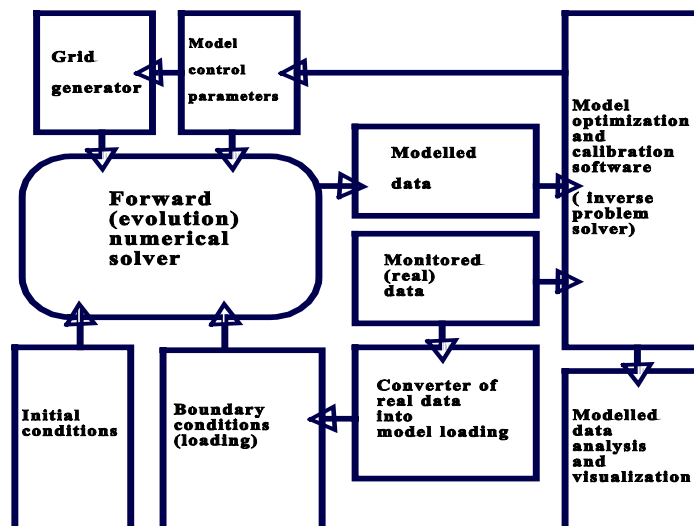
### Restrictions imposed on numerical models by the integration paradigm

Not every numerical model currently in use in the South African mining industry is suitable for integration with real seismic data. The basic requirements to be met by an integration-ready numerical model of rock-mass response to mining are:

- ! It must be designed to simulate the evolution with time of the physical state of the rock-mass.
- ! It must be equipped with the capability of converting the parameters of a real seismic event into a corresponding model-compatible input in the form of an additional loading on the rock-mass.
- ! It must allow for an unambiguous identification and quantification of seismic events among the model-generated data.

### Structure of an integrated numerical model

The functionality interrelations between the different components of a software package designed to implement the general principles of integrating real seismic data with mining-oriented numerical modelling can be illustrated by the following diagram:



### Review of numerical models potentially useful for integration

A study was performed aimed at revealing the potential for upgrading to integrated models of the software packages currently in use by the South African gold mining industry. Special attention has been paid to the ability of different models to emulate the basic patterns of mining-induced seismicity. In particular, it was concluded that the ability of a model to reproduce the power-law behaviour of the size-distribution of

local seismicity is not a decisive factor in selecting the models which are best-suited for integration. On the other hand the deviations from the above-mentioned linear trends seem to be more informative about the state of the rock and an integration-ready model should be capable of emulating such characteristic deviations from the underlying power-laws.

### **Clustering in time and migration of seismicity**

The observed temporal and spatio-temporal patterns of mining-related seismicity cannot be simulated by purely static stress modelling or by model types referred to as cellular-automata. At the core of the concept of integrating seismic monitoring with numerical modelling is the requirement for synchronizing the time-stepping of the numerical solution with the pace of the actual elapsed time. This motivates the requirement that an integrated model should be able to reproduce the main features of the local seismicity in the time domain. Studies involving existing numerical models such as DIGS , MAP3di , PFC , Point Kernel and the Integrated Damage Rheology Model (IDRM) have been carried out to explore the patterns of model-generated data in the time domain as well as to search for signatures of seismic migration.

### **Control of errors in monitored and modelled data.**

Errors are present both in observed and model-generated data-sets. The concept of integrating seismic monitoring with numerical modelling highlights the requirements for error-control in all components of an integrated seismic system. The problems related to the origin and quantification of statistical and systematic errors have been studied in the light of the corresponding requirements and limitations imposed both on the monitoring systems and on the numerical integration-ready models.

### **Integration-ready models**

A numerical model of rock-mass response to loading is suitable for functional integration with real seismic data when:

- ! It implements a reasonable approximation of the fundamental relationships between the parameters describing the physical state of the rock-mass.
- ! It is designed to solve a forward problem about the evolution of the physical state of the modelled rock-mass under the given initial and boundary conditions.
- ! It can convert the parameters of a real seismic event into a corresponding addition to the loading applied at the correct moment of time.
- ! It can itself simulate seismic activity in a quantifiable way so that a calibration to the observed local seismicity would be possible.
- ! It must have an adequate resolution in size, location and time for model-generated seismic events.
- ! The computer code of the numerical solver must run sufficiently fast on available computers to allow data-generation ahead in time.

### **Recommendations to the developers of integrated models**

Some recommendations for developing and using integrated models for the needs of the mining industry can be made, namely:

- ! Special care must be taken in specifying the initial state of the modelled rock-mass. This implies that a suitable stress-modelling module may be added as a part of the integrated software.
- ! The quality of the data provided by the local seismic monitoring system must be adequate.
- ! The geometrical discretization of the model must be done in an artefact-free manner and in accord with the available computer resources.
- ! The loading on the modelled rock-mass due to the existing and planned mining must be evaluated as accurately as possible.
- ! The reaction of the rock-mass surrounding the modelled domain to the (non-linear and inelastic ) processes which occur in the modelled material must be properly included in the numerical procedure. In practice this may require a combination of boundary element methods with finite-differences or finite elements schemes.
- ! The model must be designed with the capability for quantifying the perturbations to the physical state of the modelled rock-mass caused by real seismic events in the area so that corresponding modifications to the existing loading conditions could be made at the appropriate moment of time.
- ! In a situation when an integrated numerical model can both accept real seismic events as an input and can itself simulate seismic activity, special care must be taken for avoiding double-counting of seismic events.
- ! The design parameters of an integrated model must include sufficient flexibility for the

calibration of model-generated events to the observed seismicity.

### **Expected outcome from the use of integrated models**

The integration of numerical models with real seismic data will improve the reliability of forecasts of the stability of rock-mass while mining. In particular, the data generated by an integrated model should allow, after a proper analysis, to make definite statements about:

- ! The elastic and plastic deformations within the modelled rock-mass at a particular moment of time.
- ! The distribution of static stress, the localization of stress concentrations and their migration with time.
- ! The level of micro-seismic activity.
- ! The over-all stability of the rock-mass within a given interval of time as well as the formation and localization of damaged zones in the material.

The integration of seismic monitoring with numerical modelling is essential to improve the assessment of seismic hazards and the understanding of large scale rock-mass deformation.

### **Other Outputs:**

During the course of this project some useful tools and algorithms have been developed:

- ! The Aseismic skeleton® method of analysing catalogues of seismic events for revealing any underlying seismogenic geological structures.
- ! The methodology for identifying and quantifying connected spatial clusters of model-generated failures in the rock-mass.

### **Direct spin-offs for industry:**

The work carried out as part of project GAP603 has stimulated directly a number of initiatives that are being pursued to construct numerical tools that can be used to effect the integration of seismic observations with numerical modelling. Specific examples of these efforts are as follows:

- \$ The computer code MAP3D developed by Mining Modelling Pty Ltd has been extended to include interface and solution capabilities that allow observed fault slip episodes to be interactively included in a modelling/ review cycle.
- \$ A new Integrated Damage Rheology Model (IDRM) is under development by ISS International Ltd. This model will allow integration of observed seismic events as well as the forward modelling of mining-induced seismic activity. The model is designed to include elastodynamic effects as well as progressive creep activity in the rock-mass.
- \$ A boundary element based code termed Point Kernel is being investigated by the CSIR Division of Mining Technology to capture slip episodes, identified by ongoing seismic records, and to perform forward extrapolations of expected seismic activity. This code differs from MAP3D in that an attempt is made to construct slip patches in the rock mass in a general manner that does not require traditional fixed element shape functions.
- \$ A special purpose boundary element code called MINF has been developed at the CSIR Division of Mining Technology to simulate seismic activity associated with panel advances in tabular mining.

# Acknowledgements

The product names FLAC, UDEC and PFC are property of the Itasca Consulting Group, Inc.

The product names MAP3D and MAP3Di are property of Mining Modelling Pty Ltd.

The product name ELFEN is a property of Rockfield Software Ltd.

The product names DIGS and Point Kernel are property of CSIR Miningtek

The product name IDR is a property of ISS International Ltd.

The product names MINSIM and MINSIM-W are the property of CSIR Miningtek.

# Table of contents

Acknowledgements .....	v
Table of contents .....	vi
List of figures .....	viii
List of tables .....	xi
Glossary .....	xii
<b>1. Introduction .....</b>	<b>21</b>
1.1. Formulation of the problem .....	21
1.2. Model - data interaction .....	21
1.2.1. Visual inspection .....	21
1.2.2. Calibration .....	22
1.2.2.1. Sensitivity analysis .....	22
1.2.2.2. Practical issues of model calibration .....	22
1.2.3. Model optimisation .....	23
1.3. Integration of seismic monitoring with numerical modelling .....	24
1.3.1. Forward and inverse modelling .....	24
1.3.2. The concept of integration .....	25
1.3.3. Restrictions imposed on models by the integration paradigm .....	25
1.4. Structure of an integrated seismic monitoring-modelling system .....	26
<b>2. Review of numerical models potentially useful for integration .....</b>	<b>28</b>
2.1. Generic modelling methods .....	28
2.1.1. Discrete Models .....	28
2.1.2. Continuum models .....	34
2.1.3. Boundary Element Models and discrete fault planes .....	36
2.1.4. Static vs. dynamic modelling .....	39
2.1.5. Stochastic vs. deterministic models .....	40
2.2. Numerical models currently being developed for use in SA mining Industry .....	40
2.2.1. MINSIM/MAP3D .....	40
2.2.1.1. Boundary element basics .....	40
2.2.1.2. Simulation of seismic activity using the displacement discontinuity boundary element method .....	42
2.2.2. MAP3Di/Point KERNEL .....	45
2.2.2.1. MAP3Di .....	45
2.2.2.2. Point Kernel .....	46
2.2.3. DIGS .....	47
2.2.4. The Integrated Damage Rheology Model (IDRM) .....	48
2.2.4.1. Physical basis of IDRM .....	49
2.2.4.2. Material Stability and Seismic Events in IDRM .....	51
2.2.4.3. Typical Problems treated by the IDRM .....	51
2.2.4.4. Integration of real seismic events in IDRM .....	52
<b>3. Examples of the simulation of seismicity patterns by different numerical models ....</b>	<b>55</b>
3.1. Size distribution .....	55
3.1.1. Case study 2 - modelled seismic data .....	86
3.1.2. Case study 1 versus case study 2 – Relative changes .....	89
3.2. Time distribution .....	96
3.3. Clustering in space and time .....	98
3.3.1. Cluster identification: connected clusters .....	98
3.3.2. Cluster analysis of model-generated data .....	99
3.3.3. Quantitative analysis of spatial seismic clusters .....	99
3.3.4. Analysis of a set of clusters .....	100
3.3.5. Modelling with IDRM .....	104
3.4. Migration of Seismicity .....	111
<b>4. Seismic Monitoring: Requirements and Limitations .....</b>	<b>118</b>
4.1. Requirements .....	118
4.2. Uncertainties .....	122

4.3. Limitations .....	126
<b>5. General issues and future developments .....</b>	<b>130</b>
5.1. Validation of model representations of seismicity.....	130
5.2. Definition of a seismic event in the context of a particular model .....	131
5.2.1. Quasi-static Boundary Element Tessellation/space filling codes .....	131
5.2.2. IDR.....	132
5.3. Computational geometry issues in numerical modelling practice .....	132
5.3.1. The continuum limit and finite-size scaling .....	135
5.4. Error analysis of real and modelled data.....	135
5.4.1. Types of errors.....	136
5.4.1.1. Systematic errors.....	136
5.4.1.2. Accidental (random) errors.....	136
5.4.1.3. Control of random errors.....	136
5.4.1.4. Control of systematic errors .....	137
5.4.2. Errors due to the discretization (grid-size and grid-quality effects).....	138
5.5. Specifying the initial and boundary conditions for a particular model .....	139
5.6. Constitutive relations .....	140
5.6.1. Theoretical derivation of constitutive relations .....	141
5.6.2. Empirical constitutive relations .....	141
<b>6. Conclusions.....</b>	<b>144</b>
6.1. Requirements imposed by the integration on the numerical models .....	145
6.2. Numerical models that are suitable for seismic integration .....	145
6.2.1. Existing models.....	145
6.2.2. Future model development .....	146
6.3. Recommendations for integration in practice .....	146
<b>7. References .....</b>	<b>149</b>

# List of figures

Figure 1.1 .....	27
Figure 2.1.1 Two dimensional block-slider model (Ito and Matsuzaki, 1990).....	29
Figure 2.1.2 Frequency (R) - size (w) distribution plots of block slider models (Shaw 1995) ..	30
Figure 2.1.3 a: Clustering and b: size distribution of events for a 2-D slider block model (Ito and Matsuzaki, 1990).....	30
Figure 2.1.4 Change in power law statistics due to change in velocity boundary conditions (Rundle and Klein, 1993).....	31
Figure 2.1.5 Two methods for obtaining power law statistics from a lattice type model (Wilson et al., 1996). top: Counts of lattice breaks; bottom: box counting method.....	32
a: .....	33
b:.....	33
Figure 2.1.6 a: PFC model of a triaxial test with dots representing fractures (light dots indicate early initiation times and dark dots occurred later) and b: frequency magnitude statistics showing the dependence of the b-value on the processing procedure (Hazzard, 1998). ....	33
Figure 2.1.7 A statistical finite element model with random element properties (Tang, 1997) ...	35
Figure 2.1.8 Frequency magnitude statistics for a 2-D strike slip fault (Cochard and Madariaga, 1996).....	38
Figure 2.1.9 a: model of two parallel faults. b: Frequency magnitude statistics (Robinson and Benites 1995).....	39
Figure 2.1.10 Frequency magnitude statistics for model of multiple layers parallel to a tabular stope (Spottiswoode, 1999).....	39
Figure 2.2.1. Schematic of a virtual element at point Q transmitting influence to point P.....	46
Figure 3.1.1 Effect of element size on frequency magnitude statistics (Cochard and Madariaga (1996) using 513 grid points (top) and 1025 grid points(bottom).....	55
Figure 3.1.2 Frequency-magnitude plot for AE magnitudes derived from kinetic energy of the sample (Method 4), compared to magnitudes derived from individual bond breakages (Method 1) (After Hazzard 1999).....	57
Figure 3.1.3. Frequency-magnitude plot resulting from the syn-processing crack combination algorithm (Method 5). The plot resulting from each crack being considered individually is shown for comparison (Method 1) (After Hazzard 1999). ....	58
Figure 3.1.4 Comparison of frequency magnitude curves for all of the events recorded in Test I clustered using different space windows (Hazzard, 1998). ....	58
Figure 3.1.4 PFC3D model used for mining model. ....	59
Figure 3.1.5 Cumulative frequency – magnitude plot from PFC3D stope models using different space windows for clustering.....	60
Figure 3.1.6 a: Detail of a finite/discrete element model of a tabular stope and b: The frequency-magnitude curve based on incremental kinetic energy release.....	61
Figure 3.1.7 Typical off-reef energy release increments observed in the simulation of mining a parallel-sided panel. ....	63
Figure 3.1.8 Plots of cumulative frequency against energy release increment size in mining a parallel-sided panel at different depths. (a) Stope width = 1.0m. (b) Stope width = 0.5m. ....	64
Figure 3.1.9 Comparison of cumulative fracture length, as a function of time and excavation span, for two different tessellation densities. ....	65
Figure 3.1.10 Cumulative off-reef energy release plotted against cumulative fracture length for different mining depths and mesh grid densities.....	65
Figure 3.1.11 Result of tessellation analysis of Carbon Leader stope using Mohr Coulomb failure criteria. ....	67
Figure 3.1.12 Frequency - Moment plots for the tessellation analysis of a Carbon Leader stope using Mohr Coulomb failure criteria. ....	68
Figure 3.1.13 Maximum moment with span for the tessellation analysis of a Carbon Leader stope using Mohr Coulomb failure criteria. ....	68
Figure 3.1.14 Result of tessellation analysis of Carbon Leader stope using weak flaw and tension crack model of failure.....	69
Figure 3.1.15 Frequency - Moment plots for the tessellation analysis of a Carbon Leader stope using weak flaw and tension crack model of failure. ....	69



Figure 3.1.16 Randomly placed asperities (constant strength).....	72
Figure 3.1.17a Resultant asperity placement over the structure surface – asperities (variable size) and surrounding gouge.....	72
Figure 3.1.17b Resultant asperity placement over the structure surface – asperities only.....	72
Figure 3.1.18 Map3d three-dimensional model of the Rautenbach dyke and surrounding mining.....	74
Figure 3.1.19 Cumulative frequency-magnitude relation derived from observed data along the Rautenbach dyke.....	74
Figure 3.1.20 Cumulative frequency-magnitude relation – original method.....	76
Figure 3.1.21a Cumulative frequency-magnitude relation – new method 1.....	76
Figure 3.1.21b Cumulative frequency-magnitude relation – new method 2.....	77
Figure 3.1.22 Cumulative frequency-magnitude relation comparison – new methods 1 & 2.....	77
Figure 3.1.23 Cumulative frequency-magnitude relation comparison – all methods.....	77
Figure 3.1.24 Cumulative frequency-magnitude relation comparison – modelled versus observed.....	78
Figure 3.1.25 Coseismic slip occurring over the Rautenbach dyke for a particular model step.....	78
Figure 3.1.26 TauTona 336 area (Break fault) case study.....	80
Figure 3.1.27 E-M Relation along the Break fault.....	81
Figure 3.1.28 Cumulative Frequency-Magnitude Relation from the Break fault.....	81
Figure 3.1.30 Resultant asperity placement over the Break fault's surface.....	82
Figure 3.1.31 Observed seismic data analysis – Robust straight line fit.....	83
Figure 3.1.32 Observed seismic data analysis – Aki method.....	83
Figure 3.1.33 Case study 1: modelled seismic data analysis – Robust straight line fit.....	85
Figure 3.1.34 Case study 1: modelled seismic data analysis – Aki method.....	85
Figure 3.1.35 Case study 1: comparative modelled and observed data b-values.....	86
Figure 3.1.36 Case study 2: modelled seismic data analysis – Robust straight line fit.....	88
Figure 3.1.37 Case study 2: modelled seismic data analysis – Aki method.....	88
Figure 3.1.38 Case study 2: comparative modelled and observed data b-values.....	89
Figure 3.1.39 Comparison of b-values derived from case studies 1 & 2.....	90
Figure 3.2.1 Example of space-time distributions of seismicity from a block slider model of fault slip (Shaw, 1995).....	97
Figure 3.2.2 Energy release rate for a mine stope analysis (Napier and Malan, 1997).....	97
Figure 3.2.3 Effect of fault rheology on slip distribution through time (Cochard and Madariaga, 1996).....	98
Figure 3.3.1 Cylindrical PFC3D sample (Hazzard, 1999) showing a) cutaway view of sample and b) localisation and clustering of events along final plane immediately after failure.....	102
Figure 3.3.2 a) Square PFC3D sample for loading in compression or extension (test II) clusters recorded prior to failure in Test I. b) Clusters of events for tests I (Hazzard, 1999).....	102
Figure 3.3.3. Frequency-magnitude plots for two tests with different stress paths. Test I is a compression tests and test II is an extension test. (Hazzard, 1999). .....	103
Figure 3.3.4. Comparison of frequency-magnitude plots for events with different space windows. The value of $R_e$ in particle diameters is shown on each curve. (Hazzard, 1999). .....	103
Figure 3.3.5. Comparison of frequency-magnitude plots with different time windows ( $T_e$ ). The value of $T_e$ in $\mu s$ is shown on each curve. The radius of the space window ( $R_e$ ) is 5 particles diameters in each case (Hazzard, 1999). .....	104
Figure 3.3.6. All IDR elements which failed at $t=-55083.9$ sec (the model was started at $t_0 = -148000.0$ sec). The spheres are at the centroids of the failed tetrahedral elements. Some spheres which could be wide apart can look close together in this projection. ....	105
Figure 3.3.7a. ....	106
Figure 3.3.7b. ....	106
Figure 3.3.8. Connected cluster number 63 (of 111) from two different viewpoints: a) In the plane of the principle and the secondary axis; b) in the plane of the principle and the tertiary axis.....	107
Figure 3.3.9. IDR-generated seismic events during the first 20000 sec.....	108
Figure 3.3.10. IDR-generated events during the second 20000 sec period.....	108
Figure 3.3.11. IDR-generated events during the third 20000 sec period. ....	108
Figure 3.3.12. All IDR-generated seismic events (about 35 hours of real time). ....	109

Figure 3.3.13 Failure initiation position normal to the reef plane as a function of time. 20 time step intervals occur between each face advance increment of 2m. ....	110
Figure 3.3.14 Relative horizontal position of element failure as a function of time.....	110
Figure 3.4.1. Four successive stages of fault slip corresponding to removal of the bracket pillar in the regions 0 to 50m, 50m to 100m, 100m to 150m and 150m to 200m respectively....	112
Figure 3.4.2 Incremental area of fault plane (m <sup>2</sup> ) mobilised as a function of time. Pillar removal stages occur at times 20, 40, 60 and 85. ....	112
Figure 3.4.3 Incremental energy release values corresponding to relaxation of the fault plane in successive time intervals.....	113
Figure 3.4.4 Cumulative fracture length activated after the simulated “blast”. ....	114
Figure 3.4.5 Average distance from the center of the stope face of activated fracture segments in each time step after the simulated blast.....	114
Figure 3.4.6 Energy release increments in each time step following the simulated blast.....	115
Figure 3.4.7. Point kernel analysis of stope showing distance of events to stope with time with magnitude indicated by size of the circles. ....	115
Figure 4.1a Waveforms of a complex seismic event of m = 3 recorded at distance of 420m from the source. In this relatively homogeneous medium complexity of waveforms is caused mainly by the complexity of the source. ....	126
Figure 4.1b Source time function of the event above obtained from the moment tensor inversion in time domain. Amplitudes are normalised to 1. ....	126
Figure 5.2.1 Problem of non-unique clustering in a tessellation analysis. Problems include determination of a: order of events, b: geometry of cluster and c: cluster extension in later steps. ....	132

# List of tables

Table 3.1.1 List of parameters used in PFC3D modelling. .... 56  
Table 3.1.2 Material properties for Carbon Leader tessellation ..... 67  
Table 3.1.3 Material properties used in tessellation using weak flaw and tension crack model .69  
Table 3.1.4 Case 1 - parameter assumptions utilised to attain partial model calibration..... 84  
Table 3.1.5 Parameter assumptions utilised to attain the partial model calibration..... 87  
Table 3.1.6 Model 1&2 parameter assumptions ..... 93  
Table 3.1.7 Model 3&4 parameter assumptions ..... 94  
Table 4.1 ..... 119  
Table 4.2 ..... 122

# Glossary

The following Glossary offers short, simple and context-oriented explanations of the terms related to numerical modelling of rock mass response to loading due to mining. The reader who may require the corresponding rigorous definitions is referred to the specialised mathematical literature on the subject.

<b>Term</b>	<b>Description</b>
<b>Algorithm</b>	Detailed, step-by-step description of the numerical procedure for solving a mathematical problem. An algorithm can be implemented into computer code by means of a programming language such as FORTRAN, C, Java etc.
<b>Asperity</b>	A region of a fault where a high stress drop can occur relative to the surrounding regions.
<b>b-value</b>	A common reference to the absolute value of the slope of the Gutenberg-Richter plot of cumulative frequency vs. magnitude for observed seismic events in a given region.
<b>Barrier</b>	A region on a fault where slip is restricted or halted.
<b>Boundary Element method (BEM)</b>	A numerical technique for solution of problems in solid mechanics that involves only the significant boundary surfaces in the problem region.
<b>Boundary Integral Equation Method (BIEM)</b>	An alternative name for the Boundary Element method.
<b>Boundary Value Problem (BVP)</b>	The term refers to Partial Differential Equations (PDE) and covers all additional conditions which need to be specified to guarantee the uniqueness of the solution.
<b>Boundary condition</b>	In a BVP: requiring that the unknown function or its derivatives assume prescribed values at the points of the boundary which encloses the domain of the partial differential equation.
<b>Calibration</b>	The procedure of bringing one or more of the modelled quantities maximally close to their observed counterparts by tuning the variable parameters of the model.
<b>Cellular model</b>	A class of numerical models in which individual components ("cells") interact with each other according to defined rules.
<b>Constitutive relations</b>	The relationships which govern the response of some measured physical quantity to a variation of the state variables. In the context of solid mechanics the constitutive relations usually relate stress to strain.
<b>Continuum models</b>	A class of models that represent the region of interest as a continuous medium whose properties may vary from point to point but where no break occurs in the displacement field.
<b>Cost function</b>	A function of some independent variables which usually has a single local minimum. Finding the position of this minimum in the space of the independent variables is the objective of optimisation.
<b>Damage rheology</b>	The laws which govern the temporal evolution of material deformation due to loading and damage.
<b>Delaunay mesh</b>	a grid of triangles connecting a set of points on a surface with the property that the circumcircle of each triangle does not enclose any other point of the mesh. The Delaunay triangulation ensures that the generated triangles are as "equiangular" as possible for the given set of points.
<b>Deterministic algorithm</b>	A set of rules for solving a mathematical problem which leads to a unique solution for a given set of initial and boundary conditions.
<b>Deterministic model</b>	A description of the behaviour of a system in which key variables assume unique values that are computed according to a set of rules that are not subject to alterations by random chance.
<b>Dirichlet problem</b>	The problem of finding the solution of a partial differential equation for given prescribed values of the function on the boundary
<b>Discontinuum models</b>	A class of numerical models that simulate the interaction between discrete solid elements or which solve the interaction between assemblies of fractures in the region of interest.

<b>Term</b>	<b>Description</b>
<b>Displacement discontinuity</b>	A general term to describe the jump in the displacement vector across the surface of a crack in a solid material.
<b>Displacement discontinuity method (DDM)</b>	A particular form of the boundary element method in which the displacement discontinuity is solved on specified crack surfaces.
<b>Distinct element method (DEM)</b>	A particular type of discontinuum model in which the interaction of an assembly of polyhedral blocks or particles is analysed.
<b>Dynamic modelling</b>	A numerical model of some physical process in which the state of the modelled system changes with time. A typical example of dynamical modelling is the numerical treatment of seismic waves.
<b>Elastic modulae</b>	The material constants in the expression for the density of the elastic energy as a function of the strain invariants. In the case of a linear elastic body the elastic modulae are the coefficients in the linear relationship between stress and strain.
<b>Element</b>	A small surface patch of volumetric region chosen to represent the local variation in the slip or displacement in the numerical solution of a problem in solid mechanics.
<b>Energy dissipation</b>	The part of the mechanical work done on a solid which is irreversibly transformed into non-mechanical forms of energy e.g. heat, chemical energy etc.
<b>Empirical</b>	As opposed to theoretical: derived directly from the observations and measurements performed on concrete physical systems (usually laboratory samples).
<b>Entropy</b>	A thermodynamical quantity which measures the portion of the internal energy which cannot be converted to work done by the system.
<b>Equations of motion</b>	For a system of material particles: the equations relating the rate of change of linear momenta to the net forces acting on material particles. For a continuum: the equations which govern the time evolution of the state variables (e.g. the local strains).
<b>Euler's approach (to the equations of motion of continua)</b>	The description of the motion of a continuum relative to fixed points in space.
<b>Excess shear stress</b>	The difference between the resolved shear stress and the shear resistance at a particular point of a specified discontinuity surface.
<b>Fault slip</b>	A loose reference to the jump in the shear discontinuity across an assumed fault surface.
<b>Finite element method (FEM)</b>	A general numerical analysis technique for solution of fluid mechanics, diffusion and stress analysis problems.
<b>Forward modelling</b>	The methods for finding the (unique) solution of a problem for specified values of the model parameters and for fixed initial and boundary conditions.
<b>Frequency-magnitude plot</b>	A plot of the cumulative frequency of seismic events in a designated region against the magnitude of these events.
<b>Fundamental solution</b>	The influence of unit excitation in an elastic medium, expressed as a function of the distance between the excitation point and the observation point in the medium.
<b>Global minimum</b>	For a function of one or several independent variables defined in a domain D: the point in D for which the function assumes its minimum value.
<b>Gouge</b>	A generic reference to fine particulate material, on the interface of a discontinuity or fault surface that is generated by slip at the surface.
<b>Grid size</b>	The dimension of a unit "zone" or "element" forming the basis of a numerical solution method.
<b>Hybrid model</b>	A combination of two or more categories of numerical modelling methods
<b>Integration</b>	In the context of numerical modelling for the needs of the mining industry: enabling a numerical model to use as a direct input real data from a seismic monitoring system through converting the seismic source parameters into a corresponding additional loading on the modelled rock-mass.

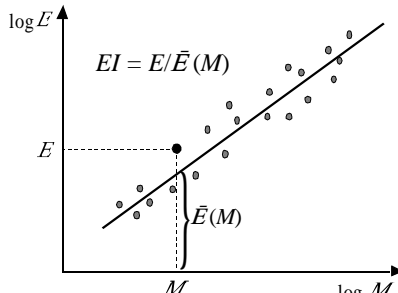
<b>Term</b>	<b>Description</b>
<b>Inverse modelling</b>	The methods whereby a given solution of a certain problem is employed to find one or more of the following: <ul style="list-style-type: none"> <li>- model parameters</li> <li>- initial conditions</li> <li>- boundary conditions</li> </ul>
<b>Lagrangian variables</b>	The description of the motion of a continuum by following individual points of the moving medium.
<b>Matrix</b>	A rectangular table of numbers. Square matrices have equal number of rows and columns. Matrix of a single column and n rows is called vector of length (or dimension) n. The basic algebraic operations are defined for matrices and vectors of compatible dimensions. Matrix notations offer a convenient way of writing systems of simultaneous linear equations.
<b>Mixed boundary value problem</b>	The problem of finding the solution of a partial differential equation for prescribed values of the unknown function on part of the boundary and prescribed values of the normal derivative on the remainder of the boundary.
<b>Neumann problem</b>	The problem of finding the solution of a partial differential equation for given prescribed values of the normal derivatives on the boundary.
<b>Non-linear physical system</b>	One for which the response to an external loading which is the sum of two components is not equal to the sum of the responses to the individual loading components.
<b>Optimisation</b>	For a given (cost-) function: the problem of finding its (local or global) minimum. For a numerical model: the problem of formulating and minimising an appropriate cost-function of the model parameters.
<b>Particle model</b>	A form of distinct element model in which the basic units are spherical particles that interact with their neighbours through specified contact forces and in which each particle is allowed to move according to the laws of Newtonian mechanics.
<b>Percolation model</b>	Any model of connected clusters which are generated on some lattice for a fixed occupation probability. Percolation models exhibit critical behaviour and, consequently, scaling laws. Large percolation clusters have fractal geometry.
<b>Percolation threshold</b>	The critical value of the occupation probability for which a percolation model can have an infinite cluster (a clusters which spans across the whole lattice).
<b>Random mesh</b>	A network of interconnected links between points placed randomly on a plane. The concept can be extended to higher dimensions.
<b>Rheology</b>	A generic term used to designate the rules governing creep-like behaviour in a medium or across discontinuity surfaces.
<b>Seismic event</b>	The occurrence of an abrupt movement in the rock mass.
<b>Seismic migration</b>	The movement, over a period of time, of observed clusters of seismic events through space.
<b>Seismic monitoring</b>	Automated detection and recording of the temporal and spatial location of seismic event activity in a given region.
<b>Slip interface</b>	The assumed narrow region of intense local movement between two relatively intact regions.
<b>Slip weakening</b>	The function describing the decrease in bond strength at a discontinuity interface as a function of the relative slip.
<b>Static modelling</b>	A numerical model of a system at equilibrium in which the physical state does not change with time. A typical example of static modelling is the computation of the stress field in a loaded material.
<b>Stiffness</b>	A generic term used to describe the proportionate change in stress at a given location in relation to some characteristic movement at that location.
<b>Stochastic process</b>	A sequence of events (or the mathematical equivalent of real events) in which the next event cannot be predicted with absolute certainty.
<b>Stochastic model</b>	A numerical model which employs a computer generated stochastic process for evaluating some or all of the relevant quantities.

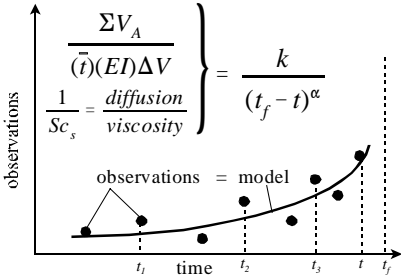
<b>Term</b>	<b>Description</b>
<b>Stress drop</b>	The decrease in the resolved shear stress following a decrease in strength and accompanying slip at a given position on a discontinuity surface.
<b>Tessellation</b>	A generic term used to describe a space-filling or “tiling” pattern.
<b>Validation</b>	the procedure whereby the output of a numerical models is compared against the observed or expected behaviour of the modelled physical system.
<b>Verification</b>	of a numerical model: to establish the degree to which the model is a truthful representation of the physical reality. Strictly speaking a model can never be fully verified.

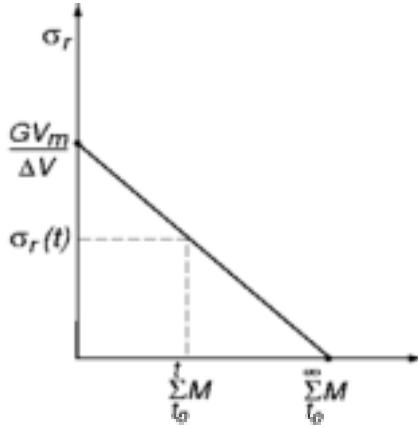
(From: Mendecki, A.J., van Aswegen, G. and Mountfort, P. *A Guide to Seismic Monitoring in Mines*. In: *A Handbook on Rock Engineering Practice for Tabular Hard Rock Mines*, A J Jager and J A Ryder (eds.), published by the Safety in Mines Research Advisory Committee (SIMRAC), 1999)

Parameter, relevant formula	Description
<p><b>Magnitude, <math>m</math></b>  <math>m = \log(A/T) + C</math>  <math>A/T</math> - the maximum displacement over associated period in the P- or S- wave group  <math>C</math> - corrections for path effects, site response and source region</p>	<p>Magnitude is a relative measure of the strength of a seismic event based on measurements of maximum ground displacement at a given frequency at multiple seismic sites. A unit increase in magnitude corresponds to a 10-fold increase in amplitude of ground displacement. Gutenberg and Richter related seismic energy and magnitude derived from P-waves recorded at large distances from the source at 1sec period as <math>\log E(\text{ergs}) = 2.4m + 5.8</math></p>
<p><b>Seismic moment, <math>M</math>, [Nm]</b>            And  <b>Moment-magnitude, <math>m</math></b>  <math>m = 2/3 \log M - 6.1</math></p>	<p>A scalar that measures the coseismic inelastic deformation at the source. Since seismic moment is proportional to the integral of the far field displacement pulse it can easily be derived from recorded waveforms. A relation that scales seismic moment into magnitude of a seismic event is called moment-magnitude.</p>
<p><b>Seismic moment tensor</b>  <math display="block">M_{ij} = \int_V c_{ijkl} \Delta \epsilon_{kl} dV = \int_V \Delta \sigma_{ij} dV, \text{ where}</math>  <math>c_{ijkl}</math> - elastic constants  <math>\Delta \epsilon_{kl}</math> - strain change at the source  <math>\Delta \sigma_{ij}</math> - stress change or change in moment per unit volume    <math>\Delta \theta = \text{tr}(M_{ij}) / (3\lambda + 2G)</math>, where  <math>\lambda</math> - the second Lamé constant  <math>G</math> - rigidity</p>	<p>The most general description of the processes at the seismic source <math>V</math> is by the distribution of forces or moments equivalent to the inelastic deformation. One can describe the inelastic processes at the source as the stress-free change of size and shape of an elastic body without alteration of the elastic properties of the region. If change in size and shape can be expressed as a change in strain <math>\Delta \epsilon_{kl}</math>, then the equivalent stress change, or change in moment per unit volume is proportional to the strain change. The total moment integrated over the source volume is the seismic moment tensor, <math>M_{ij}</math>. For long waves compared to the source size, the whole source volume <math>V</math> can be considered to be a system of couples located at, say, the centre of <math>V</math>, and the moment tensor components can be defined by the equation at left. The moment tensor measures the inelastic deformation at the source during the seismic event and its value at the end of the source process measures the permanent inelastic strain produced by the event. The seismic moment tensor can be decomposed into isotropic (or volume change) and deviatoric components providing an additional insight into the nature of the coseismic strain drop. For a homogeneous body, the coseismic volumetric change, <math>\Delta \theta</math>, can be calculated from the second equation at left. The eigenvalues and corresponding eigenvectors of the deviatoric component of the seismic moment tensor describe the magnitude and orientation, respectively, of the principal moment axes (neglecting gravity) acting at the source. These principal moment axes are uniquely determined by moment tensor inversion. Principal moment orientation data can provide sufficient information to find the best stress tensor.</p>
<p><b>Radiated seismic energy, <math>E</math>, [J]</b></p>	<p>The portion of the energy released or work done at the source that is radiated as seismic waves. Seismic energy is proportional to the integral of the squared velocity spectrum in the far field and can be derived from recorded waveforms. Radiated seismic energy increases with stress drop, seismic moment and with the traction rate i.e., stress oscillations at the source.</p>



Parameter, relevant formula	Description
<b>Corner frequency, <math>f_0</math>, [Hz]</b> And <b>Source size, <math>l</math>, [m]</b> $l = c_1 / f_0$ $c_1 \approx 2500$ for S-wave in hard rock	The frequency at which a source radiates the most seismic energy observed as the maximum on the source velocity spectrum or as the point at which a constant low frequency trend and a high frequency asymptote on the recorded source displacement spectrum intersect. The corner frequency is inversely proportional to the characteristic size of the source.
<b>Stress drop, <math>\Delta\sigma</math>, [Pa]</b> $\Delta\sigma = c_2 M f_0^3$ $c_2 \approx 1.8 \times 10^{-10}$ for S-waves in hard rock $\Delta\sigma = G\Delta\epsilon$ , and $\Delta\epsilon$ - strain drop	Stress drop estimates the stress release at the seismic source. Although it is model dependent it provides reasonable estimates and a fair comparison amongst different sources from the same region recorded by the same seismic system.
<b>Source area, [m<sup>2</sup>]</b> $A = M / (Gu)$ $u$ - average displacement at the source.	The area of coseismic inelastic deformation over the planar source.
<b>Source volume, [m<sup>3</sup>]</b> $V = M / \Delta\sigma$	The volume of coseismic inelastic deformation of the order of $\Delta\sigma/G$ .
<b>Apparent stress, [Pa]</b> $\sigma_A = GE / M = E / (\Delta\epsilon V)$ or $\sigma_A = E / (uA)$ .	Apparent stress is recognised as a model independent measure of the stress change at the seismic source.
<b>Apparent volume, [m<sup>3</sup>]</b> $V_A = M / (c_3 \sigma_A) = M^2 / (c_3 GE)$ $c_3$ - scaling factor $\approx 2$ .	The apparent volume scales the volume of rock with coseismic inelastic strain of an order of apparent stress over rigidity. The apparent volume $V_A$ is less model dependent than the source volume $V$ .
<b>Energy index, EI</b> 	The notion of comparing the radiated energies of seismic events of similar moments can be translated into a practical tool called Energy Index ( $EI$ ) – the ratio of the radiated energy of a given event ( $E$ ) to the energy $\bar{E}(M)$ derived from the regional $\log E$ vs. $\log M$ relation for a given moment $M$ . Since $\log \bar{E}(M) = c + d \log M$ , then $\bar{E}(M) = 10^{c+d \log M}$ where $c$ and $d$ are constant for a given $\Delta V$ and $\Delta t$ . In general $d$ -value increases with the system's stiffness and $c$ increases with stress. A small or moderate event with $EI > 1$ suggests a higher than average shear stress at its location. The opposite applies to the $EI < 1$ case.
<b>Seismic strain,</b> $\epsilon_S (\Delta V, \Delta t) + \Sigma M / (2G\Delta V)$ and <b>Seismic strain rate, [s<sup>-1</sup>]</b> $\dot{\epsilon} (\Delta V, \Delta t) = \epsilon_S / \Delta t$	Seismic strain measures strain due to cumulative coseismic deformations within the volume $\Delta V$ over the period $\Delta t$ . Its rate is measured by $\dot{\epsilon}_S$ .
<b>Seismic stress, [Pa]</b> $\sigma_S (\Delta V, \Delta t) = 2G\Sigma E / \Sigma M$	Seismic stress measures stress changes due to seismicity.
<b>Seismic stiffness modulus, <math>K_s</math> [Pa]</b> $K_S (\Delta V, \Delta t) = \sigma_S / \epsilon_S = 4G^2 \Delta V \Sigma E / (EM)^2$	Seismic stiffness measures the ability of the system to resist seismic deformation with increasing stress. The stiffer systems limit both the frequency and the magnitude of intermediate and large events but have time-of-day distribution with larger statistical dispersion, thus are less time predictable.
<b>Seismic viscosity, [Pa · s]</b> $\eta_S (\Delta V, \Delta t) = \sigma_S / \dot{\epsilon}_S$	Seismic viscosity characterises the statistical properties of the seismic deformation process. Lower seismic viscosity implies easier flow of seismic inelastic deformation or greater stress transfer due to seismicity.

Parameter, relevant formula	Description
<b>Seismic relaxation time, [s]</b> $\tau_S(\Delta V, \Delta t) = \eta_S / G$	Seismic relaxation time quantifies the rate of change of seismic stress during seismic deformation processes and it separates the low frequency response from the high frequency response of the system under consideration. It also defines the usefulness of past data and the predictability of the flow of rock. The lower the relaxation time, the shorter the time span of useful past data and the less predictable the process of seismic deformation.
<b>Seismic Deborah number</b> $De_S(\Delta V, \Delta t) = \tau_S / \text{flowtime}$ , where <i>flowtime</i> is a design parameter not necessarily equal to $\Delta t$ .	Seismic Deborah number measures the ratio of elastic to viscous forces in the process of seismic deformation and has successfully been used as a criterion to delineate volumes of rockmass softened by seismic activity (soft clusters). The lower the Deborah number the less stable is the process or the structure over the design <i>flowtime</i> - what may be stable over a short period of time (large $De_S$ ) may not be stable over a longer time (lower $De_S$ ).
<b>Seismic diffusivity, [m<sup>2</sup>/s]</b> $D_S(\Delta V, \Delta t) = (\Delta V)^{\frac{2}{3}} / \tau_S$ , or in a statistical sense $d_S = (\bar{X})^2 / \bar{t}$ .	Seismic diffusivity can be used to quantify the magnitude, direction, velocity and acceleration of the migration of seismic activity and associated transfer of stresses in space and time. There is an inverse relationship between the diffusivity $D_S$ and the friction parameters.
<b>Seismic Schmidt number</b> $Sc_{sd}(\Delta V, \Delta t) = \eta_S / (\rho D_S)$ or $Sc_{sd} = \eta_S / (\rho d_S)$ where $\rho$ is rock density.	Seismic Schmidt number measures the degree of complexity in space and time (the degree of turbulence) of the seismic flow of rock. Note that seismic Schmidt number $Sc_{sd}$ , encompasses all four independent parameters describing seismicity: $\bar{t}, \bar{X}, M, E$
<b>Time to failure, (<math>t_f - t</math>)</b> $d\Omega / dt = k(t_f - t)^\alpha$ $\Omega$ - measurable quantity $t$ - current time $t_f$ - time of failure $k, \alpha$ - constants 	This concept describes the behaviour of materials in the terminal stages of failure. It views instability as a critical point, then precursors should follow characteristic power laws in which the rate of strain or other observable, measurable, quantity $\Omega$ is proportional to the inverse power of remaining time to failure. Observed oscillations in $\Omega$ of an increasing frequency as the failure approaches are part of the solution to time-to-failure equation with a complex exponent, where the imaginary part relates to discrete scale transformation and introduces log-periodic oscillations decorating the asymptotic power law. The observations $\Omega$ can be a combination of different seismic parameters that would exhibit power law type increase before failure. For well behaved data sets the time at failure $t_f$ can be estimated from the times of three successive maxima ( $t_1, t_2, t_3$ ) of the observed process $t_f = (t_2^2 - t_1 t_3) / (2t_2 - t_1 - t_3)$ . Note that, in theory, $t_3 - t_2 < t_2 - t_1$ .

Parameter, relevant formula	Description
<p data-bbox="199 190 686 246"><b>Seismic moments, volume mined and relative stress</b></p> 	<p data-bbox="710 190 1428 369">If a volume of rock, <math>V_m</math>, is mined out at time <math>t_0</math> and if the altered stress and strain field can readjust to an equilibrium state through seismic movements only, the sum of seismic moments released within a given period of time would be proportional to the excavation closure and in the long term at <math>t = t_\infty</math></p> $M = GV_m$ <p data-bbox="710 459 1428 616">where <math>M</math> is the scalar seismic moment. The relative stress level at the time, <math>t</math>, in a given volume of rock <math>\Delta V</math> surrounding the excavation, can be calculated from the difference between <math>GV_m</math> and the cumulative moments released to date:</p> $\sigma_r(t) = (GV_m - \sum_{t_0}^t M) / \Delta V .$
<p data-bbox="199 723 622 779"><b>Seismic moments and volume of elastic convergence</b></p> <p data-bbox="199 784 343 817"><math>\Sigma M = \gamma GV_e</math></p>	<p data-bbox="710 723 1428 994">The amount of strain energy stored when mining in elastic rock is directly proportional to the volume of elastic convergence, <math>V_e</math>. It has been found that the total amount of seismic moment resulting from mining within a large area and time period is related to the change in elastic convergence <math>V_e</math>. The proportional constant gamma, <math>\gamma</math>, has been found to vary between about 0.03 and 1.0. There is some evidence that <math>\gamma</math> is a function of the geotechnical area being mined.</p>



# 1. Introduction

## 1.1. Formulation of the problem

The needs of the mining industry for effective and safe production have stimulated research and development effort in two strategic directions:

- design and exploitation of seismic monitoring systems
- numerical modelling of rock-mass response to loading.

To this date there has been very little cross-pollination of ideas and methodologies between the designers of seismic monitoring systems on the one side and the developers of numerical models of mining-induced seismicity and related phenomena on the other. As a result the modern seismic monitoring systems use little more than the most basic model assumptions about the seismic source dynamics and the properties of the medium supporting the propagation of seismic waves. At the same time the existing numerical modelling tools use the available real seismic data merely as a touch-stone for model validation through visual inspection or calibration and seldom for model optimisation.

The development of seismic monitoring systems seems to proceed independently from the progress in the numerical modelling of mining-induced seismicity. It is true that the analysis of seismic data depends on model assumptions but these are about the propagation of elastic waves in heterogeneous media. A monitoring system is designed to register and analyse seismic events as they occur and not to attempt an explanation of the processes in the rock-mass leading to such behaviour.

Explaining and predicting constitute the realm of physics-based models which reformulate the questions asked about the state of the rock into mathematical problems and implement numerical algorithms for solving them. In the process of solving such mathematical problems, specific information about the physical state of the material under study can be obtained either by referring to a particular moment in time or to a sequence of time steps. When such information is properly interpreted it constitutes **model-generated data**.

## 1.2. Model - data interaction

A physics-based model of rock-mass response to loading in the conditions of active mining is designed to be a reflection of the real-world situation. This reflection always turns out to be somewhat distorted due to simplifying model assumptions and input incompleteness. The measure of this distortion determines the usefulness of a particular model as a provider of answers to specific questions in a given situation.

### 1.2.1. Visual inspection

It is not always straightforward to even assess the distortion introduced by a model to say nothing of controlling and minimising this distortion to an acceptable level. The assessment is usually done by comparing the real data with the model-generated data. A simple visual inspection of the model-generated data in comparison with the data provided by the local seismic network is the first step in deciding whether a given model is at all applicable to the concrete situation in the context of the mining design and production plans. Although the visual inspection of numerical models is based on a passive and quite limited interaction between the monitored and the modelled data it is still an indispensable tool for discarding unsuitable models and for turning the efforts of the numerical modelling practitioners in the right direction.

## 1.2.2. Calibration

Once a particular type of numerical model has been chosen as the most appropriate for a given mining situation it needs to undergo the process of calibration. This involves a new level of interaction between the model-generated data and the data collected through observation of the real system. To begin with, **data interpretation** is needed as a bridge between the numerical output of the model and the values of the real physical quantities which are measured and recorded by the monitoring system. A numerical model uses variables whose values are pure numbers. In contrast the observable physical quantities have values in accordance with the chosen system of units. The lack of units (such as kg for mass or sec for time) in numerical models is compensated by supplying each model variable with a physical interpretation (i.e. pointing to the physical quantity it corresponds to) and with a scale coefficient for comparing the numbers generated by the numerical procedure with the corresponding measured quantities. **Calibration is the procedure whereby the scale coefficients of the model variables are determined.** The calibration of a model is performed by comparing a sample model output with a selected subset of the observed (monitored) data. The scaling of the modelled data makes it possible to plot it on the same graph with the corresponding observed data thus making the deviations introduced by the model visible. In all cases of practical interest to the mining industry there would be not just one such plot but several: one for each modelled quantity and its observed counterpart. The calibration must bring the model closer to the reality it describes. This is achieved by varying some of the parameters in the model in order to minimise the discrepancies between the modelled data and the corresponding observed values. Therefore a model must be subjected to a thorough **sensitivity analysis** first and only then it can be calibrated.

### 1.2.2.1. Sensitivity analysis

The formulation of every numerical model includes a number of variable parameters which cannot be specified *a priori*. As a result of this one and the same numerical model can generate different sets of data according to the values chosen for the variable parameters. **The sensitivity analysis must reveal the way in which the modelled data values respond to changes of the parameters.**

A complete sensitivity analysis could be prohibitively expensive and in practice it is only the effect of some parameters which has to be studied before a calibration of the model can be attempted. Those are the parameters which, when varied, lead to significant changes in the performance of the models and for that reason are called **critical parameters**. As a first stage in the sensitivity analysis the response of the model to all its parameters is measured and the critical parameters are identified. The next stage of the sensitivity analysis involves the detailed study of the response of the model to the simultaneous and independent variation of all critical parameters. This process could require significant time and effort especially when the number of critical parameters is more than three.

### 1.2.2.2. Practical issues of model calibration

There are different approaches to calibration. The simplest approach is to consider one observed quantity and to tune the model by varying its parameters so that the modelled variable would have the same numerical value as the observed one. Such "**one-point calibration**" is not likely to greatly improve the model and in practice a simultaneous minimisation of the differences between several pairs of modelled-monitored quantities is needed. This process is related to the mathematical problem of multivariate optimisation in which the (global or local) minimum of a function of many variables needs to be found. The final stage of the calibration of a numerical model is performed on the critical parameters only.

### 1.2.3. Model optimisation

In the context of model improvement the calibration can be regarded as a form of optimisation where the function to be minimised (**the cost function**) is a measure of the discrepancy between the modelled data and the monitored data. The cost function of a model depends on the variable model parameters but this dependence is not known analytically and the cost function of a model can be evaluated only through running the model itself. This makes it impractical to attempt a model optimisation by means of the standard algorithms for functional optimisation. There is a more fundamental difference between model optimisation and the mathematical problem of finding the minimum of a function though: the output of a model and hence the optimisation cost function is determined not only by the values of the variable parameters but also by specifying a set of additional restrictions known as initial and boundary conditions. The initial conditions of a model refer to the physical state of the rock-mass at a given moment of time while the boundary conditions correspond to the loading. The lack of detailed knowledge about the initial and the boundary conditions is the main reason for the discrepancy between the modelled and the monitored data. So, just as model sensitivity analysis was a necessary precondition for performing calibration, a study of the response of the modelled data to variations in the initial and boundary conditions is needed for carrying out model optimisation.

**Optimisation is the procedure of minimising the discrepancy between model-generated data and monitored data through varying all factors affecting the performance of the numerical model**

It may seem that the above definition of model optimisation covers all avenues along which the process of bringing a model closer to reality may follow. This is not the case since the concept of optimisation just as the lower-level concept of calibration is based on a **passive form of interaction between modelled and monitored data**:

- the model runs for certain values of the parameters and under given initial and boundary conditions;
- the model-generated data is collected and compared with the corresponding data provided by the seismic system. The degree of the discrepancy between modelled and monitored data is evaluated;
- the values of one or more parameters are changed: the prescribed values and possibly even the type of initial and boundary conditions are changed and the model is run again.

In this scheme the monitored data plays the role of a touch-stone and does not influence in any way the performance of the numerical model. In static modelling the object of interest is the state of equilibrium certain rock-mass assumes under a given load and a direct comparison of modelled data with a real data stream provided by a seismic system is not possible: there is no seismicity in static models. The situation is different for dynamical numerical modelling based on continuum mechanics, fracture dynamics, damage rheology and thermodynamics. The common feature of the models in the above group is that they employ equations of motion and thus are capable, at least in principle, to simulate the evolution of the physical state of the material in real time. In other words, **physically based dynamical models of rock-mass response to loading can produce data in the form of a stream of values similar in structure to the output from the seismic monitoring systems.**

## 1.3. Integration of seismic monitoring with numerical modelling

### 1.3.1. Forward and inverse modelling

Two types of mathematical problems can be formulated within the framework of a physics-based dynamical model:

- Forward problem: Given are the properties of the material, the initial state and the loading conditions. Find the evolution of the physical state of the rock-mass.
- Inverse problem: Given is the evolution of the system as a time-series of physical states and either the material properties or the loading conditions but not both. Determine the properties of the material if the loading conditions were given or determine the loading conditions if the material properties were given.

The forward-type of problems are well defined and have usually a single, unique solution since continuum mechanics is a deterministic theory. **The practical applications of forward modelling are obvious: this is the only physically acceptable method of making predictions about the response of the material to given loading conditions.** When the governing equations are essentially non-linear the system can exhibit instabilities: infinitesimally small variations in the initial state and/or the loading conditions could lead to significant changes in the evolution of the system resulting in chaotic behaviour. The reliability of the predictions based on forward modelling strongly depends on the accuracy of the initial and the boundary conditions. This problem casts a shadow of doubt on the feasibility of predicting seismicity even in principle.

Predicting seismicity is such a thorny issue that any definite statement made about it is certain to meet with vigorous opposition. Nevertheless it is possible to restrict the context in which one considers the predictability of seismic phenomena and to look for some causative relationships limited to relatively small space-time regions. This is precisely the situation with mining-induced seismicity. Here are some arguments in this respect:

- The processes in rock-mass subjected to loading are fully covered by the theoretical framework of contemporary physics at least at the microscopic level.
- Predictive statements need to cover relatively short periods of time and can refer to a limited volume of rock.
- The loading conditions are partially under control as they can be estimated from the design of the mine, the records of the local seismicity and the current production rates.
- Some information is available about the material properties of the rock under study and, possibly, about existing geological structures.

Inverse modelling is much more difficult than forward modelling because:

- There are infinitely many different formulations of inverse problems hence there is no universal approach to solving such problems
- There are no guarantees that a particular inverse problem will have a solution or, even if the existence of a solution can be established, it may turn out that it is not unique which is as bad as not having a solution at all.
- The numerical methods for solving inverse problems are more complex and computationally expensive than the methods for solving forward problems



In spite of the difficulties listed above formulating and solving inverse problems is an important component of the whole complex of mining-related modelling as a provider of information about the material properties of the rock-mass and the loading conditions needed for running the predictive part of the numerical model.

### **1.3.2. The concept of integration**

The demand for a greater reliability imposed on the numerical models of rock-mass response to loading dictate a further development of the ideas and practice of model optimisation. The road to go is in the direction of increasing the role played by the real data supplied by the seismic monitoring systems for reducing the discrepancy with the model-generated data. This can be achieved by developing predictive models capable of taking direct numerical input both from a catalogue of seismic events and from an in-lined seismic system. The input from real events has to be quantified and converted to either loading (boundary conditions) or to initial conditions according to the concept of the numerical model. In addition, the assimilation of real events in a running model can further specify the local material properties and the state of damage of the rock-mass immediately after a seismic event. The implementation of these ideas in functional software constitutes an integration of seismic monitoring with numerical modelling.

**A numerical model of mining-induced seismicity is truly integrated with the local seismic network when:**

- **it is designed to take as direct input all the available information about the seismic events recorded in the area prior and during the time-window of the model-generated data**
- **it uses this input to systematically improve the predictive power of the model.**

There is very little experience in the creation and exploitation of integrated seismic models in the above sense. Yet even at this stage it is possible to outline some of the fundamental principles which should be embedded in such systems. The assimilation of real seismic data in a running numerical model and the dynamical interaction between monitored and modelled data can be achieved only in dynamical, forward-in-time numerical models in which the pace of time is scalable to that of physical time. The integration of seismic monitoring with numerical modelling requires a synchronisation between real, observed events and their modelled analogues (e.g. loss of cohesion, local loss of stability, material failure etc.).

### **1.3.3. Restrictions imposed on models by the integration paradigm**

Not every numerical model of mining-induced seismicity can be upgraded to an integrated version capable of absorbing the information provided by the local seismic monitoring system in real time. Here are some of the requirements which have to be met by numerical models if the latter are to be integrated with real seismic data:

- The numerical model must run in time steps which are re-scalable to the pace of the actual (physical) time
- The numerical model must include a procedure or procedures for converting real events of particular location, time of occurrence and size characteristics into corresponding additional loading of the system.
- The numerical model must allow for an unambiguous identification of “seismic events” among the generated data.

The above conditions must be regarded as necessary for models which are to be integrated with real data. To illustrate how restrictive the above requirements really are it suffices to mention that numerical packages do not include forward-modelling in physical time cannot be integrated with monitoring systems.

The class of models which are best suited for upgrading to an integrated system are those based on dynamical evolution equations. Such models treat problems referring to the physical state and processes in a certain volume of rock-mass in given surroundings for specified initial conditions and under a prescribed external loading. This presupposes a definition of the rock-mass under study as a physical system. In the context of the problems of interest to the mining industry, such a definition should include:

- a clear description of the set of states in which a given volume of rock-mass can exist under the specified conditions
- a list of the relevant degrees of freedom of the physical system, such as: the field of local strains, the field of stresses, the distribution and the degree of local damage of the material, temperature etc.
- a formulation of all relevant macroscopically observable quantities which must serve as a bridge between the model-generated data and the data provided by the seismic monitoring system.
- a clear and unambiguous definition of seismic events within the numerical model. The definition must provide for the extraction of seismic source parameters for the purpose of model calibration.

## **1.4. Structure of an integrated seismic monitoring-modelling system**

The integration of seismic monitoring with numerical modelling does not smear the differences between the two main components of an integrated system: the monitoring complex and the numerical modelling software.

The structure of a seismic monitoring complex can be considered as well established. It comprises of the network of seismic stations, the software for on-line processing of seismic events and the seismic database.

In contrast, the structure of the numerical modelling part of an integrated system is less rigidly determined and can undergo significant evolution following the progress in the theory of damage rheology, rock-mass stability, energy dissipation in fractured solids, granular flow and other related areas of fundamental and applied physics. Another source of influence on the composition of the modelling software is the progress in the development of new numerical methods for solving difficult mathematical problems such as systems of non-linear partial differential equations, ill-posed integral equations, large unstructured and dense linear systems, variational problems in infinitely dimensional (functional) spaces etc.

The functionality of an integrated seismic system must be facilitated by appropriately developed graphical software. In fact, the development of graphical tools for seismicity-oriented modelling is so vital, that it could be attributed to a third domain of the integrated system. The complexity of seismic data makes it extremely difficult for visualising and beyond the scope of general-purpose graphical software. Even more difficult is the visualisation of the state variables of a given volume of rock. On the other hand it is the evolution of the physical state of the system under study which, if properly monitored, could reveal the patterns preceding the loss of stability in the material. It is highly desirable, therefore, to develop specific graphical tools for visualising strain distribution, stress distribution, damage and other relevant quantities. When building an integrated seismic monitoring-modelling system one must not regard the development of graphical tools as a mere convenience and part of the product packaging but rather as an essential data-interpretation and monitored-modelled data interaction facilitator.

The functional inter-dependence between the components of an integrated monitoring-modelling system is shown on the following chart:

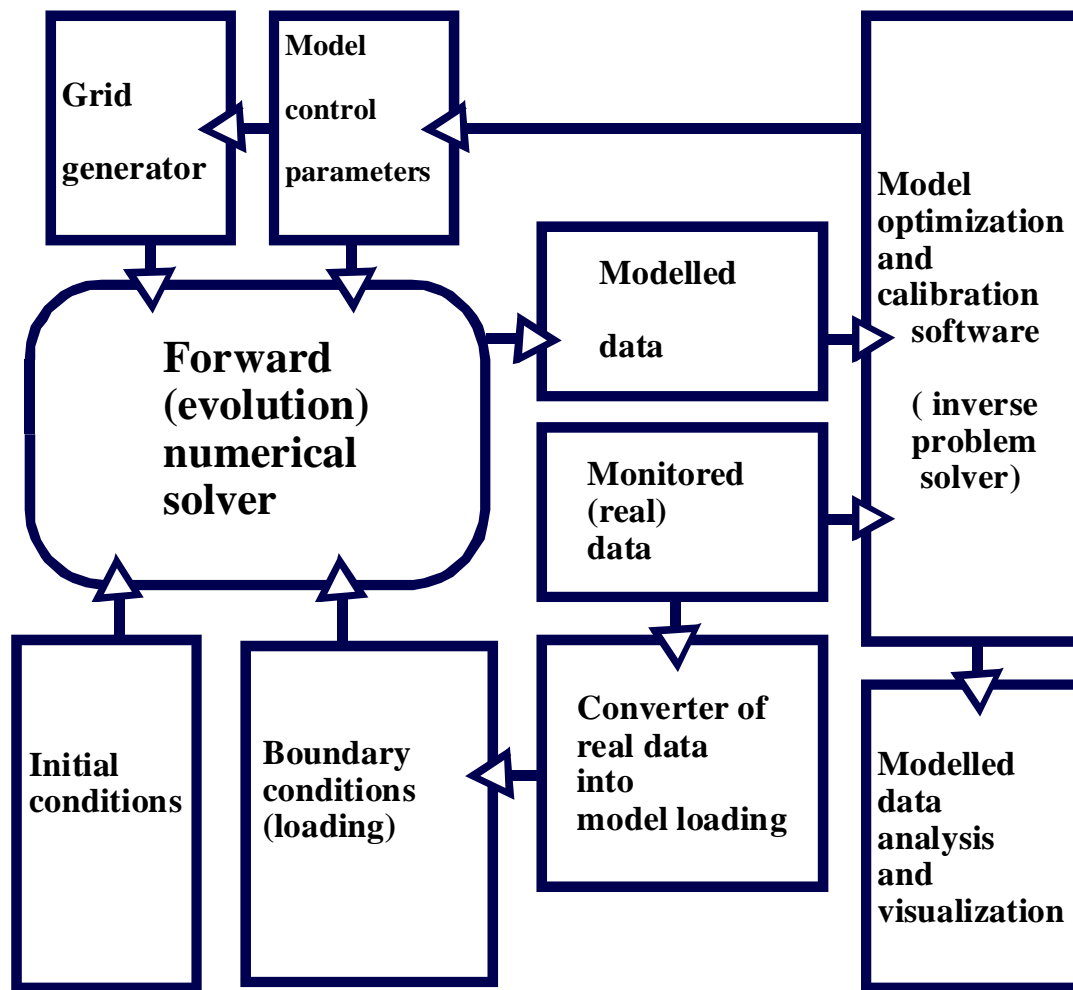


**Figure 1.1**

The interaction between the model and the real data stream goes along two channels: from one hand, the monitored data is juxtaposed to the modelled data for optimising the model parameters and from the other hand the real seismic events affect directly the running of the forward solver by modifying the boundary conditions (the loading).

The integration of monitoring and modelling implies that the real data input will, to a certain extent, drive the numerical model. On the other hand, the same model is driven by the pre-set initial and boundary (loading) conditions and itself is capable of generating the model-analogues of seismic events. The question arises of whether the model-generated seismic activity would not be in conflict with the input from real events. To understand better the situation one can imagine that the model is “perfect” in the sense that it generates seismic activity with almost exactly the same spatial, temporal and size distribution as the observed local seismicity. In that case an integration of the model with the monitoring system would lead to a “double counting” of seismic events and will drive the model away from the observed data instead of bringing it closer to it. One may, of course, argue that such a model would not need integration being itself the perfect predictive tool so badly needed in the mines. Quite apart from the fact that the considered scenario is not likely to materialise in the foreseeable future, the above analysis highlights the possibility of double counting in the integration process. A procedure would be needed in each integrated model whereby such double counting would be eliminated. The concrete approach to solving this problem would depend on the structure of the model.

## 2. Review of numerical models potentially useful for integration

### 2.1. Generic modelling methods

This literature survey is focussed on determining the ways in which seismic data can be integrated with numerical modelling programs. There is very little data on the subject of integration and so the review has been broadened to evaluate techniques and methods that may be used to accomplish the integration. Examples where some seismic parameters have been extracted from numerical models are presented. The focus has been to consider the reproduction of the power law statistics encapsulated within the Gutenberg-Richter law. The different types of numerical techniques that are able to represent seismicity in some way are discussed.

If the modelling techniques are able to represent seismicity, they may not be readily accessible, and model output parameters may have to be processed in order that they can be related to observed seismic parameters and patterns. Methods for deriving seismic patterns from numerical modelling outputs are described for different modelling techniques. The processing techniques are broadly grouped into methods for obtaining size, space and time distributions even though the methods and the outputs are generally interlinked.

Finally, methods and issues relating to the comparison and integration of modelled and observed seismicity are discussed. Initially the concepts of validation and calibration of models are explored to determine how to decide on a successful implementation of the integration. The common features of a number of techniques from the simplest visualisation tools to more complex back analyses and recalibrations to models that can explicitly include seismicity as input are considered in the context of integration.

#### 2.1.1. Discrete Models

This class of model would incorporate so-called "lattice" or "cellular" representations such as Cundall's distinct element code 3DEC or the particle assembly code PFC3D. Again, the large-scale nature of the problem and issues of scaling and the choice of the basic particle or block size have to be assessed. A copy of the PFC3D program was purchased to assist in this study.

Lattice or discontinuum models rely on simple Newtonian mechanics to update interacting particle or block positions in an evolutionary manner. In full dynamic mode, the critical time step that is necessary for the stable integration of the equations of motion of all interacting particles is determined by the smallest mass of particle and by the stiffest contact between particle pairs. This generally makes a fully dynamic simulation prohibitively time consuming for large assemblies of particles. However, in dynamic mode the PFC does, in principle, allow seismic events to be simulated. The building blocks of these events are individual particle bond breakage events which may cause subsequent neighbouring breakage as the inter-particle forces are redistributed. Attempts to use this facility to develop synthetic moment-magnitude statistics in laboratory scale samples have been successfully initiated at Keele University, UK (*Hazzard, 1998*).

The large scale application of codes such as PFC3D to problems comprising as many as one million particles are probably impractical at present. This then poses the question as to whether the PFC approach can be applied in some hierarchical or embedded form to sub-regions of interest. This should be one of the topics of investigation in trials with PFC3D together with the problem of accumulating moment-magnitude statistics. A second area of investigation should centre on the feasibility of including observed seismic activity in the model and the implications of this on subsequent mining activity. This, in turn, implies that the suitability of PFC for

performing a series of mining step analyses together with the representation of known seismic deformations has to be assessed.

The most common discrete model in seismic modelling is the block-spring or Burridge-Knopoff model. These can be one-dimensional (*Shaw, 1995, Rundle and Klein, 1993, Jordan, 1999*) or two - dimensional (*Ito and Matsuzaki, 1990*). The fault is represented by a series of blocks connected by springs to a rigid plate (see e.g. Figure 2.3.1). The plate is moved along at a displacement rate related to the tectonic field. Seismicity is represented by considering the repeated slip response of each of the sliding blocks. *Cochard and Madariago (1996)* note that discrete models of the Burridge-Knopoff type exhibit moments that are proportional to the slip length for the large events. This is due to the flat springs linking the fault elements to the driving block leading to the fault slip becoming independent of fault length for large events. Thus complexity is limited, as is the case for models of fault slip with rate independent friction laws.

*Shaw (1995)* considers the effect of different friction laws on the block - slider model, shown in Figure 2.1.1. In these models, the frictional resistance is provided by either velocity or slip weakening friction laws. The model is able to demonstrate complexity on a number of scales. The frequency – magnitude response depends on the size of the slip zones and thus does not scale over the entire range of fault slips. The smallest events are limited by the size of a single block and the moment is proportional to the product of the stress drop and the cube of the slip zone length. The largest events activate the entire fault and are independent of the stress drop so that their equivalent seismic moment scales in proportion to the length of the largest event. Velocity weakening models show similar response to slip weakening models and both models exhibit power law response with  $b = 1$  for small fault slips. Both models show a “bump” of large events that extend above the rate extrapolated from the small events (Figure 2.1.2). The differences at larger scales occur due to the selection of the slip weakening or viscosity parameters that alter the size distribution over different size ranges. *Shaw (1995)* also emphasises that the model considers a single fault only, whereas natural systems consist of fault sets. The two dimensional model of *Ito and Matsuzaki (1990)* exhibited clustering of the slip zones and a  $b$ - value close to 1 for certain choices of parameters (Figure 2.1.3)

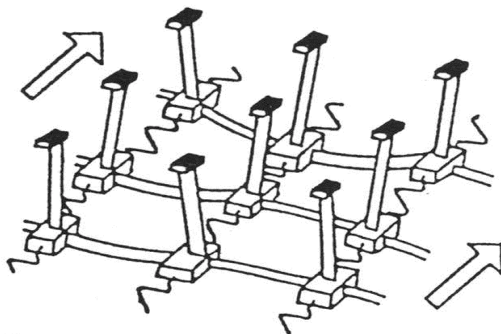
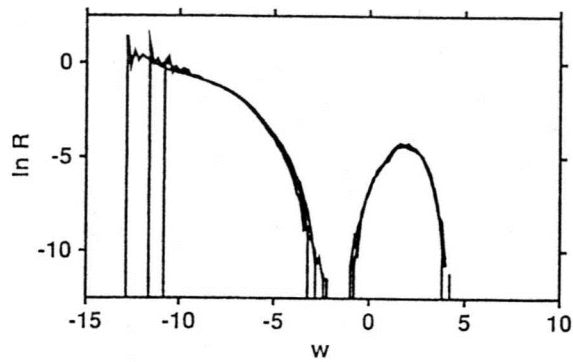
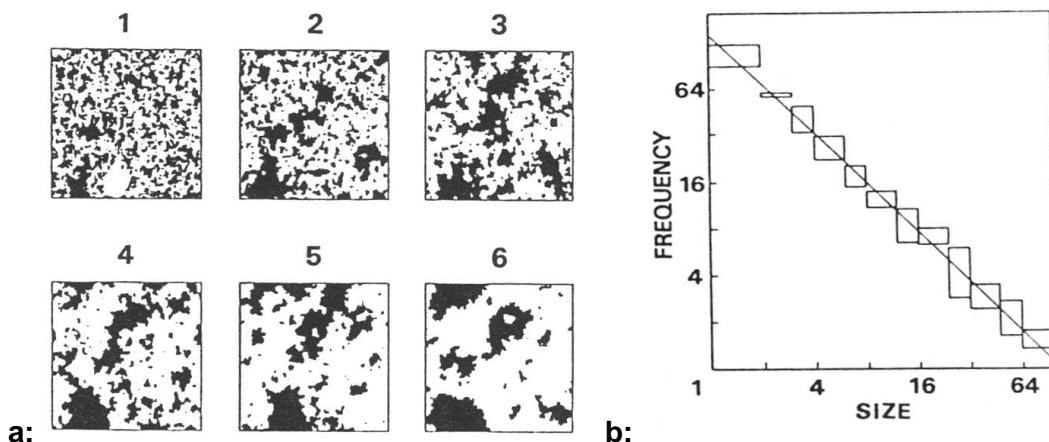


Fig. 1. Schematic representation of a portion of the two-dimensional mechanical model of earthquakes [after *Otsuka, 1971*].

**Figure 2.1.1 Two dimensional block-slider model (*Ito and Matsuzaki, 1990*).**



**Figure 2.1.2** Frequency ( $R$ ) - size ( $w$ ) distribution plots of block slider models (Shaw 1995).



**Figure 2.1.3 a: Clustering and b: size distribution of events for a 2-D slider block model (Ito and Matsuzaki, 1990).**

Similar block slider models, but with a friction law that only permits a transition between discrete static and dynamic friction values, have been applied to model seismicity by *Rundle and Klein (1993)*. With a constant failure threshold, the model exhibited power law response with an exponent that was independent of the driving velocity and can be considered to result in a state of self organised criticality. Randomisation of the failure threshold caused the power law response to alter with increasing velocity (Figure 2.1.4). For slow plate velocities there were relatively more small events and the model evolved to produce power law scaling as the velocity was increased.

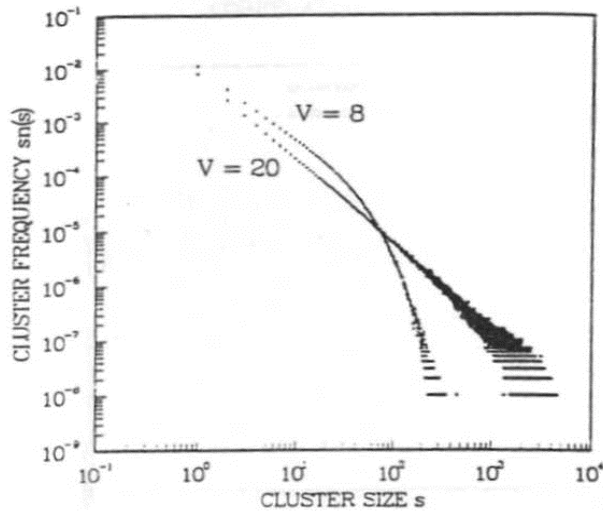


**Figure 2.1.4 Change in power law statistics due to change in velocity boundary conditions (Rundle and Klein, 1993).**

Wilson *et al.* (1996) used a lattice model consisting of a lattice pattern of bonds that could be broken if sufficient tension was applied. The entire model was given an initial distribution of tensile strengths and loaded in tension. Frequency magnitude plots were obtained (Figure 2.1.5), but were stepped due to the discrete nature of the fractures and the finite sized grid. The initial distribution of strengths affected the fracture pattern and the shape of the frequency magnitude plots. When the initial strength distribution was uncorrelated, the frequency - magnitude data did not show power law scaling. Input of a fractal representation of the strength resulted in power law scaling.

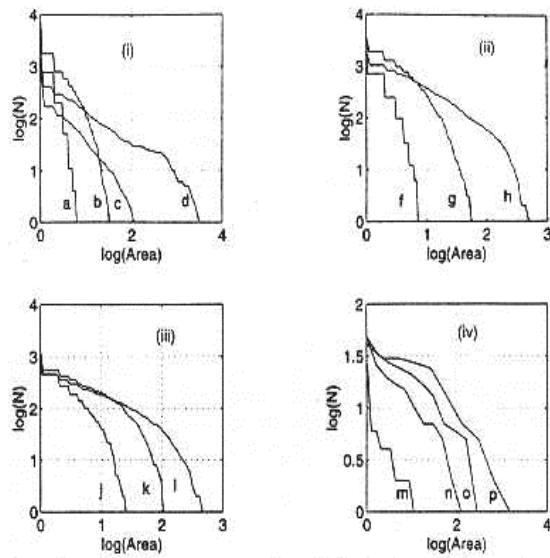


Fig. 4. Size distribution analyses of the fracture patterns shown in Fig. 3, where  $N$  is the number of fractures greater than area, and area is measured in the number of lattice elements.

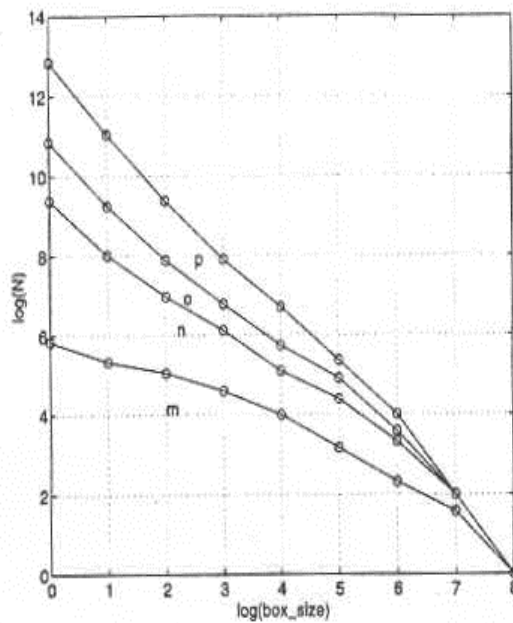


Fig. 5. Box counting analysis of the fracture patterns shown in Figs. 3(m-p), where  $N$  is the number of filled boxes and box size is measured in lattice elements.

**Figure 2.1.5 Two methods for obtaining power law statistics from a lattice type model (Wilson et al., 1996). top: Counts of lattice breaks; bottom: box counting method**

The block - slider models have a number of advantages for modelling of earthquake statistics, including the reproduction of Gutenberg- Richter statistics, characteristic size events that



dominate the cumulative slip, complex space-time patterns of seismicity, and the propagation of pulse type events. The models have disadvantages in that they are unable to model large scale dynamic effects, the loading using tectonic velocities may be unphysical, the friction laws are often ad hoc and the output complexity may be altered by the choice of the grid size (Jordan, 1999).

Morrison *et al.* (1993) considered the problem of mining towards a fault using the UDEC discrete element code. The continuously yielding joint model was applied on the fault to permit stress locking and stick slip response. The fault exhibited a range of slip event sizes, but the number of events was too low to permit the use of a frequency magnitude plot or to attempt to fit a power law.

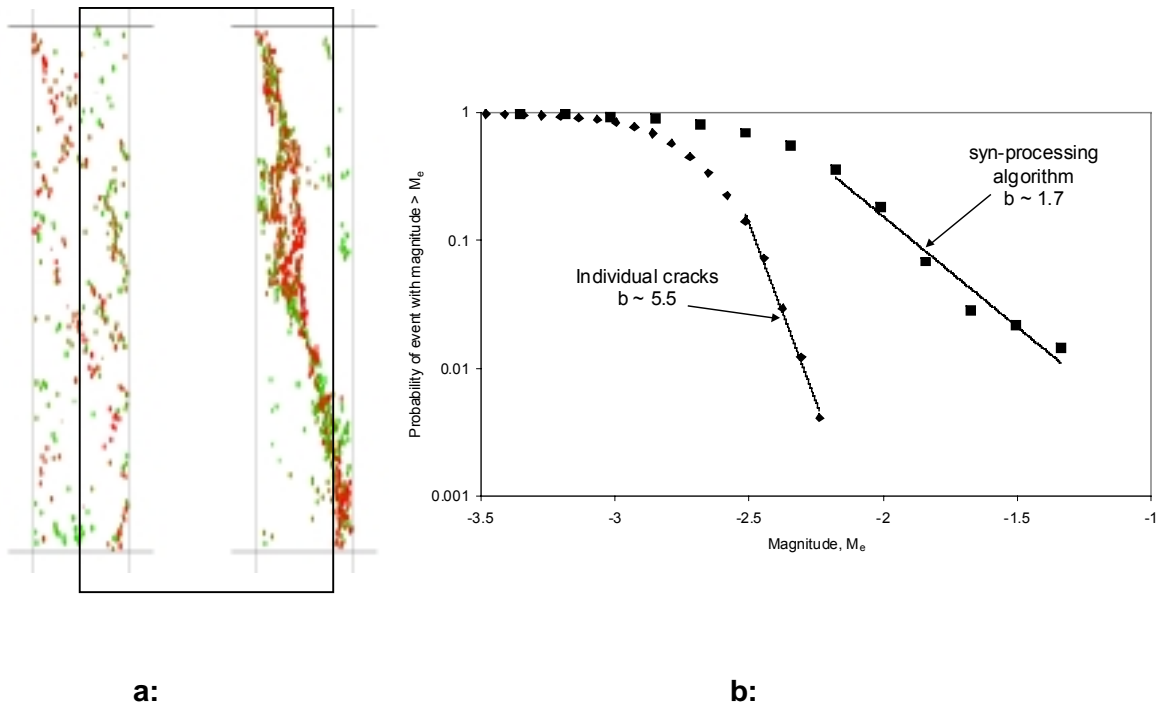


**Figure 2.1.6 a: PFC model of a triaxial test with dots representing fractures (light dots indicate early initiation times and dark dots occurred later) and b: frequency magnitude statistics showing the dependence of the b-value on the processing procedure (Hazard, 1998).**

Discrete models can be used to model dynamic slip on fault planes. When the analysis is dynamic, the seismic parameters must be calculated from the energy released (Cundall and Lemos, 1990). This can be done in two ways. Firstly as the incremental work done by far field loads less the work done by joint friction and less the elastic strain energy. The second method considered the energy released to be the sum of the kinetic energy, the work done by damping and the work done by absorbing boundaries. Both methods produced similar results in studies of the slip on a fault (Cundall and Lemos, 1990).

Lattice models of solids consisting of bonded particles have been applied to the modelling of faults containing gouge by Mora *et al.* (1997) The two-dimensional model consists of two blocks with a rough interface being driven past one another. Grains within the blocks are modelled as groupings of 3-10 bonded round particles. The model consists of 128 x 128 particles. The model exhibits multi-linear power law distributions of event magnitudes. The presence of gouge is found to enrich the distribution of event sizes. Without gouge, only events of a characteristic size are observed.

A discrete element method, in which the rock material is represented by a set of circular particles, was applied to the modelling of acoustic emissions arising from tunnel breakout by *Potyondy and Cundall (1998)*. The acoustic emissions were defined to occur once the stress on an inter-particle bond had exceeded the specified strength level. The method was extended by *Hazzard (1998)* who modelled the acoustic emission processes observed in a variety of laboratory tests (Figure 2.1.6).

## 2.1.2. Continuum models

This class of model is exemplified by finite element or finite difference programs such as ABAQUS, ELFEN or FLAC3D. It must be accepted that compromises are required at the present time to represent regional deformations covering volumes of the order of one cubic kilometre. A rough calculation shows that if the area of interest is a cube with a side length of one kilometre, then one million zones are required to achieve a nominal resolution of 10m. The biggest problem is the manner in which seismic activity would be simulated. Continuum representations require the specification of some form of strain softening to reflect stress drop effects. If this occurs in the solid rockmass then the resulting shear band is usually defined with a thickness of at least three grid zones. This implies a thickness of at least 30m using the assumed grid size of 10m. An alternative scheme is to postulate the existence of ubiquitous joint sets with given orientations. Ideally the joint set orientation would have to be introduced adaptively as seismic information is incorporated progressively into the model. Some numerical experiments will need to be performed to determine whether such behaviour can be incorporated “on the fly” in codes such as FLAC. It is not clear whether meaningful seismic event statistics could be generated in this manner. It should be noted that in many cases, material damping is incorporated in the model as an expedient device to reduce spurious instabilities that may accompany material failure. The effect of this damping on the true “physics” of the problem is unclear.

A simulation of seismicity in a tectonic plate was performed by (*Lyakhovsky et al., 1997a, b*) using a finite difference solution technique. The rock was modelled using a continuum damage model (*Lyakhovsky et al., 1997a, b*). The damage is related to a scalar parameter based on the deviatoric strain invariant. The damage accumulates due to an increase in the deviatoric strain and the rate of accumulation decreases as the mean strain increases. A logarithmic decrease in damage with time is introduced to model the healing observed in experiments of the rate and state dependent nature of friction. The extension of a tectonic plate is modelled. The assumption of a random initial damage state is necessary for localisation of the damage into large-scale shear zones. Modelling of a strike slip zone with an initial, localised, damage zone generates a series of earthquake cycles with distinct inter, pre, co and post seismic periods (*Lyakhovsky et al., 1997a, b*). The seismic features resulting in the strike slip zone with an initially random damage zone depend on the rate of healing. High values of the healing parameter leads to regular fault geometries and a characteristic earthquake size. Low healing results in a disordered fault network that exhibits Gutenberg -Richter statistics. Certain parameter choices lead to switching between the two types of response.

The finite difference method has also been applied for modelling seismic wave propagation and interaction with existing fault zones (*Coates and Schoenberg, 1995*). Solution of 3-D dynamic wave propagation problems in elastic media requires efficient solution techniques such as the staggered grid finite difference method (*Graves, 1996*). Seismicity can be explicitly included in continuum models using the staggered grid approach by using the moment tensor solution of a known event and applying the relevant point forces and the event source position (*Graves, 1996*). Only waveforms were considered to be important and no events were triggered by the induced waves and so no frequency magnitude statistics were presented.

Acoustic emissions associated with bond failure in laboratory tests and seismicity on a mine scale can be simulated with the finite element method (*Tang, 1997*). The method uses a linear elastic finite element code where each element is assigned a random strength and stiffness (Figure 2.1.7). After failure the strength is reduced and the stiffness is set to a negligible value.

An event is defined to occur when an element fails. The method is applied to an uniaxial compression test and the failure of the pillar between two underground excavations. The model exhibits power law response for small events, but the number of large events is limited.

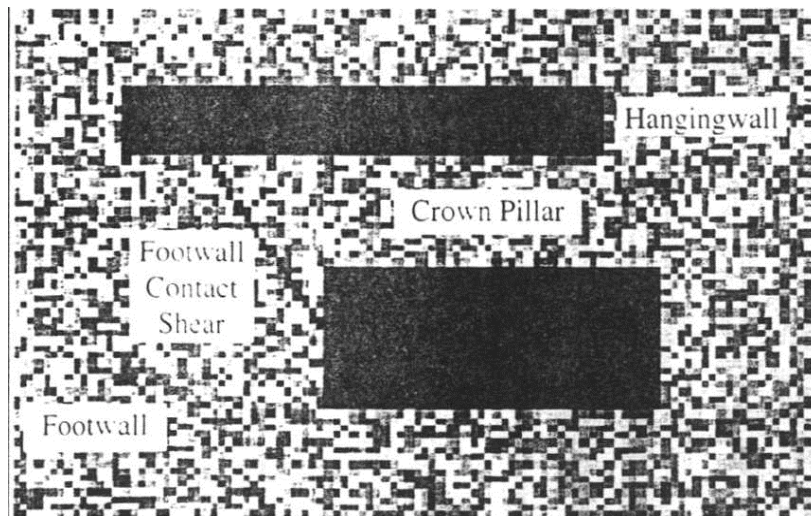


**Figure 2.1.7 A statistical finite element model with random element properties (Tang, 1997)**

Other means of applying the finite element method to multiscale problems may lie in the hierarchical methods that have been developed recently (e.g. *Oden et al, 1999*). These methods are based on the hybrid element formulation and can represent different material behaviour on a number of scales.

A method for introducing seismicity into a model of the lithosphere was presented by *Sornette et al. (1990)*. The rock is assumed to yield at some failure criterion dependent on the stress and the strain. The average stress is assumed to be constant within the tectonic plate under consideration. The deformation of the plate is related to the time dependent applied stress by means of a global balance equation that assumes that the average stress in a volume is constant. This leads to a diffusion equation relating the rate of change of stress to the gradient of the strain. Earthquakes are introduced as nonlinear corrections to the strain gradient i.e. they are considered to be noise that is superimposed onto the overall level of strain. The strain gradient depends on the strain, the average stress and the gradient of the average stress and thus introduces nonlinearity into the model. The noise includes inhomogeneities and anisotropy of the geometry and composition. The noise is assumed to be uncorrelated and non-conservative i.e. it is not governed by any global law, other than the assumption that the average noise is zero. This approach, with a global conservation law on average, and non conservative noise terms are the minimum requirements for a system to exhibit self organisation.

An alternative approach was taken by *Sornette et al. (1990)* in which the faults were explicitly introduced as internal boundary conditions. The organisation that results from each approach is different. In the approach with superimposed noise, the changes to the strain and time fields introduced that are characterised by a power law distribution that features long range correlations in time and space. In the internal boundary condition approach, a fractal structure of faulting develops that is controlled by a power law that is different to the input law. The underlying conservation law is seen as the crucial component in causing the power law (self similar) fluctuation of the strain field. The nonlinear feedback in the strain field forces the effects of a local change to be distributed through space and time, and not to die off locally. Thus an initial disturbance (an earthquake) spreads out through time and space. The introduction of dissipation would lead to a limit to the distance and time that are affected by the disturbance.

The presence of self organised criticality in the model leads to the power law distribution of the frequency of the average energy of earthquakes. The way in which the average energy is determined by *Sornette et al. (1990)* is not clearly defined. An equivalent value of  $b = 1$  for the  $b$  parameter in the Gutenberg Richer frequency magnitude relation is obtained.

Another method for producing a numerical simulation of seismicity was presented by *Salamon (1993)*. A rectangular region of the rock mass is assumed to contain a set of random flaws. The locations, orientations, and sizes of each of the flaws are specified using a Monte-Carlo technique. Mining progresses within the block of potential events, with each flaw visited after each mining increment. The stresses in the rock mass are calculated from the analytical solution for mining of a single panel. When the driving shear stress exceeds the frictional and cohesive resistance, the flaw is considered to have produced a seismic event. Equivalent seismic parameters, such as moment, kinetic energy, seismic efficiency, can then be calculated. Four assumptions were made regarding the flaw activations and interactions. There is no interaction between flaws, flaws that experience tensile stresses are ignored, flaws that have been triggered may not be re-activated, and flaws that are mined out are not triggered. The major assumption, that is not listed, is that the slips do not alter the stress state within the elastic continuum. The model therefore produces a catalogue of events, but there is not cumulative inelastic response generated by the events.

The model was applied to the problem of mining a single panel dipping at 20 degrees, and having a dip length of 100m. The panel was mined for a span of 2500m at 2.5m increments. Correlations with observed mining seismicity were obtained by altering the flaw density, the random distribution and the friction coefficients. The events are found to cluster around the mining face. A correct choice of the input parameters, based on a flaw density of 16 000 flaws/km leads to correspondence of the simulated slip distances, and stress drops with data from the ERPM mine.

### **2.1.3. Boundary Element Models and discrete fault planes**

This generic category of model exploits the proposition that off-reef deformations can be considered to be concentrated on distinct discontinuity surfaces (faults, joints, burst fractures). This is compatible with general seismological methodology. In this case, it is natural to assume that some form of boundary element code (MAP3D, FRANC3D, FRACMAN, 3DIGS) could be adapted to represent the off-reef seismic behaviour. Questions that are unresolved though are whether elastodynamic effects should be explicitly treated and the extent to which discontinuities on multiple (fractal) length scales can be represented by these models.

The discontinuities can be pre-specified as random flaws, joint sets, faults or inter-connected random meshes as might arise in describing a bonded granular material. The interaction between discontinuities can be resolved by explicit joint constructs in Finite Element or Finite Difference codes (e.g. ELFEN, WAVE/ NUWAVE) or by treating the discontinuities as small strain dislocations as in boundary element programs (MAP3D, MINSIM, 3DIGS, FRANC3D, FRACMAN, POLY3D). When using a finite element or finite difference formulation, it is necessary to represent the whole space or to erect suitable bounding surfaces or to use special mapping functions for infinite element shape variation. The formulation is inherently inertia sensitive and is able therefore to simulate dynamic effects directly with the usual proviso on the choice of time step size to ensure numerical stability. An important limitation of this approach, in the context of the integration of seismic activity, is the difficulty of including adaptively the observed seismic strain information. This will require some form of re-meshing the model to include explicit discontinuities. Alternatively some form of damage tensor is required to allow a continuum inelastic strain tensor to be included in the model. This is a challenging requirement in three dimensions.

The boundary element codes must be carefully distinguished as being either static or dynamic. Most of the readily available codes (as listed previously) are static and, consequently, the rock mass is implicitly assumed to have no inertia (zero density/ infinite wave speed). This apparently

gross assumption is of little consequence in the analysis of stress redistribution caused by mining or due to specified joint or fault slip increments. In certain cases, it may even be legitimate to represent the rheological behaviour of the rock mass by postulating that the slip rate of a discontinuity is related to the driving shear stress by a fluidity parameter. This allows the simulation of pseudo-seismic event sequences. This viscous behaviour is included in the computer codes MAP3D and DIGS. It has not yet been demonstrated whether realistic moment-magnitude statistics can be generated by the surface fluidity formulation. The boundary element formulation does offer some advantages in only requiring the active discontinuity surfaces to be represented and can readily accommodate the subsequent addition of extra surfaces which might represent observed seismic activity.

A second variety of boundary element formulation does allow elastodynamic movements to be analysed. This can be readily derived from the Stokes solution for a time-dependent point force in an infinite elastic medium but the method is difficult to implement numerically. Extreme care is required in the selection of time step and shape function representations. An initial feasibility of implementing some form of dynamic boundary element code that is periodically invoked in conjunction with a static code (continuum, lattice or boundary element) should be investigated to address the issue of multiple time scales (e.g. *Ben-Zion and Rice, 1993*).

A considerable amount of research has been focussed on modelling of the behaviour of single fault planes. For example, the time and space distributions of slip on a single fault have been studied using an elastodynamic formulation of the boundary integral method in two (*Cochard and Madariaga, 1996*) and three dimensions (*Fukuyama and Madariaga, 1998, Madariaga et al., 1998*). The fault surface is assigned rate and state variable friction laws in which the friction depends on the amount of slip, and the velocity of the slip. In these implementations, the friction decreases linearly with distance and with the inverse of the slip velocity.

In the two-dimensional model of *Cochard and Madariaga (1996)* a random stress state that increased slowly with time was applied. They observed “seismic” slips if the fault slipped more than the characteristic minimum length chosen for the friction laws. Two time scales were observed, one related to the selected rate of increase in the tectonic stress and the second is determined by the ratio  $\Delta x / \beta$  where  $\Delta x$  is the element length and  $\beta$  is the shear wave velocity. The rate dependent friction laws cause complexity in the response of the fault set within a homogeneous medium. The complexity introduces events that are smaller than the entire fault length due to premature locking and healing of the slip. The partial stress drops are associated with the rate dependent friction and cause disorganisation of the fault behaviour. If rate independent friction laws were used, full stress drops would occur across the fault, unless some heterogeneity of the frictional properties was specified. Seismic events are defined as regions of slip, and followed an L2 scaling law in which seismic moment scaled as the product of the partial stress drop and the square of the length  $L$  of the zone that slipped. The frequency magnitude data does not show Gutenberg-Richter behaviour. The frequency magnitude distribution can also be obtained directly from the numerical results and is shown for two different element sizes in Figure 2.1.8. Each analysis shows that there is a different distribution for small and large events. The distribution for larger sizes reflects the events in which the influence of the boundaries dominates the response of the fault.

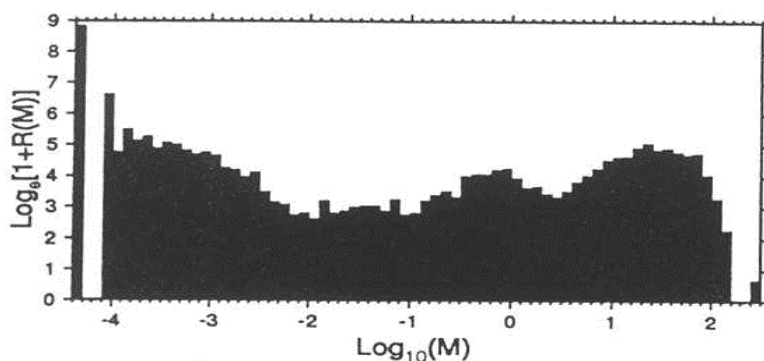


**Figure 2.1.8 Frequency magnitude statistics for a 2-D strike slip fault (Cochard and Madariaga, 1996).**

The distribution of fault slip in time and space on a two-dimensional strike slip fault was studied by *Tse and Rice (1986)* using a series of line-screw (Mode III) dislocations. The fault exhibited periodic earthquake formation that was attributed to the quasi-static assumption and the simple rate dependent slip law.

*Rice (1993)* applied a boundary element formulation to model a single fault plane. A quasi-static approach was used, with a viscous damping term to approximate the dynamic effects. The response was found to be related to the size of the elements. Larger elements failed independently, whereas smaller elements had to co-operate and fail in clusters. The critical element size depends on the parameters of the rate dependent friction law. The correct solution of the stresses at the edges of a spreading fault source requires very small elements and the space-time distribution was found to be periodic, not complex. Oversized elements were able to act independently. A conflict arises between the requirement for smaller element size to ensure numerical accuracy and ability of the oversized elements to represent the complexity that is observed in real seismic data, even though the stress distribution was not modelled properly.

*Ben-Zion and Rice (1993)* and *Rice (1993)* indicated that random element strengths are required to produce self organised criticality, or scaling behaviour. Variations in strength of more than 10% of the average strength were required in order to activate self-ordered clusters. The size distribution found by *Ben-Zion and Rice (1993)* showed a linear log Frequency - log Moment response for small and intermediate events and constant size, or characteristic, earthquakes at large magnitudes. This is because the larger events are unstoppable and the maximum earthquake size is only limited by the size of the model. They found that the numerical frequency-magnitude distribution depended on the parameters that were selected for the rate and state dependent friction laws.

A distribution of asperity strengths was required by *Lachenicht and van Aswegen (1999)* in order to compare the results of a boundary element model with the distribution of seismicity resulting from mining towards a fault. The strength distribution of asperities was specified to be a power law determined from the observed power law of seismicity. The regions of the fault surrounding the asperities were modelled with a viscoplastic friction model. The modelled seismicity exhibited similar b-values and energy - moment relationships to the observed data.

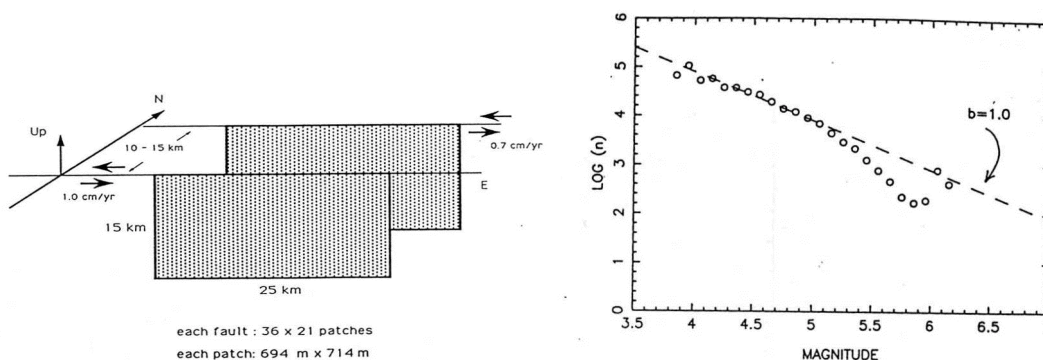
Models consisting a number of interacting slip planes have been developed by *Robinson and Benites (1995)* and *Spottiswoode (1999)*. The model of Robinson and Benites consists of a three-dimensional boundary element formulation with elements that are allowed to slip whenever the pre-existing strength is exceeded. The friction parameters vary from 0.1 to 0.2 resulting in a stress drop of 10% of the static stress. A model of two parallel strike slip faults generated 500 000 events over a simulated time period of 28 900 years (Figure 2.1.9a). The b-value depended on the fault parameters, but is close to 1 for the selected values (Figure 2.1.9b).

In Extended MINSIM models, off-reef seismic activity is "condensed" onto the reef plane using special constitutive constructs. An initial example is Spottiswoode's MINF routine with "capped" stress levels ahead of the stope face. A somewhat different approach is to follow the proposal by Salamon to represent off-reef features as "virtual" random flaws that are assigned according to postulated orientations and density. These "flaws" are triggered by the mining induced stresses sweeping past them as on-reef mining increments are simulated. This approach needs to be calibrated using local gold mine seismic data.

It may be possible to extend the capped stress model of Spottiswoode to allow for the representation of off reef deformations as equivalent "plastic" strains in a boundary element formulation. In this case it would be possible to analyse near-field discontinuity interactions directly using the actual discontinuity surfaces (without any loss of accuracy) and to determine

far-field influences by the use of plastic volumetric strains. A hybrid model of this type is similar in spirit but different in implementation to the multipole method introduced by Peirce and Napier. The multipole method, however, seems to be limited to 2D applications because of the proliferation of influence kernel functions required in 3D. It would appear that a more effective strategy in 3D would be to represent the off-reef strain as a high order variation field whose influence can be evaluated by numerical means. The strain field could be constructed by the multipole strain moment expansion technique. This strategy could be more effective than the “equivalent crack” approach proposed by Napier and could be readily tested initially in two dimensions. This approach would also allow a very flexible means of including seismic information adaptively either as explicit discontinuities or directly in moment tensor form. The extension to elastodynamics is not yet formulated.

Spottiswoode (1999) considered a number of planes parallel to a tabular stope excavation. A spectral boundary element approach was used to facilitate the solution of a large number of elements. In this approach, fast Fourier transforms methods are used to compute the inter-element influences very efficiently. Each plane can fail when the Mohr Coulomb failure threshold is exceeded. A growth rule is applied that only permits slip at the element with the highest excess shear stress and any subsequent slips must be associated with elements on the boundary of the current slip. The elements experience viscoplastic slip (creep) once the element has failed and the stress state has dropped to a seismic residual value. The model indicates power law response over certain size ranges, with a b-value of 1 at intermediate sizes (Figure 2.1.10).



a: **Figure 2.1.9 a: model of two parallel faults. b: Frequency magnitude statistics (Robinson and Benites 1995).**

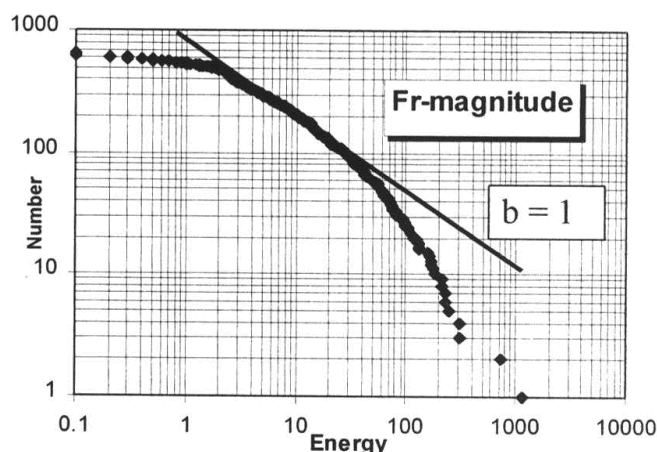


**Figure 2.1.10 Frequency magnitude statistics for model of multiple layers parallel to a tabular stope (Spottiswoode, 1999).**

## 2.1.4. Static vs. dynamic modelling

In the context of integrating seismic activity with numerical modelling, it is necessary to consider when inertial effects, controlling wave propagation through the rock mass are important, 2. computer memory capabilities but are extremely flexible in allowing variable material properties to be accommodated. It is possible that future developments in computer parallel processing technology may relieve the memory constraints associated with these methods.

### **2.1.5. Stochastic vs. deterministic models**

An essential feature of the integration of numerical modelling with seismic monitoring is the ability to be able to simulate the statistical patterns of seismic activity. This will generally require that the numerical model has some form of “cellular” structure in which individual elements interact with one another and coalesce to form damage regions covering many size scales. This can only be achieved to a limited extent by current computer tools. One future aspect of studies of integration of seismic activity with numerical modelling will be the formulation of computational methods that can accommodate the representation of damage on many length scales. In this respect, the “renormalisation group” methods of statistical physics can be expected to provide useful guidance in the formulation of these models.

## **2.2. Numerical models currently being developed for use in SA mining Industry**

### **2.2.1. MINSIM/MAP3D**

The computer programs MINSIM and MAP3D are widely used in South Africa for the analysis of stress distributions in the vicinity of tabular mine openings. MINSIM is a boundary element code, based originally on Salamon’s “Face Element Principle” (*Salamon, 1964*) which uses the displacement discontinuity method to solve tabular excavation and fault slip interaction problems. MAP3D (*Wiles, 2000*) has a number of more general features than are catered for in the MINSIM code, including the ability to model cavities, multiple material zones, and limited volumetric plasticity. In addition to MINSIM and MAP3D, a number of generically similar computer tools have been employed for the analysis of stress patterns near deep level openings. These include, specifically, the programs MINAP and MSCALC developed by Crouch; the basic principles are described in detail by *Crouch and Starfield (1983)*. In the context of exploring the integration of seismic monitoring with numerical modelling, it is important to highlight certain broad attributes of these computer programs rather than attempting a detailed comparison between each particular code.

#### **2.2.1.1. Boundary element basics**

All boundary element methods rest on the assumption that any solution can be expressed as a linear superposition of fundamental solutions. The fundamental solution provides the response to a local excitation, at a given time and position in space, at all other points in space and at all succeeding times. By using such a fundamental solution and classic results from vector analysis, a boundary integral representation can be established in terms of the values of key variables defined on the surfaces surrounding the medium and on any special surfaces (such as fractures) within the problem region. The computational advantages of such a surface representation are clearly manifest in the analysis of steady state, three-dimensional problems. These advantages are reduced as the controlling surface area is increased relative to the volume and if transient problems are to be solved. In addition, the fundamental solutions may only be known for simplified approximations to the actual medium behaviour (such as linear isotropic elasticity). Despite these shortcomings, the boundary integral method provides a very useful tool in the analysis of stress distribution problems in solid mechanics. The particular approach, referred to as the displacement discontinuity method (DDM), is ideally suited to the analysis of tabular excavation and fault interaction problems although detailed numerical



difficulties may arise in its implementation and efficient solution, particularly with regard to intersecting or acutely angled discontinuities.

The implementation of the DDM for the solution of tabular excavation or fault sliding problems requires that the excavation or fault surface be divided into discrete areas termed “elements”. Each element is assigned a “shape function” which controls the variation of the displacement discontinuity density within the element. Boundary conditions must be matched at one or more “collocation” points within each element or must be satisfied in some average sense over the element area. In the simplest approximation, the discontinuity vector is assumed to be constant over a flat polygonal element and the boundary condition is enforced at a single representative point within the element. In the solution of tabular mine problems, it is often assumed that each element has a square shape and that the boundary condition is matched at the center of the element. This scheme is used by the current versions of the MAP3D, MINSIM and MSCALC codes in the solution of discontinuity problems.

In order to highlight some of the properties of the constant element assumption, consider the expression for the normal stress,  $\tau_{zz}$ , induced by a single square element of side  $2a$ , centred at the origin of the  $x$ - $y$  plane. This is given by the formula

$$\tau_{zz}(x, y) = \frac{G}{4\pi(1-\nu)} I_{,zz} D_z^0 \quad (2.2.1)$$

where  $G$  is the shear modulus and  $\nu$  is the Poisson’s ratio of the assumed isotropic rockmass.  $D_z^0$  is the value of the normal ( $z$  direction) displacement discontinuity component across the element. (This is interpreted as the stope closure in tabular mining problems). The quantity  $I$  is the Newtonian potential, integrated over the surface area of the element:

$$I = \int_{-a}^a \int_{-a}^a \frac{d\xi d\eta}{r} \quad (2.2.2)$$

where  $r^2 = (x - \xi)^2 + (y - \eta)^2 + z^2$ .  $I_{,zz} = \partial^2 I / \partial z^2$  represents the second derivative of this function, evaluated in the limit  $z \rightarrow 0$ , and is given by:

$$I_{,zz} = \frac{\sqrt{(x+a)^2 + (y+a)^2}}{(x+a)(y+a)} - \frac{\sqrt{(x+a)^2 + (y-a)^2}}{(x+a)(y-a)} - \frac{\sqrt{(x-a)^2 + (y+a)^2}}{(x-a)(y+a)} - \frac{\sqrt{(x-a)^2 + (y-a)^2}}{(x-a)(y-a)} \quad (2.2.3)$$

Equation (2.2.3) determines the normal stress component induced by the element with a normal DD component  $D_z^0$ . General relationships for the full stress tensor, induced by the DD vector  $(D_x^0, D_y^0, D_z^0)$ , are documented by *Crouch and Starfield (1983)*. Equation (2.2.3) reveals a number of interesting properties relating to the DD method that are not always appreciated. Specifically, it can be observed that if  $x = \pm a$  or  $y = \pm a$ , the expression contains apparently singular terms. However, on closer inspection it can be seen that these terms cancel in pairs. This in turn implies that some care must be taken in implementing the influence computation procedures in any computer code. Setting  $y = 0$  in equation (2.2.3) gives the expression for the stress induced by the element along the  $x$ -axis:

$$I_{,zz} \Big|_{y=0} = \frac{2\sqrt{(x+a)^2 + a^2}}{a(x+a)} - \frac{2\sqrt{(x-a)^2 + a^2}}{a(x-a)} \quad (2.2.4)$$

Consider a position  $x = a + \varepsilon$  close to the edge of the element. For  $|\varepsilon| \ll a$ , equation (2.2.4) tends to

$$I_{,zz}|_{y=0} \rightarrow -2/\varepsilon \quad (2.2.5)$$

Equation (2.2.5) demonstrates that the stress becomes infinite adjacent to the edge of the element and changes sign on each side of the edge. (In the present case a positive value of  $D_z^0$  represents stope closure). The induced stress component  $\tau_{zz}$  changes from infinitely positive (tension) to infinitely negative (compression) as  $x$  changes from a position just inside the element ( $\varepsilon < 0$ ) to a position just outside the element ( $\varepsilon > 0$ ). It is important to note that this singularity is much stronger than the  $\sqrt{\varepsilon}$  crack tip singularity encountered in fracture mechanics analysis (*Lawn and Wilshaw, 1975*). Furthermore, it is not possible to integrate the expression (2.2.1) for  $\tau_{zz}$  over the area of the element. In fact, the point value  $\tau_{zz}(0,0)$  should be interpreted as the *average* stress induced over the element. The presence of the strong singularity represented by equation (2.2.5) also means that considerable care must be taken in interpreting stress values at points near element edges and displaced normal to the plane of the element. This has particular importance in attempting to perform seismic modelling integration by inserting near-reef strain influences to represent observed seismic activity.

The integration of seismic activity and numerical modelling can be simplified enormously if the seismic behaviour is associated with discrete, non-intersecting fault planes. In these cases it is possible to adapt most of the displacement discontinuity boundary element codes currently in use to perform basic integration studies and to attempt to predict future seismic activity. Specifically, the following steps can be followed if seismic information in a given mining area is reviewed at regular time intervals.

1. Translate the observed seismic activity over the review period into the required slip vectors acting over one or more fault plane areas.
2. Assign the slip to an already identified fault plane area or create a new fault plane. Re-compute induced stress values in the areas of interest.
3. The slip assignment can be carried out easily if the existing planes are pre-gridded into square elements. This ensures that no element overlap or intersection occurs.
4. To predict future activity, it is necessary to determine the slip propensity (measured, for example, by the excess shear stress level) on the currently unslipped portions of each fault plane. The actual slip can be computed and used to estimate potential event magnitudes.
5. Return to step (a) for the next review period.

The simple procedure outlined in steps (a) to (e), allows observed fault related seismic activity to be incorporated adaptively into the modelling framework. This scheme will, however, need to be extended if, at any stage, the inserted slip values are incompatible with the pre-existing stress states at the identified event positions. This will arise if incorrect assumptions have been made about the field stress orientation or if additional deformation has occurred that is not reflected in the modelled configuration. In general, it may be found that it is also necessary to cater for intersecting fault planes, occasional fault-reef intersections and the effect of structures such as dykes. It should be noted as well that the integration process in steps (a) to (e) relates mainly to large event activity. Detailed procedures for the integration of local stope face damage will probably require more complex numerical approaches such as that used in special purpose boundary element programs or nonlinear continuum codes.

### **2.2.1.2. Simulation of seismic activity using the displacement discontinuity boundary element method**

One advantage of the displacement discontinuity method is that nonlinear behaviour at slip interfaces (friction sliding or cohesion breaking) can be incorporated readily into the solution procedure (*Ryder and Napier, 1985*). In particular, it is straightforward to introduce simple "creep" relaxation laws into the solution procedure. For example, the shear slip rate on mobilised fault elements can be assumed to be proportional to the difference between the local

driving shear stress and shear resistance acting on the element, provided the shear stress exceeds a defined strength “barrier”. This, in turn, allows the simulation of intermittent rapid slip episodes on a fault surface having a distribution of intact and creep elements. More elaborate rate laws can be used that involve velocity-dependent friction and slip healing. At present these relationships must be regarded as speculative at the mine scale although they may be empirically descriptive at the laboratory scale. Nevertheless, it seems that a multiple, interactive assembly of discontinuity surfaces can provide a good geometric representation of large-scale rock mass deformation for the purposes of integrating seismic activity with numerical modelling. The main challenge is to demonstrate the validity of postulated slip constitutive relations and to be able to identify the orientation and extent of existing and induced fracture surfaces.

The integration process requires that observed seismic behaviour must be incorporated in some manner into the modelling framework and that this should also be capable of inferring subsequent deformation processes. Most observations of seismic behaviour involve the determination of event locations and, in some cases, the nature of the event source. This can be expressed in terms of the seismic moment tensor defined as

$$M_{ij} = G(D_i n_j + D_j n_i)A \quad (2.2.6)$$

where  $D_i$  are the components of the slip vector,  $G$  is the shear modulus and  $A$  is the area of slip. The scalar moment  $M_0$  is defined with respect to the average slip  $\bar{D}$  by

$$M_0 = G\bar{D}A \quad (2.2.7)$$

Knowledge of the six independent components  $M_{ij}$  of the symmetric moment tensor is insufficient to allow equation (2.2.6) to be solved uniquely for the  $D_i$  and  $n_i$  values since

$$n_i^2 = 1. \text{ However, if some rule is available to fix the orientation of the slip plane, the}$$

components of the displacement discontinuity vector can be assigned and the stress induced by the event can be determined by appropriate influence relationships. In a local coordinate system,  $x,y,z$ , and assuming constant values of the DD vector ( $D_x, D_y, D_z$ ), the stress induced within the slip region is given by

$$\begin{bmatrix} \Delta\tau_{xz} \\ \Delta\tau_{yz} \\ \Delta\tau_{zz} \end{bmatrix} = \frac{G}{4\pi(1-\nu)} \begin{bmatrix} I_{,zz} + \nu I_{,yy} & -\nu I_{,xy} & 0 \\ -\nu I_{,xy} & I_{,zz} + \nu I_{,xx} & 0 \\ 0 & 0 & i_{,zz} \end{bmatrix} \begin{bmatrix} D_x \\ D_y \\ D_z \end{bmatrix} \quad (2.2.8)$$

where  $I$  is given by equation (2.2.2). Let the 3 X 3 influence matrix in equation (2.2.8) be designated by  $K$ . For a square-shaped slip area of side  $g$  this is equal to

$$K = \frac{8\sqrt{2}}{g} \begin{bmatrix} 1-\nu/2 & 0 & 0 \\ 0 & 1-\nu/2 & 0 \\ 0 & 0 & 1 \end{bmatrix} \quad (2.2.9)$$

It is interesting to note that for a circular shaped slip area of radius  $R$ , the influence matrix is equal to

$$K = \frac{2\pi}{R} \begin{bmatrix} 1-\nu/2 & 0 & 0 \\ 0 & 1-\nu/2 & 0 \\ 0 & 0 & 1 \end{bmatrix} \quad (2.2.10)$$

For equal slip areas,  $g = \sqrt{\pi}R$ , and the ratio of the influence coefficients for the square area to the coefficients for the circular area is approximately equal to 1,015. If the pre-existing stress at the source location is  $\tau_{ij}^p$ , the total stress is given by

$$\tau_{ij} = \tau_{ij}^p + \Delta\tau_{ij} \quad (2.2.11)$$

where  $\Delta\tau_{ij}$  is computed using equations (2.2.8) and (2.2.9) or (2.2.8) and (2.2.10).

In cases where additional slip is to be estimated in some proposed position relative to an existing population of discontinuities and mined regions, some law must be used to determine the equilibrium stress condition. The simplest rule is to assume that the equilibrium shear stress at a potential site is equal to the frictional sliding resistance. For example, if slip is in the local y-coordinate direction, on a flat, square crack whose normal is in the local z-direction, it is required that

$$|\tau_{yz}| = -e(\tau_{yz}^p + CK_{22}D_y) = -\mu\tau_{zz} \quad (2.2.12)$$

where  $\tau_{zz}$  is the normal stress across the crack (compression negative),  $\mu$  is the coefficient of friction and  $e$  is a slip indicator variable equal to the sign of the slip component  $D_y$ .  $C$  and  $K_{22}$  are, from equations (2.2.8) and (2.2.9), given by

$$C = \frac{G}{4\pi(1-\nu)} \quad (2.2.13)$$

and

$$K_{22} = 8\sqrt{2}(1-\nu/2)/\sqrt{A}, \quad (2.2.14)$$

respectively. Solving equation (2.2.12) gives

$$|D_y| = eD_y = \tau_e / CK_{22} \quad (2.2.15)$$

where the excess shear stress (or stress drop)  $\tau_e$  is given by

$$\tau_e = -e\tau_{yz}^p + \mu\tau_{zz} \quad (2.2.16)$$

Now, from equations (2.2.13) and (2.2.14), it can be seen that  $CK_{22} = \alpha G / \sqrt{A}$  where  $\alpha$  depends on the element shape and on Poisson's ratio,  $\nu$ . The energy release,  $\Delta E$ , is given by

$$\Delta E = \frac{1}{2} A \tau_e |D_y| = A^{3/2} \tau_e^2 / 2\alpha G \quad (2.2.17)$$

The scalar moment  $M_0$  is given by

$$M_0 = GA |D_y| = A^{3/2} \tau_e / \alpha \quad (2.2.18)$$

Finally, combining equations (2.2.17) and (2.2.18) gives

$$\Delta E = M_0 \tau_e / 2G \quad (2.2.19)$$

Equations (2.2.17) to (2.2.19) are equivalent to the basic relationships of elementary seismology (see *Scholz, 1990*). However, it should be noted that the assumption of a constant slip leads to a value of  $\alpha$  which over-estimates the average slip by a factor of approximately two when compared to the average slip computed for a penny shaped crack (Brune model). (This error is reduced if the slip variation is smoothly reduced to zero near the edges of the patch). In addition, considerable care must be exercised in assigning crack slip elements to designated spatial positions in order to avoid spurious singular stress interactions. In general, it will be necessary to use point influences (Section 2.2.2) or to ensure continuity at crack intersection lines by means of higher order discontinuity variations. These detailed difficulties have to be resolved in the actual scheme that is designed to integrate seismic observations with numerical modelling.

## **2.2.2. MAP3Di/Point KERNEL**

### **2.2.2.1. MAP3Di**

Map3Di is an advancement of the standard MAP3d programme that permits the superposition of external field loading effects onto a standard Map3D model. The field loading can arise from thermal heating, fluid pressure, non-linear behaviour, etc. In addition, the magnitudes of the external effects can be determined from many forms of in situ monitoring including for example fluid pressures (e.g. well drawdown, dams, hydrofracturing), heating (e.g. natural heating, nuclear waste storage), and deformations (e.g. monitored with extensometers). Another important source of in situ field loading information arises from seismic activity. By definition, the presence of seismicity indicates that the rock mass is yielding to load and hence deforming in some way. The seismicity could indicate shearing on a fault plane or 3D material non-linearity possibly resulting from a weak lithological feature. The deformations indicated by the seismicity can be superimposed onto the Map3D mine model, thereby redistributing the stresses to accommodate the deformations.

The field loading information is specified as ride and dilation components on a segment of a slip plane, and/or deformation of a 3D zone. Slip or dilation on a fault plane would be applied by subdividing the known extent of the fault into small planar zones and then specifying the slip or dilation components in each zone. If the seismic observations suggest that entire volumes of the rock mass are deforming and other parts are not, the whole rock mass can be divided into up into small 3D zones with the deformation components specified in each zone based on the observed seismic strain deformations. The overall stress state is then updated to accommodate the contribution of the integrated field loading. Note that the Map3D model can contain all of the regular features including excavations, stiff dykes, faults etc. The effects of the field loading and all of these other features will be superimposed to provide a final composite prediction of the stresses, strains and displacements throughout the rock mass.

The wealth of information that comes from seismic monitoring is enormous. Seismic monitoring provides the volume and spatial distribution of information on the rock mass response that can be obtained in no other way at reasonable cost. Map3Di provides a mechanism to directly use this information for model calibration and assists in applying Terzaghi's Observational Approach to Design (???). Owing to the real-time nature of seismicity, it becomes practical to traverse the mine/monitor/redesign loop for every increment of mining. Thus, instead of spending years making visual observations to develop a history of rock mass response, there is potential to calibrate the model much more quickly. Perhaps the most important part of this is that it provides the possibility of adapting to changing rock mass conditions.

The applications of Map3Di to the modelling of seismicity in mines could result in improved accuracy of prediction of spatial seismic hazards. The calculation of the redistribution of stresses due to the occurrence of large events allows the assessment of the extent that a large event might diminish the seismic hazard and should improve the temporal prediction of seismic hazard as a result of the superimposition of measured displacement onto modelled displacement for both historic and planned mining steps. If direct linking could be provided between a seismic database and a super fast computer, Map3Di modelled stresses could be updated in “real time”, where the time step would be controlled by the feed of seismic data and the ability of the system to update the model. General boundary element limitations, discussed in section 2.2.1 still apply and include the limited ability to model the spatial temporal distribution of seismicity.

### 2.2.2.2. Point Kernel

The point kernel method is a combined meshed/meshless methodology that builds on the mine analysis program MINSIM and incorporates the fracturing processes in a meshless representation. Planar features such as tabular orebodies, and geological discontinuities can be modelled conveniently by means of displacement discontinuity elements in the same way as the standard MINSIM. It is then proposed that the rock mass contains an additional set of discontinuities for which the displacement components are known. These correspond to slips on pre-existing planes, and new fractures or slip planes that may form. The multitude of different scales implies that element intersections and geometrical discretizations will consume much of the already scarce computation resources and new approaches must be sought. A move to meshless methodologies has been taken in computational fluid dynamics (*Oden et al. 1999*) – another field where the consideration of nonlinearities on multiple scales is required. The integration of seismic information with numerical modelling codes emphasises the need for meshless methods as predefined mesh structures will be unable to cope with the introduction of measured nonlinearities at arbitrary positions in space and time.

The basis of the point kernel method is the assumption that each surface in space can be represented by a “virtual” element, of known orientation, size and with a given displacement discontinuity. The influence of these discontinuities become an effective load to the mine layout and hence reduces the memory requirements if the loading points are decoupled from the layout solutions. The influence on the stress state  $\sigma_{ij}$  in the global axis system of any virtual element centred at any other point  $P$  can be expressed as

$$\Delta\sigma_{kl}(P) = -\Gamma(Q_{ij}, P_{kl})D_j(Q)n_j(Q)\Delta S_q \quad (2.2.20)$$

where the  $D_j(Q)$  is the displacement discontinuity and the virtual element is assigned an area  $\Delta S_q$  and normal  $n_j$  as shown in Figure 2.2.1. The influence matrix  $\Gamma(Q_{ij}, P_{kl})$  is defined in *Crouch and Starfield (1983)* and is not presented here.

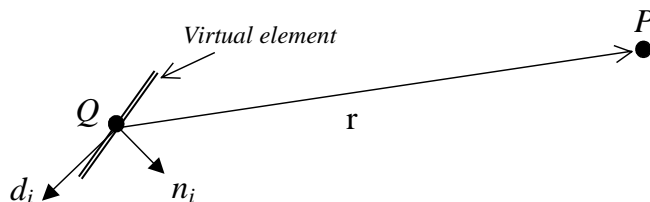


**Figure 2.2.1. Schematic of a virtual element at point Q transmitting influence to point P.**

As the displacements at the virtual elements are assumed to be known, the sum of the influences at all  $M$  cracks at points  $Q_i$  on the center of the  $N$  existing mine elements  $P_j$  provides the influence matrix of all the virtual surfaces. This method is an approximation, but the concept of a meshless model, using only virtual elements, introduces considerable savings in the

computational and programming effort required for the housekeeping functionality that is otherwise needed to track new elements and intersections with pre-existing elements.

Two types of virtual elements can be defined. Passive elements are associated with known displacement discontinuities. These can be inputs from external data such as fault slip components obtain from structural mapping, or as the first step towards integration with seismic systems, the observed data can be imported into the model to condition the solution to take account of information about the actual rock mass response. Thus, explicit failures on structural features can be included into a purely elastic model. Stress will be distributed in such a way that new failure surfaces may be highlighted allowing improved predictions of future seismic events.

This step, however, can be seen as merely an advanced post processing of the seismic data unless the modelling can be allowed to predict forward. Thus, the introduction of active elements that have rheological properties that permit failure and slip in the future is required to be able to provide input for mine planning.

The displacement discontinuities on passive elements can be calculated from the moment tensor of seismic events or the slip plane directions must be assumed e.g. determined from known geological structures, assumed to be vertical, or in the calculated direction of maximum shear.

Active virtual elements require some assumptions regarding the constitutive response and the rheology. It is postulated that the rate of shear slip on a virtual element is proportional to the net shear stress acting at the point  $Q_0$  associated with the element. The point effect reflects the influence of a “virtual” element centered at the point in question. The self-effects have been chosen to reflect a square, constant displacement discontinuity element.

### 2.2.3. DIGS

DIGS (Discontinuity Interaction and Growth Simulation) is a computer program that is designed to solve plane strain interacting crack problems. The original concept for this code (*Napier, 1990*) was to provide a tool which would enable the fracture zone ahead of a deep level gold mine stope to develop according to simple growth initiation rules. This would, in principle, allow the impact of factors such as the primitive stress field, backfill and pre-existing discontinuities such as joints and parting planes to be assessed. The use of the DIGS code has highlighted the role of parting plane slip in extension fracture initiation and has illustrated how fracture zone deformations can alter the in-stope hangingwall clamping stresses. Specific difficulties in applying the explicit growth model include the numerical treatment of fracture intersections that may lead to very small crack segments and wide variations in crack element sizes. Additional problems arise in solving closely parallel or acutely angled fractures.

In order to alleviate these numerical difficulties an alternative version of the original DIGS code (the “tessellation” model) was developed in which fracture paths are constrained to lie on the arcs of a predefined random mesh. A number of studies have established that the nature of the random mesh plays a strong role in determining the overall material response. If the mesh is generated according to a Voronoi polygon scheme, the average number of mesh branches meeting at each junction is equal to three. In this case, simulation of uniaxial loading of a rectangular rock sample leads to the formation of an inclined shear zone and plastic “hardening” (no load shedding) at the onset of failure. The rounded grain pattern of the Voronoi mesh leads to qualitatively “plastic” behaviour. Alternatively if the random mesh is generated as a Delaunay triangulation, the average number of mesh branches that meet at a junction is equal to six. In this case, uniaxial loading of a rectangular shaped sample leads to strong load shedding and axial splitting after the point of initial failure; a qualitatively “brittle” response. Additional studies have shown that the use of a Voronoi mesh, with internal triangles in each polygon, is also effective for the simulation of load shedding behaviour. Further work carried out by *Sellers (1997)* has addressed the progressive formation of the fracture zone at the edges of a small span stope that is incrementally enlarged. *Sellers (1997)* has demonstrated the importance of

parting planes in generating fractures ahead of the stope face and has shown as well that undulations of the parting plane surface can amplify the rate of closure with respect to the stope face advance.

*Napier and Malan (1997)* have implemented a time-dependent slip model in the DIGS tessellation model. This allows the simulation of classic primary, secondary and tertiary creep behaviour for the response of a dead-weight loaded sample covered by a random Delaunay mesh. A fraction of the mesh segments are chosen to be initial "flaws" having zero cohesion and which can creep in shear when the load is first applied. As time advances, additional loading accumulates on the intact crack elements. Once these elements start to fail, a sporadic cascade process is initiated which leads, eventually, to the ultimate catastrophic failure of the sample. This sequence has clear correspondences to theories of earthquake initiation and to the generation of mine seismic activity. Some applications are described in Section 3.1.4.

Despite the encouraging qualitative attributes of the DIGS code for the representation of seismic deformation mechanisms, it is apparent that a number of limitations exist. One limitation is that it is not obvious how to extend the random mesh scheme to three dimensions. In particular, it can be anticipated that a three dimensional tetrahedral mesh would be inappropriate for the representation of relatively smooth, extensive slip surfaces. Computational difficulties in treating multiple three dimensional interacting fracture surfaces are also formidable. It appears that the best alternative to using a pre-defined mesh in three dimensions, is to allow for the incremental development of fracture growth surfaces in the sense of the original DIGS code.

It is important to note that in the simulation of seismic behaviour, using the DIGS code, results can be sensitive to the density of the tessellation mesh. This sensitivity can be reduced by introducing a slip-weakening failure rule that defines, effectively, a specific energy for the fracture process. However, this does not fully resolve the grid size problem. It must be noted, as well, that this problem is endemic to most numerical procedures used to analyse material failure although this is seldom reported.

#### **2.2.4. The Integrated Damage Rheology Model (IDRM)**

A realistic numerical model of rock-mass response to extreme loading has to include some treatment of material damage. The study of damage evolution must provide some insight on the physical processes leading either to instability and material failure or to healing and restoration of cohesion. Unfortunately the physical theory of damage is incomplete at present. One of the reasons for this is that it spans several length scales from macroscopic down to molecular level and the relevant physical variables are macroscopically unobservable. Nevertheless it is possible to construct a state-function of a system which includes both directly observable variables and macroscopically unobservable parameters such as some measure of damage. In fact the free-energy approach to mining-oriented numerical modelling seems to be the only physically consistent way of combining the dynamics of deformable solids with damage evolution and stability analysis: in other words, the whole complex of fundamental equations which is known as **rheology**. The treatment of damage adds a new aspect to the rheological behaviour of solids since the damage itself has the effect of an induced loading. Therefore it is more proper to use the term **damage rheology** for the appropriate physical concept to be embedded in a realistic numerical model of rock-mass behaviour.

From a theoretical point of view, a numerical model is specified by postulating the expression for the free energy of the system as a function of the relevant state variables and material constants. In the case of damage-rheology models, the free energy will depend on the invariants of the deformation tensor and on one or more damage-related parameters. The partial derivatives of the free energy are treated as "thermodynamical forces" and enter in the dynamical equations of motion for the medium. The external loading corresponds to the boundary conditions needed for the uniqueness of the solution. The dynamical equations of deformable solids are solved in real, physical time in either Lagrangean variables or in the Eulerian formulation of the mechanics of continua. Thus the basic requirement for the



integration of seismic monitoring with numerical modelling can be met: the clock of the numerical model can, in principle, be synchronised with the pace of the physical time.

A great advantage of the outlined general formulation of a damage rheology numerical model is that it is sufficiently general to allow for **non-linear material response** in a most-natural way. In general, the internal energy of a deformable solid and through it the free energy will depend on the elastic moduli which are not constants but state-dependent functions of the damage distribution. The response of the material to loading is determined not only by the instantaneous value of the load but by the past history of loading. The evolution of damage can include material healing in addition to material degradation which corresponds to the actual behaviour of rock-mass.

On the ground of the presented arguments it can be concluded that damage rheology numerical modelling is the correct choice for building an integrated seismic system.

The IDR (Integrated Damage Rheology Model) (*Lyakhovskiy, Ilchev, Agnon, 2001; Ilchev and Lyakhovskiy, 2001*) software is an integrated system for numerical modelling of damage evolution, elastic and plastic deformations as well as the occurrence of sudden material failure leading to the formation, localisation and propagation of cracks within solids subject to some prescribed external loading. The IDR solves a forward problem in actual (calendar) time and is designed to assimilate the damage associated with real events both from a seismic catalogue and as they occur in real time. The damage evolution and the material rheology are derived from fundamental physical principles as opposed to models with random input. The resolution of the time-clock of the model is determined by the speed of propagation of seismic waves and the spatial discretization scale.

#### **2.2.4.1. Physical basis of IDR**

IDR considers either a homogeneous or a heterogeneous solid which occupies some finite volume. The IDR volume is discretized by a set of tetrahedral elements. The nodes of the tetrahedra are treated as material points of mass determined by the local density of the material and the volumes of the tetrahedra to which the node belongs. The variations of the stress field materialise in forces acting on the nodes. The latter subsequently move according to the laws of mechanics. The resulting displacements induce corresponding changes in the stress field via the variation of the free energy of the system. The (Helmholtz) free energy of the system is a thermodynamical function which depends on all relevant state variables and produces, through its partial derivatives, all macroscopically observable physical characteristics of the material body. The IDR body is treated here as a thermodynamical system. The free energy is the difference between the internal energy and the product of the entropy and the temperature:

$$F = U - ST$$

In the case of interest for the IDR the internal energy will be equal to the elastic potential energy of the solid body (the considered volume of rock).

The Free energy of a system determines the states of stable equilibrium according to the general variation principle: the physical equilibrium state minimises the free energy as compared to all (conditions permitted) virtual states. The system can exist in a stable state only when the free energy is a convex function of the strains. Material failure is identified with the loss of stability due to a loss of convexity of the free energy of the system. In IDR, the convexity of the specific (per element) free energy is tested at every time-step and the beginning of a seismic event (crack formation, slip...) is marked by a loss of convexity of the elastic potential energy.

The free energy of a physical system depends on state variables some of which can be "hidden" in the sense that they are associated with microscopic degrees of freedom and hence not directly observable. IDR is based on the introduction of one such hidden variable, denoted by  $\alpha$  and describing the local state of damage in the rock-mass. The damage variable (or just

damage)  $\alpha$  is a dimensionless (pure number) quantity taking its values in the interval [0,1].

Damage equal to zero corresponds to intact rock while damage equal to one means completely destroyed material (gauge, powder...). The damage parameter is simply an estimate of the state of damage in a given location and at a given time on a scale from 0 to 1. It is possible to associate the damage parameter with the local density of microscopic cracks (after a suitable normalisation).

The state of damage in a solid affects:

- the elastic modulae of the material
- the state of strain in the material
- the state of stress in the material

It is therefore necessary to include the degree of damage in the free energy of the system. In IDRM this is done by postulating the density of the elastic potential energy after Lyakhovskiy and Myasnikov :

$$U = \frac{1}{\rho} \left( \frac{\lambda}{2} I_1^2 + \mu I_2 - \gamma_1 \sqrt{I_2} \right)$$

where  $\lambda$  and  $\mu$  are the Lamé parameters,  $\gamma$  is a new elastic module which vanishes from intact rock and  $I_1, I_2$  are the two strain invariants. The dependence on the damage variable is in the elastic modulae:

$$\begin{aligned} \lambda &= \lambda_0(1-\alpha) + \lambda_1\alpha + \dots \\ \mu &= \mu_0(1-\alpha) + \mu_1\alpha + \dots \\ \gamma &= \gamma_1\alpha + \dots \end{aligned}$$

The response of the material to loading is not Hookean and non-linear due to the term  $I_1\sqrt{I_2}$ .

The effect of this term does not vanish even when the strains are small as long as the material is (partially) damaged and  $\gamma$  is not zero.

IDRM does not use *ad hoc* constitutive relations but generates them by means of the free energy according to the fundamental relationship:

$$\sigma_{ij} = \rho \frac{\partial F}{\partial \varepsilon_{ij}}$$

The evolution of damage follows from one of the fundamental principles of non-equilibrium thermodynamics i.e. that the rate of entropy production should be maximum (corresponding to a maximum dissipation power). This leads to the following equation:

$$\frac{d\alpha}{dt} = -C \frac{\partial F}{\partial \alpha}$$

Where C is positive and controls the temporal scale of the damage (and HEALING) process.

The rheological law incorporated in IDRM is:

$$\frac{dg_{ij}^0}{dt} = \frac{1}{2\eta} \left( \frac{\partial F}{\partial \varepsilon_{ij}} - \frac{1}{3} \frac{\partial F}{\partial \varepsilon_{kk}} \delta_{ij} \right)$$

where  $g_{ij}^0$  are the irreversible (viscous) strains.

The velocities of the nodal particles are determined from the equation of motion:

$$\frac{\partial \sigma_{ij}}{2x_j} + f_i = \rho \frac{dv_i}{dt}$$

#### **2.2.4.2. Material Stability and Seismic Events in IDRM**

Due to the damage-dependent elastic potential energy the above constitutive relations are non-linear and break down when the free energy loses its convexity. The loss of convexity of the free energy signals the beginning of a damage event accompanied by stress-drop in the failed elements as well as with induced (co-seismic) stress-drop in other elements. The latter is a process which could be localised in space and finishes with the restoration of the convexity of the free energy. Due to the full access to the stress and strain fields provided by IDRM one can extract information about the modelled events in full detail. IDRM writes the catalogue of damage events it generates. This model-generated data needs further processing in order to filter out the actual model-analogues of seismic events from the acoustic noise which would remain below the sensitivity threshold of the seismic monitoring system. In other words, IDRM like all similar models of seismic activity requires an unambiguous and quantitative definition of what is to be interpreted as a modelled seismic event. Further the said definition of modelled seismic events must be sufficiently flexible to allow for a calibration of the running model to the observed level of local seismicity. IDRM is equipped with such a definition of a modelled seismic event.

Key to the definition of seismic event within IDRM is a cluster-analysis of the model-generated data on element failures due to damage above the critical level and a loss of stability. Not every failed element is treated as a source of a seismic event. Instead, the set of all simultaneously failed elements is analysed and all connected clusters (see the corresponding entry in the Glossary) of such elements are identified. A seismic event is a connected cluster of "mass" above certain minimum value. The damaged elements which do not belong to connected cluster of sufficient size are treated as contributing to the acoustic noise.

The above definition of IDRM-generated seismic events allows for tuning the frequency and size of the modelled events to the observed local background seismicity level and achieve a maximum efficiency of the integration of real events into the running model.

#### **2.2.4.3. Typical Problems treated by the IDRM**

1. Damage evolution and local seismicity of rock-mass subjected to a constant strain rate loading. The strain rate is converted to a velocity field on the boundary nodes.
2. Damage evolution and local seismicity of rock-mass subjected to a time-dependent (e.g. blasting determined) strain rate loading. The strain rate is converted to a velocity field on the boundary nodes.
3. Damage under constant or confining stress or under variable stress distribution due to mining activity.
4. Mixed problems: prescribed velocities on some of the boundary nodes and prescribed traction values in the remaining boundary nodes. The prescribed values could vary with time in accordance with the real mining rates.

The above list of practical problems which can be successfully treated with the help of the IDRM is far from complete. The criterion for correctness of the formulation of an IDRM problem is that the boundary conditions guarantee the uniqueness of the solution of the corresponding partial differential equations.

#### 2.2.4.4. Integration of real seismic events in IDRM

The occurrence of a seismic event is associated with certain damage of the material in the neighbourhood of the seismic source. This coseismic damage is estimated from the corresponding displacements and passed to the IDRM **in the particular moment of time** as a sudden increment to the damage variable. This is how the real events can modulate the damage evolution in the running IDRM thus bringing it closer to reality. There is a difference in the methodology of assimilation for real seismic events which occur within the IDRM volume or in the immediate vicinity from the treatment of events located far from the IDRM volume. The latter are converted into corresponding loading passed to the boundary of the IDRM via a second, much bigger boundary-element shell. In this context one can say that the functional scheme of IDRM implements a hybridisation between the finite-element code of damage rheology and the boundary element method used to evaluate the loading conditions due to an ongoing mining activity and the local seismicity.





### 3. Examples of the simulation of seismicity patterns by different numerical models

#### 3.1. Size distribution

In the two dimensional elastodynamic boundary integral method (e.g. *Cochard and Madariago, 1996*) slip length and stress drop can be obtained directly from post processing of the numerical results. The seismicity resulting from the gradual increase of tectonic stresses applied to study the response of a single strike slip fault was expressed in terms of histograms of the slip length. The seismic moment can be obtained as

$$M = \mu \bar{D} L,$$

where  $\mu$  is the shear modulus,  $\bar{D}$  is the average slip, and  $L$  is the length of the slip zone. Stress drop and moment are plotted against length as shown in Figure 3.1.1b and c. The frequency magnitude distribution can also be obtained directly from the numerical results and is shown for two different element sizes in Figure 3.1.1. A similar method can be applied in three dimensions (*Robinson and Benites, 1995, Lachenicht and van Aswegen, 1999*). *Robinson and Benites (1995)* calculated the total moment for an event that slips over a number of elements as a summation of the products of the area of each element that slips and its accompanying slip deformation. *Lachenicht and van Aswegen (1999)* define the area of slip as the region having a slip deformation that is greater than a given tolerance.

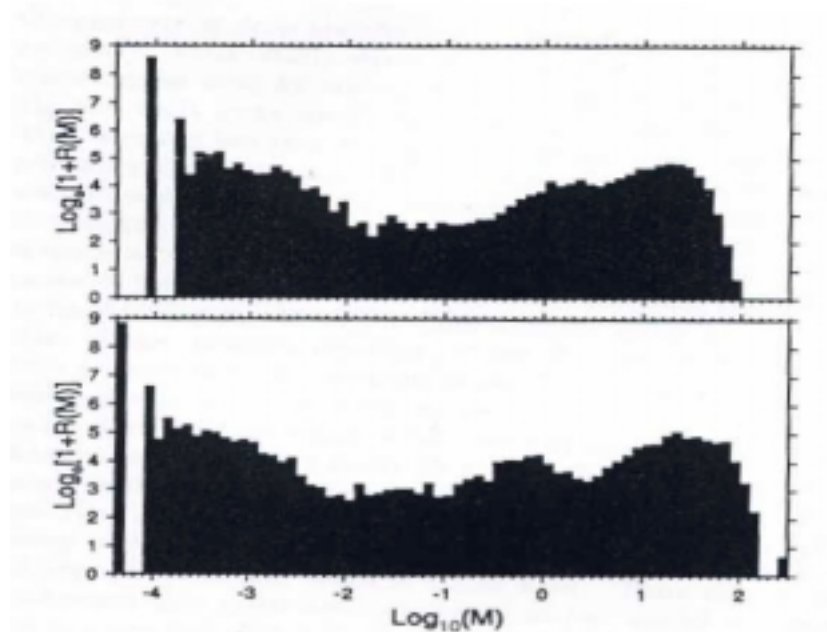


**Figure 3.1.1 Effect of element size on frequency magnitude statistics (*Cochard and Madariago (1996)* using 513 grid points (top) and 1025 grid points(bottom))**

In cellular or discrete models, the number of broken bonds is known and can be used to calculate equivalent moments. However, other methods are required to measure the clustering of events on a larger scale. A box counting method was applied, but not described in detail by *Wilson et al. (1996)* to obtain frequency magnitude plots from cellular automata. Correlation integral methods (e.g. *Turcotte, 1992*) have been used for special correlation of acoustic emissions (*Hirata et al., 1987*) and could be applied to obtain seismicity from the space-time distribution of plastic strain in continuum models.

*Ben-Zion and Rice (1993)* prefer to consider the potency  $P$  that is defined as the moment divided by the shear modulus ( $M/G$ ) instead of the moment itself as there are difficulties in

determining a unique shear modulus. The defined the magnitude of the events form the empirical relation

$$M = (2/3) \log_{10} (P) + 3.6$$

where  $P$  is given in units of  $\text{km}^2 \cdot \text{cm}$ . Then the frequency magnitude plot is found by relating  $\log_{10} P$  to  $\log_{10} A$  where  $A$  is the fracture area.

Particle based models are created using a distinct element code in which a rock is represented by an assembly of thousands of individual particles bonded together at points of contact. Cracks are induced in the rock mass during loading when particles separate and the connecting bonds are broken. The models are run dynamically with low damping, which allows seismic waves to emanate from the cracks. The particles move independently of one another and interact only at contacts. They are assumed to be rigid (non-deformable) but deformation (or overlap) can occur at the contacts. Contacts are assumed to exist only at a point and not over some finite surface area as would be the case with fully deformable particles. The forces and displacements on the particles are calculated from the force-displacement law and the law of motion. A typical code is PFC3D (*Itasca*), which uses the distinct element method (DEM). The model is a dynamic process where disturbances can propagate through the system at some speed that depends on the physical properties of the system.

Models can be created to imitate many different situations and processes, however in PFC some steps of the model creation are always the same. In general, a PFC model of rock consists of a collection of particles bonded together in a dense assembly. The micro-properties of the particles and bonds can be adjusted to simulate the desired rock type. The various micro-properties that can be specified are shown in Table 3.1.1. These micro-properties influence the macro-properties (e.g. strength and stiffness) of the modelled 'rock'.

**Table 3.1.1 List of parameters used in PFC3D modelling.**

Parameters
minimum radius
maximum radius
normal stiffness scale factor
shear stiffness scale factor
density
friction
normal bond strength scale factor
shear bond strength scale factor
bond strength deviation
damping coefficient, $\alpha$

Hazzard (1998) presented a detailed study on the ways in which seismicity could be obtained from discrete element methods, in particular the Particle Flow Code. This work indicated that there were five methods of determining the event size in order to present the frequency magnitude plots.

1. Kinetic Energy of each bond breakage. This method produced too many small events as no clustering was considered.
2. Examination of wave forms. A numerical equivalent "seismic system" consisting of a set of velocity measuring points was used to locate events and the event parameters were evaluated with the methods used by in situ seismic systems. The method permits a number of bond breakages to be considered as a single event and this introduces larger clusters. The methods is limited by the requirements for lots of data output and also the need for a "seismic system" for analysis.
3. Kinetic Energy of clusters of bond breakage. Clusters of bonds were considered together, but it was difficult to determine the events making up a single cluster.



4. External Kinetic energy release rate. The time series of kinetic energy was used to evaluate the magnitudes. The method was easy to apply and considered larger clusters, but includes too many events as one cluster. Figure 3.1.2 compares the b-values obtained from the two methods and shows that the external methods (e.g. method 4) produce lower b-values as they consider the effect of bond breakage for clusters of elements.
5. Kinetic Energy of bond breakage with space time cluster windowing. A procedure was developed for post-processing the results and determining all events within a given space-time window. The size of the window was calculated as being of the order of 5 particle diameters and the time length was determined from the time taken for the shear wave to cross that distance. Figure 3.1.3 shows that the clustering algorithm reduces the b-value. Advances were included that re-initialise the space-time window at every new event in the cluster to allow for the development of growing, localised failure zones. The method produced improved clustering and consequently a lower b-value, but the b-value is found to depend on the window size, as shown in Figure 3.1.4

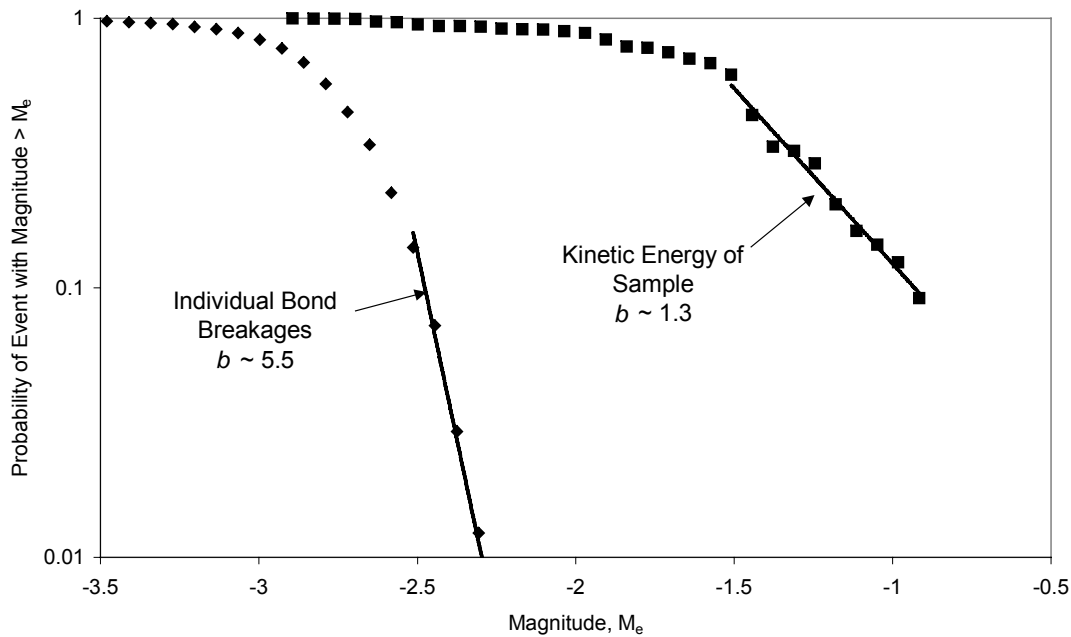


**Figure 3.1.2** Frequency-magnitude plot for AE magnitudes derived from kinetic energy of the sample (Method 4), compared to magnitudes derived from individual bond breakages (Method 1) (After Hazzard 1999).

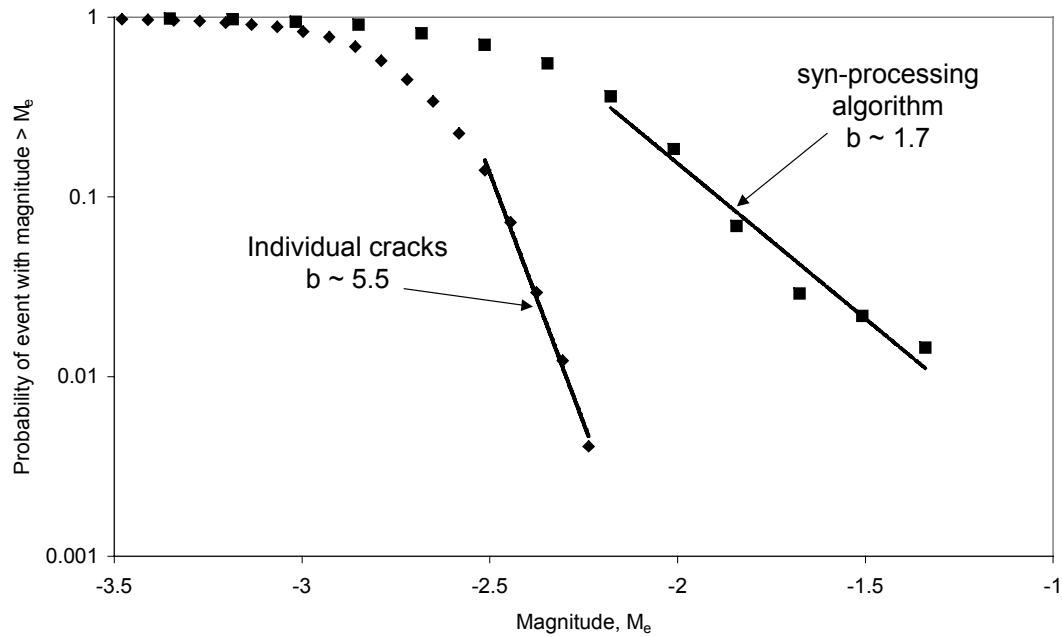


**Figure 3.1.3. Frequency-magnitude plot resulting from the syn-processing crack combination algorithm (Method 5). The plot resulting from each crack being considered individually is shown for comparison (Method 1) (After Hazzard 1999).**

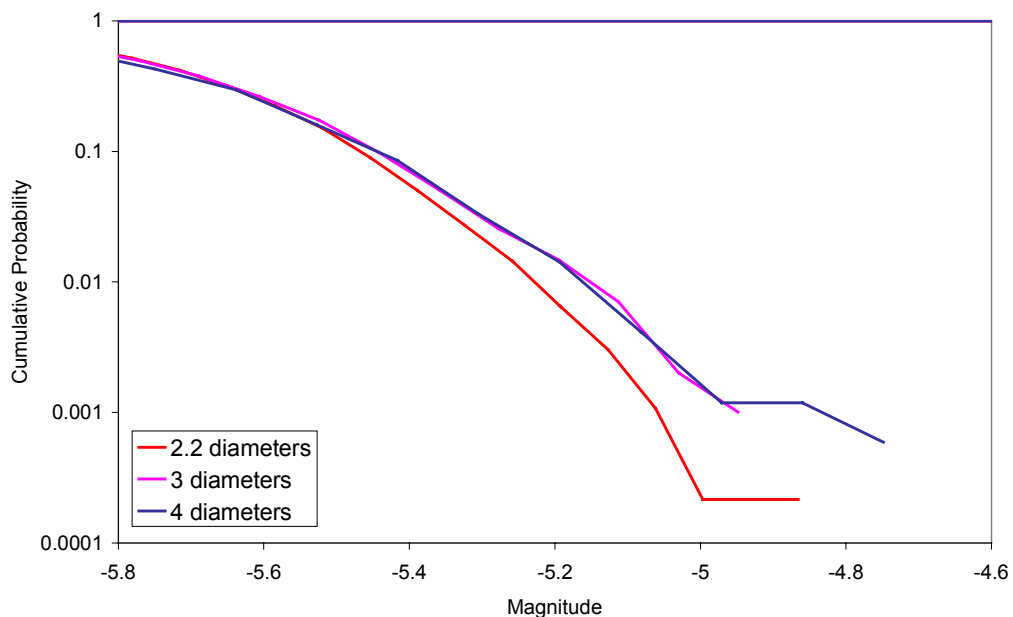


**Figure 3.1.4 Comparison of frequency magnitude curves for all of the events recorded in Test I clustered using different space windows (Hazzard, 1998).**

To study the response of PFC3D in a model that is more representative of a mining situation, a cubic set of particles of side length 80mm, which contains 71019 balls, was mined with 1 mm face advanced in 40 mining steps. As shown in Figure 3.1.4, mining was at the middle of the cube where finer balls are present. The ball sizes vary from 0.63 mm to 1.2 mm. The balls are finer where the stope is and gradually increased away from the stope both in the hangingwall and the footwall.

Four different ways of mining were considered:

1. Excavate the area (since this process is dynamic, excavating the area immediately produces shocking effects in the system).

2. (a) High damping (freeze the system)  
(b) Excavate the area  
(c) Low damping (allows the fracture to occur)
3. Decrease the ball stiffness gradually with time.
4. Decrease the forces gradually on the particles with time around the stope.

The model was loaded up to 80 MPa with a confinement of 40 MPa with the first method explained above. If the cracks occurred within some specified time and space window they were clustered together to form larger events. The event magnitudes were calculated by representing each crack's kinetic energy history by a Gauss shaped curve where the peak of the curve is equal to the peak kinetic energy associated with the crack and the width of the curve is related to the rise time (the time from the bond breakage to time of the peak KE). The Gauss curves for the cracks within each cluster were then summed to get the peak kinetic energy and therefore magnitude of the event (*Hazzard, 1998*).

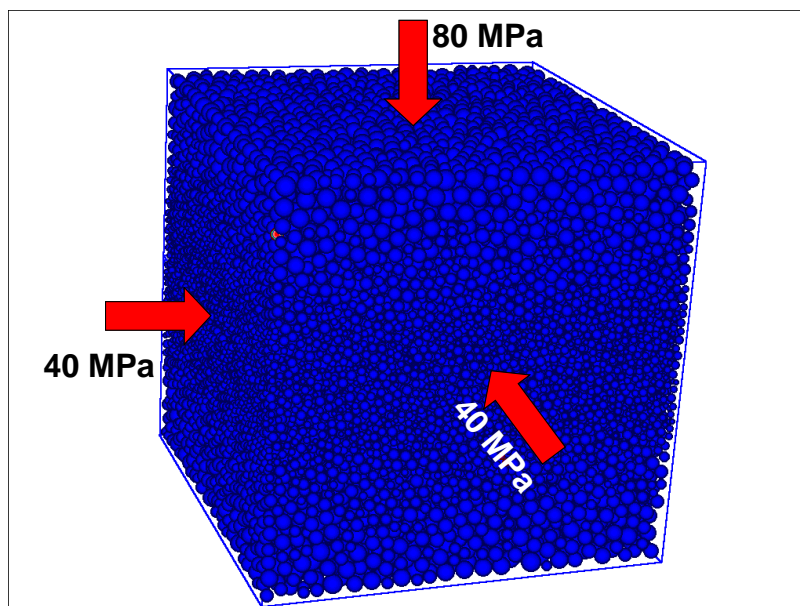


**Figure 3.1.4 PFC3D model used for mining model.**

If each bond breakage is considered a single acoustic emission then no calculations are required to obtain the AE locations in PFC. A simple function can be written that records the exact location and time of each bond breakage and these can be recovered after the model has been run.

Each bond-breakage in PFC can be assigned some event magnitude. When a bond breaks, the particles fly apart until they are stopped by local confinement. The maximum velocity of the particles can then be used to calculate the kinetic energy of the 'event'. A FISH algorithm for determining the kinetic energy of events was devised by Peter Cundall at Itasca. The method works as follows:

A bond breaks and the initial kinetic energy of the two connected balls ( $KE_0$ ) is stored in memory. At every subsequent time step the kinetic energy ( $KE$ ) of the two particles is calculated.  $KE_0$  is then subtracted from this value to get the change in  $KE$  ( $\Delta KE$ ) at each step. The maximum  $\Delta KE$  over some time interval is stored as the energy associated with that crack.

The only parameter that needs to be set is the length of time for which the  $KE$  should be recorded after each bond breakage. *Hazzard (1998)* found that on average the maximum  $\Delta KE$  occurred within 6 time steps of bond breakage. Most of the events exhibited rise times close to this value however some had much longer rise times up to a maximum of 27 steps. These long rise times are attributed to reflections causing constructive interference and a second peak

larger than the first so that the maximum  $\Delta KE$  was recorded at a significantly later time. To ensure that all peaks were recorded, a recording window of approximately twice the maximum observed rise time (50 steps) was used in this study.

The energy magnitude ( $M_e$ ) of an event can be calculated from the log of the emitted energy by (*Hanks and Kanamori, 1979*),

$$M_e = \frac{\log E - 4.8}{1.5}$$

where  $E$  is the kinetic energy in Joules.

This is emphasised further by observing a frequency-magnitude or b-value plot for all of the events recorded during loading of the sample. This plot corresponds to the Gutenberg-Richter relation

$$\text{Log}N = a - bM$$

where  $N$  is the number of earthquakes with magnitude greater than  $M$  and  $b$  is the slope of the straight part of the curve, usually close to unity. Figure 3.2.2 was constructed by plotting the cumulative number of events versus the event magnitude and then fitting a best-fit line to the straight part of the curve using a least-squares routine.

Figure 3.1.5 illustrates the b-values obtained from different space windows for the same time window. Changing the time window makes little difference to the b-value for this model. More information can be obtained from *Hazzard (1998)* for determination of time and space windows. It is interesting to note that all curves have the common asymptote in Figure 3.1.5. It was observed from the model that larger balls have a tendency to generate bigger magnitude events indicating a possible dependence on the grid size of the simulated results.

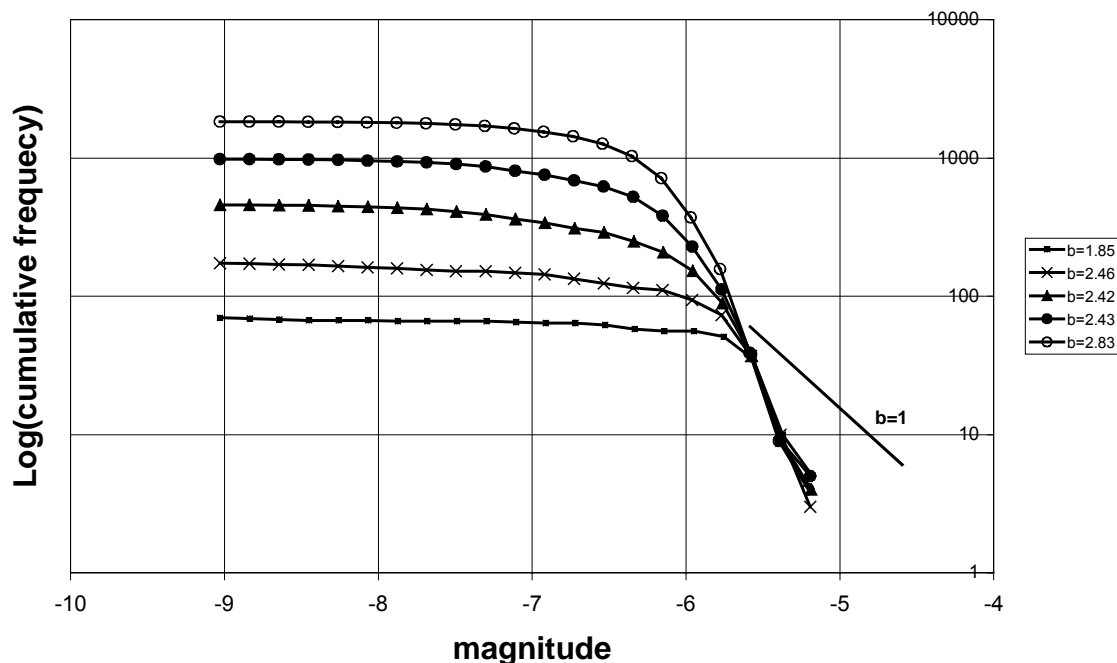


**Figure 3.1.5 Cumulative frequency – magnitude plot from PFC3D slope models using different space windows for clustering.**

Finite element and finite difference models consider the entire rock mass as a continuum. Failure can be modelled using softening constitutive models, but relating the failure to seismic events remains a problem. The ELFEN explicit finite /discrete element code allows discrete

fracturing by splitting elements internally or along their sides and introducing new, internal, boundaries into the finite element mesh. Pre-existing joints sets can be inserted into the model and will become active if the stress state exceeds a Mohr–Coulomb strength criteria. A two dimensional model of a stope was set up to investigate the frequency magnitude statistics. Pre-existing joints sets were included and simulate the observed jointing and mining induced fracturing in a carbon leader stope. The model consists of 50m of mining in 0.8m mining steps. The stope is supported with discrete stope support elements that model the force displacement response of typical elongate support elements. Backfill elements were inserted so that backfill was always kept a distance of 3m from the face. A detail of the model, showing the jointing, elongates and backfill is shown in Figure 3.1.6a. The rock mass, between the joints, was assumed to be elastic with relevant material properties for each of the stratigraphic layers. The magnitude of seismic events was calculated from the energy release in a manner similar to method 4 of *Hazzard (1998)* explained above. Frequency-magnitude plots of a time series of energy release peaks, corresponding to simulated mining in 2D, demonstrates power law behaviour in different size ranges as shown in Figure 3.1.6. The effect of plastic and viscoplastic continua and three-dimensional modelling should also be investigated, together with different schemes for identifying event clusters, based on the distribution of plastic strain and joint slip contours.

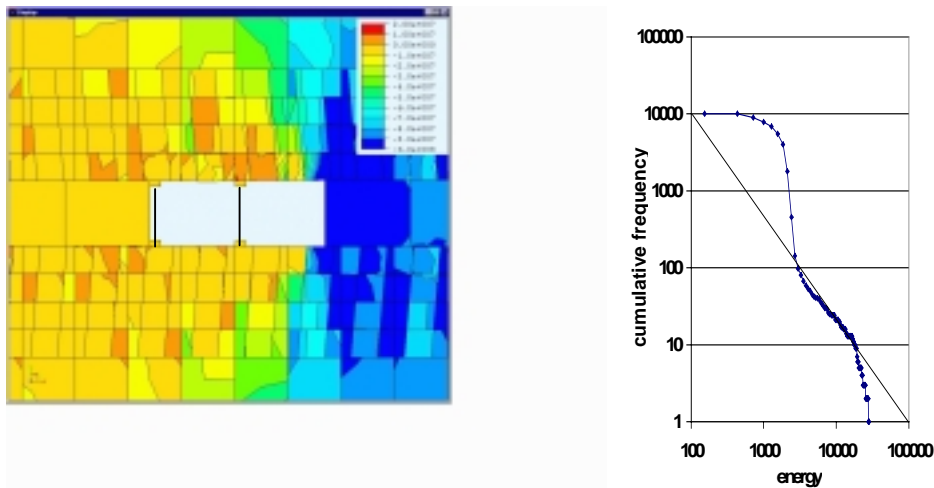


**Figure 3.1.6 a: Detail of a finite/discrete element model of a tabular stope and b: The frequency-magnitude curve based on incremental kinetic energy release.**

Boundary element solvers, are able to efficiently process interacting assemblies of displacement discontinuity elements. In the current project, the 2D displacement discontinuity program DIGS is assessed to determine its suitability for generating seismic recurrence behaviour. To study some of the concepts, the excavation of a parallel sided mining panel was simulated in 100 steps of 5m up to a total mined span of 500m. The stope was modelled using the classic tabular slit approximation with limited interpenetration of the crack surfaces to represent total closure. The surrounding rockmass was assumed to be covered by a random mesh of pre-existing planes of weakness. The mesh was generated as a Delaunay triangulation. Test runs were carried out using two mesh densities having average grid sizes of 26.5m (std. dev. = 6.6m) and 11.0m (std. dev. = 2.7m) respectively. The mesh grids which were inclined at  $\pm 10$  degrees to the horizontal mining excavation were assumed to be weak “parting” planes having a sliding friction angle of 30 degrees and zero cohesion. The other mesh grids were assumed to have a pre-failure cohesion of 25MPa and intact friction angle of 45 degrees. The cohesion was assumed to vanish when the grid was mobilised and the residual sliding friction angle was set to 30 degrees. In addition, it was assumed that after a mesh grid is mobilised, all subsequent slip movements are controlled by a viscous relaxation rule in which the rate of slip is proportional to the net shear stress acting across the crack. The mining rate is then determined by the number of time relaxation steps that are allowed to occur within each excavation step. In the present analysis this rate was chosen arbitrarily to be four relaxation steps per mining step.

Special attention must also be given to the manner in which the energy release rate and inferred “seismic” effects are computed. Since the mining simulation is artificial in respect of the assumed large excavation advances of 5m, it was considered to be inappropriate to include the energy release that is directly related to the closure of the stope as the excavation step is introduced. A two-stage procedure was adopted in which the off-reef tessellation structure was first “frozen” and the change in closure corresponding to the panel span increase of 5m was determined. In the second stage, the off-reef mesh structure was “unfrozen” and allowed to move in response to the first stage closure, for a specified number of time relaxation steps. The strain energy release in each time step was computed on all mobilised grid elements. For the case of sliding elements, this takes the form

$$E_S = \frac{1}{2} \int_A |\tau_e| |D_S| dS \quad (3.1.1)$$

where  $E_S$  is the total energy release over the time step,  $A$  is the total mobilised crack area,  $\tau_e$  is the difference between the shear stress and the shear resistance on each crack at the start of the time step and  $D_S$  is the shear slip occurring during the time step. If it is assumed that the slip in any one time step is concentrated in a specified region on a well clustered group of cracks, it can be inferred that this slip constitutes a coherent “event” with moment  $M_0$  given by

$$M_0 = GA\bar{D}_S \quad (3.1.2)$$

where  $G$  is the shear modulus and  $\bar{D}_S$  is the average slip. Hence, the energy release  $E_S$  is related approximately to the moment by

$$E_S = M_0 \bar{\tau}_e / 2G \quad (3.1.3)$$

If the cumulative number of events  $N$  having a moment greater than  $M_0$  is expressed by a power law then, in view of the proportionality between  $E_S$  and  $M_0$  expressed by equation (3.1.3), it can be postulated that

$$\log N = a - b \log E_S \quad (3.1.4)$$

Figure 3.1.7 shows a typical simulated response of the computed off-reef energy release increments when the stope width is 1m and the mining depth is 4000m. Figures 3.1.8a and 3.1.8b show plots of  $\log N$  against  $\log E_S$  for mining simulations with stope widths of 1m and 0.5m respectively. In each figure, three cases are shown corresponding to mining depths of 3000m, 4000m and 5000m. From Figures 3.1.8a and 3.1.8b it is clear that the power law relationship given by equation (3.1.4) provides a reasonable representation of the energy release statistics. It is also interesting to note that with increasing depth, the slope of these plots (parameter  $b$  in equation (3.1.4)) becomes less negative indicating an increased probability for larger size energy release “events” to occur. Contrasting Figures 3.1.8a and 3.1.8b, it is also interesting to observe that the parameter  $b$  is increased significantly when the stope width is reduced.

These results appear to be qualitatively satisfactory but rest on many ad hoc assumptions relating to the shape and dimension of the tessellation mesh, the assumed mechanism of the time relaxation process and, particularly, the mining step excavation procedure. Figure 3.1.9 compares the cumulative mobilised fracture length for two simulation sequences with a coarse mesh and a fine mesh. It is apparent that the mobilised fracture length is proportional to the mesh grid density. In Figure 3.1.10, the off reef energy is plotted against the mobilised fracture length for a number of simulation runs, using both coarse and fine mesh tessellations. This plot indicates a rough proportionality between the cumulative energy release and the mobilised fracture length.

These trends are disconcerting and indicate a lack of robustness in the 2D tessellation model for the mesh sizes used in these studies. It is clearly necessary to establish whether the fracture

length (and released energy) becomes asymptotically stable as the mesh density is increased. Define the stope width to be  $w$ , the average mesh size to be  $g$  and the mining step size to be  $s$ . In the analyses presented here it should be noted that  $s/g = 0.5$  and  $0.2$  for the fine and coarse mesh simulations respectively. Specific questions relating to the energy release and fracture length results must, however, be answered in the case when  $s/g \gg 1$ ,  $w/g \gg 1$  and  $s \approx w$ . In addition, it is necessary to evaluate the effect of geological fault set orientations on these results. The investigation of cases where  $s/g \gg 1$  places a great demand on the computational capacity of existing simulation procedures, particularly in three dimensions. It is therefore suggested that special strategies for carrying out fine level simulations should be investigated such as the concept of advancing an active region surrounding the mining face with the remaining inelastic deformations “frozen” except for larger scale fault structures. This proposal in turn demands some insight into the scaling structure of the large scale weaknesses. Seismic information such as presented by *Finney (1999)* will be essential in calibrating these models.

**Slow mining- fine grid- elastic  
(off-reef energy)**

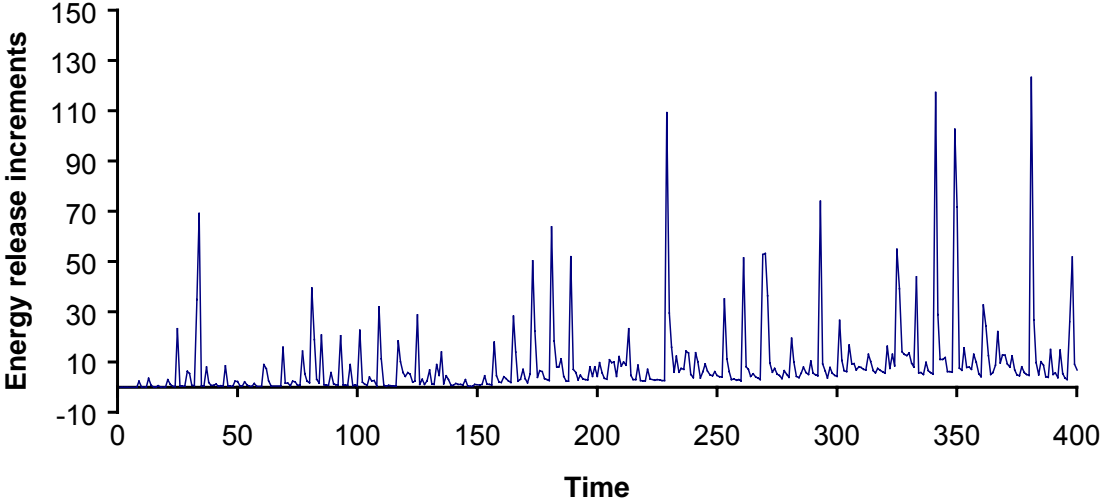
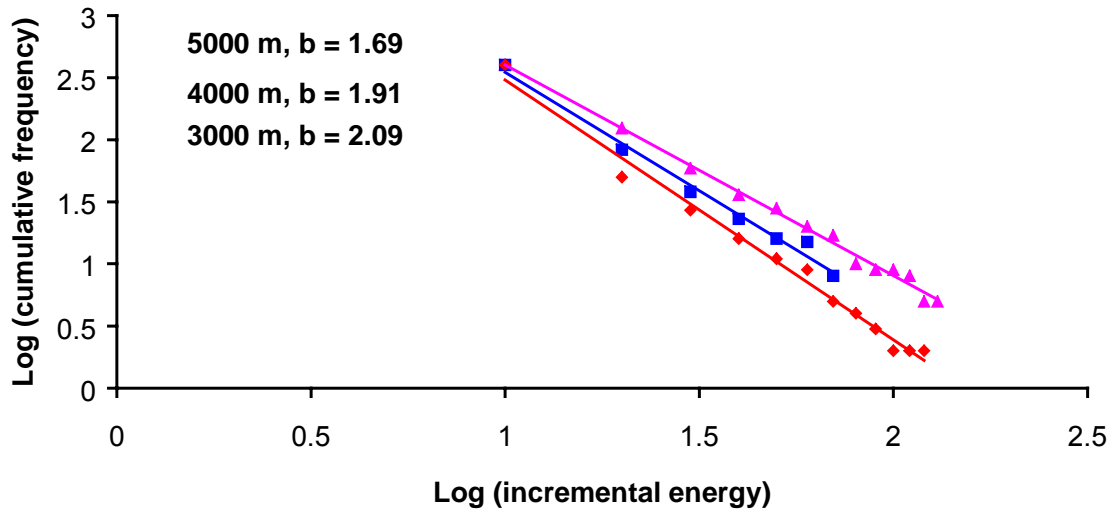


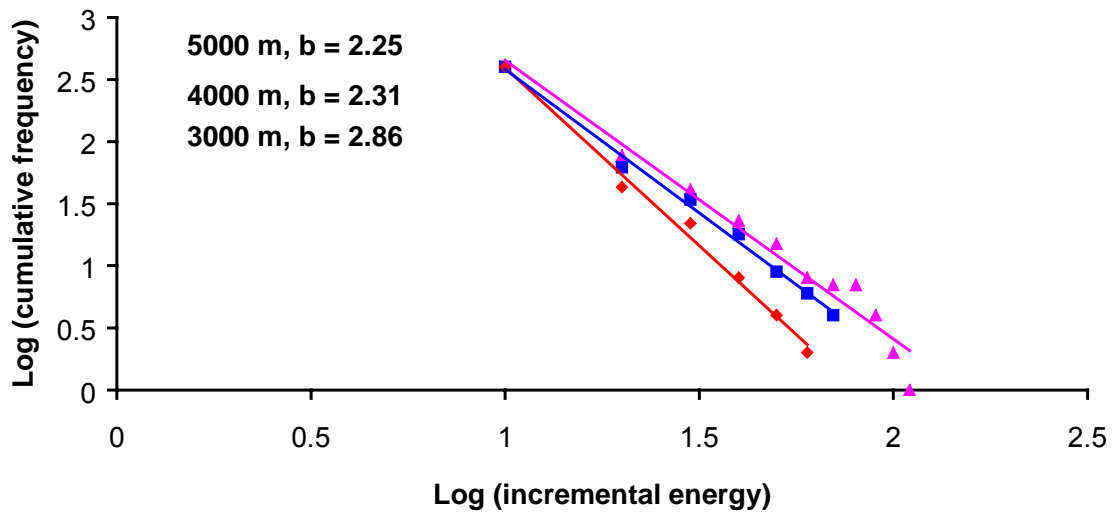
**Figure 3.1.7 Typical off-reef energy release increments observed in the simulation of mining a parallel-sided panel.**

**INCREMENTAL ENERGY RELEASE STATISTICS  
(STOPE WIDTH = 1 m)**



(a)

**INCREMENTAL ENERGY RELEASE STATISTICS  
(STOPE WIDTH = 0.5 m)**



(b)

**Figure 3.1.8** Plots of cumulative frequency against energy release increment size in mining a parallel-sided panel at different depths. (a) Stope width = 1.0m. (b) Stope width = 0.5m.



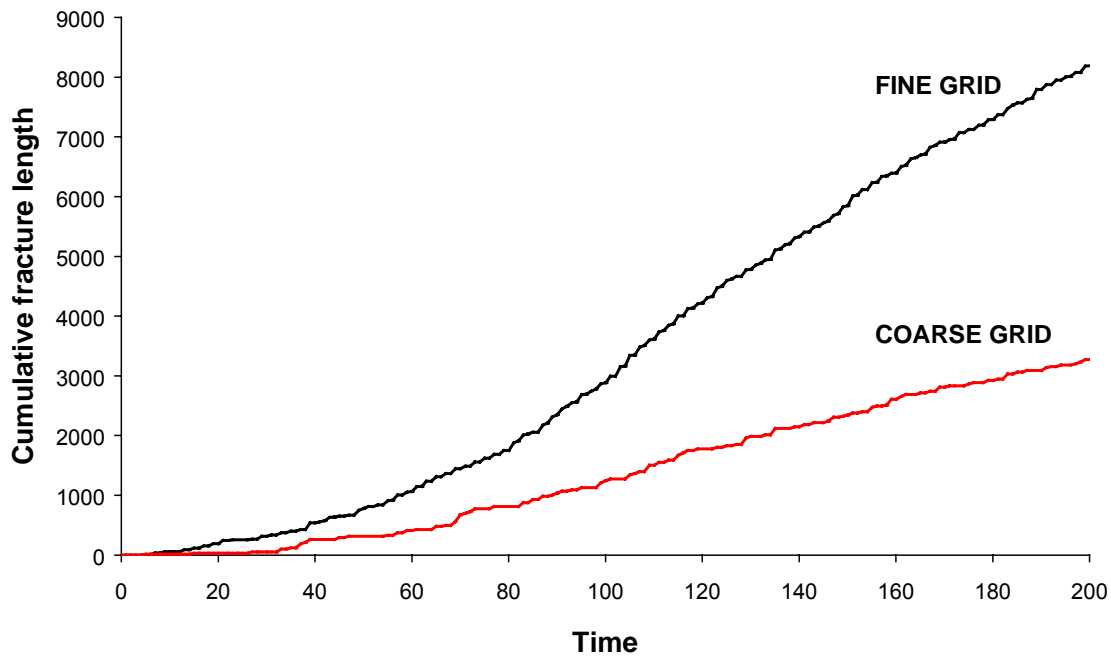


**Figure 3.1.9 Comparison of cumulative fracture length, as a function of time and excavation span, for two different tessellation densities.**

### OFF-REEF ENERGY RELEASE AS A FUNCTION OF FRACTURE LENGTH

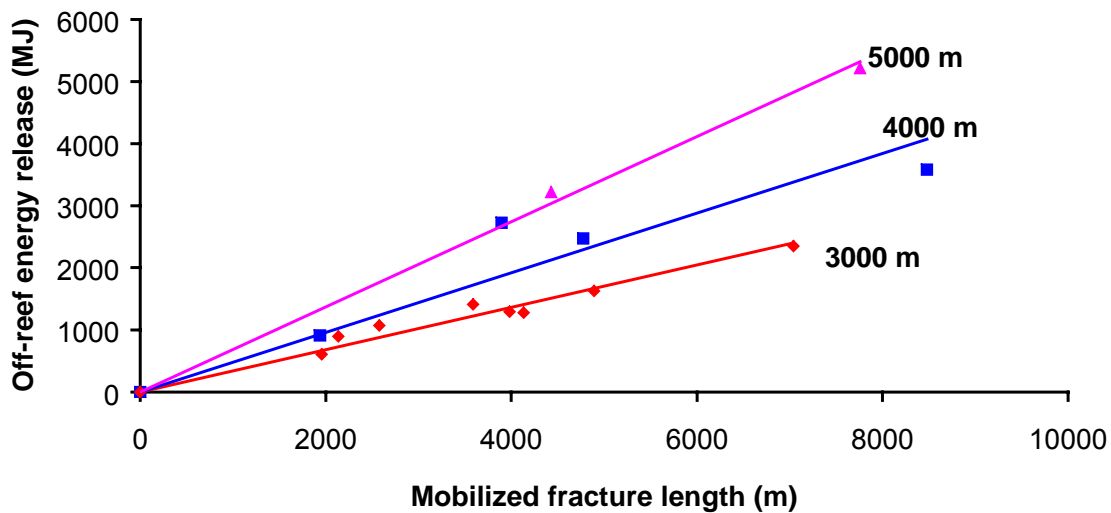


**Figure 3.1.10 Cumulative off-reef energy release plotted against cumulative fracture length for different mining depths and mesh grid densities.**

The ability of boundary element models to represent seismicity using energy based seismic magnitudes has been shown in Figure 3.1.8. However, as the DIGS tessellation program is based on the displacement discontinuity method, it is interesting to determine the moment magnitudes based on the average element slip. The method involves the construction of a grid of triangles (tessellation) around the region of interest. Applying a Delaunay tessellation procedure ensures randomness of the triangulation. Each side of the triangle is the site of a potential fracture and is assigned a failure criterion. Specification of different failure criteria in different regions permits the consideration of different strength materials. The mining is modelled as conventional boundary elements within the tessellated region. If the stress state

due to mining at any of the potential fracture sites exceeds the specified strength, the site will activate and a displacement discontinuity element will be placed at the site. The element may respond to further stress changes based on specified residual strength criteria. For fine mesh simulations, it is necessary to consider many thousands of intersecting elements. Special techniques can be employed in 2-D numerical simulations to solve these problems (see *Pierce and Napier, 1995*). However, it has proved to be possible to only solve problems that have limited mine spans, in the order of tens of metres.

A computer program was written to post process the output from a tessellation analysis to provide parameters that relate to the parameters that are used to describe seismic data. The parameter of interest was the seismic moment related to each cracking event. An event is assumed to be either a slip on a pre-existing fault, or the emplacement of a new crack. The seismic moment  $M_o$  can be expressed as

$$M_o = G\bar{A}\bar{D} \quad (3.1.5)$$

where  $G$  is the Shear modulus,  $A$  the area of the slip and  $\bar{D}$  is the average slip. An equivalent parameter must be determined for the numerical modelling results. The shear modulus of the intact rock is known. The area of the slip must be related to an assumption regarding the crack shape. In the two-dimensional plane strain model, the width out of plane is 1m. The crack can be assumed to be an infinite slit and then the area  $A$  can be related to the crack length  $L$  as

$$A = L \times 1\text{m} \quad (3.1.6)$$

or, the crack could be considered to be penny shaped, in which case the area

$$A = \pi L^2/4. \quad (3.1.7)$$

The slip can be determined easily from the current magnitude of the displacement discontinuity and can be obtained directly from the boundary element output. In order to determine the slip on a crack related to a particular mining step  $n$ , the change in slip is calculated as

$$dDD^n = |DD^n - DD^{n-1}| \quad (3.1.8)$$

where  $DD^n$  is the average shear displacement discontinuity at mining step  $n$ , and  $DD^{n-1}$  is the average shear displacement discontinuity for the previous mining step. The numerical moment is obtained by substituting equations 3.1.6 and 3.1.8 into equation 3.1.5. Then

$$M_{o(num)}^n = GLdDD^n \quad (3.1.9)$$

The cumulative frequency of events having a moment greater than or equal to a particular value can be plotted on a log-log scale to represent the numerical equivalent of the Gutenberg-Richter relationship.

The fracture pattern resulting from a tessellation analysis of a carbon leader stope after 28 mining steps of 1 m, is shown in Figure 3.1.11. The stope has a strong hangingwall layer, overlain by a weak layer representing the Green Bar. The footwall layers are all an intermediate strength. The material properties are given in Table 3.1.2. All sites in a horizontal layer have the same strength and there is no random variation of the strength of the sites.

The moments were calculated for all fractures using equation 3.1.9. The parting planes were assumed to slip in an aseismic manner and so slips along the partings are not included. The frequency magnitude plots for mining steps 7 to 24 are shown in Figure 3.1.12. The plots are reasonably linear indicating that there is a power law response occurring, even though there is no specified logarithmic variation in strength distribution. This is a significant outcome that suggests that the tessellation approach is suitable for the numerical representation of seismicity.

The slope of the line is related to the b-value of the Gutenberg Richter relationship, but cannot be compared directly due to the different definitions of the components of the seismic moments. As the mining progresses, there are relatively more smaller events and the plot becomes more linear. The maximum moment increases to a maximum and then tends to oscillate, as shown in Figure 3.1.13.

The limit on the maximum value of the moment is probably a result of relating the moment to the element length. In the model, the minimum and maximum element lengths are limited in size by numerical modelling considerations. Application of a scheme that considered the connections between sliding cracks to determine an effective sliding length would produce a different frequency magnitude relation.

A second tessellation analysis, using a different fracture criterion was tested to confirm the frequency - moment relationship. The model, shown in Figure 3.1.14, has a selection of weak flaws randomly spaced throughout the mesh. All other crack sites have a specified tensile strength and an effectively infinite compressive strength. The results are very similar to those of the Mohr Coulomb analysis. This suggests that the tessellation approach does provide a frequency moment relationship based on a power law. The cumulative frequency of fractures is lower and is related to the lower fracture density. The relative increase in smaller fractures at longer spans is also evident.

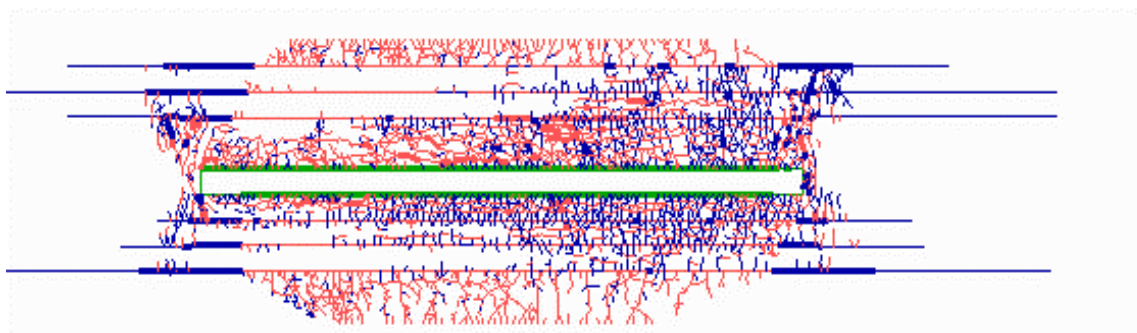


**Figure 3.1.11 Result of tessellation analysis of Carbon Leader stope using Mohr Coulomb failure criteria.**

**Table 3.1.2 Material properties for Carbon Leader tessellation**

Rock type	UCS	Cohesion	Friction angle		tensile strength
	MPa		MPa	initial	mob
Hangingwall Quartzite	320	18	52	30	5
Footwall Quartzite	200	18	43	25	5
Greenbar	180	18	32	20	5

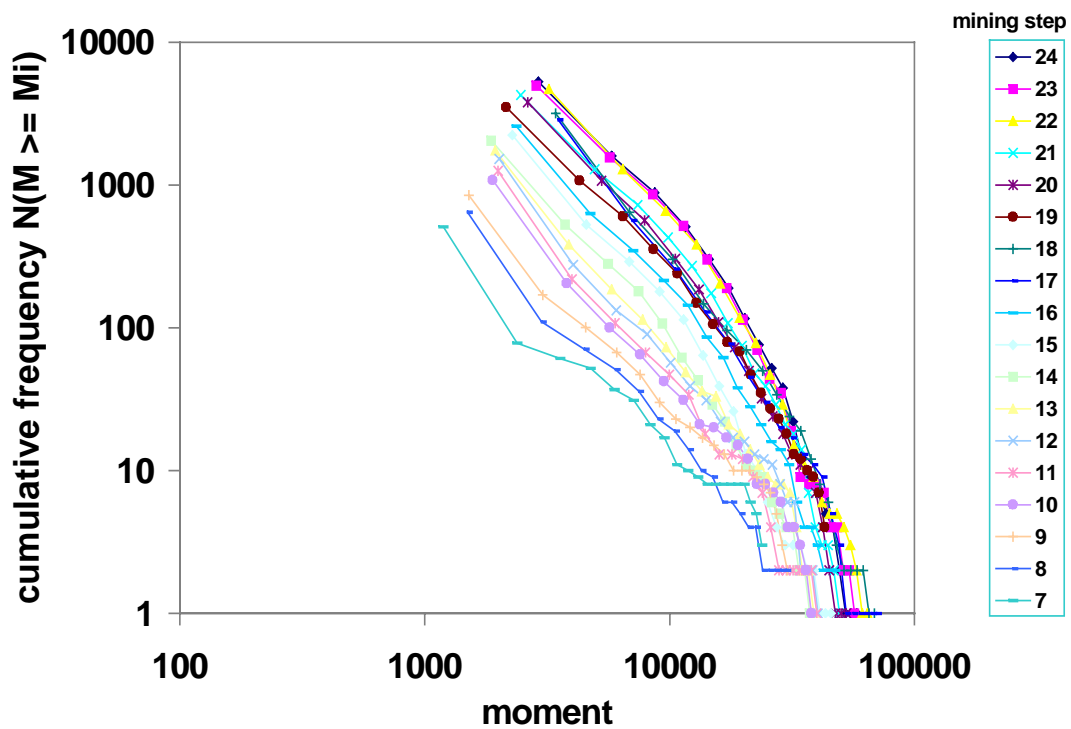


**Figure 3.1.12** Frequency - Moment plots for the tessellation analysis of a Carbon Leader stope using Mohr Coulomb failure criteria.

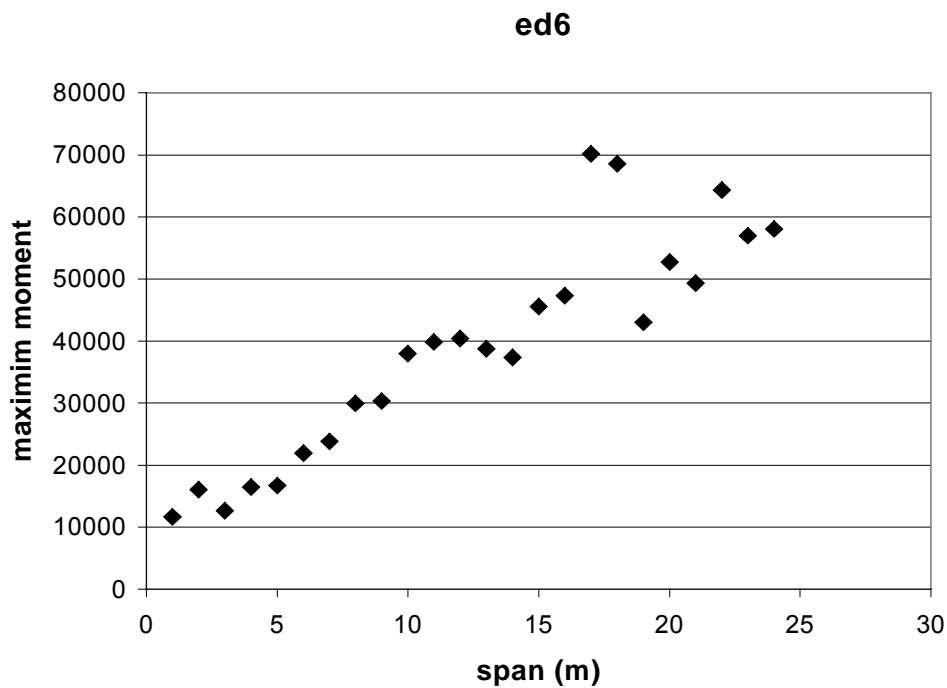


**Figure 3.1.13** Maximum moment with span for the tessellation analysis of a Carbon Leader stope using Mohr Coulomb failure criteria.

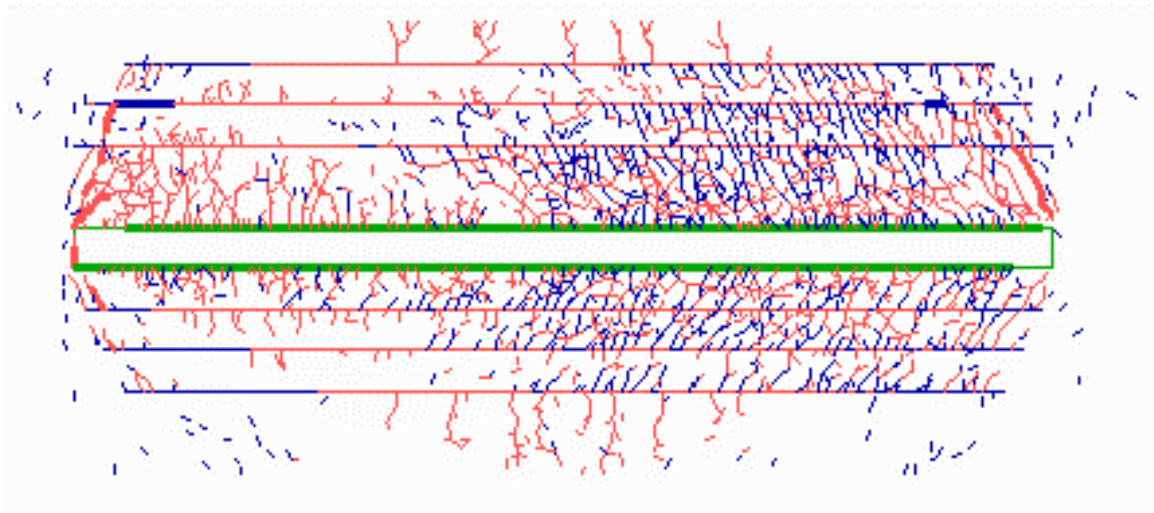


Figure 3.1.14 Result of tessellation analysis of Carbon Leader stope using weak flaw and tension crack model of failure.

Table 3.1.3 Material properties used in tessellation using weak flaw and tension crack model

	Flaw Cohesion	Cohesion C	$\phi$	$C_m$	$\phi_m$	Tensile strength
	MPa	MPa	deg	MPa	deg	MPa
HW Quartzite	5	1E5	52	10	30	5
Green Bar	5	1E5	32	10	20	5
Green Bar Parting			30		30	
FW Quartzite	5	1E5	45		25	5
Parting Planes			40		40	

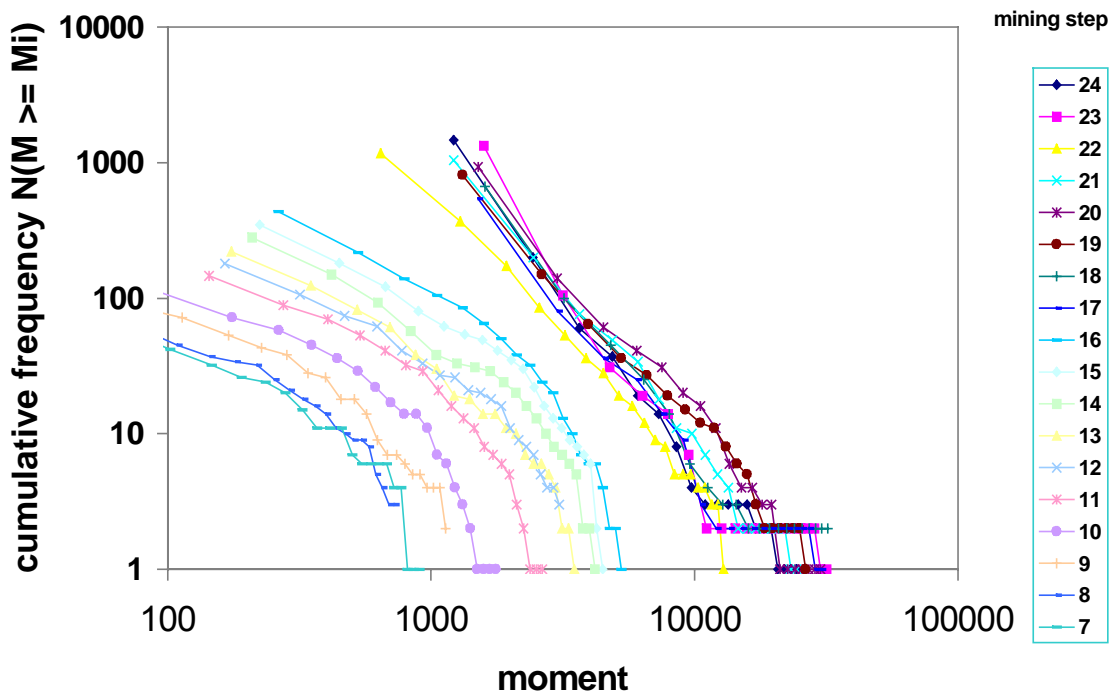


Figure 3.1.15 Frequency - Moment plots for the tessellation analysis of a Carbon Leader stope using weak flaw and tension crack model of failure.

The tessellation approach of modelling, using displacement discontinuity elements, has been shown to produce a power law distribution of equivalent seismic moments, and is therefore suitable for consideration as part of a package that integrates numerical modelling with seismic data. The technique must still be evaluated in three-dimensional analyses. The numerical counterpart to the seismic moment can be defined in a number of ways and so the magnitude of the numerical b-value will not necessarily correspond with that observed from seismic data.

## **Modelling the frequency-magnitude relationship - MAP3D on geological structure**

### **Objectives:**

Initial investigation to determine whether a boundary element numerical code is capable of generating a power law seismic event size distribution along a geological structure.

As part of SIMGAP 303 "Mine layout, geological features and seismic hazard", an engineering method is being developed and tested to evaluate the seismic potential of geological structures as a function of mine layout. Theoretical aspects and objectives of the engineering method are outlined in detail in *Lachenicht and van Aswegen (1999)* and *Lachenicht (in prep.)*. Initial investigation aimed to determine whether a boundary element numerical code is capable of generating a power law seismic event size distribution along a geological structure.

In summary, application of the method firstly permits layout options to be optimised against proposed design principles, and secondly, utilising a calibrated model, the seismic potential along the geological structure can be statistically estimated for future progressive mining. The engineering method explicitly incorporates the simulation of discrete seismic events through time. This is achieved through the concept of the 'asperity model' implemented into a numerical simulation where the distribution of strength on a geological structure is divided into two categories (*Dragoni, 1990*), namely:

- 'failed' areas creeping in a continuous and aseismic fashion according to a viscoplastic flow law
- 'asperity' areas of high strength, failure of which would result in abrupt slip, producing discrete seismic events

All the event characteristics are recorded through time by the numerical model, allowing for the calculation of the seismic event source parameters, and the eventual analysis of seismicity.

The mechanics of the simulation of discrete seismic events incorporates:

- the 'asperity model'
- viscoplastic displacement loading of asperities
- a slip-function representing unstable asperity failure
- quasi-static analyses (inertial effects are ignored)

The mechanics of the simulation of seismicity as a result of the occurrence of discrete seismic events through time is a function of the spatial heterogeneity of asperities. This controls:

- the resulting co-seismic deformation
- the frequency-magnitude relation
- seismic radiation
- triggering of the failure of adjacent asperities through the ensuing co-seismic deformation caused from static stress changes of the discrete seismic event

A model calibration process is integral to the successful application of the method. The detailed calibration incorporates strength heterogeneity across randomly distributed asperities, i.e. a power law strength distribution is imposed across the asperities. This strength distribution is altered on an iterative basis until the b-value of the modelled Gutenberg-Richter frequency-magnitude relation approximates the observed relation.

In order to set up the numerical simulations, software code was developed to generate and randomly distribute a number of asperities along a surface (*Hofmann, 1999*). The software permits different types of asperities to be specified to represent, for example, asperities of different strengths. The number of asperities assigned to each category is decided outside of

the software, for example using a power-law distribution of strengths of asperities. For each type of asperity, grid-elements along the surface are selected at random (using an appropriate random number generator), and the positions thereof are written to file and directly incorporated in the engineering analysis.

### **Problem statement:**

The analysis method outlined (original modelling methodology) utilises a boundary element numerical code and is essentially a comparative tool useful for delineating effects on the modelled event size distribution resulting from design layout changes. The method is based on the principle of assuming a power law strength distribution of asperities in such a way as to roughly emulate the observed power law seismic event size distribution (asperity sizes are constant), i.e. assuming a 'power law' results in the generation of a 'power law'.

The fundamental premise of this assumption is derived from observations of nature. *Scholtz (1998)* refers to fault populations that have a power law length distribution in which the exponent of the (cumulative) distribution is approximately  $-1$ . The contact area between two fractal surfaces follows an unique power law (*Chakrabarti and Stinchcombe, 1999*). Seismic events occurring in nature are observed to adhere to a power-law size distribution known as the Gutenberg-Richter relation (*Scholtz, 1990*).

Results from an asperity method developed by *Kemeny and Hagan (1992)* showed a very realistic pattern of earthquake rupture, with reasonable source parameters, the proper magnitude-frequency behaviour, and the development of characteristic earthquakes. The simulation method implemented was based around an imposed distribution of asperity sizes and strengths.

One could argue that asperities of a constant strength, randomly distributed across a geological structure would naturally result in different size asperities forming (power-law distribution?) from the natural density dispersion of asperities. The question arises, would this generate a power law seismic event distribution.

Thus, is it possible for a boundary element model to generate a power law seismic event size distribution without prior assumption of a power law strength distribution across the asperity spectrum? If this is true, firstly what factors present within the model attribute to the power law seismic event size distribution, and secondly, how does the modelled event size distribution compare to actual seismic observations.

### **Initial concept:**

In order to test this hypothesis, the modelling methodology and analysis routines built around the asperity model need to be redesigned. This revised modelling methodology could then be tested through the modelling of an actual case study, comparing the modelled to the observed over identical time periods.

The revised modelling methodology consists of:

- Incorporate the relevant geological structures and appropriate mining sequence into a three dimensional boundary element model (Map3d)
- Place constant size asperities randomly over the structures surface
- Cover approximately 30% of the structures surface area with asperities in order to constitute a seismogenic structure (*Gusev, 1989*) (Figure 3.1.16)
- The remainder of the structures surface is assigned a constant viscosity and failure strength, and is assumed to creep aseismically
- All the randomly placed asperities are assigned a constant strength value

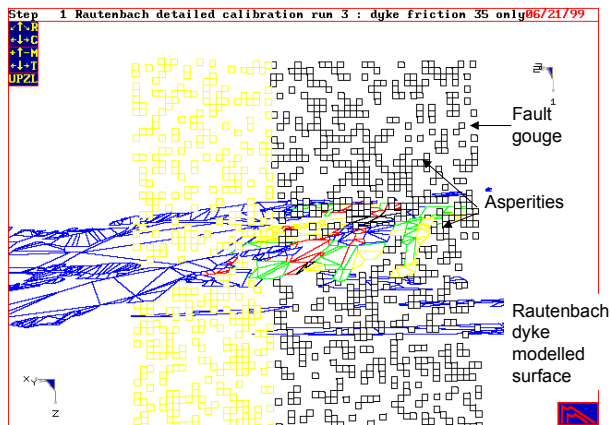


**Figure 3.1.16 Randomly placed asperities (constant strength)**

- Where asperities touch each other as a result of the random placement the sides are glued together, i.e. increased size asperities are created from the randomly placed asperities without incorporating any clustering procedures. Figure 3.1.17a,b shows an example of the resultant asperity placement over the structure surface. It can be noted that a size distribution of asperity sizes, consisting of many small asperities and few large asperities, naturally results from the randomly placed asperities.

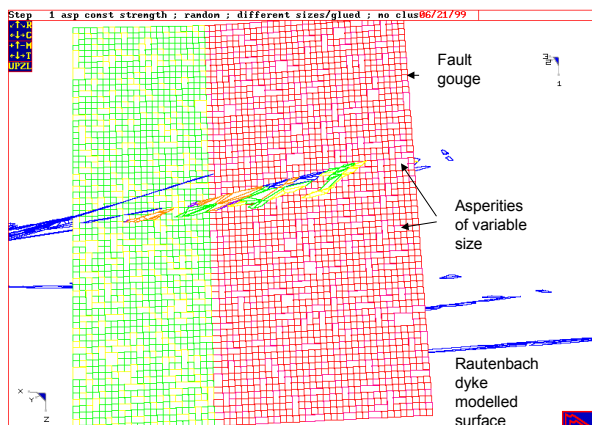


**Figure 3.1.17a Resultant asperity placement over the structure surface – asperities (variable size) and surrounding gouge.**

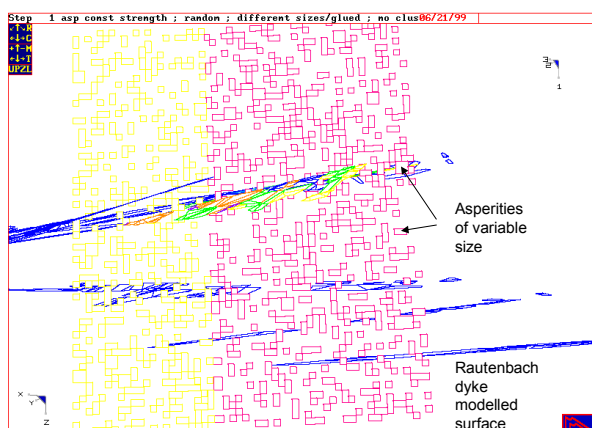


**Figure 3.1.17b Resultant asperity placement over the structure surface – asperities only.**

- Delineate and filter observed seismic events occurring along the structure.
- Analyse the observed seismic events creating the structures cumulative frequency magnitude relation over the specified time period.



- Numerically run the mining steps for the identical time period of the observed data.
- Implement filtering methods for the modelled data calculating a cumulative frequency-magnitude relation resulting from the failure of the asperities through time.
- Analyse the modelled cumulative frequency-magnitude relations and compare to the observed data.

The initial random distribution of asperities on a fault and their clustering highlight the analogy with the percolation model and critical phase transitions.

Some physical systems can exist in different phases. Crystals can melt, liquids can crystallise or evaporate. Some ceramic materials behave as insulators at room temperature but, if immersed in liquid nitrogen they suddenly become superconductors. The general properties of these processes are:

1. They occur only for certain values of the physical parameters controlling the behaviour of the system such as temperature, pressure, concentration etc. The values of the control parameters for which a given physical system undergoes a phase transition are called critical values.
2. Near the phase transition point the correlation length of the physical system diverges as a (negative) power of the distance of the control parameter to the corresponding critical value. Similar power-law behaviour near a phase transition is observed for other physical quantities. The corresponding exponents in these power laws are called critical exponents.
3. One of the central facts in the theory of phase transitions is that while the critical exponents are unique for each concrete system, there are many seemingly different types of physical systems which share the same values of the critical exponents. For such systems it is said that they form a class of universality.
4. The power-law behaviour of the observable quantities of a physical system near a phase transition point is directly related to the phenomenon of scaling (the preservation of the form of a function when the argument is scaled by a factor). It is an observed fact that many quantities related to seismic activity exhibit scaling.

A concept of a considerable following is the belief that many real physical systems are spontaneously driven to a critical state by their internal complexity. This statement is known in the literature as Self-Organised Criticality (SOC). Apart from some very attractive theoretical aspects to SOC it is of little practical importance to the mining industry.

One way of studying critical phenomena is on simple mathematical models. One such model with wide-ranging applications is the percolation model. It is perhaps the simplest system which can undergo a phase transition. The model is formulated on a regular lattice. The role of the control parameter is played by a real number  $p$  called the occupation probability. For a given value of the occupation probability one can generate many instances of the lattice system by assigning either 0 or 1 to the sites of the lattice according to the rule: the value of 1 is assigned to the current site with probability equal to  $p$ . If a site is not assigned the value 1 it is set to zero. Obviously the control parameter  $p$  must be a number between zero and one.

The main objects of interest in the study of percolation models are the connected clusters. A connected cluster is a set of occupied sites in which each site has at least one nearest neighbour which is also occupied. An infinite cluster (or spanning cluster) is a connected cluster which includes occupied sites from the opposite ends of the lattice. The model is said to percolate for a given value of the control parameter (the occupation probability  $p$ ) if it has a spanning cluster. Obviously the model does not percolate for  $p=0$  or even for  $p>0$  but very small. On the other hand the model will certainly percolate for  $p=1$  or  $p<1$  but very close to 1. The question is: how does the probability for forming a spanning cluster vary with  $p$ ? It turns out that the variation of this probability is not a smooth and monotonous increase from zero to one.

Instead the percolation model exhibits a phase transition with the corresponding critical point being the percolation threshold, that is the value of the occupation probability for which the model can for the first time generate a spanning cluster. For a two-dimensional site-percolation model the percolation threshold is near the value 0.5927.

The implications of the above result for modelling the distribution of asperities on a fault is that the control parameter of their density distribution must be below the percolation threshold unless one wants the asperities to percolate and form clusters which span the whole fault or system of faults.

**Observations:**

The case study analysed is that of the northern portion of the Rautenbach dyke at Great Nologwe mine, AngloGold. Figure 3.1.18 shows the Map3d three-dimensional model built including the mining steps surrounding the dyke and the geological structure itself. The dyke is a narrow, steeply dipping structure (approximately 80 degrees).

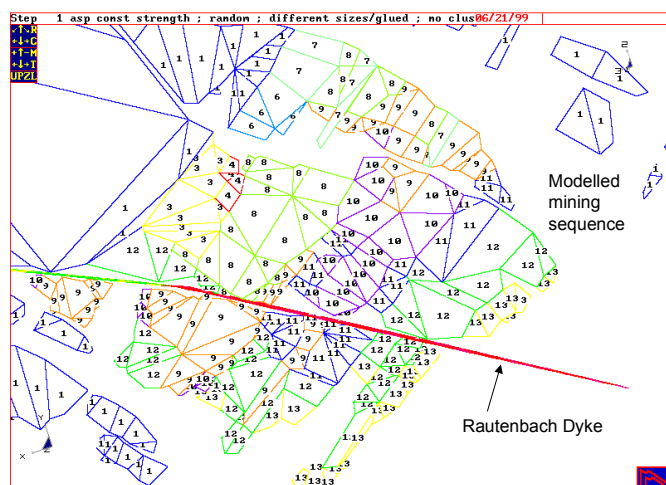


**Figure 3.1.18** Map3d three-dimensional model of the Rautenbach dyke and surrounding mining

Figure 3.1.19 shows a plot of the cumulative frequency-magnitude relation derived from the observed data in the immediate vicinity of the Rautenbach dyke. The data was accumulated from applying a spatial filter of 40m into the hangingwall and footwall along the interpreted dyke surface and an event filter of greater than magnitude 1 (increase the accuracy of the data utilised).

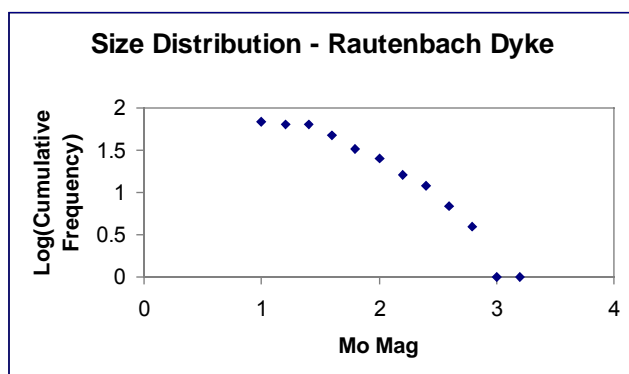


**Figure 3.1.19** Cumulative frequency-magnitude relation derived from observed data along the Rautenbach dyke

**Analysis results:**

The resulting modelled data is analysed firstly by subtracting filter runs in order to derive the co-seismic slip occurring for each time step, and secondly through separating individual events along the structure per time step (model step). The resultant discrete seismic events are influenced by the lower limit of slip utilised. That is to say, if a lower filter limit of 1mm is utilised, an increased number of smaller events and fewer larger events are delineated. For a lower limit of 0.1mm the smaller events get absorbed into larger events, affecting the event size distribution. This problem occurs as a result of the overall analysis methodology utilising large time steps (originally designed as a practical engineering analysis tool). Hence, the time stepping of the occurrence of small events is lost in the analysis results.

Application of the original filtering method presented possible problems – the presence of varying block sizes possibly affected the subtraction, sorting and filtering routines.

During the analysis the following filtering methods were tested:

- Original method:
  - Delineate events by filtering across the structure surface for co-seismic slip > 0.1mm.
  - Moment calculation:  

$$M_o = d\sigma_{\text{average}} * dV_{\text{source volume}}$$
 Where:  
 $M_o$  = seismic event moment (Nm)  
 $d\sigma_{\text{average}}$  = average stress change of asperities failing over event source volume (Pa)  
 $dV_{\text{source volume}}$  = event source volume (m<sup>3</sup>)  
 This is implemented for each discrete event derived from the filtering method implemented.
- New method 1:
  - Filtering across the structure surface for co-seismic slip > 1mm. This permits an increased number of smaller events to be separated from the overall deformation across the structure. A new filtering method is applied resulting in the quantitative values associated with each event being output to separate files for analysis.
  - Moment calculation:  

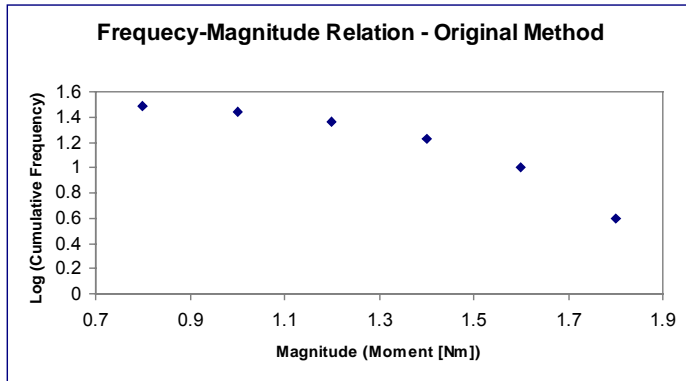
$$M_o = d\sigma_{\text{average}} * dV_{\text{source volume}}$$
 Where:  
 $M_o$  = seismic event moment (Nm)  
 $d\sigma_{\text{average}}$  = average stress change of asperities failing over event source volume (Pa)  
 $dV_{\text{source volume}}$  = event source volume (m<sup>3</sup>)  
 This is implemented for each discrete event derived from the filtering method implemented.
- New method 2:
  - Filtering across the structure surface for co-seismic slip > 1mm. This permits an increased number of smaller events to be separated from the overall deformation across the structure. A new filtering method is applied resulting in the quantitative values associated with each event being output to separate files for analysis.
  - Moment calculation:  

$$M_o = \mu * \sum_{i=1}^n (A_i * u_i)$$
 Where:  
 $M_o$  = seismic event moment (Nm)  
 $\mu$  = rigidity (3e10 Pa)  
 $A_i$  = Area of grid block i (m<sup>2</sup>)  
 $u_i$  = coseismic slip of grid block i (m)  
 $n$  = number of grid block delineated for the seismic event  
 This is implemented for each discrete event derived from the filtering method implemented.

From the seismic event data, cumulative frequency-magnitude relations are derived for each method tested.

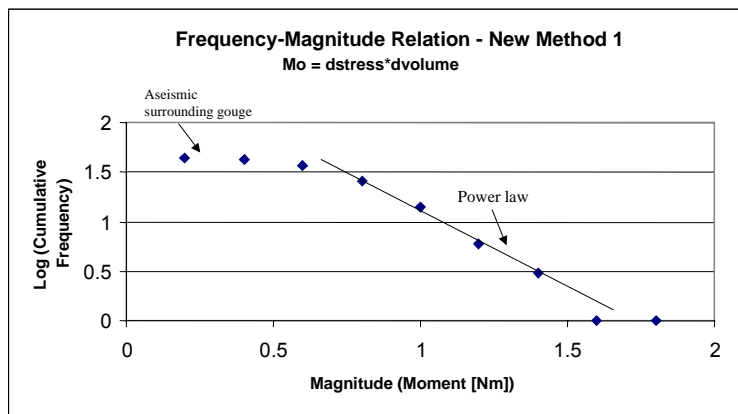
Firstly the results are analysed to determine whether a power-law seismic event distribution is present, and secondly compared for the different methods applied. Lastly, the modelled results are compared to the observed seismic event size relation to obtain an initial estimate of the differences between the modelled and observed.

Figure 3.1.20 shows the cumulative frequency magnitude relation derived from the application of the original method. Slight indications of a power law event distribution are present. Two problems are identified with this analysis. Firstly the filtering method could be experiencing problems as a result of the variable size asperities present – the method was designed to be utilised for a constant block size. Secondly the slip filter value of 0.1mm is too low to permit delineation of smaller events i.e. they are absorbed into the larger events.

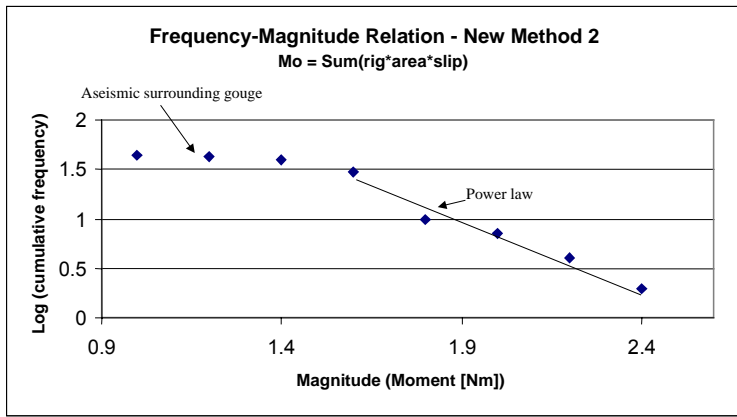


**Figure 3.1.20 Cumulative frequency-magnitude relation – original method**

Figures 3.1.21a & b show the cumulative frequency magnitude relations derived from the application of new methods 1 and 2. Much stronger indications of the presence of a power law seismic event distribution are present. This results from the increased filter value of 1mm and secondly the improved filter method adequately catering for the variable block sizes present within the analyses undertaken.

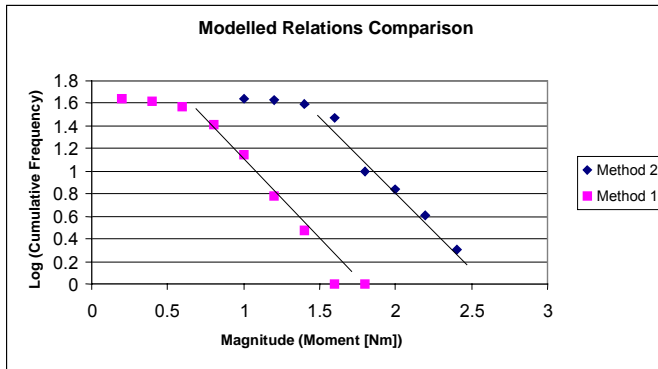


**Figure 3.1.21a Cumulative frequency-magnitude relation – new method 1**



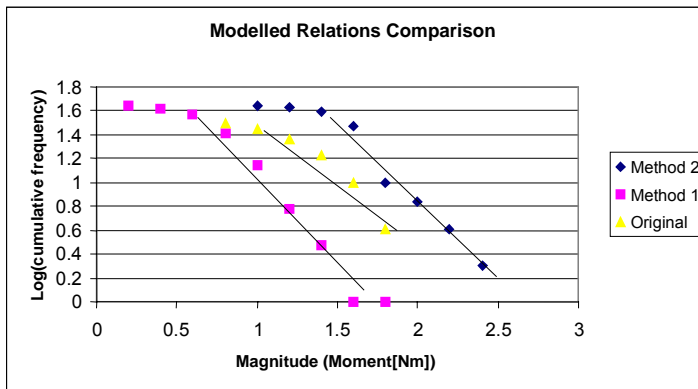
**Figure 3.1.21b Cumulative frequency-magnitude relation – new method 2**

Figure 3.1.22 compares the two methods. It can be noted that both methods result in similar b-values. The offset in the moment magnitude range results from the moment calculation method and can be simply adjusted for through the application of a factor.



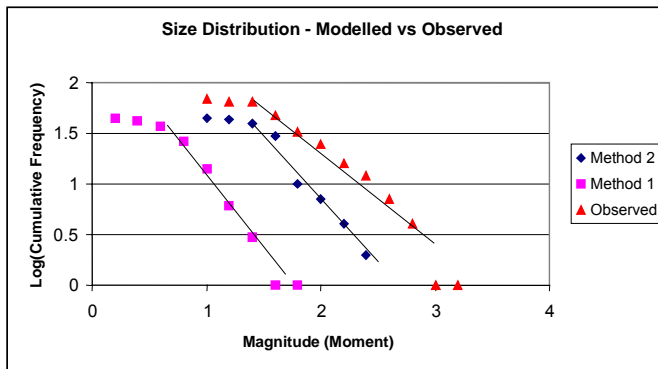
**Figure 3.1.22 Cumulative frequency-magnitude relation comparison – new methods 1 & 2**

Figure 3.1.23 compares all three methods confirming the problems associated with the original method (altered b-value, magnitude range offset and limited power law distribution).



**Figure 3.1.23 Cumulative frequency-magnitude relation comparison – all methods**

Figure 3.1.24 compares the modelled results of methods 1 and 2 to the observed data. This shows encouraging first results in terms of the overall observed power law response of the structure, although a substantially different b-value is observed.



**Figure 3.1.24 Cumulative frequency-magnitude relation comparison – modelled versus observed**

The power law event size distribution emulated through the model results from a combination of:

- the failure of different size asperities through time and the resultant static stress changes
- the random asperity locations
- the inherent asperity size distribution formed from the random asperity placement (strength heterogeneity)
- the viscoplastic flow of rock across the structures surface loading asperities
- the viscoplastic deformation retardation as a result of asperity placement
- the normal and shear stress changes spatially and temporarily occurring over the structures surface

Figure 3.1.25 shows the co-seismic slip resulting from the seismic events occurring across the structure surface at a particular time step. This co-seismic slip is derived from the failure of different size asperities failing at different locations over the structure surface for that particular step. This demonstrates the aforementioned concepts.

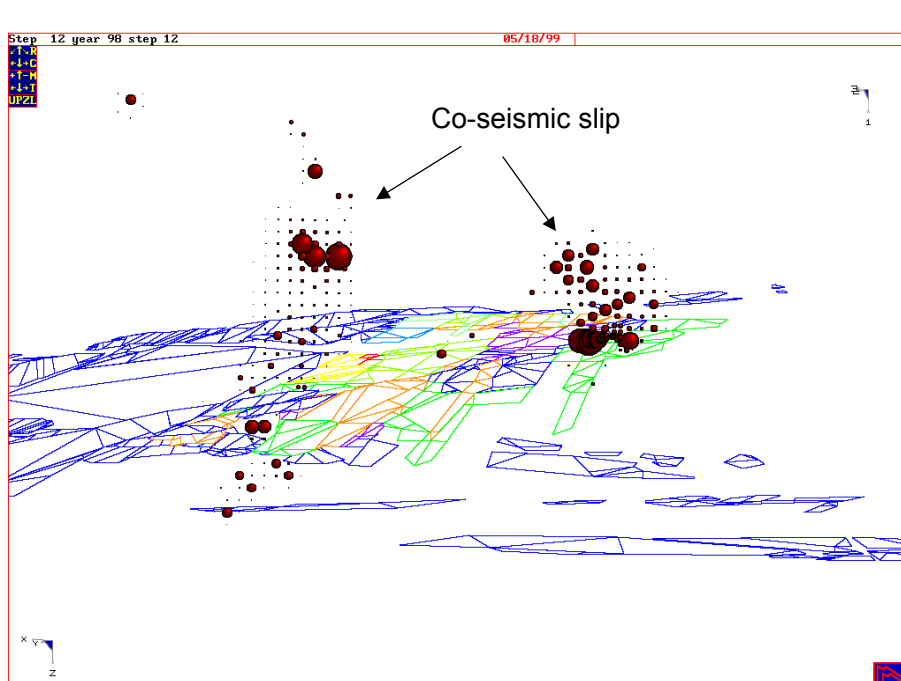


**Figure 3.1.25 Coseismic slip occurring over the Rautenbach dyke for a particular model step**

### Conclusions and future work:

The major conclusions from the initial work undertaken are:

- Boundary element codes are capable of generating a power law seismic event size distribution along geological structures without the prior assumption of a power law strength distribution.
- The analysis methods applied affect the modelled cumulative frequency-magnitude relation:
  - The minimum co-seismic slip utilised to delineate individual events controls the number of individual smaller events.
  - The original filtering method resulted in incorrect results due to its inability to adapt to variable size grid blocks.
  - The different moment calculation methods applied (new methods 1 and 2) showed a constant offset in the cumulative frequency magnitude relation. This can be adjusted for through the application of a factor to the calculated moment. The calculated b-values were similar.
- For the parameter assumptions utilised in the analyses conducted, a significant difference was observed between the modelled and observed b-values of the cumulative frequency-magnitude relation. However, the spread of the data over the magnitude range was of a similar order.

A number of outstanding issues remain that should be answered as part of future work on the integration method. These include:

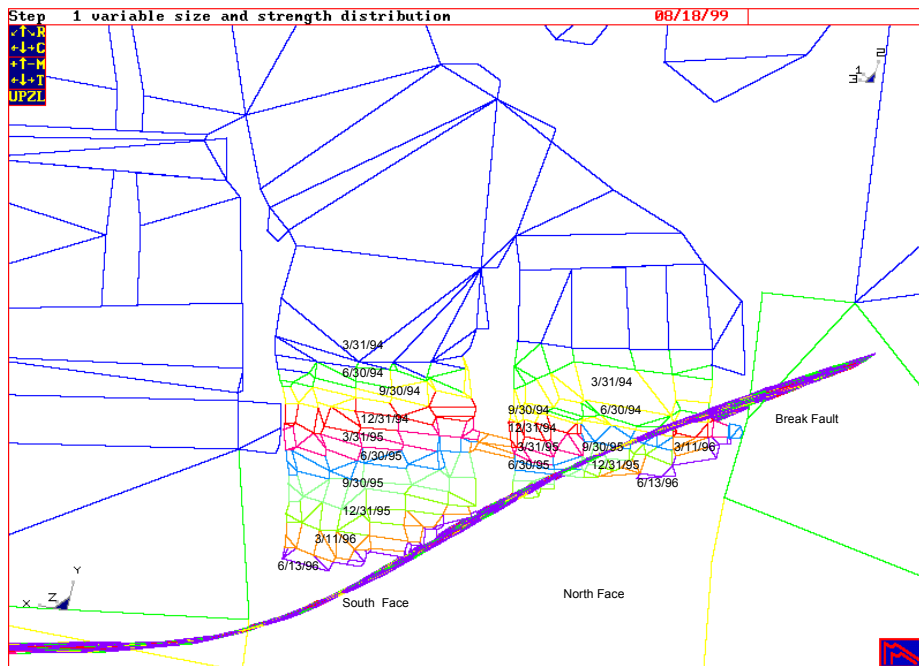
- Different random distributions of asperities over the structure surface must be tested and its affect on the resultant cumulative frequency-magnitude relation documented.
- Different material properties for both asperities and surrounding gouge must be tested and the resultant effects documented.
- The filter methods must be rechecked and analysed for different size asperities.
- The effect of including a different base grid size must be documented.
- The effects of different asperity 'glueing' procedures must be analysed.
- The effect of clustering asperities should be analysed, i.e. asperities not directly adjacent to each other 'gravitate' together.
- The effect of inserting a limited 'power law strength distribution' in addition to the random asperity placement and subsequent 'glueing' of asperities must be documented. This could possibly be closer to a natural underground environment.
- Additional model calibration strategies are currently being investigated.
- The affect of excluding 'glueing' adjacent asperities together. Will a power law be generated from the failure of constant size and strength asperities through time?
- Alter the time-steps utilised in the model to enable individual events occurring through time to be clearly delineated.

Lastly, the important question to be answered is, 'Can the seismicity generated from a model roughly emulate the observed after model calibration?' That is to say, can the modelled and observed cumulative frequency-magnitude relations form similar power law distributions with similar b-values?

To attempt to answer the most important of these questions, namely, 'can the modelled and observed cumulative frequency-magnitude relations form similar power law distributions with similar b-values?', a case study analysis of the TauTona 336 area case study has been performed.

### *Background information – TauTona 336 area*

The area of interest includes a series of longwalls situated in TauTona Mine, referred to as the TauTona 336 area. Two lagging longwalls are mining a pillar created between two previously mined longwalls. In so doing, the longwalls are mining directly towards a fault (the Break fault).



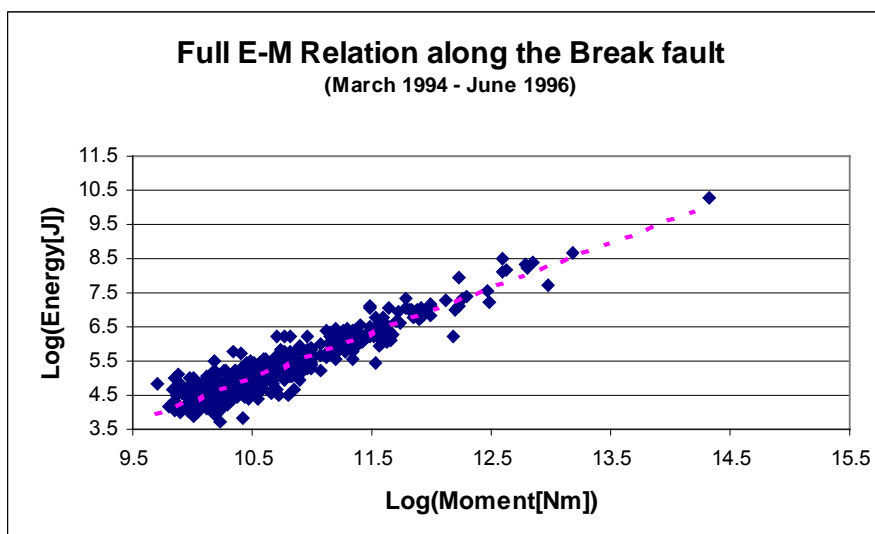
**Figure 3.1.26 TauTona 336 area (Break fault) case study**

Figure 3.1.26 shows the inferred Break fault surface (geological interpretation) and the historic mining layout and sequence used for the numerical analysis. For the purpose of the analysis the mining sequence is broken down into quarterly mining steps.

The aim of the analysis is to attempt firstly to understand and secondly to simulate the seismic response of the Break fault as a result of the approaching longwalls situated in the highly stressed pillar.

Analysis of the seismic data on the Break fault

The seismic events were selected, within the analysis time frame, along the three-dimensional geological structure from the seismic database (events located 40m in the hangingwall and footwall along the inferred surface). Figures 3.1.27 and 3.1.28 show the E-M Relation and Gutenberg-Richter cumulative frequency-magnitude plots derived from seismic data recorded along the Break fault.





**Figure 3.1.27 E-M Relation along the Break fault**

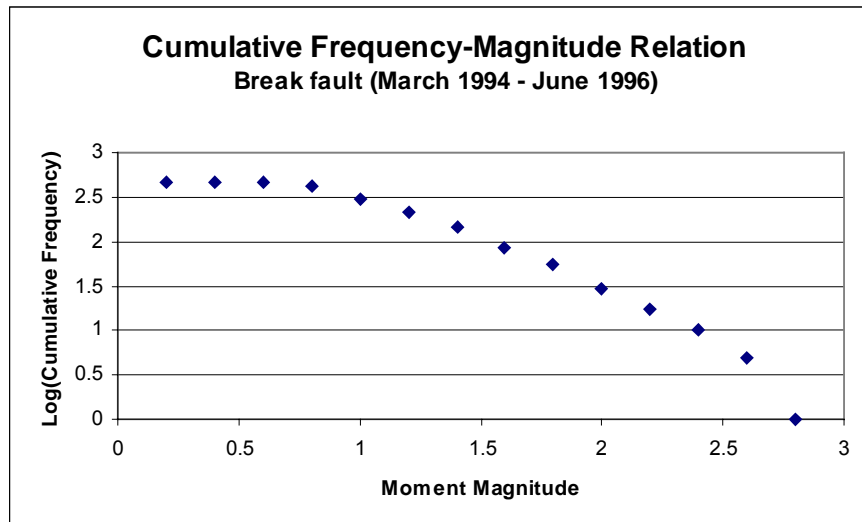


**Figure 3.1.28 Cumulative Frequency-Magnitude Relation from the Break fault**

The relation utilised to calculate the moment magnitude in Figure 3.2.28 is:

$$\text{Magnitude (Mo)} = 2/3 \log_{10}(\text{Mo}) - 6.1$$

Where Mo is the moment source parameter calculated in the seismic database.

### Experiment design overview

In both case studies partially calibrated models are utilised. It will not always be possible to attain a fully calibrated model when undertaking design analyses. The purpose behind this exercise is to test the degree of correspondence between the modelled and observed frequency-magnitude relations within the limits of the model calibration.

In accordance with the analysis methodology implemented (*Lachenicht and van Aswegen, 1999*), model calibration is attained when:

- Quantitative deformation values occurring along the structure roughly approximates observed deformation values,
- Rough correspondence is attained between the modelled and observed contours of deformation across the structure in both space and time.

Deformation is chosen as the calibration parameter. This is due to the fact that deformation values can be easily and relatively accurately inferred from the seismic data. In addition, it is the simplest parameter to numerically emulate whilst ensuring that the model is deforming at the correct locations during the correct time frame. This provides the foundation for more complex analyses as viscoplastic displacement loading forms the fundamental driving mechanism for the analysis and interpretation of seismicity.

The model deformation values are derived from a heterogeneous strength model. The detailed concepts behind the calibration procedure are outlined in *Lachenicht (in prep.)*. The procedure utilised to calibrate the model is:

- The Break fault surface and appropriate mining sequence are incorporated into a three dimensional boundary element model (Map3d)
- The surface is divided into a grid consisting of square blocks
- Different analysis time spans, fault strength and fault rheological properties are tested until an initial correlation is attained between the modelled and observed fault deformation through space and time (iterative process)

- The homogeneous strength model is initially used to calibrate the model due to its simplicity, but once a degree of correlation is achieved, the procedure can immediately be extended to encompass asperities and hence the explicit simulation of seismicity:
- Constant size asperities are randomly distributed over the Break fault
- Approximately 30% of the Break fault is covered with asperities
- The remainder of the Break fault is assigned a constant viscosity and failure strength, and is assumed to creep aseismically
- Where asperities touch each other, within individual planes, as a result of the random placement, the sides are glued together, i.e. increased size asperities are created from the randomly placed asperities without incorporating any clustering procedures. Figure 3.1.30 shows the resultant asperity placement over the Break fault's surface. It can be noted that a size distribution of asperity sizes, consisting of many small asperities and few large asperities, naturally evolves from the randomly placed asperities.
- In addition to the natural size distribution derived from the random asperity placement, an additional strength distribution is assigned to the asperities in accordance with the asperity size. This increases the strength of the larger asperities, and hence the spread of the modelled seismic data.

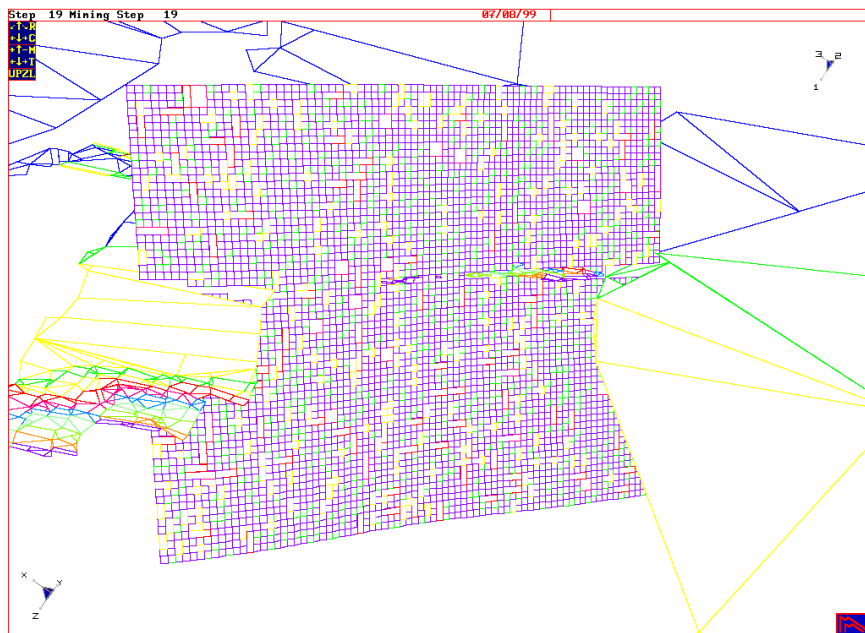


**Figure 3.1.30 Resultant asperity placement over the Break fault's surface**

The detailed comparisons between the modelled and observed deformation values along the Break fault, through both space and time, are included in *Lachenicht (in prep.)*, and only the seismic events derived from the partially calibrated models are examined in this report.

### Experiment results

#### Observed seismic data

An analysis of the cumulative frequency-magnitude relation derived from the observed seismic data selected along the Break fault yields the plots shown in Figures 3.1.31 and 3.1.32. Figure 3.1.31 shows the cumulative frequency-magnitude relation analysed using a robust straight line fit (*Vetterling et al., 1986*) over a selected portion of the relation. Figure 3.1.32 analyses the relation utilising the Aki method (*Aki & Richards, 1980*). The line fits yield b-values of 1.17 and 1.12 respectively.

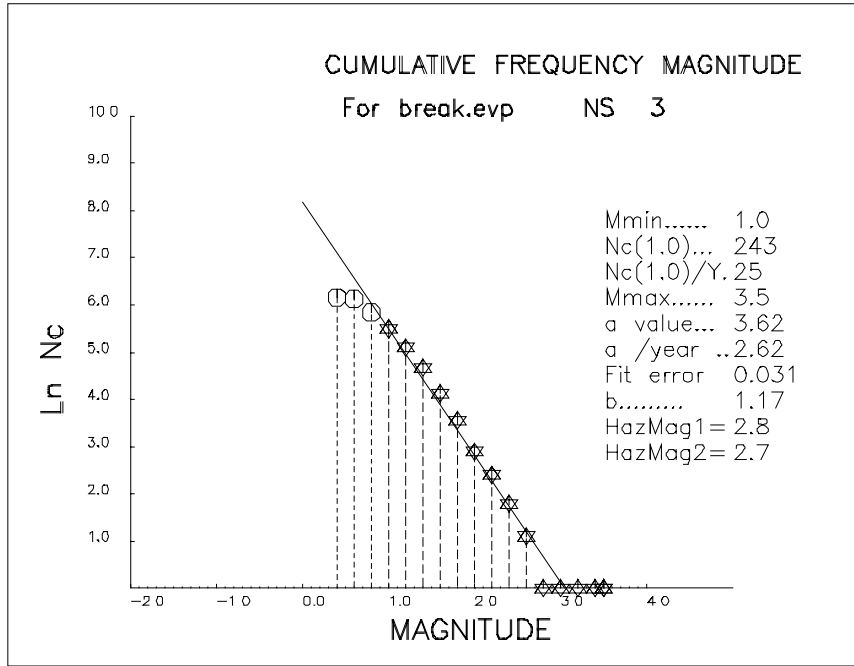


**Figure 3.1.31 Observed seismic data analysis – Robust straight line fit**

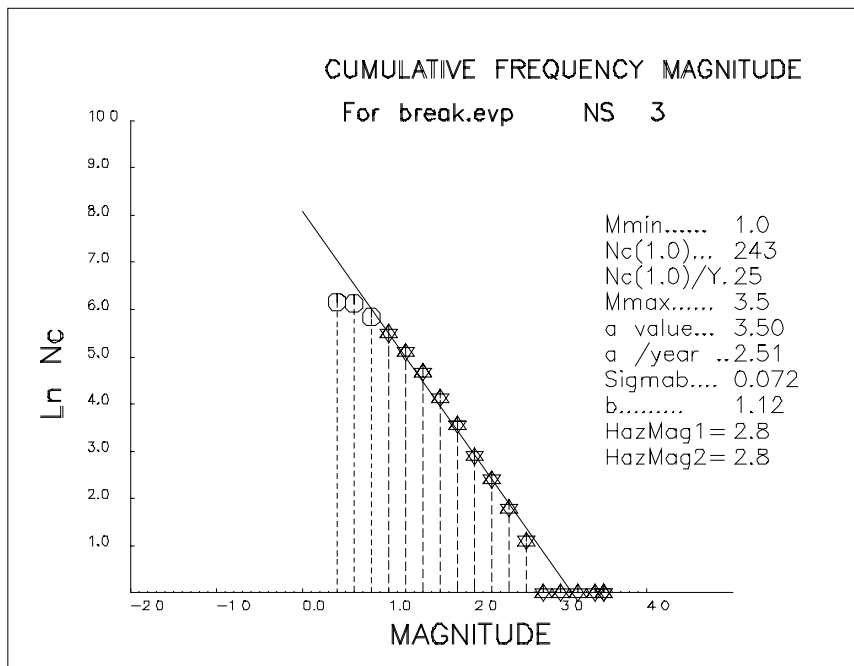


**Figure 3.1.32 Observed seismic data analysis – Aki method**

Case study 1 - modelled seismic data

Table 3.1.4 lists the parameter assumptions utilised in the numerical analyses to achieve the partial model calibration for case 1.

**Table 3.1.4 Case 1 - parameter assumptions utilised to attain partial model calibration**

Parameter	Parameter Assumption
Gouge Constitutive Model (Break fault)	Mohr-Coulomb
Gouge friction (Break fault)	25-18 degrees (strain softening)
Gouge viscosity (Break fault)	1e16 Pa·sec
Gouge cohesion (Break fault)	0 MPa
Gouge Young's Modulus	40GPa
Gouge Poisson's Ratio	0.2
Asperity distribution (Break fault)	Random / Spatial clustering (80x80m blocks)
Asperity strength distribution (Four asperity sizes from spatial clustering)	Friction 45-18 (size 1) Friction 48-18 (size 2) Friction 51-18 (size 3) Friction 54-18 (size 4)
k-ratio	0.5 (constant in all directions)
Vertical in-situ stress gradient	0.027 MPa/m
Host rockmass Constitutive model	Elastic
Host rockmass Young's Modulus	70GPa
Host Rockmass Poisson's Ratio	0.25
Time interval	3 months / model step
Modelled mining sequence	As specified in Figure 2.1
Closure of excavations	In excess of 2m closure permitted
Additional structures	Not included for simplicity

The comparison of the modelled versus observed deformation for case study 1 essentially yields:

- The deformation along the Break fault is under estimated in the model. This could be a function of the displacement taper function applied when estimating the observed displacement (apparent strain method).
- The deformation along the Break fault occurs predominantly lower in the footwall than indicated from the observed seismicity. This could be a function of z location error.

An analysis of the cumulative frequency-magnitude relations derived from the modelled seismic data of case study 1 yields the plots shown in Figure 3.1.33 and 3.1.34.

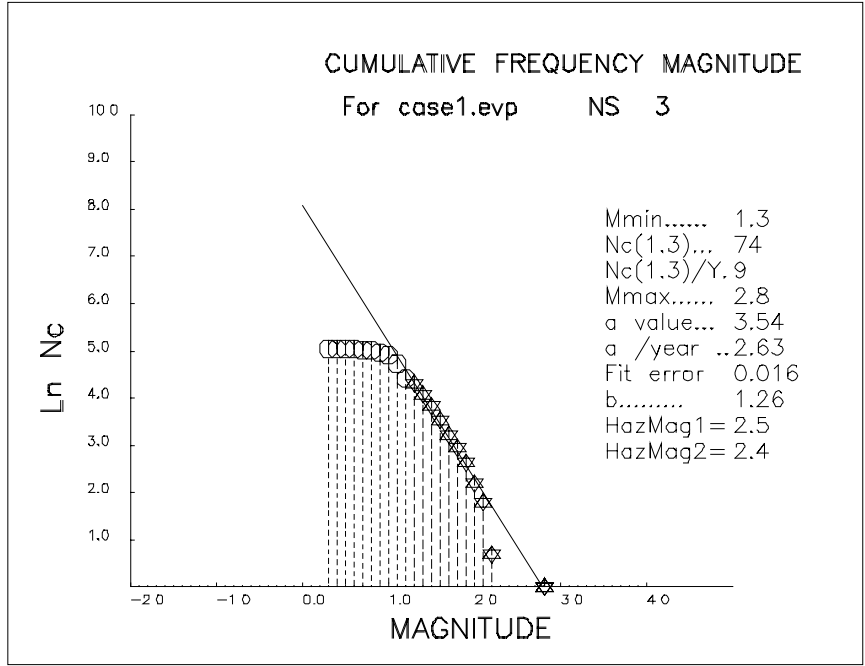


**Figure 3.1.33 Case study 1: modelled seismic data analysis – Robust straight line fit**

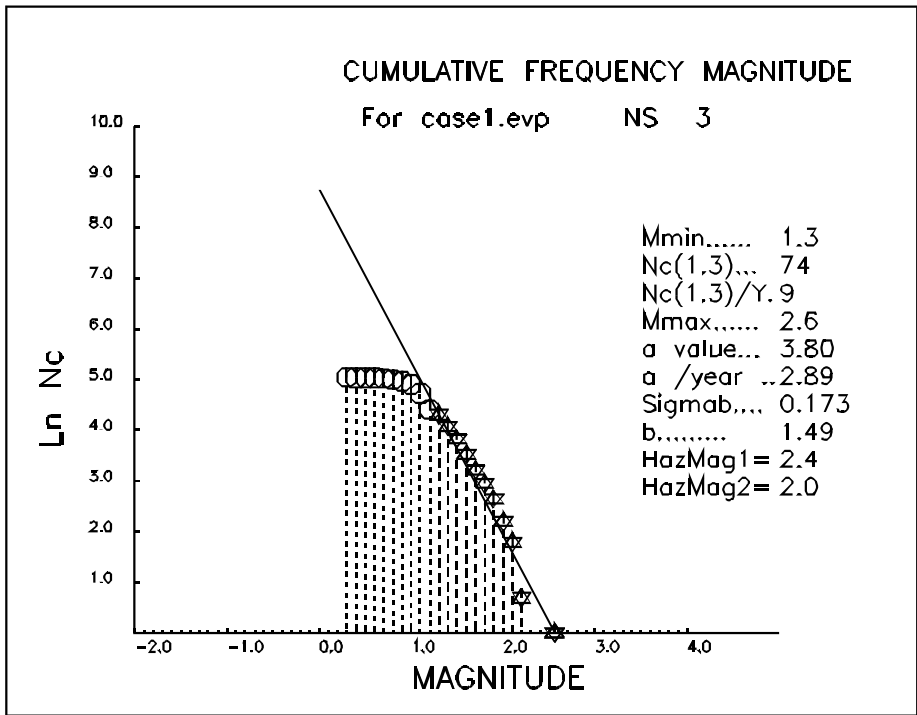


**Figure 3.1.34 Case study 1: modelled seismic data analysis – Aki method**

The line fits yield b-values of 1.26 (versus 1.17 from the observed data) and 1.49 (versus 1.12 from the observed data) respectively. Hence, the difference in b-values between the modelled and observed data is 0.09 (robust line fit) and 0.37 (Aki method). Practically, b-values derived from seismic data sets can be interpreted as being significantly different if differences between b-values of the order of 0.1 are calculated. Hence, the modelled cumulative frequency-magnitude relation of case 1 can be said to be significantly different to the relation derived from the observed seismic data.

However, when examining the relative differences between the relations, it is of interest to note that the b-value derived from the modelled data is higher. This is indicative of a stiffer system (Mendecki, van Aswegen and Mountfort, 1999), and is in accordance with the earlier deformation comparison.

The relative differences between the two methods are highlighted in Figure 3.1.35 using a least squares fit (0.2 bin ranges).

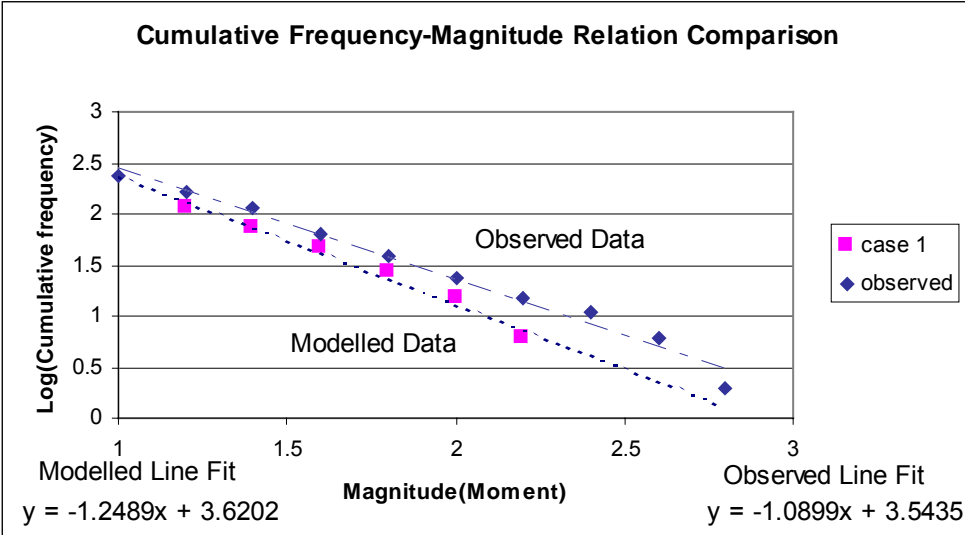


Figure 3.1.35 Case study 1: comparative modelled and observed data b-values

### 3.1.1. Case study 2 - modelled seismic data

Table 3.1.5 lists the parameter assumptions utilised in the numerical analyses to achieve the partial model calibration of case study 2.

**Table 3.1.5 Parameter assumptions utilised to attain the partial model calibration**

Parameter	Parameter Assumption
Gouge Constitutive Model (Break fault)	Mohr-Coulomb
Gouge friction (Break fault)	30-15 degrees (strain softening)
Gouge viscosity (Break fault)	4e15 Pa·sec
Gouge cohesion (Break fault)	0 MPa
Gouge Young's Modulus	40Gpa
Gouge Poisson's Ratio	0.2
Asperity distribution (Break fault)	Random / Spatial clustering (80x80m blocks)
Asperity strength distribution (Four asperity sizes from spatial clustering) Higher friction areas where model versus observed asperity failures significantly differ (iterative basis)	Friction 45-18 (size 1) Friction 48-18 (size 2) Friction 51-18 (size 3) Friction 54-18 (size 4)
k-ratio	0.7(east-west)/0.3(north-south)
Vertical in-situ stress gradient	0.027 MPa/m
Host rockmass Constitutive model	Elastic
Host rockmass Young's Modulus	70Gpa
Host Rockmass Poisson's Ratio	0.25
Time interval	3 months / model step
Modelled mining sequence	As specified in figure 13.1 and 13.8
Closure of excavations	Maximum of 1m closure permitted
Additional structures	Portion of the Grey fault intersection with the Break fault

The comparison of the modelled versus observed deformation for case study 2 essentially yields:

- The deformation along the Break fault is roughly emulated in the model. Various parameters in the model are changed to allow the overall system to soften sufficiently, and hence increase the modelled deformation along the Break fault.
- The deformation along the Break fault still occurs predominantly lower in the footwall than indicated from the observed seismicity. Again, this could be a function of z location error. However, in this analysis, this deformation is restricted due to the growth of higher friction areas (stronger asperities).

An analysis of the cumulative frequency-magnitude relation derived from the modelled seismic data of case study 2 yields the plots shown in Figure 3.1.36 and 3.1.37.

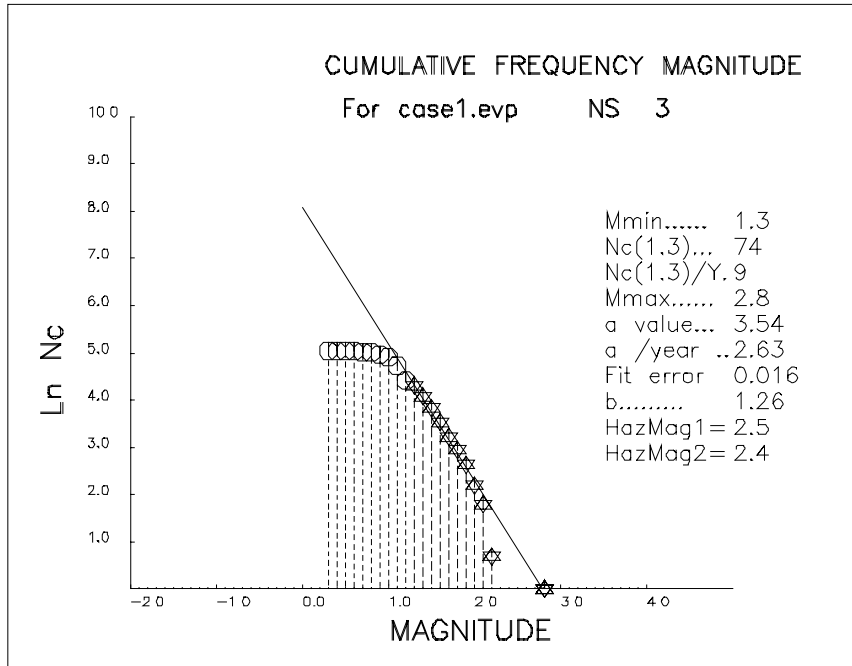


**Figure 3.1.36 Case study 2: modelled seismic data analysis – Robust straight line fit**

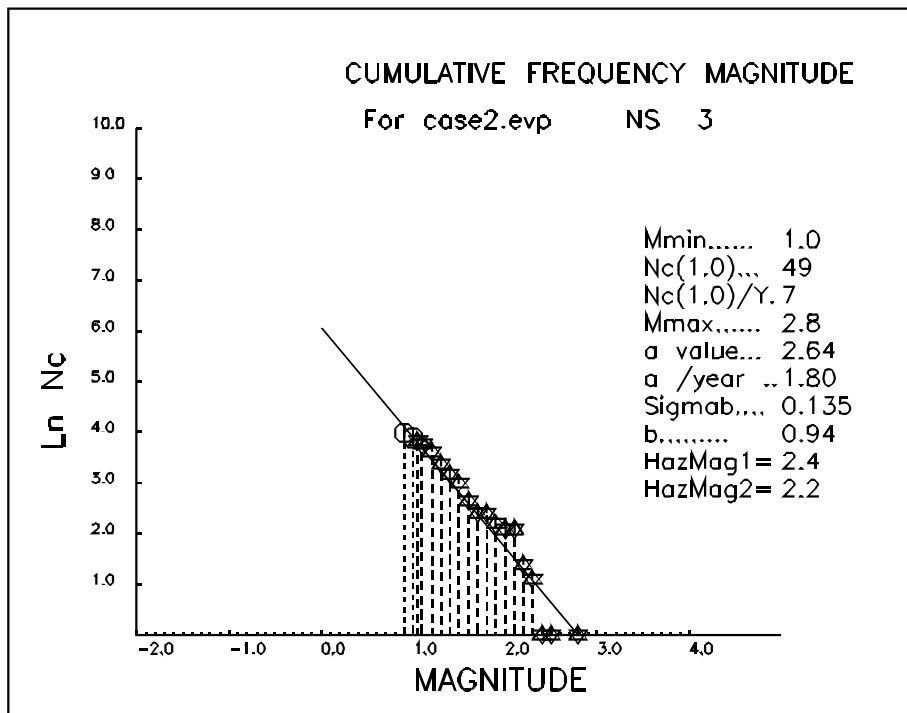


**Figure 3.1.37 Case study 2: modelled seismic data analysis – Aki method**

The line fits yield b-values of 0.85 (versus 1.17 from the observed data) and 0.94 (versus 1.12 from the observed data) respectively. Hence, the difference in b-values between the modelled and observed data is 0.32 (robust line fit) and 0.18 (Aki method). Again the difference between the modelled (case 2) and observed b-values can be interpreted as being of significance.

However, examining the relative differences between the relations, the b-value derived from the modelled data is lower. This is indicative of a relatively softer system (*Mendecki, van Aswegen*



and Mountfort, 1999). This is again in accordance with the earlier deformation comparison – the reduction in the overall system stiffness in order to permit increased deformation to occur along the Break fault. However, the resultant frequency-magnitude relation comparison indicates that the modelled system stiffness degradation was excessive, dropping the b-value to below that of the observed. This occurred even though a relatively good qualitative comparison was achieved between the modelled and observed deformation along the Break fault.

The relative differences between the modelled and observed b-values are highlighted in Figure 3.1.38 using a least squares fit (0.2 bin ranges).

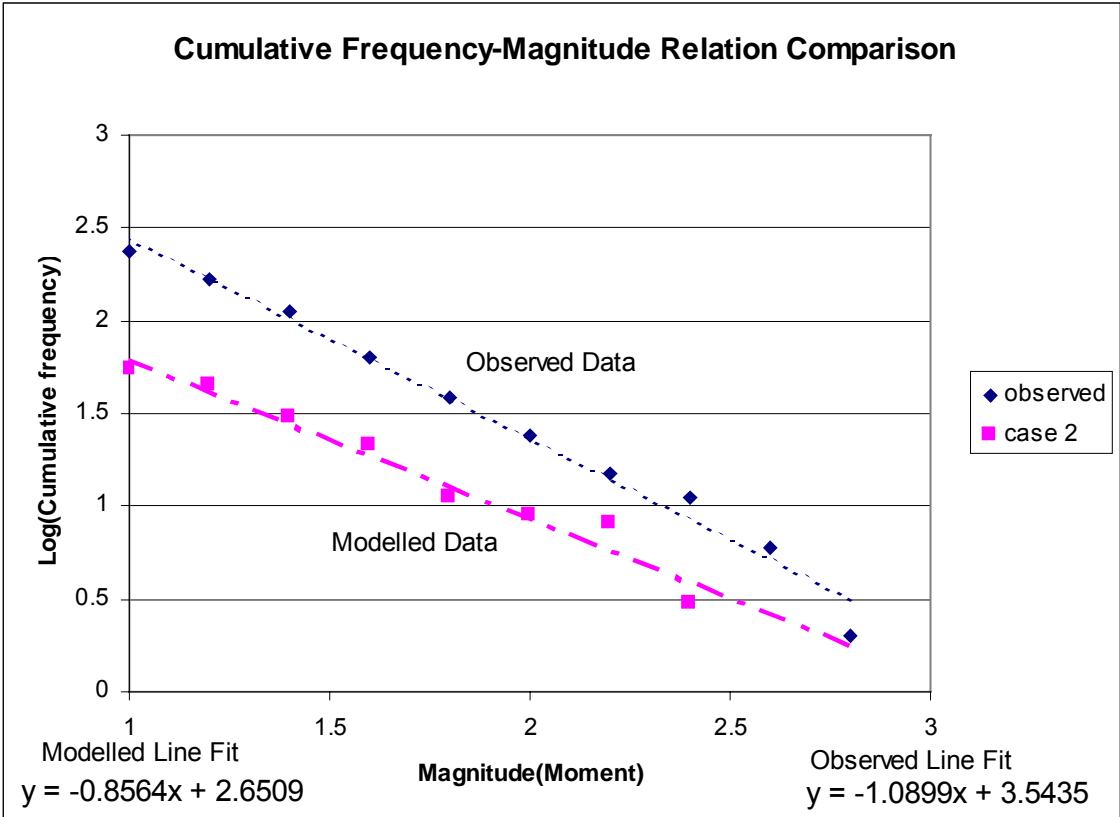
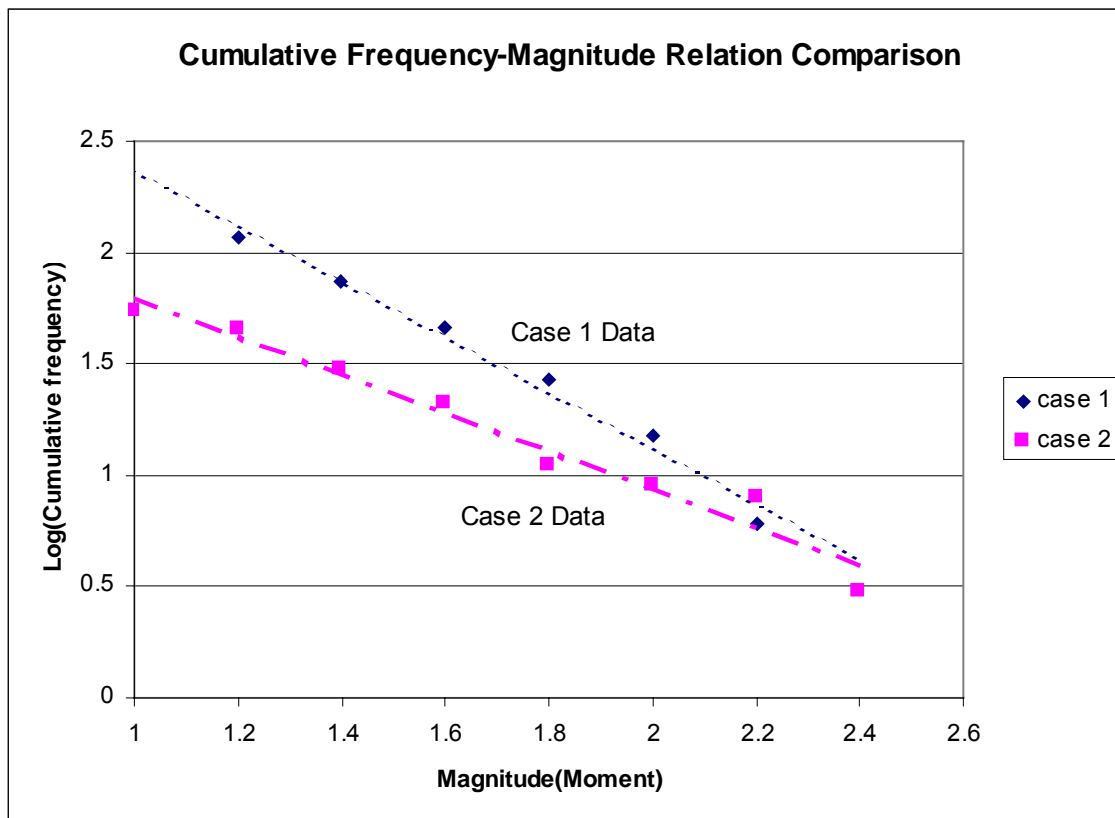


Figure 3.1.38 Case study 2: comparative modelled and observed data b-values

### 3.1.2. Case study 1 versus case study 2 – Relative changes

Figure 3.1.39 compares the b-values derived from case study 1 and case study 2. The relative changes are indicative of a stiffer system (case1) versus a softer system (case 2), and are in accordance with the comparative changes made to the model during the model calibration exercises.



**Figure 3.1.39 Comparison of  $b$ -values derived from case studies 1 & 2**

### Conclusions

The main objective of the analyses undertaken was to determine whether modelled and observed cumulative frequency-magnitude relations could form similar power law distributions with similar  $b$ -values. A direct comparison between the  $b$ -values derived from the two modelled case studies and the observed data indicate the  $b$ -value differences to be significant ( $>0.1$ ). From this one could conclude that although the model generated power law distributions, the model is not capable of generating  $b$ -values that approximate the observed data.

However, a more detailed analysis showed that through tuning/calibrating the model parameters to improve the emulation of the inferred observed deformation, the modelled  $b$ -value was significantly changed (softened system). The resultant  $b$ -values from the two case studies bracketed the  $b$ -value of the observed data. Thus, through an intensive calibration effort, it is possible that the model (intermediate solution) could reproduce the observed  $b$ -value. However, as a result of the effort required to correctly calibrate the model it doesn't represent a practical tool. The method is optimally utilised on a comparative basis from a partially calibrated model.

Lastly, it is of interest to note that the relative changes to the modelled  $b$ -value and estimated  $m_{max}$  resulting from 'softening' the system are in accordance with observations. That is to say, 'stiffer' systems results in an increased  $b$ -value, lower  $m_{max}$  and an increased frequency of smaller events (*Mendecki, van Aswegen and Mountfort, 1999*). The corresponding relationships will be examined in greater detail in future reports (parametric studies).

### Introduction

The case study of TauTona mine 336 area investigated whether a boundary element numerical code was capable of generating a power law seismic event size distribution along a geological structure and compared modelled and observed cumulative frequency-magnitude relations along the Break fault. A specific conclusion of this study was that through an intensive

calibration effort, it is possible that the model could reproduce the observed b-value. However, as a result of the effort required to correctly calibrate the model it doesn't represent a practical tool. The method is optimally utilised on a comparative basis from a partially calibrated model.

Further studies were undertaken with the objective of moving towards defining the relative effects of changing the model parameter assumptions on the modelled seismic event size distribution. The long term objective is to delineate the parameter assumptions that control the resultant power law distribution. Specific aspects dealt with in this study are:

- Seismic data selection sensitivity
- Modelled material properties sensitivity
- Seismic event delineation method sensitivity (modelled data)
- Alternative seismic event simulation methods
- Asperity size distribution sensitivity
- Comparison between frequency magnitude relations

(all of the modelled and observed seismic event data analysed originate from the Break fault at TauTona mine).

### Seismic data selection sensitivity

A general problem associated with seismic monitoring is that of location error. In the analyses undertaken, the seismic data utilised is assumed to be associated with the Break fault, i.e. a specific geological structure. However, this data is subject firstly to location errors and secondly could be spatially intermixed with data derived from alternative sources – such as events occurring in the direct vicinity of mining faces. Different spatial filter windows were selected around the estimated position of the Break fault surface in order to test the robustness of the cumulative frequency-magnitude relation derived from the data. Firstly data was selected around the surface of the Break fault using a 40m hangingwall and footwall search distance, and secondly using a 20m footwall and 150m hangingwall search distance.

### **Conclusions:**

- The robustness of the frequency-magnitude relation should be improved if data is gathered between long time intervals. The data utilised in the analysis of the Break fault was gathered over a period of approximately two years, representing a relatively short time interval in terms of the long term fault response – potentially affecting the robustness of the cumulative frequency magnitude relations derived from the data.
- If data is gathered for the specific purpose of examining the response of a specific structure, depending on the sensitivity of the seismic monitoring network, the data could firstly be subject to a location error, and secondly be intermingled with data derived from alternative sources. As such, sensitivities of different spatial windows must be tested in order to delineate the robustness of the frequency magnitude relation derived from the data.

### **Modelled material properties sensitivity**

As part of the analysis of the seismic response of the Break fault, modelled seismic events have been generated using a number of different material properties. In all the case studies analysed, the material properties significantly influence the resultant seismic statistics derived from the model.

To summarise, examining the relative changes between modelled cumulative frequency magnitude relations as a result of changing material properties, increased the material strengths and imposing a higher material viscosity results in a general stiffening response of the system. That is to say, a 'stiffer' system results in an increased b-value, lower Mmax and an increased frequency of smaller events (*Mendecki, van Aswegen & Mountfort, 1999*). An example of this is shown in Section 5.4 GAP 603 September progress report (*Lachenicht, 1999<sub>2</sub>*).

## **Seismic event delineation method sensitivity (modelled data)**

In the September 1999 progress report, seismic events were delineated automatically utilising a cut-off co-seismic slip value. All spatially connecting co-seismic slip above the cut-off value was combined into a single event. The main problem with this method of event delineation, is that if a large cut-off co-seismic slip distance is selected a large amount of detail of the individual event responses is lost. If a very small cut-off value is used, the events are lumped together into a single event. This problem is essentially a function of the large time windows utilised in the model, i.e. a number of events occurring sequentially through time will be lumped into a single event, even though they actually do not directly interact through time.

As a result, a new method of delineating seismic events was devised. This permits the analyst to visually delineate and separate individual seismic events using polygons.

## **Alternative seismic event simulation methods**

### **Co-seismic slip filters**

All the analyses of modelled seismic events up to this point have been based on events derived from filtered co-seismic slip values. Thus the viscous relaxation of the surrounding fault gouge is filtered out in order to allow the co-seismic slip to be calculated and associated to individual seismic events. However, this filtering process is computationally intensive.

To circumvent this problem, an alternative procedure was tested where seismic events are delineated (utilising polygons) from raw data, which includes the viscous relaxation component. Application of this method shows the simulated seismic event data analysed to still exhibit a power law response.

### **Approximation of the three dimensional non-linear rockmass response**

In the previous analyses of the seismic response along the Break fault, the response of the surrounding rockmass was assumed to be linear elastic. This methodology can, however, be improved by simply incorporating non-linear displacement discontinuity elements along the plane of the reef. This permits both compressive and shear failure to occur in the vicinity of mining excavations, approximating the surrounding three-dimensional rockmass response and its subsequent interaction with the Break fault (refer to section 6). The method is also computationally efficient, hence presenting a viable design tool.

### **Asperity size distribution sensitivity**

All the seismic events extracted from the models have been derived from the failure of asperities placed over the Break fault surface (*Lachenicht, 1999 1&2*). These have been associated with specific assumptions, namely:

- Random distribution of asperities over the fault surface (30% areal coverage)

And with one or more of the following:

- A specific assumed strength distribution of asperities
- A specific assumed size distribution of asperities
- Spatial clustering of randomly distributed asperities allowing the formation of larger asperities

All of the modelled seismic data derived from the above assumptions exhibited a degree of power law behaviour. However, the question arose, 'Would it be possible to generate a power law frequency magnitude size distribution from an experiment which incorporates constant strength and size asperities randomly distributed over the fault surface. If this were true, it would imply that the power law size distribution is inherent in the mechanics of the model.'

Both frequency-magnitude relations exhibit strong power law behaviour.

### Comparison between frequency magnitude relations

For both the 'model 1' and 'model 3' data, the seismic moment of each event is calculated by:

$$M_o = \mu * \sum_i^n (A_i * u_i) \quad (\text{Kostrov \& Das, 1988})$$

Where:

- $M_o$  = seismic event moment (Nm)
- $\mu$  = rigidity (3e10 Pa)
- $A_i$  = Area of grid block I (m<sup>2</sup>)
- $u_i$  = estimated co-seismic slip of grid block i (m)
- $n$  = number of grid blocks delineated for the seismic event (polygon method)

For the 'model 2' and 'model 4' data, the seismic moment of each event is calculated by:

$$M_o = d\sigma_{\text{average}} * dV_{\text{source volume}} \quad (\text{Madariaga, 1979})$$

Where:

- $M_o$  = seismic event moment (Nm)
- $d\sigma_{\text{average}}$  = average stress change of asperities failing over the event source volume (Pa)
- $dV_{\text{source volume}}$  = event source volume (m<sup>3</sup>)

Thus it can be noted that different methods of moment calculation alter the resultant b-value of the cumulative frequency magnitude relation.

The parameter assumptions utilised to attain the modelled seismic event data are listed in Tables 3.1.6 and 3.1.7.

**Table 3.1.6 Model 1&2 parameter assumptions**

Parameter	Parameter Assumption
Gouge Constitutive Model (Break fault)	Mohr-Coulomb
Gouge friction (Break fault)	30-25 degrees (strain softening)
Gouge viscosity (Break fault)	1e16 Pa-sec
Gouge cohesion (Break fault)	0 MPa
Gouge Young's Modulus	40GPa
Gouge Poisson's Ratio	0.2
Asperity distribution (Break fault)	Random / Spatial clustering (80x80m blocks)
Asperity strength distribution (Four asperity sizes from spatial clustering)	Friction 45-18 (size 1) Friction 48-18 (size 2) Friction 51-18 (size 3) Friction 54-18 (size 4)
k-ratio	0.3(east/west)/0.7(north/south)
Vertical in-situ stress	0.027 MPa/m
Host rockmass Constitutive model	Elastic
Host rockmass Young's Modulus	70GPa
Host Rockmass Poisson's Ratio	0.25
Time interval	3 months / model step
Modelled mining sequence	As specified
Closure of excavations	1m maximum closure permitted
Additional structures	Not included for simplicity

**Table 3.1.7 Model 3&4 parameter assumptions**

Parameter	Parameter Assumption
Gouge Constitutive Model (Break fault)	Mohr-Coulomb
Gouge friction (Break fault)	35-25 degrees (strain softening)
Gouge viscosity (Break fault)	1e16 Pa·sec
Gouge cohesion (Break fault)	0 MPa
Gouge Young's Modulus	40GPa
Gouge Poisson's Ratio	0.2
Asperity distribution (Break fault)	random
Asperity strength distribution	Constant – friction 45-25 degrees
k-ratio	0.3(east/west)/0.7(north/south)
Vertical in-situ stress	0.027 MPa/m
Host rockmass Constitutive model	Elastic
Host rockmass Young's Modulus	70GPa
Host Rockmass Poisson's Ratio	0.25
Time interval	3 months / model step
Modelled mining sequence	As specified
Closure of excavations	1m maximum closure permitted
Additional structures	Not included for simplicity

Additional points that can be noted:

- Model 1&2 (full data) show a higher b-value to that of the observed data (1.62 & 1.76 versus 1.18 & 1.35)
- Model 3's b-value emulates that of the observed data (40m h/w f/w filter), i.e. 1.18.
- There is a high variability of b-value between model 3 & 4 (1.18 to 2.07), i.e. resulting purely from the alternative moment calculation method.
- Model 3 shows a lower b-value to that of model 1 (1.18 versus 1.62). This can be attributed to the fact that spatial clustering of asperities is not present, the asperity strength assigned is on average lower and non-linear displacement discontinuity elements are incorporated in the model on reef elevation – leading to an overall softer system response.
- The power law size distribution is more noticeable in the model 3 data (no size or strength distribution imposed) than for the model 1 event data (imposed size and strength distribution).

## Conclusions

This work forms the first part of a sensitivity analysis necessary to delineate the parameter assumptions that control the resultant power law distribution. The major conclusions derived from the work can be summarised as follows:

Observed cumulative frequency-magnitude relations are sensitive to:

- Spatial filtering of the data
- Length of analysis time windows (amount of available data)

Modelled cumulative frequency-magnitude relations are sensitive to:

- Material properties (strength & viscosity)
- Event delineation methods
- Alternative source parameter calculation methods (moment)

In addition, the following points were noted:

- Modelled cumulative frequency-magnitude b-values can reflect the observed data. However, the underlying physics between the two might significantly differ. This can be confirmed through an analysis of the associated time and space distributions
- Cumulative frequency-magnitude relations derived from modelled energy still exhibit power law characteristics which are shown to be less sensitive than that of moment magnitude (analysis of differences between models)
- Cumulative frequency-magnitude relations derived from asperities distributed randomly in space, with no assumed size or strength distribution still exhibit power law behaviour in the resultant cumulative frequency-magnitude relations

Other aspects investigated as part of this report were:

- Less computer intensive event filtering methods (co-seismic slip filters)
- Optimised event delineation methods (polygon method)
- A seismic event simulation method incorporating an approximation of the surrounding three dimensional non-linear rockmass response

The remaining sensitivity associated with the frequency magnitude size distribution that must still be investigated is that of the analysis of the effect of variable grid block sizes on the resultant frequency magnitude size distribution.

Some physical systems can exist in different phases. Crystals can melt , liquids can crystallise or evaporate. Some ceramic materials behave as insulators at room temperature but , if immersed in liquid nitrogen they suddenly become superconductors. The general properties of these processes are:

1. They occur only for certain values of the physical parameters controlling the behaviour of the system such as temperature, pressure, concentration etc. The values of the control parameters for which a given physical system undergoes a phase transition are called critical values.
2. Near the phase transition point the correlation length of the physical system diverges as a (negative) power of the distance of the control parameter to the corresponding critical value. Similar power-law behaviour near a phase transition is observed for other physical quantities. The corresponding exponents in these power laws are called critical exponents.
3. One of the central facts in the theory of phase transitions is that while the critical exponents are unique for each concrete system, there are many seemingly different types of physical systems which share the same values of the critical exponents. For such systems it is said that they form a class of universality.
4. The power-law behaviour of the observable quantities of a physical system near a phase transition point is directly related to the phenomenon of scaling (the preservation of the form of a function when the argument is scaled by a factor). It is an observed fact that many quantities related to seismic activity exhibit scaling.

A concept of a considerable following is the belief that many real physical systems are spontaneously driven to a critical state by their internal complexity. This statement is known in the literature as Self-Organised Criticality (SOC). Apart from some very attractive theoretical aspects to SOC it is of little practical importance to the mining industry.

One way of studying critical phenomena is on simple mathematical models. One such model with wide-ranging applications is the percolation model. It is perhaps the simplest system which can undergo a phase transition. The model is formulated on a regular lattice. The role of the control parameter is played by a real number  $p$  called the occupation probability. For a given value of the occupation probability one can generate many instances of the lattice system by assigning either 0 or 1 to the sites of the lattice according to the rule: the value of 1 is assigned

to the current site with probability equal to  $p$ . If a site is not assigned the value 1 it is set to zero. Obviously the control parameter  $p$  must be a number between zero and one.

The main objects of interest in the study of percolation models are the connected clusters. A connected cluster is a set of occupied sites in which each site has at least one nearest neighbour which is also occupied. An infinite cluster (or spanning cluster) is a connected cluster which includes occupied sites from the opposite ends of the lattice. The model is said to percolate for a given value of the control parameter (the occupation probability  $p$ ) if it has a spanning cluster. Obviously the model does not percolate for  $p=0$  or even for  $p>0$  but very small. On the other hand the model will certainly percolate for  $p=1$  or  $p<1$  but very close to 1. The question is: how does the probability for forming a spanning cluster vary with  $p$ ? It turns out that the variation of this probability is not a smooth and monotonous increase from zero to one. Instead the percolation model exhibits a phase transition with the corresponding critical point being the percolation threshold, that is the value of the occupation probability for which the model can for the first time generate a spanning cluster. For a two-dimensional site-percolation model the percolation threshold is near the value 0.5927.

The properties of sub-critical and super-critical (spanning) clusters in percolation models could be of relevance for modelling of faults and specifically when choosing a distribution density of the asperities.

## 3.2. Time distribution

Space-time distributions of fault slip were plotted by (Cochard and Madariaga, 1996, Rice 1993, Shaw, 1995). The fault epicentres or slip lengths are plotted on a fault position - time plot, as shown in Figure 3.2.1. Low values of rate dependence lead to slip across the entire fault whereas higher values cause a distribution of smaller events within the fault boundaries. Time dependent energy release cycles were observed by Napier and Malan (1997) using a boundary element representation of longwall mining of tabular stopes as shown in Figure 3.2.2. The energy release can be considered to be analogous to the seismic energy release and can be used as a measure of seismicity.

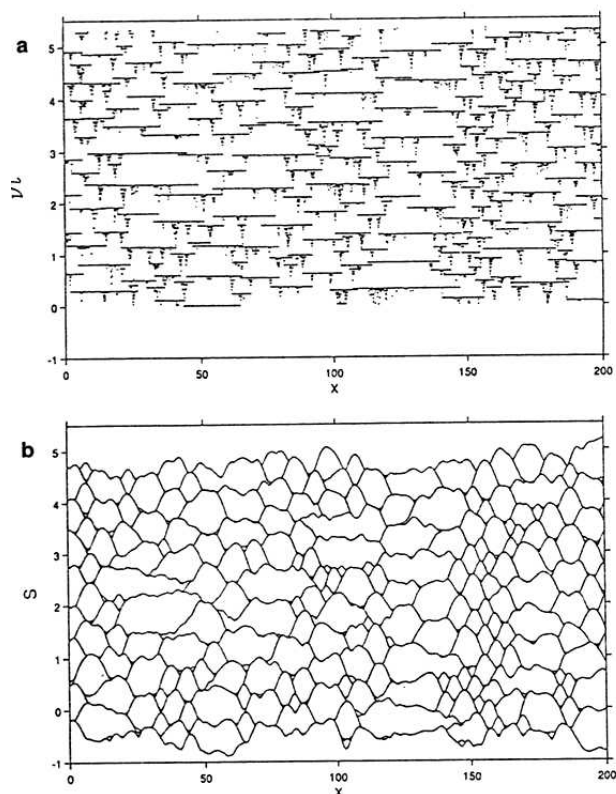




**Figure 3.2.1 Example of space-time distributions of seismicity from a block slider model of fault slip (Shaw, 1995)**

A comparison of inter-event times was used by *Robinson and Benites (1995)* to assess the difference between the modelled results and a random, Poisson process. The results indicated that there was very little difference over most of the size range, although larger sizes demonstrated quasi-periodic recurrences. *Ito and Matsuzaki (1990)* compared the time distribution of events in a two-dimensional Burridge-Knopoff cellular automaton model with the Omori law and indicated that the model response could approximate the Omori law if the manner in which the events were defined was modified. Thresholds of frictional force were introduced that defined the start and the end of an event. Any subsequent increase in force over the initiation threshold was considered to be an aftershock. Thus, in numerical models, the event statistics and size, space and time distributions depend on the way that events are defined.

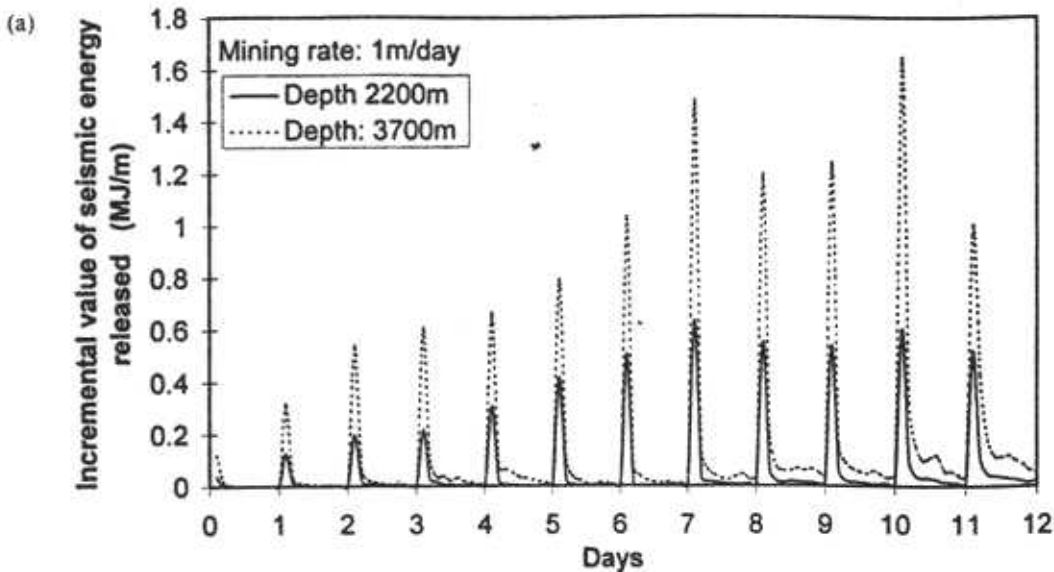


**Figure 3.2.2 Energy release rate for a mine stope analysis (Napier and Malan, 1997).**

*Evena and Ben-Zion (1997)* evaluated numerical seismicity as generated with a model of a fault segment 70km long by 17.5 km deep, using 550m long elements. They used pattern recognition algorithms to assess the generation of seismicity in terms of spatial randomness, correlation dimension, repetitiveness, average depth, time interval for recurrence of a constant number of events and the ratio of numbers of events in two magnitude ranges.

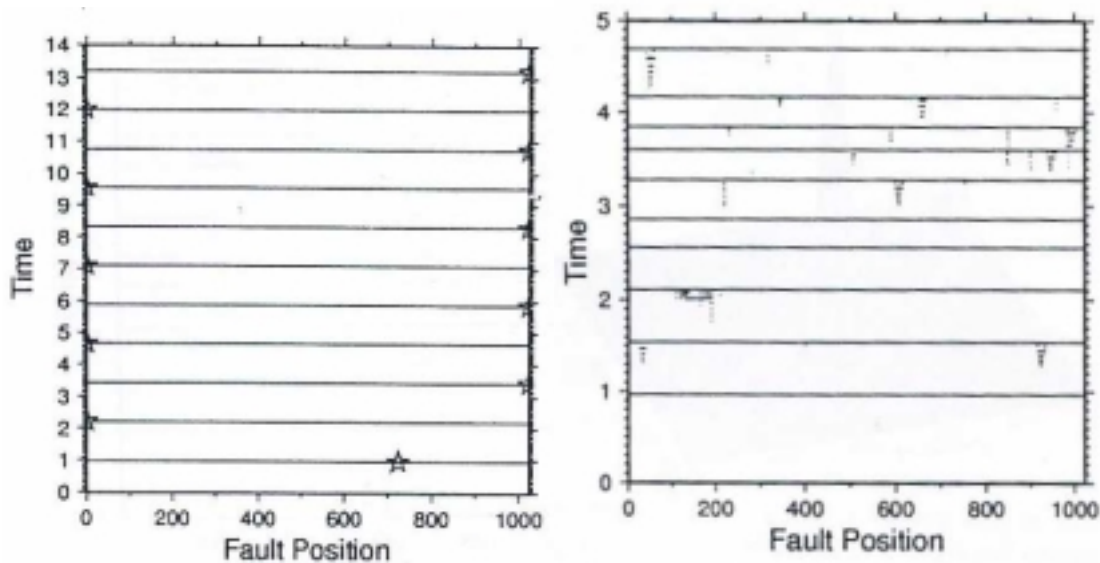


**Figure 3.2.3 Effect of fault rheology on slip distribution through time (Cochard and Madariaga, 1996)**

The importance of applying the correct constitutive relation on the slip plane is illustrated in Figure 3.2.3. The model in Figure 3.2.3a uses a rate independent model and slip events occur once and then no further relaxation is allowed. The Model in Figure 3.2.3 uses a visco-plastic rheological model and demonstrates a number of slip events extending across the fault plane subsequent to each initial slip.

### **3.3. Clustering in space and time**

The term “clustering” as applied to seismic phenomena corresponds to the property of seismic events to form distinguishable groups according to some criterion. A seismic cluster is a group of seismic events formed in the above sense. It is obvious that specifying of clustering criterion or criteria is crucial for cluster identification within a given seismic catalogue. A clustering criterion must lead to a metric relationship (distance or a sense of closeness) between any pair of seismic events. Here are some examples to illustrate this idea:

1. Temporal seismic clusters: the grouping criterion is based on the time interval between two events. Another way of defining temporal seismic clusters is by the time interval between an event and a fixed moment of time. When the additional criterion of causal relationship between the events is added to the time-clustering criterion one arrives at the idea of fore-shocks and after-shocks as a typical example of clustering in time.
2. Spatial seismic clusters: the criterion is the Euclidean distance between the locations of the events. This is the most intuitively acceptable idea of clustering because the clusters are groups of seismic events swarmed together in physical space.
3. Clustering in size: the criterion is the absolute value of the difference between the size of any two events. Since the size of a seismic event cannot be uniquely specified by a single number there are different criteria by which one could identify seismic size clusters.
4. Spatio-temporal clusters: the criterion is the simultaneous fulfilment of the requirement for closeness in Euclidean space and for a short time-interval between a pair of seismic events. The importance of the identification and analysis of spatio-temporal seismic clusters lies in the possibility of revealing a causal relationship between some events.
5. Projective spatial clusters: the criterion is a weakened spatial closeness condition applied to the projections of the locations of seismic events on some plane or line.

#### **3.3.1. Cluster identification: connected clusters**

Cluster identification is the procedure whereby a seismic catalogue is subdivided into individual seismic clusters.

Selecting a clustering criterion is only the first step towards cluster identification. The criterion has to be applied in order to decide whether an event belongs to a cluster and if it does to which particular cluster it has to be assigned. This procedure is not unique. To specify the clustering criterion means to define the distance between events. The cluster identification procedure is a specific way of using this distance. The simplest and intuitively most acceptable cluster-identification idea is the search for connected groups of seismic events. Connected groups of seismic events or connected clusters are defined through the definition of a connected pair of seismic events. Two seismic events are said to be connected if the distance between their locations is less than some chosen value - the connectivity range. The choice of

the connectivity range depends on the concrete situation and could be related to the error in determining the locations of seismic events. The algorithm for the identification of connected clusters can be derived inductively from the following statement: Given are a connected cluster and a seismic event. The event belongs to the cluster if it is within the connectivity range of at least one of the events already assigned to the cluster.

The separation of a seismic catalogue into connected clusters strongly depends on the choice of the connectivity range: if it is chosen too small there will be many separate clusters of one or two events each; if the connectivity range is too big then there will be only a few very big connected clusters and, in the extreme case, the whole catalogue will be one cluster. The whole idea of the cluster analysis is to reveal some patterns in the local seismicity or some structural features of the rock mass. Therefore the two extreme cases: each event - a cluster and all events - one cluster are equally uninformative. Choosing the best value for the connectivity range is not a simple task and strongly depends on the local seismicity, the properties of the seismic system, the geological structures etc.

### **3.3.2. Cluster analysis of model-generated data**

The numerical models capable of simulating seismic activity invariably use some form of spatial discretization hence they possess some fixed length scale. This simplifies the choice of a connectivity range when the objective is an analysis of the clustering in space of some set of model-generated seismic data. The natural choice of the connectivity range in this case is some multiple of the discretization length of the model. For instance, if the model is three-dimensional and uses some subdivision of the volume of interest into non-intersecting tetrahedral elements, the connectivity range could be taken as the maximum distance between the centroids of adjacent tetrahedra. The same choice of connectivity range will be appropriate for clustering analysis of the projections of seismic events' locations on a fixed plane.

### **3.3.3. Quantitative analysis of spatial seismic clusters**

An important component of the cluster analysis of seismic data (either real or model-generated) is the quantification of every individual connected cluster. The simplest quantity which can be associated with a cluster is its "mass" or weighted sum of the events which make the cluster. The weights can be chosen according to the size of the events or set to unity for all events in the cluster. Clusters can have a different shape and location and the problem of associating numerical characteristics with these features does not have a unique solution. One possible way of quantifying spatial seismic clusters is to embed each cluster in its best-fitting ellipsoid (or ellipse in two dimensions). In the three-dimensional case the numerical characteristics of a cluster will be:

- the position of the centroid of the ellipsoid
- the lengths of the three main axes of the ellipsoid
- the unit vector along the principle axis of the ellipsoid.

The characteristics of two-dimensional clusters are defined in the same way:

- the position of the centroid of the ellipse
- the lengths of the two main axes of the ellipse
- the unit vector along the principle axis of the ellipse.

The procedure for computing the above characteristics in the three dimensional case may read as follows:

- Preliminary step: the given seismic catalogue is decomposed into several connected clusters and, perhaps, a number of diffuse events which cannot be assigned to a cluster for the chosen value of the connectivity range. If it turns out that the catalogue contains connected clusters one can proceed with the quantification of the individual clusters.

- Finding the centroid of a cluster: If the singled-out cluster contains N elements (seismic events) located at  $P_i = (x_i, y_i, z_i)$ ,  $i = 1, 2, \dots, N$ , the centroid of the cluster is at  $P_C = (x_C, y_C, z_C)$  where the coordinates are computed as the centre of gravity of material points of “mass”  $w_i$  at  $P_i$ .

$$x_C = \frac{\sum_{i=1, N} w_i x_i}{\sum_{i=1, N} w_i}$$

$$y_C = \frac{\sum_{i=1, N} w_i y_i}{\sum_{i=1, N} w_i}$$

$$z_C = \frac{\sum_{i=1, N} w_i z_i}{\sum_{i=1, N} w_i}$$

The weights can be correlated to the size of the events or alternatively all weights could be set equal to unity.

- Determining the principle axis of the cluster: Measure the distance of each event-point  $P_i$  to the centroid of the cluster and single out the point  $P_k$  which is furthest from the centroid. Then the length of the principle axis of the cluster ellipsoid is equal to the length of the vector  $(P_k - P_C)$  and the unit vector along the principle axis is collinear with  $(P_k - P_C)$ .
- Determining the secondary axis of the ellipsoid: Measure the distances of all points of the cluster to the line of the principle axis. Single out the point  $P_m$  which is the furthest from the line of the principle axis. Then the vector  $(P_m - P_C)$  determines the secondary axis of the ellipsoid.
- Determining the third axis of the ellipsoid and the corresponding length: calculate the cross-product of the unit vectors of the principle and the secondary axis. The result is the unit vector of the third axis of the cluster ellipsoid. Measure the distances of all points in the cluster to the line of the third axis and determine the point  $P_n$  for which this distance is maximum.

Special cases:

- spherical clusters: for which the three axes have approximately the same length
- a pancake-shaped cluster: two of the axes are of approximately the same length while the third is much smaller
- a cigar-shaped cluster: the secondary and the tertiary axes of the ellipsoid are approximately equal and much smaller than the principle axis.

The procedure described above has a straightforward adaptation to the two-dimensional case.

### 3.3.4. Analysis of a set of clusters

Consider a catalogue of the local seismicity in an area of interest for a given period of time. By applying the cluster identification procedure the catalogue is decomposed into a set of connected clusters. The mass and the shape characteristics of each cluster are evaluated according to the above formulated rules. The next step is to study the distribution of the clusters according to one or more of the cluster characteristics. The spatial distribution of the centroids of the clusters can be related to the locations of stress concentrations and seismogenic geological structures. Additional information about the seismogenic structures can be extracted from the orientation of the principle axes of the cluster ellipsoids. The temporal evolution of spatial seismic clusters can be related to the local mining activity and can specify the input to numerical models which is one of the form of integration of modelling with monitoring.

The simplest means of evaluating the spatial distribution of seismicity is to plot the data on mine plans with the size of the symbol being proportional to some parameter obtained from the seismic event e.g. magnitude or moment. This does not allow for evaluation of the patterns.

The application of numerical or analytical models based on the theory of elasticity led to the development of parameters based on stress or strain measures that could be used to indicate the spatial variability of seismicity.

*McCreary et al. (1993)* suggest that reasonable estimates of seismic potential could be obtained at the Ansil Mine in Canada by consideration of modelled principal stresses. A three-dimensional boundary element code was used to model the mine layout. Known seismic events were plotted along with the principal stress contours. The seismicity correlated to regions in which the principal stress was greater than 55 MPa and less than 80 MPa. Regions with a principal stress greater than 80 MPa did not exhibit seismicity and were considered to have failed completely. *McCreary et al. (1993)* commented that parameters such as the principal stress change due to mining, the stress difference and the extension strain should also be considered. *Bek et al. (1996)* noted that the majority of events in a deep copper mine lay on pre-existing fault planes. They plotted the stresses at each event location, obtained from an elastic model, in the Mohr Coulomb space, to obtain an estimate of the elastic stresses at which the events were occurring. They stressed the need for inelastic models to be able to address the issue of path dependence of rock failure on the evolution of seismicity.

The excess shear stress ESS can be defined as the shear stress acting on an existing or potential plane in excess of the dynamic rupture strength (*Ryder, 1988*). Reasonable estimates of seismic event magnitude were obtained by *Ozbay et al. (1993)* and *Webber (1990)* using the MINSIM-D program and considering the modelled ride on a plane of potential failure below the stope. The integral of the ride over the expected area of slip was used to calculate an equivalent seismic moment. Seismic location accuracy must also be considered when comparing the predictions of numerical modelling with actual seismic event locations (*Webber, 1990*). The extension to three dimensions can be made by considering the volume excess shear stress VESS (*Spottiswoode, 1990*). Comparison with seismic events in mines indicates that the maximum VESS corresponds to regions of high seismicity and that the maximum event magnitudes can be related to the maximum VESS. The importance of explicitly including the co-seismic strain changes to model inelastic response is stressed by *Spottiswoode (1990)*.

The energy release rate ERR is defined as the amount of strain energy released per unit area of mining. The ERR can be related to the volume of closure. *Minney and Naismith (1993)* attempted to match the rate of change of stored energy with the seismicity from mining a remnant pillar. They noted, however, that the elastic models were only useful in hindsight for understanding the sequence of seismic events. A method to introduce inelastic response by limiting the maximum stress carried by pillars and the rock mass ahead of the face produced better correlations between the ERR and the locations of events (*Spottiswoode, 1997*).

*McGarr (1976)* proposed that a link between seismicity and the area that had been mined out could be obtained through the relationship

$$M_o = \gamma G \Delta V$$

where  $M_o$  is the cumulative seismic moment,  $G$ , is the shear modulus and  $\Delta V$  is the volume of closure in the stope. The dimensionless parameter  $\gamma$  is determined from back analysis of mine seismic data (*Milev and Spottiswoode, 1997*) for a particular region.

In models where the fault zones are treated explicitly, the frictional properties affect the space and time distributions of slip (*Cochard and Madariaga, 1996, Tse and Rice, 1986*). Plots of slip, or stress drop against position on the fault for various time contours can provide insight into the space-time correlation of events for different parameter ranges.

A series of tests to investigate clustering in the particle flow code (PFC3D) were performed by (Hazzard, 1999). The numerical models were compared against physical laboratory experiments. The model used in a test with uniaxial loading of a cylinder is shown in Figure 3.3.1a. The plot of events occurring immediately after failure is shown in Figure 3.3.1b and indicates how the events are clustered along a single failure plane.

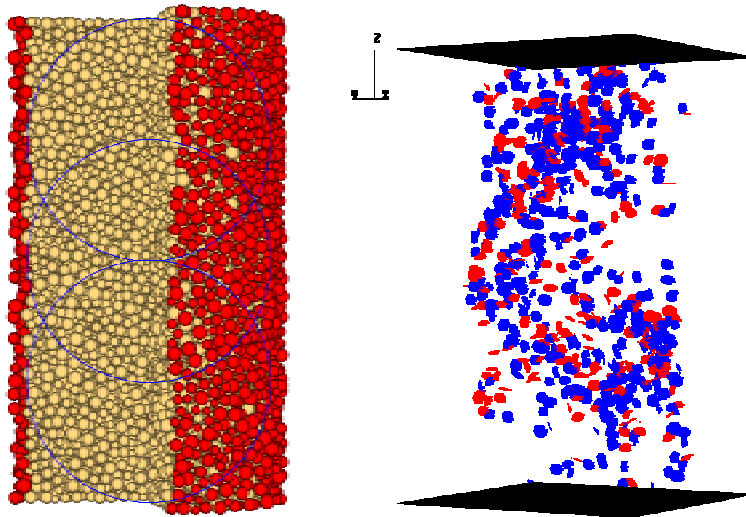


**Figure 3.3.1** Cylindrical PFC3D sample (Hazzard, 1999) showing a) cutaway view of sample and b) localisation and clustering of events along final plane immediately after failure.

Hazzard (1999) also performed a series of tests on a square sample to investigate the effect of the parameters of a proposed clustering algorithm. The sample and final set of event clusters are shown in Figure 3.3.2. As shown in Figure 3.3.3, the size distribution depends on the stress path applied to the model. Test I considered hydrostatic compression followed by compression of one side of the cube to failure. Test II was an extension test, where the stress on one side was relieved until the sample failed. Figure 3.3.4 and 3.3.5 show that the cluster size also depends on the choice of the space and time windows in the clustering algorithm.

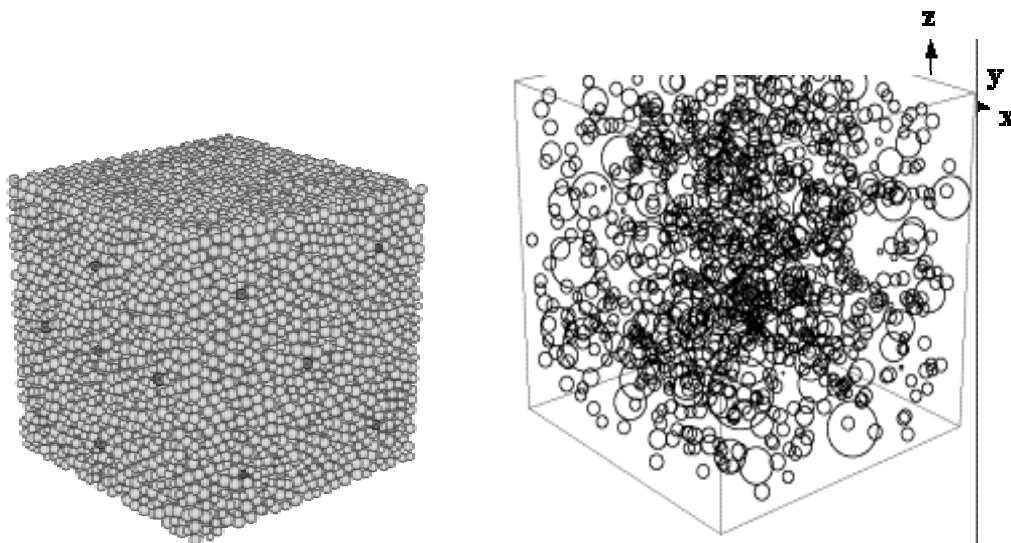


**Figure 3.3.2** a) Square PFC3D sample for loading in compression or extension (test II) clusters recorded prior to failure in Test I. b) Clusters of events for tests I (Hazzard, 1999).

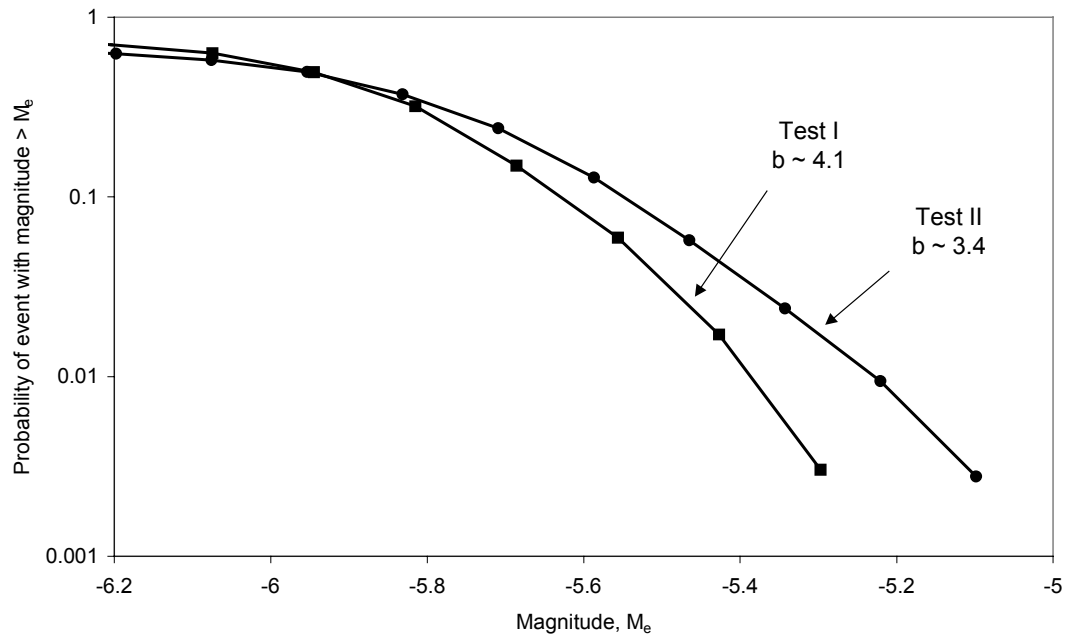


**Figure 3.3.3. Frequency-magnitude plots for two tests with different stress paths. Test I is a compression tests and test II is an extension test. (Hazzard, 1999).**

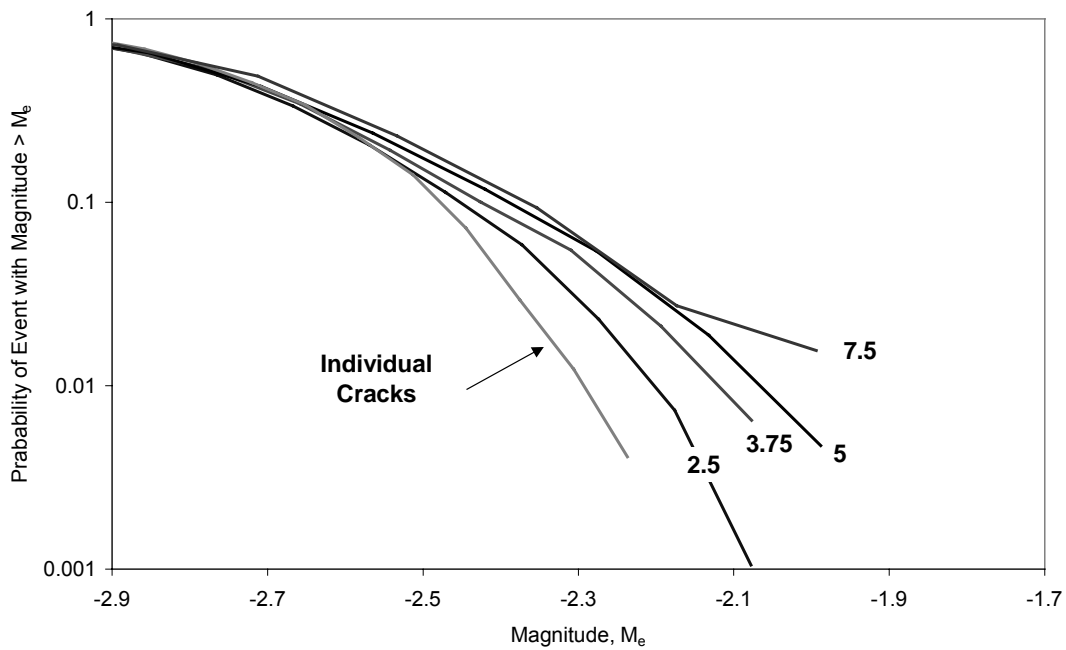


**Figure 3.3.4. Comparison of frequency-magnitude plots for events with different space windows. The value of  $R_e$  in particle diameters is shown on each curve. (Hazzard, 1999).**

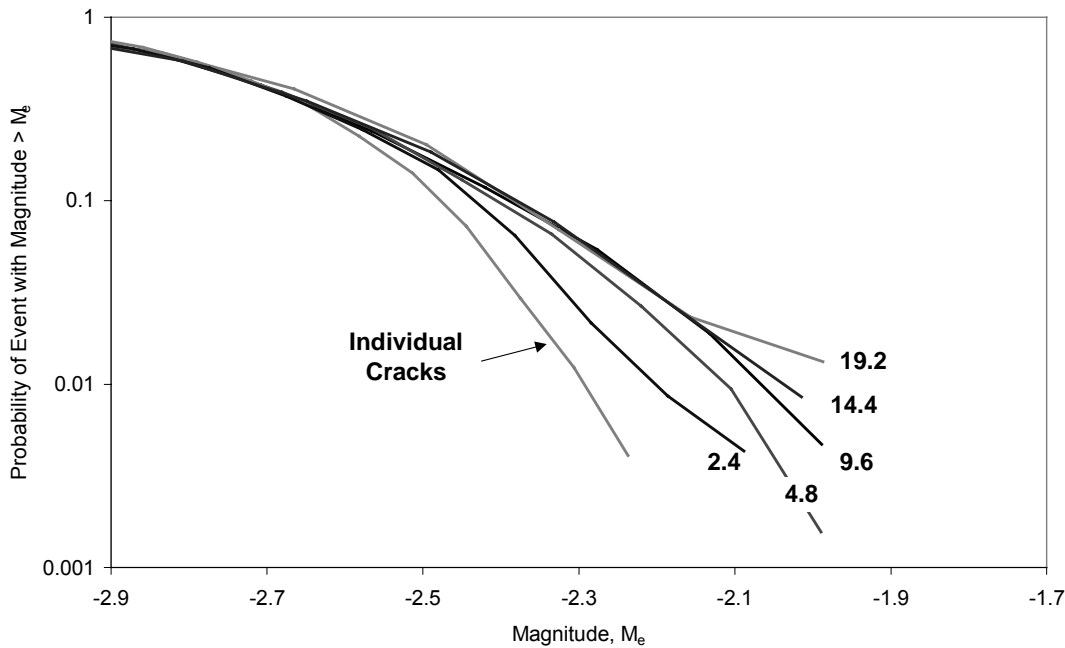


**Figure 3.3.5. Comparison of frequency-magnitude plots with different time windows ( $T_e$ ). The value of  $T_e$  in  $\mu s$  is shown on each curve. The radius of the space window ( $R_e$ ) is 5 particles diameters in each case (Hazzard, 1999).**

### 3.3.5. Modelling with IDRM

The methods of cluster identification and quantification have been applied to the analysis of model-generated data about instabilities in rock-mass under loading. The numerical model (which is named IDRM for Integrated Damage Rheology Model) implements the fundamental equations of continuum mechanics with damage rheology. A set of self-consistent equations describe the evolution of the physical state of a given volume of rock for certain initial distribution of the stress tensor and under prescribed boundary conditions. The state of damage of the material is described by a scalar variable which takes its values in the interval  $[0, 1]$ . The material properties and, in particular, the elastic modulae depend on the local state of damage. The material response to loading is non-linear and is governed by the density of the elastic potential energy (in the iso-thermal case). The numerical algorithm implements a finite-difference FLAC-like procedure for describing the distribution of the deformations within the volume of interest. The model does not postulate empirical constitutive relations but recalculates the stress-field directly from the Helmholtz free energy of the physical system. Since the numerical procedure is based on equations of motion, the model solves a forward problem in the actual, physical time and hence is perfectly suitable for integrating with real seismic data. The model-generated seismic events correspond to local loss of stability (the local density of the free energy loses its convexity) or damage above the critical level. The loss of stability and consequently the failure in elements is associated with stress-redistribution which affects the entire volume and can cause failure in other elements in which the level of damage happened to be just under the critical value. Thus a single record in the model-generated data stream refers to a particular moment of time and a number of elements which have failed simultaneously at this time are not necessarily connected in a spatial cluster. A further processing of the data generated by the IDR is required in order to separate seismic events (connected clusters of elements which were failed by the model at the same moment of time) from the acoustic noise (diffuse set of simultaneously failed elements which do not belong to connected clusters).

Once the actual model-generated seismic events are separated from the acoustic noise, one can proceed to write a seismic catalogue of modelled data. Such a catalogue can in turn be analysed by means of the technique for identifying and quantifying connected clusters either in



real space (spatial seismic clusters) or in any other abstract space of the modelled observables. In this report we shall restrict ourselves to spatial clustering of seismic data generated by means of the IDR model. Correlations will be sought between spatial clusters and the distribution of stress, damage, damage rate and other relevant quantities.

The model was set for a prismatic volume of rock just under the mining face of section 336 , TauTona mine. The initial distribution of stress was produced by MAP3D. Since the objective of the study is the clustering of data in Euclidean space, no change of loading due to advance of the face was considered. A seismic catalogue of real events which is available for the area was used as an additional input to IDR which constitutes a *de facto* integration of numerical modelling with seismic monitoring.

Stage 1 involves the separation of IDR-generated seismic events from the acoustic noise. A typical set of simultaneously failed elements is shown on Fig.3.3.6.

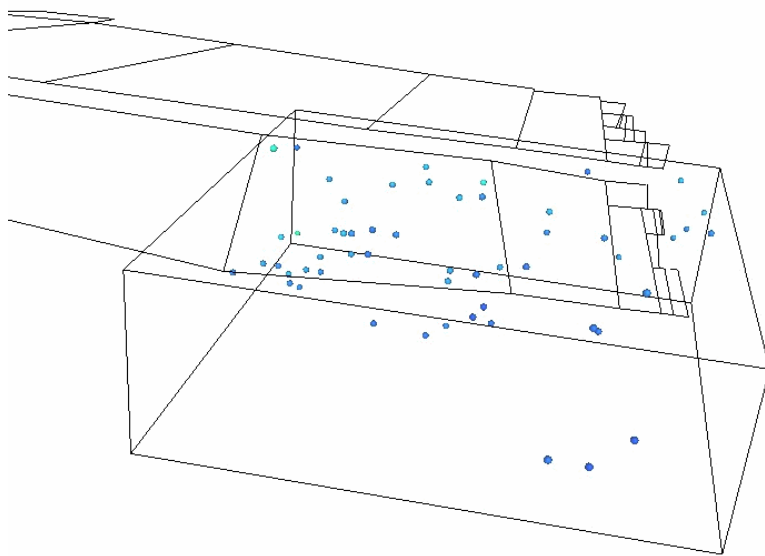


**Figure 3.3.6. All IDR elements which failed at  $t=-55083.9$  sec (the model was started at  $t_0 = -148000.0$  sec). The spheres are at the centroids of the failed tetrahedral elements. Some spheres which could be wide apart can look close together in this projection.**

The procedure for identifying connected cluster was applied for the set of failed tetrahedra shown in Fig.3.3.6. The connectivity range was chosen as 1.5 times the minimum distance between tetrahedral nodes for the whole grid. Groups of less than three connected failed tetrahedra were not considered as clusters but were assigned to the acoustic noise instead.

It turned out that the above set of failed elements contains only two connected clusters (for the chosen connectivity range) and the reminder of the IDR event contributes to the acoustic noise. The two connected clusters (the model-analogue of seismic events) are shown on Fig. 3.3.7a and Fig. 3.3.7b respectively.

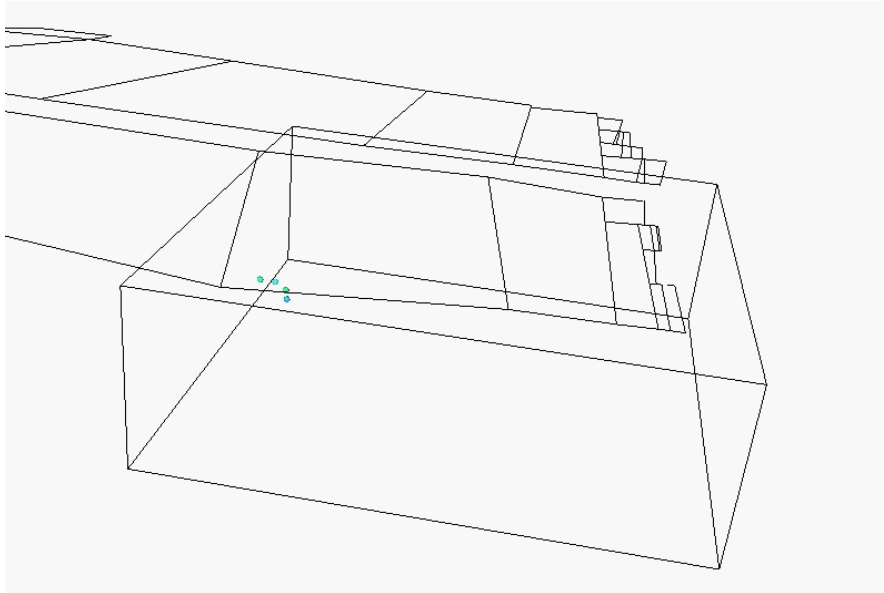


**Figure 3.3.7a.**

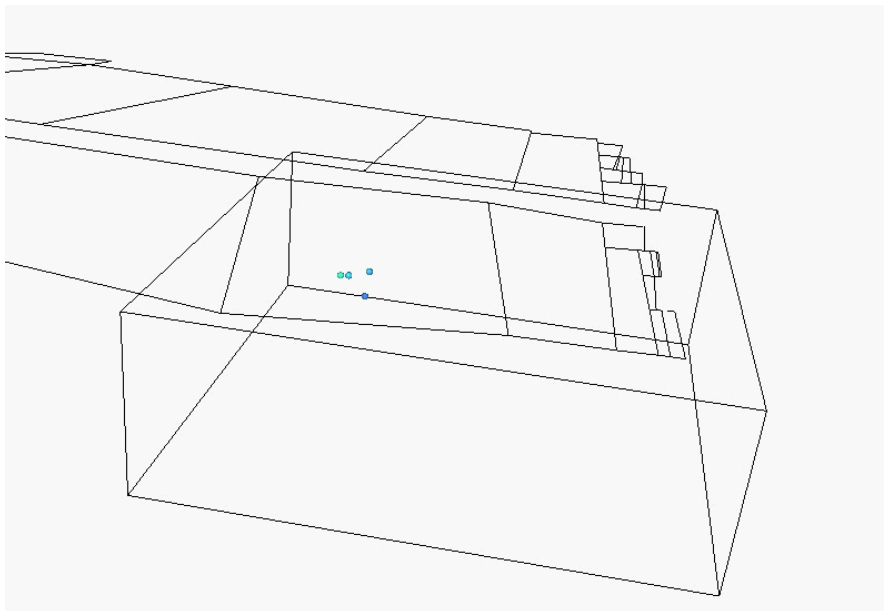
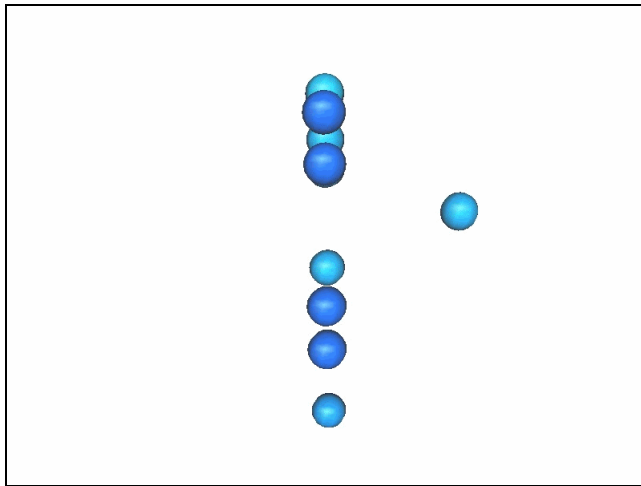
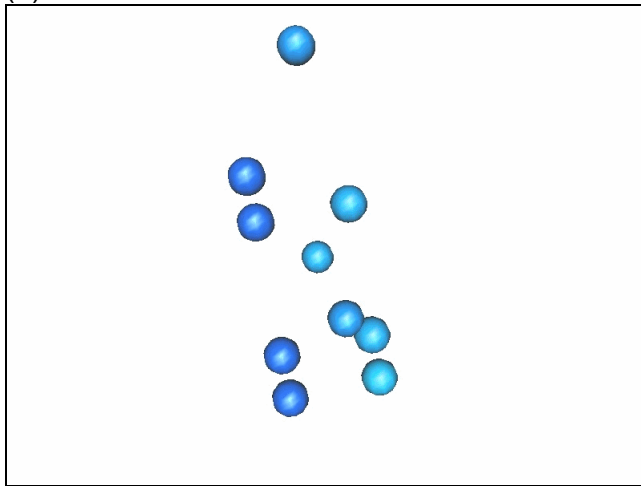


**Figure 3.3.7b.**

In a subsequent analysis, the model was run through about 40 hours of real time (considerably less in computer time because of an adaptive inertial mass re-scaling). The total number of failed elements for this simulation was 21371 but the number of seismic events (connected clusters of simultaneously failed elements) turned out to be just 111, the number of elements in a cluster ranging from 3 to 12. The clusters varied in shape as well. A cluster of 10 elements is shown on Fig 3.3.8 from two different viewpoints: in the plane of the principal and the secondary axes (Fig. 3.3.8 a) and in the plane of the principal and the tertiary axes of the cluster-ellipsoid (Fig. 3.3.8 b) This particular IDR cluster can be interpreted as a planar seismic event. Indeed, 9 of the 10 elements in this cluster are coplanar as it can be seen from Fig. 3.3.8 a.



(a)



(b)

**Figure 3.3.8. Connected cluster number 63 (of 111) from two different viewpoints: a) In the plane of the principle and the secondary axis; b) in the plane of the principle and the tertiary axis**

Stage 2: cluster analysis of IDRМ-generated seismic events begins once the model-generated seismic events have been identified (in Stage 1). One can apply a connected-cluster identification procedure on the whole catalogue of IDRМ-events or to parts of it, corresponding to shorter time intervals. This would correspond to the observed clustering of events that are associated with the swarming of model-generated seismic events near the base of the pillar and under the active face of section 336, TauTona mine are shown on Fig. 3.3.9-3.3.11. Fig. 3.3.9 represents the data from the first 20000 sec. (Physical time) of simulations. Fig. 3.3.10 and Fig. 3.3.11 correspond to the subsequent periods of 20000 sec. each. The first of these intervals begins with the start of the model and thus bears the mark of a certain transient period. This explains the lower level of seismicity in the first of the three figures.

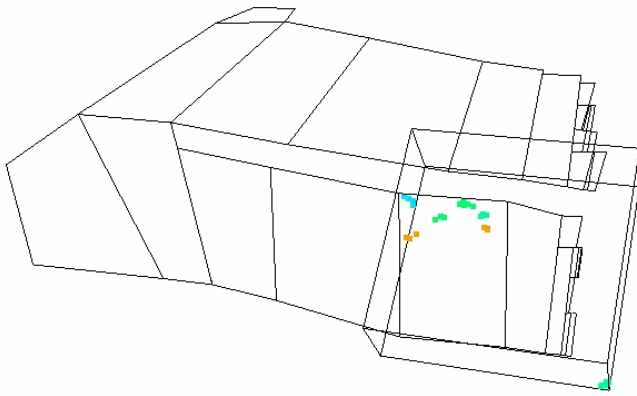


**Figure 3.3.9. IDR-generated seismic events during the first 20000 sec.**

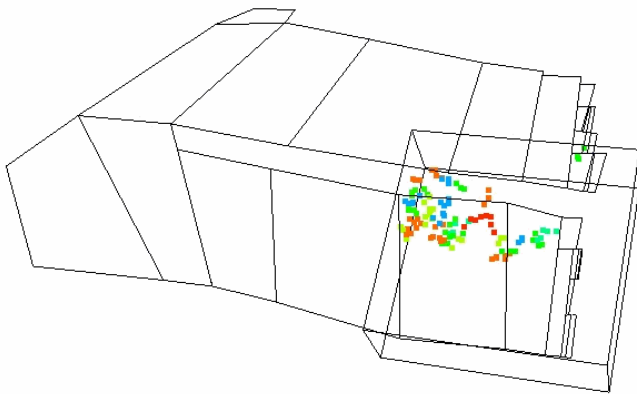


**Figure 3.3.10. IDR-generated events during the second 20000 sec period.**

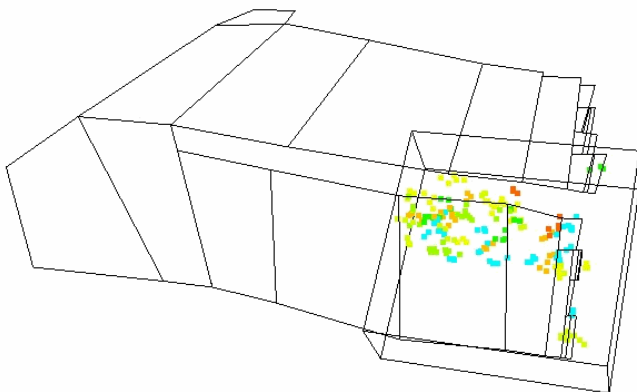


**Figure 3.3.11. IDR-generated events during the third 20000 sec period.**

Finally, the cumulative plot of all IDR-generated events for this simulation is shown in Fig. 3.3.12

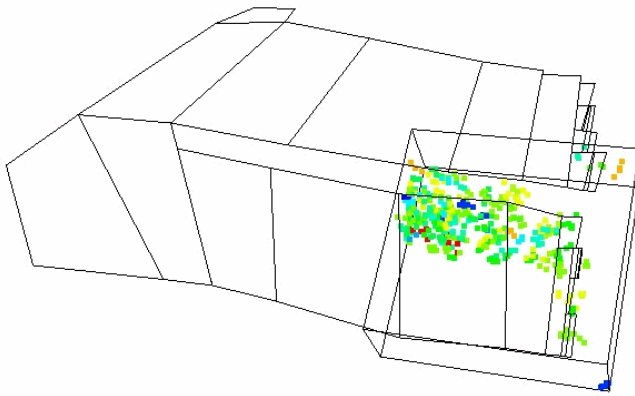


**Figure 3.3.12. All IDR-generated seismic events (about 35 hours of real time).**

The spatial clustering of model-generated seismic events depends on the choice of the connectivity range and on the threshold separating seismic events from acoustic noise. These parameters have an obvious importance for calibration purposes when model-generated data is compared with the records from the local seismic monitoring network.

Another factor which affects the results of the cluster analysis of model-generated data is the geometry of the spatial discretization. Quite apart from the obvious dependence on the grid size (which simply limits the resolution power of the model) there is a more subtle dependence on the aspect ratios of the elements of the grid (local factors) as well as on any anisotropies of the mesh as a whole: i.e. privileged planes and/or directions. The effect of these factors can be assessed and eliminated by running the model for several different grid sizes. A preliminary analysis shows that the results produced by IDR are not very sensitive to the distribution of the aspect ratios of individual tetrahedral elements but could be affected by the presence of privileged planes in the three-dimensional grid. In order to eliminate this effect a new meshing algorithm was developed which randomises the grid and improves the quality of individual tetrahedra at the same time.

## Modelling with DIGS

Slip weakening and tension weakening laws have been included in the DIGS code to try to reduce grid size effects in the simulation of random crack assembly failure. This model has also been extended to allow time-dependent cohesion and friction weakening. A problem of concern in simulating seismic activity, using random crack assemblies, is the identification of seismic event clusters. A simple test run in which a parallel sided stope is mined up to a span of 96m, using face advance steps of 2m, was carried out to attempt to gain some insight into the spatial positions of fracture clusters. In this analysis, the time and mean position of failure of each element in the random mesh was recorded. Figure 3.3.13 displays a plot of the normal distance to the reef plane at the time of failure of each element. This shows the dispersion of failure away from the reef plane as mining proceeds. It is also interesting to observe certain organised failure trajectories curving away from the reef plane as time advances. These paths correspond to fractures initiating at the stope face and then growing away from the stope horizon. Figure 3.3.14 shows a second plot in which the horizontal position of failure is plotted against time. It is apparent from this plot that failure generally follows the stope face position. (The stope face advance of 2m is assumed to occur after every 20 time step intervals). Coherent groups of points in Figure 3.3.14, for which the distance decreases as time increases, correspond to the same crack elements that form the associated point groups in Figure 3.1.13 and show that these cracks grow backwards over the mined region and away from the stope face. The group of points occurring near the relative horizontal position of 12m, corresponds to ongoing failure at

the “passive” end of the advancing slope panel. The analysis presented here is a first step towards formulating a procedure to identify the link between temporal and spatial clustering of failure sites. However, the results show that in this model very few fractures initiate ahead of the slope face. It is still uncertain how to identify the participating crack elements in a particular seismic “event”. Effects of random or selective material strength orientations would also affect the analysis.

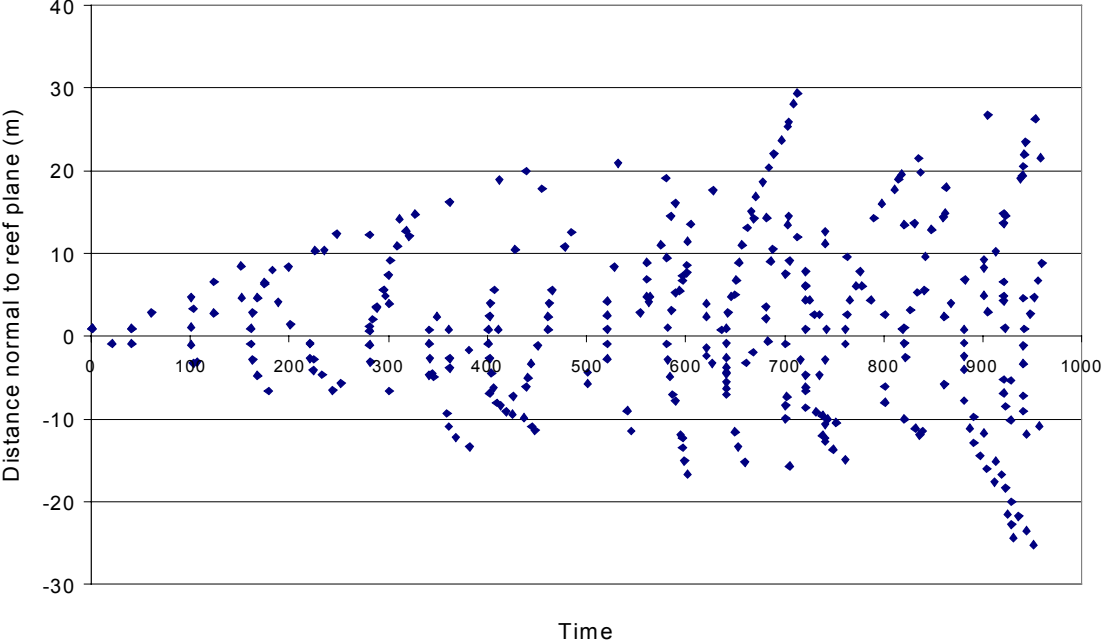


**Figure 3.3.13** Failure initiation position normal to the reef plane as a function of time. 20 time step intervals occur between each face advance increment of 2m.

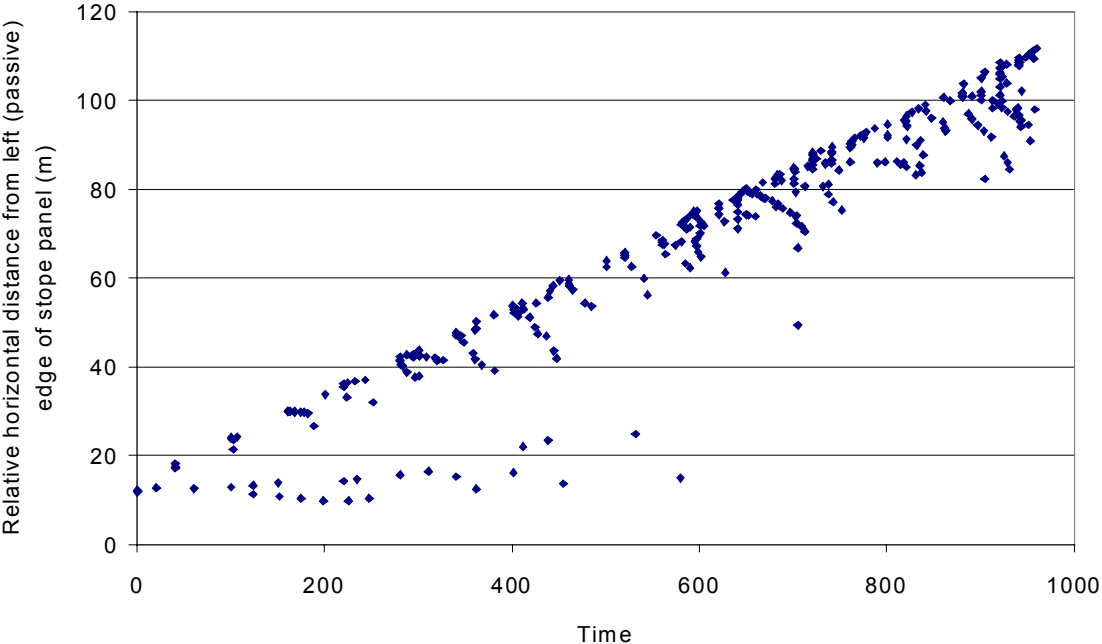


**Figure 3.3.14** Relative horizontal position of element failure as a function of time.

### 3.4. Migration of Seismicity

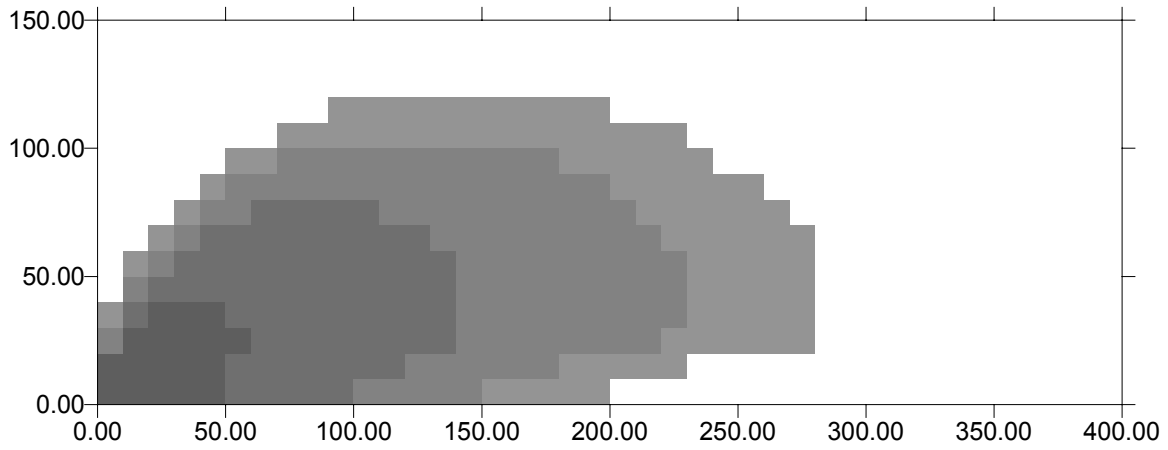
Studies carried out in this project have established that a number of simulations of mining induced seismic behaviour lead to exponential frequency-magnitude distributions of the number of events and their moment or magnitude. In these cases it has been found that the displacement discontinuity boundary element method (DDM) is an effective tool for the representation of random discontinuity assemblies or slip on a fault with random strength properties. It is noted, however, that an important feature of observed seismic behaviour in deep level mining is the migration of seismic activity along geological structures as a function of time.

In order to gain some initial insight into the representation of this phenomenon with the DDM, a simple mining geometry was considered. In this case, a rectangular shaped, horizontal stope, with dimensions of 400m by 190m, was analysed adjacent to a vertical fault plane situated 10m from the long axis of the stope. Four 50m by 10m rectangular segments of the effective pillar between the stope and the fault plane were then removed in successive steps, starting from one edge of the stope. Following each mining stage, the fault was allowed to slip according to a “creep” rule specifying that the rate of creep is proportional to the net shear stress acting across the fault. An important feature of the simulation is that all elements of the fault plane are initially intact. During each time step, the shear stress is computed at each fault plane element. If the specified fault strength is not exceeded no slip is allowed. If the strength is exceeded, the fault element is mobilised and is permitted to slip by an amount proportional to the net driving shear stress. The number of time steps between each pillar removal stage is nominally set to 20 or 25 time units.

Figure 3.4.1 shows the successive areas on the fault that are mobilised in each of the four mining stages. In the first stage, where the bracket pillar is removed in the region 0 to 50m from the left hand edge of the fault, it can be seen that an approximately rectangular patch of the fault, with area 50m by 40m, is mobilised. However, as successive portions of the pillar are removed, it is clear that the slip patch extends both vertically and laterally to the right hand end of the fault plane. Within each stage it is also observed that the mobilised elements migrate upwards and towards the right as a function of time. It is also particularly significant that the bracket pillar does not “insulate” the fault from movement when part of the pillar is removed and fault-stope intersection is allowed. The results shown in Figure 3.4.1 correspond to the assumption of uniform Mohr-Coulomb strength properties on the fault. The slip patterns are found to be similar if random properties are used.

Figure 3.4.2 shows the incremental area mobilised on the fault plane in each time step. It is interesting to note the randomness of this time series despite the assumed uniform fault strength properties. Figure 3.4.3 shows the corresponding energy release increments which show nearly regular decay rates following each pillar removal step.

It appears that the simple model presented here demonstrates some of the mechanistic elements of seismic migration or “diffusion” that arise in practice. However, it is necessary to assess how sensitive this model is to the assumed time-dependent creep law and to compare results to observed activity.



Fault area activated in each of four mining steps.

**Figure 3.4.1.** Four successive stages of fault slip corresponding to removal of the bracket pillar in the regions 0 to 50m, 50m to 100m, 100m to 150m and 150m to 200m respectively.

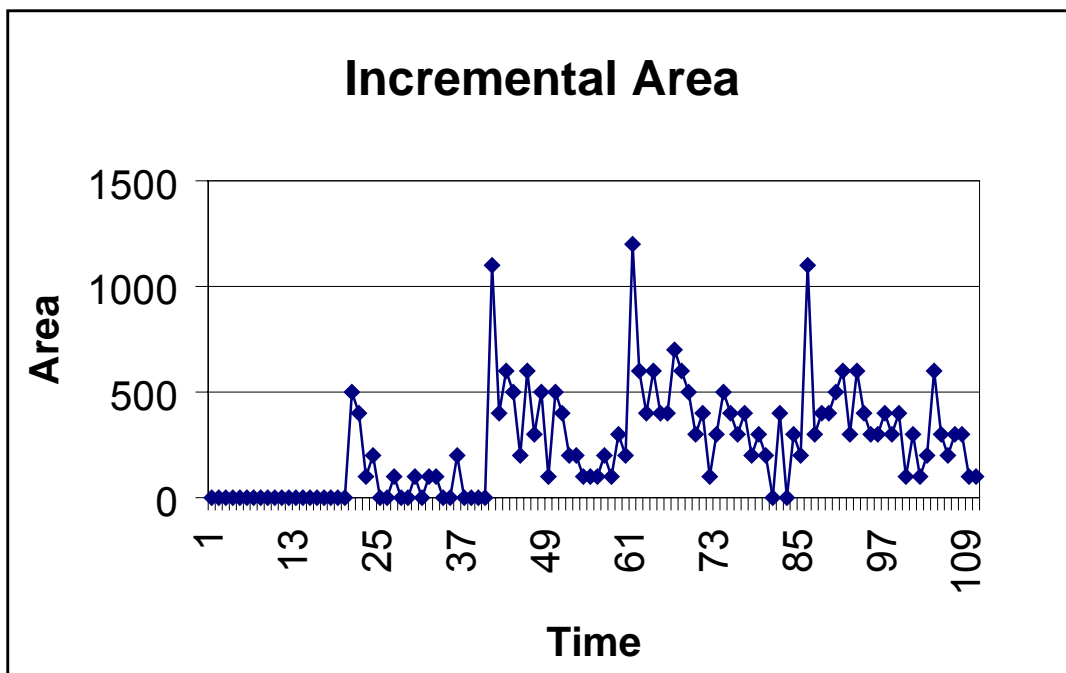


**Figure 3.4.2** Incremental area of fault plane ( $m^2$ ) mobilised as a function of time. Pillar removal stages occur at times 20, 40, 60 and 85.



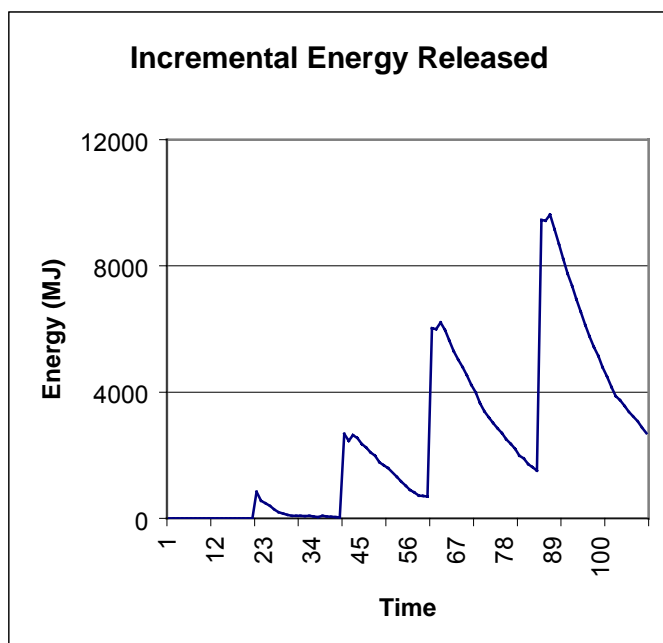


**Figure 3.4.3 Incremental energy release values corresponding to relaxation of the fault plane in successive time intervals.**

The integration of seismic migration and aftershock activity with numerical modelling requires an assessment of the capabilities of models to represent observed behaviour. On a smaller scale, smaller than the slope-fault interaction problem described above, it is necessary to assess whether models can replicate detailed migration effects following slope face blasting. An initial simulation of these effects has been carried out by considering the time-dependent formation of the fracture zone around a mining face. In this case a small region of approximately 10m × 10m is covered by a random mesh of grid elements and the edge of the slope is simulated as a rectangular slot adjacent to this region. The height of the slot (slope width) was set to one metre and fractures were then allowed to activate ahead of the slot. The average mesh element size was approximately 0.2m. The mesh was assumed to comprise intact elements interspersed with a population of weak flaws (one in every twenty mesh elements) having no cohesion. Figure 3.4.4 shows the cumulative length of flaws and mesh elements that are activated following the introduction of the slot adjacent to the mesh area. This displays a decreasing activation rate of the mesh segments as a function of time. (The model is uncalibrated and the time units have been omitted deliberately but could be considered to be in hours). To check for migration effects, the distance of the center of each sequentially activated mesh element from the center of the slope face was computed and averaged within each time step. This average distance has been plotted in Figure 3.4.5 as a function of time. Figure 3.4.5 shows that the fracture activation occurs in a region of approximately 5m radius from the center of the slope face. The graph also indicates that the locus of fracture activation does not show any clear trend as a function of time and continues to occur randomly within the 5m radius face region. Figure 3.4.6 shows the time-dependent trend of the energy release increments that arise within each time step after the implicit face “blast”. It must be appreciated that this model is extremely simplistic with respect to the manner in which the loads are applied to the face region as well as the local assumptions concerning the time-dependent fracture movement constitutive relations. It is therefore essential to compare this first step with observed data and to refine the face advance procedure.

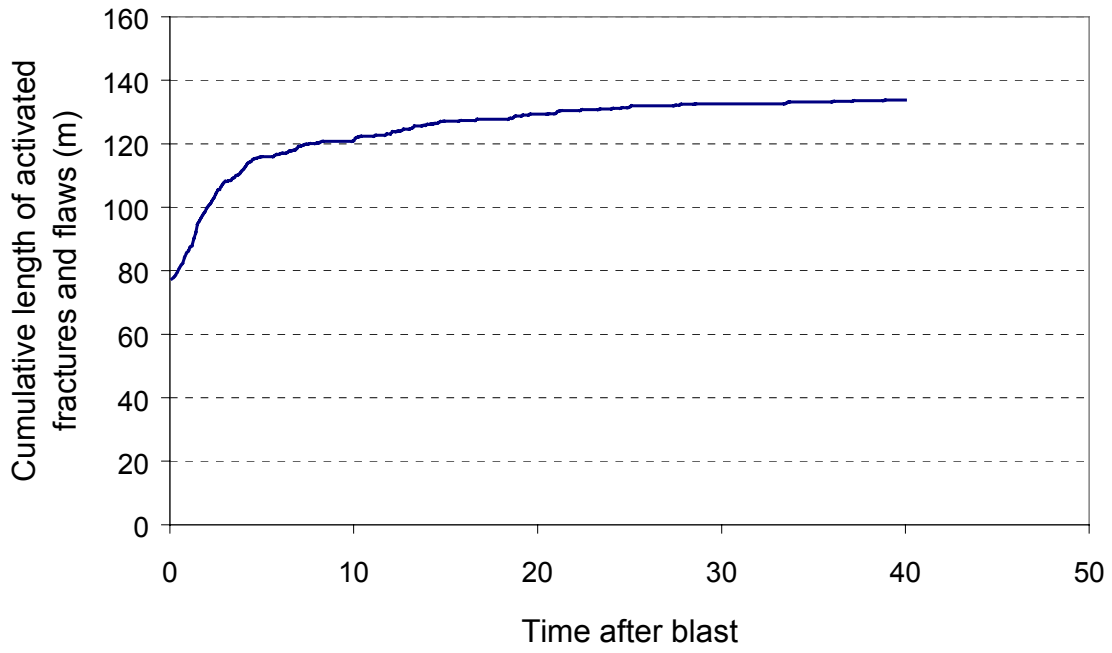


**Figure 3.4.4** Cumulative fracture length activated after the simulated “blast”.

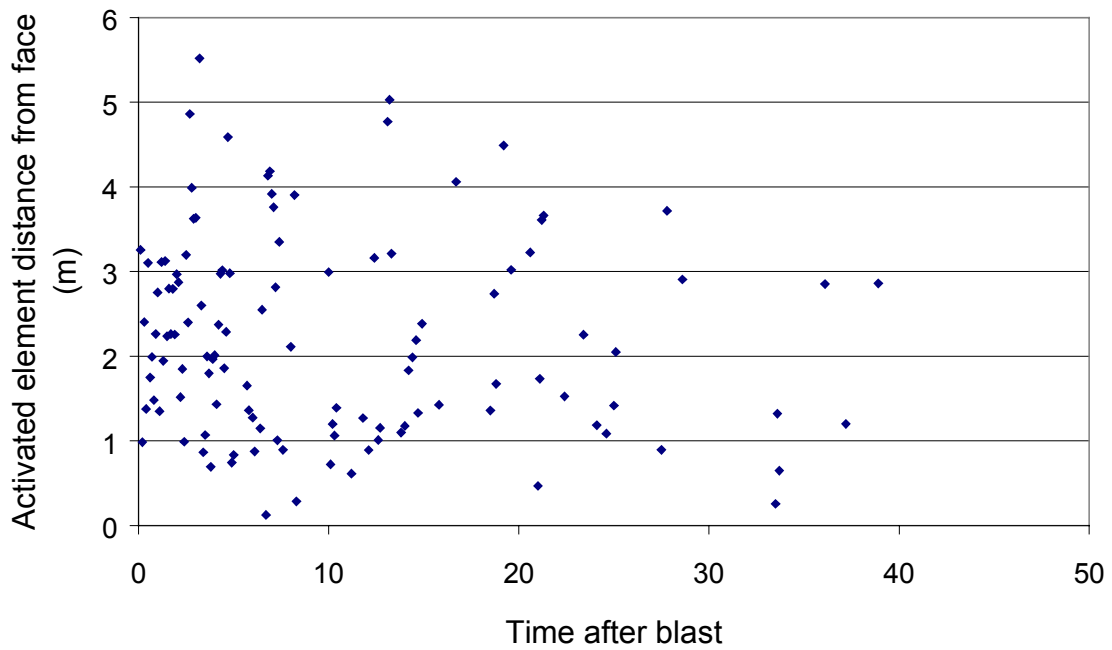


**Figure 3.4.5** Average distance from the center of the stope face of activated fracture segments in each time step after the simulated blast.

## Incremental energy release

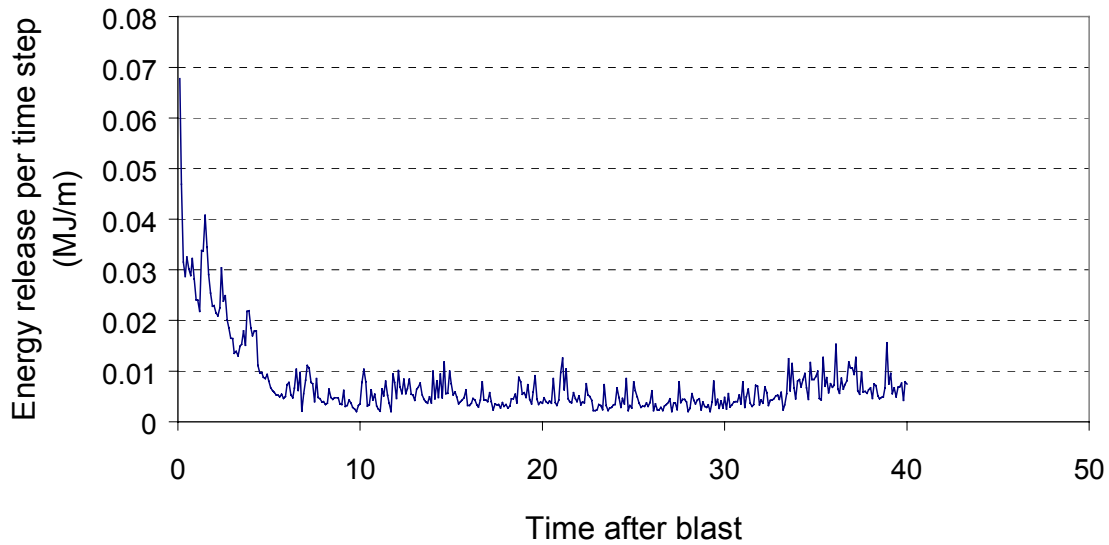


**Figure 3.4.6** Energy release increments in each time step following the simulated blast.

The Point kernel method has been extended to include viscoplastic discontinuities randomly distributed throughout space. This will enable the program to consider forward modelling of the potential for formation and interaction of new seismic events, based on a set on input seismic events and a known and planned mining layout. As an illustration, a two panel stope model was mined from a central raise line for 10 mining steps. The element size was 10m and 12 relaxation time steps were allowed for each mining step. The resulting time sequence of moment releases is shown in Figure 3.4.7. The figure indicates that events tend to cluster together in space and time. Migration effects are possibly evident in later mining stages where events are observed to be induced subsequent to the mining step. Further studies are required to investigate the effects of geometric, material and rheological properties.

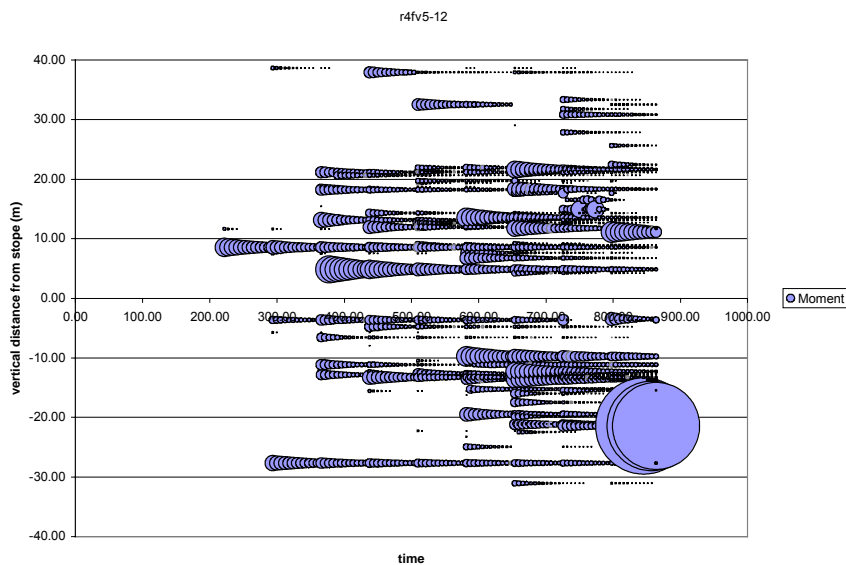


**Figure 3.4.7.** Point kernel analysis of stope showing distance of events to stope with time with magnitude indicated by size of the circles.





## 4. Seismic Monitoring: Requirements and Limitations

### 4.1. Requirements

**Location:** The location of a seismic event is assumed to be a point within the seismic source that triggered the set of seismic sites used to locate it. The interpretation of location, if accurate, depends on the nature of the rupture process at the source - if a slow or weak rupture starts at a certain point, the closest site(s) may record waves radiated from that very point while others may only record waves generated later in the rupture process by a higher stress drop patch of the same source. One needs to be specific in determining the arrival times if the location of rupture initiation is sought, otherwise the location will be a statistical average of different parts of the same source.

A reasonably accurate location is important for the following reasons:

- to indicate the location of potential rockbursts;
- all subsequent seismological processing, e.g. seismic source parameter and attenuation or velocity inversion, depends on location;
- all subsequent interpretation of individual events depends on location, e.g. events far from active mining, close to a shaft or, in general, in places not predicted by numerical modelling, may raise concern;
- all subsequent interpretation of seismicity, e.g. clustering and specifically localisation around planes, migration, spatio-temporal gradients of seismic parameters and other patterns are judged by their location and timing.

Location error depends on the accuracy of the data. Table 4.1 lists the major aspects of the data and their minimum precision required for accurate location (*Mendecki et al. 1999*).

The location depends also on the numerical procedure adopted to solve the system of nonlinear site equations. The denser the network and the more accurate the data, the smaller is the influence of the numerical procedure. With high quality data from at least 5 sites of reasonable configuration, the location error may be reduced to less than 3% of the average hypocentral distance of the sites used.

In the case of the velocity model not being known adequately, or if velocities change significantly with time, one can attempt to improve the location by the arrival time difference method, also known as 'master event' location or relative location. This procedure requires an accurately located master event (e.g. blast), in the proximity of the event to be relocated, that has reliable arrival times at sites used in the relocation procedure. It is inherently assumed here that the velocities of the seismic waves from the master event to the sites and those from the target event are the same. Since this is not always the case, it is important that the two events should be close to each other; less than 10% of average hypocentral distance would be a good rule of thumb.

In general the accuracy of location should be approximately half of the event size.

**Table 4.1**

<b>Parameters Affecting Location Accuracy</b> <i>Seismic site = the set of sensors with the same co-ordinates</i>	<b>Recommended Minimum Precision</b>
common time among seismic sites in the network	500μs
arrivals of P and/or S-waves at site	500μs or one sample
P and/or S-wave velocity model	7.5%
site coordinates	1m
sensors orientation at site, used to constrain the location by direction(s) or azimuth(s) of recorded waveforms; also used in seismic moment tensor determination	5 degrees
number of seismic sites	at least 5
the distribution of sites with respect to the position of the event to be located, e.g. as measured by the normalised orthogonality between straight ray paths from the hypocentre to the sites, $QC$ : $QC = 0.3873\sqrt{ns}[\det(C)]^{\frac{1}{3}}$ , where $C = \begin{vmatrix} \cos^2 \alpha_i & \cos \alpha_i \bullet \cos \beta_i & \cos \alpha_i \bullet \cos \gamma_i \\ \cos \alpha_i \bullet \cos \beta_i & \cos^2 \beta_i & \cos \beta_i \bullet \cos \gamma_i \\ \cos \alpha_i \bullet \cos \gamma_i & \cos \beta_i \bullet \cos \gamma_i & \cos^2 \gamma_i \end{vmatrix}$ and $\alpha_i, \beta_i, \gamma_i$ are directional angles between the hypocentre and the i-th site; $\sum$ runs over the number of sites, $ns$ .	0.3

**Static source parameters:** A seismic event, at its source, is a sudden inelastic deformation within a given volume of rock that radiates detectable seismic waves.

The velocity of that deformation varies on average from a few centimetres per second to a few meters per second, generally being slower within softer rock at lower differential stress. The average strain change varies from  $10^{-4}$  to  $10^{-2}$  and stress change can be as low as  $10^4$ Pa and as high as  $10^8$ Pa. The source size for small events of magnitude  $m = -2$  would vary between 2 and 4 meters and for larger events of  $m = 3$  could go from 100m, for fast sources in highly stressed, homogeneous rock to a few hundred meters in low stress, heterogeneous rockmass. The shape of the source can not be defined routinely and is frequently assumed to be circular or, at best, rectangular over the fault plane. More sophisticated inversion techniques need to be used to unravel the complex deformation and/or stress change distribution at the source(s) of seismic radiation.

Since the definition of the source of a seismic event in numerical models is not unique, one needs to derive as much useful information from waveforms as possible to constrain the guesswork.

The following static parameters, apart from the origin time and location, pertaining to seismic source are considered essential for the purpose of integration with numerical modelling:

- Scalar seismic moment,  $M$ , that measures coseismic inelastic deformation and it is related to the average slip  $\bar{u}$  over the planar source curve  $A$  or to the strain drop  $\Delta\varepsilon$  or stress drop  $\Delta\sigma$  at the volume source  $V$ ,

$$M = \mu \bar{u} A \quad \text{or} \quad M = \mu \Delta \varepsilon V = \Delta \sigma V, \quad 4.1.1$$

where  $\mu$  is rigidity. The inclusion of rigidity here may be misleading since linear elastic waves generated by a slip event have no information on material properties at the source (Ben-Zion, 2001). It is therefore better to replace moment with the observable product, called seismic potency  $P$ ,

$$P = \bar{u} A \quad \text{or} \quad P = \Delta \varepsilon V. \quad 4.1.2$$

- Seismic moment tensor,  $M_{ij}$ , that can be decomposed into isotropic (or volume change) and deviatoric components providing an additional insight into the nature of the coseismic strain drop. The eigenvalues and corresponding eigenvectors of the deviatoric component describe the magnitude and orientation, respectively, of the principal moment axis (neglecting gravity) acting at the source. These principal moment axes are uniquely determined by moment tensor inversion (Michael, 1987) and can provide sufficient information to find the best stress tensor, thus very useful for integration. For homogeneous body, the coseismic volumetric change,  $\Delta\Theta$ , can be calculated from (Aki and Richards, 1980)

$$\Delta\Theta = \text{tr}(M_{ij}) / (3\lambda + 2\mu),$$

where  $\lambda$  and  $\mu$  are the Lamé constants.

- Characteristic length,  $l$ , associated with the narrowest dimension of the source, which is inversely proportional to the higher predominant frequency at the velocity spectrum at the source,  $f_0$ , also known as the second corner frequency from the displacement spectrum,  $l = \text{constant} / f_0$ . For a circular source there is one corner frequency and  $l = 2 \times \text{source radius}$ .
- Stress drop  $\Delta\sigma$ , which is equal to the difference of initial  $\sigma_0$  and final  $\sigma_1$  stress values at the source:  $\Delta\sigma = \sigma_0 - \sigma_1$ . It follows from the linearity of the basic equations that  $\Delta\sigma$  and  $\bar{u}$  must be proportional to one another, thus

$$\bar{u} = c \frac{\Delta\sigma}{\mu} l \quad \Delta\sigma = \frac{M}{c l A} \quad 4.1.3$$

where  $c$  is a dimensionless constant depending on the shape of the source and for the most important cases, varies by a factor of two. Thus, if we know  $M$ ,  $A$  and  $l$ , the stress drops,  $\Delta\sigma$ , may be found with a precision better than a factor of, at most, 2. However, in most cases, only one source size parameter is obtained from waveforms and then stress drop is approximated by

$$\Delta\sigma = \frac{M}{c A^{3/2}}, \quad 4.1.4$$

which, for long thin sources may produce errors much larger than a factor of two.

**Seismic energy:** Seismic energy is defined as the total energy transmitted by seismic waves through a surface surrounding the source, and as such is inaccessible to the static or quasi dynamic numerical models used in the South African mining industry. In terms of source parameters the exact formula is given by Kostrov (1974) and Kostrov and Das (1988),

$$E = -2\gamma_{\text{eff}} A + \frac{1}{2} \Delta\sigma_{ij} u_i n_j dA + \int_0^{t_{\text{cs}}} dt \dot{\sigma}_{ij} u_i n_j dA \quad 4.1.5$$

where:



$\gamma_{eff}$  effective surface energy, which includes the total loss of mechanical energy, in particular inelastic work, and heat flow from the fracture edge;  
 $A$  fracture area with the displacement  
 $\Delta\sigma_{ij}$  difference between the final (at the end of the event) and the initial stress;  
 $n_j$  unit vector normal to the fracture plane;  
 $t_{cs}$  source duration;  
 $\dot{\sigma}_{ij}$  traction rate.  
 Summations over repeated indices is assumed.

From dimensional analysis it follows that the last two terms in equation (4.1.5) vary with the fracture area as  $A^{3/2}$ , whereas the fracture work,  $2\gamma_{eff} A$ , is proportional to  $A$  (Kostrov and Das, 1988). Thus, the relative contribution of the fracture work to seismic energy increases with a decrease in the size of the fracture. Consequently for sufficiently small fractures the first term may almost cancel the second term, suppressing the acoustic emission so that 'silent' fracture would occur.

The second term in equation (4.1.5) is determined by the static quantities – stress drop and final slip. The last term, containing the traction rate, strongly depends on how the fracture propagates and correlates with slip. The faster the oscillations of stress, the greater their contribution to the radiated energy due to the presence of the time derivative of stress. The energy due to radiation of high frequency waves during accelerating and decelerating rupture is called radiational friction. It usually occurs when the moving zone of slip pulse reaches regions of differing resistance to deformation. If traction rate and slip are uncorrelated the third term will vanish, and then

$$E = \frac{\Delta\sigma M}{2\mu} \tag{4.1.6}$$

In the far field the P and S wave contributions to the total radiated energy are proportional to the integral of the square of the P and S velocity spectrum. For a reasonable signal to noise ratio in the bandwidth of frequencies available on both sides of the corner frequency, the determination of that integral from waveforms recorded by seismic networks is fairly objective.

The high frequency component of seismic radiation needs to be recorded by the seismic system if a meaningful insight into the stress regime at the source region is to be gained.

Table 4.2 lists the major aspects of data used in source parameter calculations and the minimum precision required for reasonable results.

**Table 4.2**

Parameter Affecting Source Parameter Calculation	Recommended Minimum Precision/Value
calibrated, resonance free frequency range $\pm 3\text{dB}$ $m_{max}$ - the maximum magnitude event to be measured $m_{min}$ - the magnitude that defines sensitivity of the network geophone natural frequency geophone damping factor geophone sensitivity accelerometer sensitivity number of sites  location accuracy hypocentral distance $\text{SNR} = A_{max}/\text{pretrigger noise level}$ P and S wave velocities P and S wave attenuation & scattering Q rock density at the source window length for source parameters $T(A_{max})$ - period associated with maximum amplitude on velocity waveforms Uncertainties between the observed displacement spectra, corrected by the average radiation pattern, and the model.	$f_{min} = 0.5f_0(m_{max})$ $f_{max} = 5f_0(m_{min})$ 5% 5% 5% 5% 5 x 3 component each, or 3 x 3 comp. plus 6 single comp. 5% of AHD $> \lambda = \text{wave velocity} / f_0$ 10 7.5% 20% 10% $4 \cdot T(A_{max})$ 75%

**Quantification of seismicity:** Apart from general patterns of seismicity, e.g. size and time distributions, clustering and migration that have been described earlier, one can quantify the following seismic components of strain, stress or rheology change in the rockmass:

- Seismic strain and its rate,
- Normalised strain orientation tensor,
- Seismic stress and relative stress,
- Seismic viscosity and stiffness,
- Seismic relaxation time and Deborah number.

Since most routine numerical modelling packages used in the South African mining industry are static, the radiated seismic energy needed for most of those parameters can only be derived from

$$E = \xi \Delta W, \tag{4.1.7}$$

where  $W$  is the change in strain energy at the source and  $\xi$  is the seismic efficiency which can not be obtained by purely seismological observations and needs to be assumed by calibrations.

## 4.2. Uncertainties

**Location:** The location uncertainties depend on the following factors:

- The errors in arrival time determination: this source of errors can never be fully eliminated, since not only are both automatic and human pickers subject to errors but also the effective sampling rate of the instruments puts a bound on the accuracy of arrival times.
- Inadequate knowledge of the velocity model.

- Inaccuracy in the station coordinates.
- The method of solution: if the system is linearised a different location error will be found than if a nonlinear minimisation technique is used. The applied norm used will also play a role in the location error.
- The spatial distribution of stations with respect to the event to be located.

The estimate of the uncertainty depends on the method used to solve the system of station equations. If the location algorithm resorts to solving the linearised system, say

$$r = Ax \quad 4.2.1$$

where  $r$  is the vector of residuals,  $A$  is the matrix of derivatives and  $x$  is the vector of origin time and hypocenter corrections, then the covariance matrix can be calculated by

$$C = \sigma_d^2 (A^T A)^{-1} [(A^T A)^{-1}]^T, \quad 4.2.2$$

where  $\sigma_d^2$  is an estimate of the data variance, usually based on the variance of the fit to the arrival times (residuals). Individual uncertainties are simply the square root of the corresponding diagonal elements of  $C$ . The covariance matrix can be used to estimate confidence regions, which is usually a 4-dimensional ellipsoid using

$$(x - x_0)^T C_m^{-1} (x - x_0) = k^2, \quad 4.2.3$$

where  $k^2 = m\sigma_d^2 [F(m, n - m)] / (n - m)$ ,

where  $m$  is the number of unknowns, in this case 4,  $n$  is the number of equations and  $F$  is the  $F$ -statistic at a given confidence level. This type of estimate does not take into account errors in the velocity model, so that actual errors will generally exceed this estimate.

If a nonlinear programming method, e.g. Nelder-Mead algorithm, is used to solve the system of station equations, then there is no information on errors associated with the solution. In their original paper, *Nelder and Mead (1965)* pointed out that such errors could be evaluated by adding a few selected points and generating the Hessian matrix. The error estimation associated with the nonlinear method is performed using the standard approach, which entails calculations of the travel time derivatives with respect to the hypocentral parameters. Confidence ellipses are computed via:

$$(h - \bar{h})^T C^{-1} (h - \bar{h}) \leq k_\alpha^2 \quad 4.2.4$$

Where  $\bar{h}$  is the estimated hypocentre,  $C$  is the covariance matrix associated with the matrix of the partial derivatives evaluated at the estimated hypocentre. The value of  $k_\alpha$  depends upon the distribution of the residuals, usually assumed to be normally distributed. Under the assumption that picking and velocity model errors are normally distributed, *Flinn (1965)* proposed the following formula for  $k_\alpha$ :

$$k_\alpha^2 = 4s^2 F_\alpha(4, n - 4) \quad 4.2.5$$

where  $F_\alpha(4, n - 4)$  is an  $F$  statistic with 4 and  $n-4$  degrees of freedom for the critical level  $\alpha$  and

$$s^2 = \frac{1}{(n - 4)} \left( \frac{1}{n} \sum_{i=1}^n r_i^2 \right)^{1/2} \quad 4.2.6$$

where  $n$  is the number of observations and  $r_i = t_i^{obs} - t_i^{cal}$ .

The confidence ellipsoids that are calculated using this relation may be unrealistically large in the case of a small number of observations (Evernden, 1969). Jordan and Sverdrup (1981) suggested a modification in this relation by taking into account *a priori* information on the residual distribution:

$$k_\alpha^2 = \frac{4K + 4s^2(n-4)}{K + (n-4)} F_\alpha(4, K + n - 4) \quad 4.2.7$$

where  $K$  is the parameter that controls the amount of *a priori* information. For  $K = 0$  Flinn's relation is retained, while for  $K = \infty$ , it is assumed that there is exact *a priori* information. Jordan and Sverdrup (1981) recommended a value of  $K = 8$  (Thurber and Rabinowitz, 2000).

**Source parameters:** Seismic source parameters are often estimated from the velocity and displacement power spectra (Andrew, 1986) with corrections for the effect of the bandwidth limitations (Di Bona and Rovelli, 1988, Mendecki and Niewiadomski, 1997).

The power spectra approach does not use the objective function, consequently no information regarding the resolution of the parameters can be obtained directly from the inversion process. One may then use the conventional statistical testing to estimate the confidence intervals for the parameters. Extent of confidence intervals is controlled by the shape of the probability distributions function. A possible way to estimate the distribution of parameters is by using bootstrapping techniques, whereby repeated samples are drawn from the data enabling a distribution to be built up and to construct confidence regions. This type of simulation required to generate large numbers of the replicate time series and inversions. The method is suitable in all cases, where usage of CPU time is not an issue.

The alternative approach is to assume the shape of the probability distribution and then estimate the mean, variance and covariance matrix.

The computational advantage is that the estimation of statistical moments required far fewer replicated time series than that needed to reconstruct the probability distribution function.

The whole data set has to be divided into several subgroups to generate the replicated time series. There are several possibilities for selecting subgroups:

- Application different techniques of selection P-wave and S-wave windows
- Resampling of original data
- Using different station combinations ( $N-1$  in rotation)
- Resampling in the frequency domain

Power spectra are then calculated for each subgroup. The data for each subgroup are chosen arbitrarily, therefore one can calculate the variations of source parameters for every event.

The uncertainties of measured quantities are often produced from many factors which contribute to the final statistical error. There are two ways of combining individual errors in the final uncertainty of a measured quantity: additive and multiplicative. It is a rigorous result from the mathematical theory of probability that the additive combination of similarly distributed errors leads to a normal (or Gaussian) distribution while a multiplicative combination of component-errors leads to a log-normal distribution of the final uncertainty of the measured quantity.

The normal distribution of a random  $x$  is characterised by two parameters,  $\mu$  and  $\sigma$ , in terms of which the corresponding probability density function is given by:

$$f^{nor}(x, \mu, \sigma) = \frac{1}{\sigma\sqrt{2\pi}} \exp\left(-\frac{(x-\mu)^2}{2\sigma^2}\right) \quad 4.2.8$$

The mean value and the variance of the normal distribution are given by  $\mu$  and  $\sigma^2$  respectively.

The log-normal distribution can be defined by means of the normal in the following way: a random variable,  $x$ , is said to obey the log-normal distribution if  $\log(x)$  is found to obey the normal distribution. Using the same parameters  $\mu$  and  $\sigma$  to describe the log-normal distribution, one can write the corresponding probability density function, mean value and variance as:

$$f^{\log-nor}(x, \mu, \sigma) = \begin{cases} \frac{1}{\sigma\sqrt{2\pi}} \exp\left(-\frac{(\ln x - \mu)^2}{2\sigma^2}\right) & x > 0 \\ 0 & x \leq 0 \end{cases} \quad 4.2.9$$

$$\langle x \rangle = \exp(\mu + 0.5\sigma^2)$$

$$\text{var}(x) = (e^{\sigma^2} - 1)\exp(2\mu + \sigma^2)$$

The errors associated with seismic moment  $M$  and the source size,  $l$ , are assumed to be log-normally distributed (*Archuleta et al. 1982, Fletcher et al. 1987*). The error associated with seismic energy was assumed to be normally distributed.

**Seismicity parameters:** Once we have the uncertainties in the fundamental seismic parameters - time,  $t$ , location,  $X$ , radiated seismic energy,  $E$ , and scalar seismic moment,  $M$  - we can estimate the errors in quantities that are derived from these. These other forms are either microscopic, in the sense that the quantity is computed on a single-event basis, like apparent volume or apparent stress drop, or macroscopic quantities computed for a collection of seismic events within some volume of interest, like seismic Schmidt number or diffusion.

In what will follow we shall assume that the underlying probability density functions (pdf's) of the estimated seismic parameters are Gaussian, with the variances directly related to the standard deviations. This assumption can only be tested accurately by a time sequence of identical fractures occurring at exactly the same point in space, something that does not occur in nature. Nevertheless the central limit theorem dictates this to be a reasonable default assumption.

If the standard deviations of the underlying seismic quantities are small compared to the quantities themselves, then a simple analytic approximation may be used. For some function of the directly estimated underlying seismic quantities from some catalogue, we have a straightforward expression for the error of  $F(t_i, X_i, E_i, M_i)$  that parameter in terms of the underlying errors:

$$\sigma_F = \sqrt{\sum_i \left[ \frac{\partial F}{\partial t_i} \sigma_{t_i} \right]^2 + \sum_i \left[ \frac{\partial F}{\partial X_i} \sigma_{X_i} \right]^2 + \sum_i \left[ \frac{\partial F}{\partial E_i} \sigma_{E_i} \right]^2 + \sum_i \left[ \frac{\partial F}{\partial M_i} \sigma_{M_i} \right]^2}$$

### 4.3. Limitations

The fundamental limitation of seismic monitoring is our limited understanding of the deformation and radiation processes at seismic sources and the inability to recover all useful information from recorded waveforms. Specifically, larger seismic events in mines have proven to be complex rather than simple fracture-like sources with multiple subevents and non-uniform distribution of inelastic strain or slip, e.g. see Figure 4.1 after *Cichowicz, 2001*.

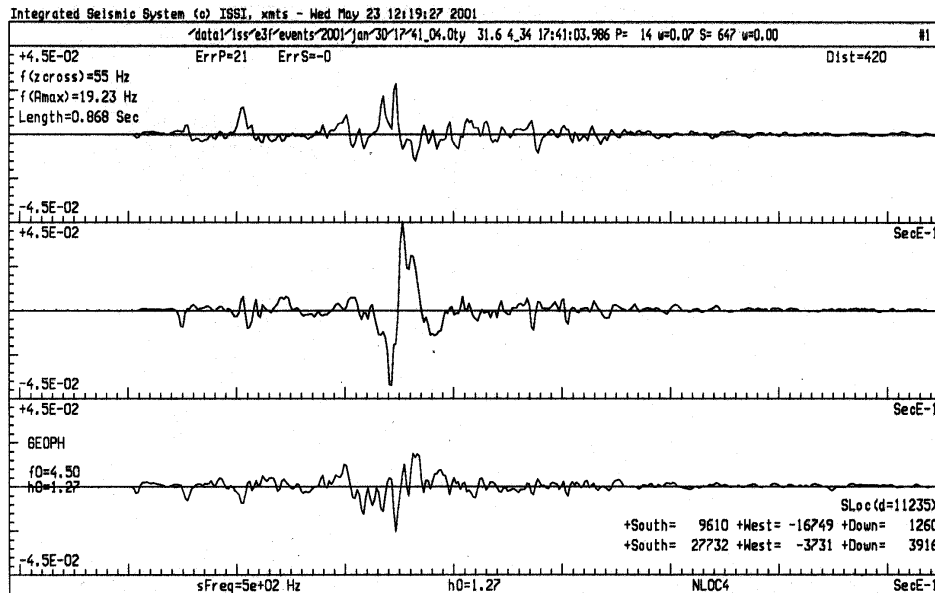


**Figure 4.1a** Waveforms of a complex seismic event of  $m = 3$  recorded at distance of 420m from the source. In this relatively homogeneous medium complexity of waveforms is caused mainly by the complexity of the source.

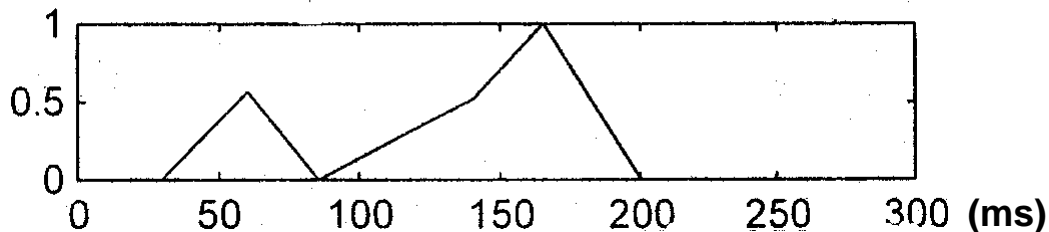


**Figure 4.1b** Source time function of the event above obtained from the moment tensor inversion in time domain. Amplitudes are normalised to 1.

The same limited understanding applies to seismic processes leading to rockbursts where certain recognisable spatio-temporal patterns exist only over a limited time period after which a dynamical reorganisation occurs that leads to the appearance of a new but still temporary pattern of events. The nature of the processes responsible for this complex dynamic is not as yet understood and it severely limits the predictability of rockmass response to mining by either the numerical modelling or seismic monitoring techniques. Specifically important is to understand the spatio-temporal mechanics of an extended system and to distinguish its characteristic time and length scales associated with processes of excitation, dissipation and correlation. It is the ratios of these times and lengths to each other and to the characteristic system size that determines the state of the dynamics and the extent of the influence between the different points of the system.

In general we cannot claim to understand a phenomenon unless we can prescribe a rule, e.g. an equation or a computerised algorithm, that allows us to say something about the future behaviour of a system, given information about its present state.







## 5. General issues and future developments

### 5.1. Validation of model representations of seismicity

Validation and verification are terms that are often applied in numerical modelling to describe the process of determining whether the results of the model are reliable and can be used for making predictions. *Oreskes et al. (1994)* present a philosophical discussion on the application and reliability of models. They consider that the term “verification” implies that the “truth” of the model has been demonstrated. They argue that it is impossible to demonstrate “truth” in the context of a numerical model. The individual mathematical components or computational algorithms may be verified as they are part of a closed system, in which each part is well defined and hence the correctness of the result can be proven, or verified. In contrast, models are an incomplete representation of an open system. They require input parameters that may not be well defined or known, and there is a loss of information regarding the system due to a choice of the scale at which the system is described.

Validation is considered by *Oreskes et al. (1994)* to mean the process of ensuring that there are no errors of logic or detectable flaws within a computer program. A model cannot be validated in this sense, as the results depend on the input parameters and hypotheses. They present a number of cases that indicate that the general usage of the two words is inconsistent, and usually are both meant to suggest that the model can represent reality. A comparison of the model results with in-situ or laboratory tests data is still not sufficient to validate the model. They note that comparison of the results of a numerical model with an analytical solution can show that the program is verified in a limited sense, but does not say anything about the ability of the model to describe reality or to provide correct predictions in other situations. In a similar manner, calibration of the model to conform to a set of observed data is still not a guarantee that the model predictions will be relevant in other circumstances.

The usefulness of models is not however questioned by *Oreskes et al. (1994)*. Models can be applied to provide additional information regarding the consequences of hypotheses. They can be used for sensitivity analyses to understand the relationships between the input parameters and the outputs and to define requirements for new empirical data. Comparison with other models can highlight shortcomings in different hypotheses. Alternatively, the model may be used for prediction into the future, as long as relevant changes are made to the input parameters over the considered time period.

*Oreskes et al. (1994)* consider that the “main reason for modelling is the lack of full access in time or space, to the phenomena of interest.” This view can be challenged by asking if the purpose of the model is in fact not to be a replica of the real system, but is instead a distillation of the important features. Then, the usefulness of the model is that the system can be understood, and predictions made, without the complications of unnecessary detail. If this view is taken, the validation must be the process of ensuring that the output reflects the main features of the system.

In the context of the modelling of seismic patterns, *Ben-Zion and Rice (1993)* consider that the reproduction of a Gutenberg-Richter power law with a b-value of 1 is not a sufficient condition for concluding that the model correctly represents real seismic data. The correctness of the model should be determined by its ability to model observed deviations from the power law. In many models, the b-value is observed to remain invariant regardless of chaotic response in the time series of events resulting from small changes to the input parameters (*Robinson and Benites, 1995*). The value of  $b = 1$  is a nearly universal outcome of self organised models (*Robinson and Benites, 1995*) and can be obtained from boundary

element based discrete fault plane models (*Eneva and Ben-Zion, 1993*), cellular automata (*Wilson et al, 1996*), spring slider models (*Shaw, 1995*), particle models (*Hazzard, 1998*), and even continuum models, assuming that the elements have a random strength distribution.

The essential element for prediction of power law response is that there is some type of randomness in the input parameters (*Ben-Zion, 1993, Eneva and Ben-Zion, 1995, Wilson et al. 1996, Rundle and Klein, 1993, Rundle, 1988, Lyakovsky et al, 1998*). The randomness results in self organisation and scaling behaviour. Uniform or uncorrelated properties lead to characteristic events that relate to a specific size. The number of size scales represented in the model can also change the response from scaling to characteristic size events (*Ben-Zion, 1998*). A wider range of scales is needed to develop a power law output. Alternative effects such as dynamics and conservation parameters can also change the event statistics, even in the same model. The inclusion of inertial dynamics does not necessarily lead to complexity. Strong heterogeneities, or special friction laws are also needed.

The event statistics may also depend on the space-time window that is used to observe the events (*Ben-Zion and Lyakovsky, 1999, Hazzard, 1998*). The model must also be relevant to the physical situation (*Sammis et al, 1999*). Thus, a model of a crack in an elastic half space produces extremely high stress drops compares to events observed in a creeping fault zone at Parkfield U.S.A.

A number of problems arise in comparing numerically generated seismicity with observed data (*Eneva and Ben-Zion, 1997, Rundle, 1988*). There is considerable non-uniqueness in the representation of seismicity by numerical models, as well as non-universality in earthquake models. Models should be constrained by comparison with geological and seismological data. The degree of predictability varies depending on the choice of the properties of the numerical fault. The relative performance of different models varies when measured against different seismic parameters. Precursory or long-term trends vary from model to model. Finally, all models may vary from the observed data, but the amount of correlation may be optimised for certain models. Thus, there is a considerable degree of subjectivity and non-uniqueness in the selection of the modelled seismicity.

## **5.2. Definition of a seismic event in the context of a particular model**

### **5.2.1. Quasi-static Boundary Element Tessellation/space filling codes**

- The incremental moment,  $M_0$ , for each element is computed and summed for the whole crack assembly. This is easy to apply and considers larger clusters but the definition of a cluster is a problem. As shown in Figure 5.2.1, there is no unique definition of what constitutes a cluster. Problems with this approach also include determination of the order of events, geometry of the cluster and the cluster extension in later steps.
- Calculation of released energy for each time step is easy to apply and considers larger clusters, but may incorporate too many events in one cluster.

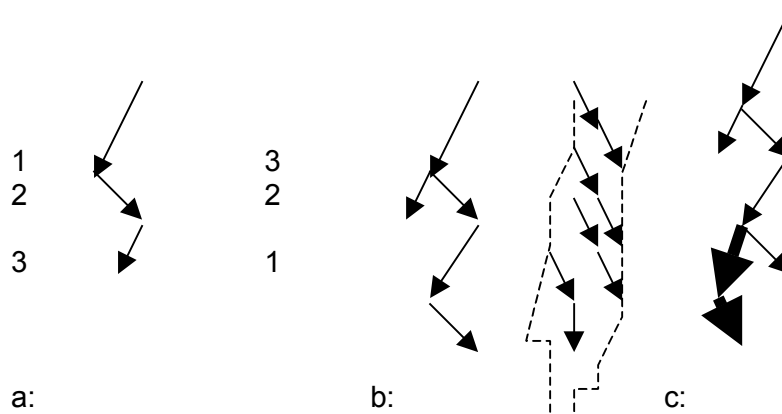


**Figure 5.2.1 Problem of non-unique clustering in a tessellation analysis. Problems include determination of a: order of events, b: geometry of cluster and c: cluster extension in later steps.**

## 5.2.2. IDRM

Due to the damage-dependent elastic potential energy the constitutive relations of IDRM are non-linear and break down when the free energy loses its convexity. The loss of convexity of the free energy signals the beginning of a damage event accompanied by stress-drop in the failed elements as well as with induced (co-seismic) stress-drop in other elements. The latter is a process which could be localised in space and finishes with the restoration of the convexity of the free energy. Due to the full access to the stress and strain fields provided by IDRM one can extract information about the modelled events in full detail. IDRM writes the catalogue of damage events it generates. This model-generated data set needs further processing in order to filter out the actual model-analogues of seismic events from the acoustic noise which would remain below the sensitivity threshold of the seismic monitoring system. In other words, IDRM like all similar models of seismic activity requires an unambiguous and quantitative definition of what is to be interpreted as a modelled seismic event. Further the said definition of modelled seismic events must be sufficiently flexible to allow for a calibration of the running model to the observed level of local seismicity. IDRM is equipped with such a definition of a modelled seismic event.

Key to the definition of seismic event within IDRM is a cluster-analysis of the model-generated data on element failures due to damage above the critical level and a loss of stability. Not every failed element is treated as a source of a seismic event. Instead, the set of all simultaneously failed elements is analysed and all connected clusters (see the corresponding entry in the Glossary) of such elements are identified. A seismic event is a connected cluster of “mass” above a certain minimum value. The damaged elements which do not belong to connected clusters of sufficient size are treated as contributing to the acoustic noise.

## 5.3. Computational geometry issues in numerical modelling practice

Computational geometry is a new discipline dealing with the algorithms of representing geometrical object in a manner suitable for computer programming and especially for the development of computer graphics applications and for solving boundary value problems. The scope of computational geometry includes algorithmic development for the following problems:

- draw the best-fitting smooth curve to a given set of points
- draw the best-fitting smooth surface to a given set of points
- given a smooth surface, cover it completely with elements or “tiles” which do not overlap.
- given a three-dimensional body, subdivide it into elements of a given geometry. The elements should not overlap and the coverage must be complete i.e. it must cover the whole body.
- given a coverage of a geometrical body with elements, refine the coverage by adding additional elements or make the coverage coarser by removing and merging elements.

These and similar problems arise in a natural way from the needs of the applied and engineering sciences. The interest in computational geometry has been steadily increasing and has led to the creation of an independent scientific discipline. The development of numerical modelling depends strongly on the progress in computational geometry especially for the discretization of problems originally formulated for a continuum in two or three dimensions.

Of interest to the numerical modelling of seismicity-related phenomena is the generation of two- and three-dimensional grids constrained within some specified domain. The process of generating such grids is known as meshing or gridding. Grids are used for transforming problems formulated initially for a continuum into approximately equivalent discrete problems. The term “approximate equivalence” as applied to two problems needs some clarifying: two problems are said to be equivalent if they have the same set of solutions. Two problems are approximately equivalent if the solutions of one problem can be regarded as approximations to the corresponding solutions of the other problem. The idea of numerical modelling consists in reformulating a given “tough” problem into an approximately equivalent and easier to solve problem. The problems of continuum mechanics are considered as tough while the problem of solving a system of simultaneous algebraic equations is considered as “easy” even when the number of equations is large.

By imposing a grid over the spatial domain occupied by a solid it is possible to reformulate a boundary value problem for the partial differential equations of continuum mechanics into some approximately equivalent problem of solving a system of algebraic (often even linear) equations. There are three different ways of achieving this:

- One can use the nodes of the grid to obtain discrete analogues of the operators of taking partial derivatives. This idea is implemented in the various finite differences methods.
- One can seek an approximate solution to the given boundary value problem as an assembly of “pieces”, each piece being a combination of some basis functions and defined within one of the sub-domains into which the grid has partitioned the whole domain. Such “piecewise” approximations are at the basis of various finite element schemes.
- It is possible to regard a solid as a heterogeneous assembly of homogeneous “grains” or “blocks” and to identify the latter with the elements of a grid. This is the underlying idea of the discrete or distinct element models.

All numerical models of importance to the mining industry fall into one of the above categories. In a sense, the choice of the discretization scheme is inseparable from the choice of modelling strategy. Therefore it is important to understand the effect of the geometrical or grid factors on the performance of a numerical model.

A grid or mesh which has been generated for a particular model can be characterised by:

- Its length-scale or grid-size which is defined as the minimum distance between nearest-neighbour nodes. The grid-size is a local parameter and can, in principle, vary from one part of the grid to another. For regular grids, though, the grid-size is an over-all constant.
- Its connectivity index which is determined by the number of connected nearest-neighbour nodes of the grid. The connectivity of a grid is closely related to the dimensionality of the gridded manifold as well as to the geometry of the unit cell. For regular square grids the connectivity index is equal to twice the Euclidean dimension of the manifold. For tetrahedral grids in three dimensions the connectivity index of a grid-node is defined as the number of tetrahedra to which the node belongs.
- Its topology or deformation-invariant properties. For instance a grid of a sphere is different from any grid of a dough-nut-shaped body.
- The quality of the grid elements or cells. The quality factor of a grid element is sometimes expressed in terms of the so-called aspect ratio. The aspect ratio is defined in a different way for different types of grid elements even if they have the same Euclidean dimension. Alternatively the quality of the grid elements and hence of the discretization procedure as a whole can be measured by a quality factor which is the normalised ratio of:
  1. the square root of the area over the circumference for two-dimensional elements
  2. the cubic root of the volume over the square root of the boundary area for three-dimensional elements.

The grid topology is not a matter of choice but is dictated by the geometry of the rock-mass to be modelled. The connectivity index of the grid is determined to a great degree by the dimensionality of the problem and to a lesser degree by the choice of the unit cells for the grid to be generated. The other two characteristics of a grid are entirely subject to choice and determine the resolution and accuracy of the approximation provided by the model.

The smaller the grid-size (i.e. the finer the grid) the smaller will be the minimum size of the seismic events generated by the model. The grid size affects also the accuracy of the discrete solution of the continuum problem: the finer the grid, the better the approximation since the latter is related in one way or another to some interpolation procedure. But the limitations of the present day computers in processor speed and in core memory restrict the minimum grid size for a given volume of the modelled body.

The quality factor of the individual grid elements does not alter the resolution power of the model but does affect the accuracy of the approximation. For instance, in a finite differences scheme, the partial derivatives of the unknown function are replaced by partial derivatives of some interpolation polynomials with nodal points defined by the grid elements and if the latter are abnormally elongated the approximation to the derivatives could be very poor. Better quality factor means better shaped elements and correspondingly more accurate representation of the derivatives. In a finite element scheme the interpolation is via some basis of shape functions and a badly-shaped element can lead to a large error in the replacement of the unknown function with the corresponding combination of the shape functions. In a boundary integral scheme the shape of the elements is directly related to the errors in the numerical integration (which again uses interpolation techniques). Finally, the shape characteristics of the grid elements are of great significance in distinct-element modelling and in molecular-dynamics inspired schemes (friction, fracture etc.). When a heterogeneous rock-mass is modelled as an assembly of homogeneous “blocks” the shape of the grid elements determines the interfacing of the blocks, the area of the contact surfaces and the contact interactions.

Apart from the grid refinement and the quality of the grid elements the accuracy of a numerical model can be affected by global grid artefacts. For instance, the algorithm for meshing the target body could produce a grid in which most of the nodes sit on preferred

planes or lines which would introduce artificial anisotropies. This problem is common for structured grids and can be avoided by randomising the nodes of the grid while keeping the connections.

### **5.3.1. The continuum limit and finite-size scaling**

It is believed that the solution of a correctly formulated problem for a continuum solid will correspond to the observed behaviour of the object. Unfortunately, the problems of practical interest are essentially heterogeneous, anisotropic and non-linear which means that the exact solution cannot be found analytically. The question is to what degree a numerical solution of a discretized version of the original problem would approximate the existing and yet unknown exact solution?

There are many different numerical approaches to the same problem originally set for a continuum. Further, even within the same numerical approach there can be many different models corresponding to different grids. This means that one and the same problem has an arbitrary number of candidates for “the solution”, some very far off the target, others more acceptable.

A criterion is needed for selecting out the best numerical solution among the available approximate solutions. The following line of reasoning may lead to the formulation of such a selection rule. Suppose that we have a numerical model based on some interpolation scheme. If we could simulate the model for a sequence of grids with increasing refinement one can expect that in the limit when the grid size goes to zero the discretized version of the problem would become infinitely close to the original formulation in the continuum and hence the solution of the model would tend to the exact solution. This procedure is called the exact continuum limit of the model and cannot be carried out in practice because it would require unlimited memory and computer time. Unfortunately it is very difficult and sometimes even impossible to prove that the exact continuum limit exists and if it does that it is unique. With some sacrifice of mathematical rigour and guided by practical considerations one could look for signals of convergence in a sequence of simulations corresponding to an increasing grid refinements. If one assumes that the character of the convergence, at least after some initial transient part of the sequence, is monotonous, then the approach to the limit will be signalled by a reduced variation of the consecutive members in the sequence. In practice one will have to run the model for several grids with different degree of refinement and look for a decreased sensitivity of the modelled data on the grid size. When it is found that the last refinement of the grid did not change the modelled data by more than an acceptable margin, one can conclude that the practical continuum limit has been reached.

Strictly speaking, one cannot speak of a continuum limit for a discrete element model. Yet the same idea of reduced sensitivity of the modelled data to changes in the element size can be applied to assemblies of distinct elements. For assemblies of distinct elements it is of greater importance to study the so called finite-size scaling, which tests the sensitivity of the model to increasing the number of constituents.

## **5.4. Error analysis of real and modelled data**

Errors are always present in data. The origins of errors in a set of real data collected by a seismic monitoring system are different from those of the errors in modelled data. Yet the methods of error analysis are sufficiently general to cover all sources of errors and thus are applicable to both real and model-generated data. A systematic treatment of the theory and practice of error analysis goes far beyond the scope of these Guidelines.

### **5.4.1. Types of errors**

There are two types of errors: systematic and accidental. Errors of both types are present, in principle, in every data set be that a list of observed values or a numerical output from a running model.

#### **5.4.1.1. Systematic errors**

The systematic errors in real data can be due to some features of the electronic design of the monitoring equipment or due to the concrete conditions in which the equipment operates e.g. temperature, humidity, human factor and the like. Another source of systematic errors in observed data could be the methodology used in the processing of seismic events including all model assumptions made for this purpose. The configuration of the seismic stations in a local network also affects the results by adding a, sometimes considerable, systematic error especially in the location of the seismic sources.

The main sources of systematic errors in data generated by a numerical model are:

- The choice of basic equations
- The choice of numerical approximation to the solution of the mathematical problem formulated in the model
- The discretization scheme applied and especially its length-scales
- The choice of the prescribed values in the initial and the boundary conditions

The above lists can be enlarged by including many other sources of systematic errors in real as well as in modelled data.

#### **5.4.1.2. Accidental (random) errors**

Accidental errors are present in all measurements and their origin is not as easy to trace as was the case with the origin of systematic errors. A common feature of the accidental errors is that their values form random sequences in which there are no obvious correlations. For this reason the accidental errors are also called random errors.

The random errors in measured values are usually attributed to the sensitivity and the resolution power of the measuring instruments. In the case of model generated data the random errors can be negligibly small if the model is based on a deterministic algorithm. The situation is different, though, for stochastic modes in which the output is directly linked to some random process e.g. numerical models implementing the Monte Carlo method.

#### **5.4.1.3. Control of random errors**

The presence of random errors in a data-set can be established by studying the distribution of the numerical values with the standard tools of mathematical statistics. In particular, one can evaluate the first moments i.e. mean and variance as well as the lower-order correlation functions. The probable value of a measured quantity is associated with the statistical average while the corresponding variance provides a measure for the accuracy with which one can accept the above value. The reliability of the statistical estimates for the mean and the variance depends on the volume of the data-sample.

The analysis and control of random errors is of importance for real data since the measuring instruments and the data-acquisition units are susceptible to countless random disturbances.



Model-generated data is practically unaffected by random errors unless the algorithm is stochastic.

#### 5.4.1.4. Control of systematic errors

The control over systematic errors is more difficult than the treatment of random errors because there are no general procedures for this kind of analysis. Instead, each case must be treated individually and the actual cause for the systematic errors must be identified and quantified. The systematic deviations to the measured values by a seismic monitoring system can be separated out from the raw data by testing the equipment for:

- the susceptibility to temperature variations
- the susceptibility to variations of the humidity
- the effect of mechanical factors on the equipment
- the effect of ageing on the equipment

A very important source of systematic errors in observational data is related to the design of the measuring equipment. In order to identify and quantify systematic errors due to the design of a seismic monitoring system it would be necessary to compare different sets of data collected by different seismic system installed on the same site. The installation of two or more parallel seismic systems on the same site can be prohibitively expensive but one can double some of the components of an installed seismic system.

The above-listed possible sources of systematic errors in real data are difficult to control and, for that reason, are often ignored. A more realistic task will be to quantify the effect of the model assumptions needed for the analysis of seismograms. This includes the details of the algorithms implemented in the seismic analysis software. Finally, it is necessary to estimate the effect of the configuration of the seismic network on the data.

The systematic errors are often the only errors present in model-generated data. The main sources of systematic errors in modelled data are:

- the choice of equations implemented in the model
- the choice of numerical approximation to the exact solution of the equations
- the formulation of the initial and boundary conditions needed for solving the mathematical problem in the model
- the properties of the discretization scheme used for reducing the number of degrees of freedom in the problem (a continuum mechanics problem involves infinitely many degrees of freedom and cannot be treated in a computer unless discretized)
- errors due to the interpolation of continuous functions by a finite set of table-values
- some elements of the computer code can lead to errors in the model output due to loss of accuracy (single precision numbers used instead of double precision in sensitive segments of the code)

Most difficult to quantify are the errors due to the choice of the basic equations embedded in the numerical model. The equations of physics can have a limited domain of validity and, if applied beyond this domain, their solutions can deviate from the observed reality. A typical example is the use of the linearised version of an equation (say, the harmonic oscillator) in the region where nonlinear effects become non-negligible and even dominant. The only way to identify the contribution to the total error in modelled data due to the fundamental equations of the numerical model is by comparing different data-sets generated by different models designed to solve the same problem. Unfortunately, this recipe is far from easy to implement.

### 5.4.2. Errors due to the discretization (grid-size and grid-quality effects)

The systematic errors in modelled data due to the properties of the discretization scheme are better understood and easier to analyse and quantify. The discretization of a continuum problem is usually carried out by imposing on a region of space (or space-time) a finite grid (mesh) of nodes connected by links. The elementary cells of the mesh provide an approximation to the real material in the sense that the material properties within a cell are considered either constant or changing according to some shape function. This approach is especially well-suited for the treatment of heterogeneous and granular materials. The error due to the discretization of heterogeneous materials can be reduced by calibrating the size of the elementary grid-cell to the actual size of the homogeneous system. The errors due to the shape of the individual grid-cells are treated in a similar way.

The main reason for introducing a grid in a model is for converting a set of differential or integral equations into a system of simultaneous algebraic (usually linear) equations. In the case when the numerical model is built on differential equations, the grid is used for obtaining a discrete representation of the differentiation operator. Grids are used for solving integral equations by replacing the integrals with numerical quadrature or cubatures (as for instance in the Boundary Element Method). The errors introduced by the discretization in these cases are due to the interpolation of an unknown function by a set of nodal values.

In numerical models of seismic activity the most serious grid-size effect is an imposed cut-off on the size of the modelled seismic events. The minimum grid-cell size determines the resolution power of the model with respect to the magnitude of the seismic events and the separation of their hypocentres. The total volume of the grid used in a model puts an upper limit on the maximum size of seismic events which can be simulated. In dynamic modelling of seismic waves the grid-size imposes an upper cut-off on the frequency spectrum while the total span of the grid restricts the lowest frequency (i.e. largest wavelength) in the model.

The influence of the discretization on the modelled data is a broad subject and needs a specific treatment for different numerical models. The road to quantifying the grid-determined errors in a model is via a sensitivity analysis of the model response to variations of the parameters determining the grid.

The evaluation of the various computational methods reveals that a fundamental grid size is implied in each case. The particular grid size parameter is as follows.

- Finite element method: element mesh size
- Particle flow code: average ball size
- 2D DIGS model: tessellation mesh size
- 3D fault slip model: square element size
- FLAC model: zone size

It is important to address the following set of generic questions.

1. How does each model behave, in terms of energy release magnitudes, when the grid size parameter is varied in relation to the mining step size?
2. Is the mobilised fracture “length” (“area” or “volume”) deterministic or fractal?
3. How are the magnitude-frequency statistics affected by different fracture size populations?

The answers to these questions are related also to the constitutive rules that are used to describe failure. In particular, for slip on fault planes or on the segments of a random tessellation mesh, it is important to distinguish between conventional cohesion breaking (Mohr-Coulomb) models and models in which slip weakening or velocity dependent friction are employed and which include an implicit length scale in their formulation. The importance of the implicit slip length scale has been highlighted by *Rice (1993)* in the formulation of a San Andreas Fault (SAF) slip model. In this case, if grid sizes are too large, “inherently discrete” behaviour is observed in which power law frequency-magnitude statistics occur. Most of the simulations of seismic behaviour evaluated to date fall into this category of model. When the grid size is reduced sufficiently, it is observed on the SAF model that the complex slip behaviour is replaced by cycles of periodically repeated large earthquakes. These considerations must be evaluated in relation to local mining induced slip complexity and the spatial migration of seismic and aftershock activity.

## **5.5. Specifying the initial and boundary conditions for a particular model**

Every numerical model which solves a forward problem needs a set of initial conditions to be specified. The initial conditions must form a complete set in the sense that they must fully specify one of the accessible states of the physical system under study (e.g. a given volume of rock.) In the case of wave propagation in an elastic medium the initial displacements and the initial velocities must be specified in every point in space (note that the wave equations require two sets of quantities, namely displacements and velocities, to be specified as initial conditions. This is due to the fact that the wave equation is of second order in the time-variable). A damage rheology model needs the initial stress field and the initial distribution of damage for solving the corresponding forward problem. A cellular automation type of model would require as an initial condition the full information of an accessible state of the system under study. In short, the initial conditions set the starting point in a forward (evolution) simulation.

Initial conditions may be all that is needed for solving an evolution problem formulated in terms of Ordinary Differential Equations (ODEs) but a Partial Differential Equation (PDE) problem needs also boundary conditions to be specified for ensuring the existence and the uniqueness of the solution. The physical meaning of the boundary conditions is that they specify the concrete loading conditions for the material system under study as well as the interactions of this system with the surrounding world (heat exchange, diffusion, radiation emission and absorption, contact interactions etc.). The fundamental equations of a physics-based model are a coded form of the most general laws of nature and as such have infinitely many solutions which include all possible situations and processes. It is the set of boundary conditions which specify a concrete problem. Setting up the boundary conditions in a particular case is a very delicate task because if these conditions turn out to be too restrictive there will not be a solution of the problem and if the boundary conditions are not restrictive enough the problem will have more than one solution which is as bad as not having a solution at all. For certain classes of problems there are rigorously proven theorems which state how one must set the boundary conditions in order to guarantee the existence and the uniqueness of the solution. In particular, for the elliptic partial differential equations describing the elastic equilibrium states of a solid occupying certain volume there are three types of boundary conditions which lead to an unique solution:

- Dirichlet problem: prescribed are the values of the unknown function on the boundary of the domain
- Neumann problem: prescribed are the values of the normal derivative of the unknown function on the boundary of the domain

- Mixed problem: Dirichlet-type of conditions are set for part of the boundary and on the rest of the boundary the conditions are of Neumann-type.

Some problems exhibit an enhanced sensitivity to small variations of the boundary conditions. This leads to chaotic behaviour and is usually the consequence of some non-linearity either in the equations or in the boundary conditions.

Lattice solids and cellular automata models require specific boundary conditions to deal with the edge-effects of finite lattices. For instance, the most commonly imposed boundary conditions on lattice models of solids are periodic with the topology of a torus (dough-nut). This corresponds to an infinite crystallic structure.

## 5.6. Constitutive relations

Continuum mechanics provides a good description of the behaviour of solids and fluids and yet it is only an approximation to the reality because it does not take into account the full details of the microscopic structure of the concrete material. The basic equations of continuum mechanics are an expression of the fundamental conservation laws of physics and are universally applicable irrespective of the specific properties of the material under study. This universality means, for instance, that the dynamical equations of motion are not sufficient for determining the evolution of the physical state of a deformable solid under prescribed loading and additional information has to be supplied about the specific way in which the material responds to changes in the state variables (such the strain tensor invariants, the temperature, and other relevant degrees of freedom).

The physical state of certain volume of rock at a given moment of time is specified by the values of all relevant state variables. One can say that the accessible states of a physical system correspond to points in an abstract space of dimension equal to the number of state variables (in the case of a mechanical system of material particles this is the phase space of coordinates and momenta).

One of the fundamental assumptions of physics is that the dynamics of a physical system is determined by some function of the state variables. In the case of a system of material points this function is called the action. For a deformable solid the elastic potential energy (or, more generally the internal energy) as well as the entropy are of importance and the role of the state function is given to the so-called **Helmholtz free energy** defined as the total internal energy of the system minus the product of the entropy and the temperature.

The way in which a physical body responds to small changes in the state variables is determined by the details of the interactions between its microscopic constituents and is manifested at the macroscopic level by a set of functional relationships between the state variables and some suitably defined macroscopic (averaged) quantities. The stress tensor is one example of such macroscopic quantity which is the averaged result of the local intermolecular interactions for the material under study. A typical constitutive relation will have the form of an expression for some component of the stress tensor as a function of the components (one or more) of the strain tensor. The Hooke's law is a classical example for a constitutive relation in the case of an elastic solid and within a limited interval of small deformations.

For complex and nonlinear materials the constitutive relations are also non-linear and can include a dependence on the derivatives of the state variables and on the loading history. When the constitutive relations contain a dependence on the loading history it is said that they correspond to a material with memory.

### 5.6.1. Theoretical derivation of constitutive relations

Theoretically the constitutive relations are generated by the partial derivatives of the Helmholtz free energy with respect to the components of the strain tensor. Therefore a numerical model based on a postulated form of the Helmholtz free energy is already equipped with constitutive relations and any additional input of stress-strain relations could lead to internal inconsistencies. The generic link between the free energy and the way in which the material responds to variations of the deformation is rooted in the physical meaning of the Helmholtz free energy, namely: it is the amount of internal energy stored in the material which is available for conversion into mechanical work.

The damage-rheology model IDRM is an example of a numerical procedure in which the constitutive relations are derived from an explicit expression for the Helmholtz free energy.

Many numerical models of practical importance do not include a postulate about the free energy and are based on explicit constitutive relations which are usually derived from the analysis of experiments and observations.

### 5.6.2. Empirical constitutive relations

Empirical constitutive relations are in the form of stress-strain curves for the material under study and for different loading ranges and patterns. The data for the stress-strain curves is obtained either from laboratory experiments or from field observations. There is a considerable contamination with both systematic and statistical errors in empirical constitutive relations which may lead to significant distortion of the modelled data relative to the corresponding real data.

The constitutive description of failure in large scale volumes of rock surrounding a mining excavation can be approached in two fundamentally different ways. In the first case, it can be assumed that the medium is partitioned into representative volume elements (RVE's) and that the overall deformation is controlled by the local deformation of each RVE and the inertial interaction between these elements. This class of model embodies the theories of plasticity or damage mechanics to provide descriptions of the element strain as a function of the imposed loading and loading history. An alternative approach is to assume that the medium deformation is controlled by failure *between* constituent particles or blocks. In this case, constitutive descriptions are expressed in terms of the interface forces such as bond strength and frictional resistance. These two classes can be considered to be dual and exclusive descriptions of material failure. It is important to observe that the surface separation philosophy depends also on the divisibility of the material that is controlled, ultimately, by molecular separation forces. In practical terms, this scale is many orders of magnitude smaller than the scale of engineering interest and the possibility exists that the defining fracture surfaces may possess a fractal character with dimension falling between 2 and 3.

In terms of the specific numerical models that are considered to be potential candidates for the integration of seismic activity with modelling, the boundary integral codes, MINSIM and DIGS assume that material failure occurs on representative surfaces, whereas the ISR code assumes that failure occurs in volumetric elements. The finite element code ELFEN, boundary integral code MAP3Di and distinct element code UDEC allow failure on both separating surfaces and in volumetric elements. It is important to note that the different models demand different classes of constitutive relationships. The surface controlled models require a description of bond cohesion and friction resistance whereas the volumetric models require parameters to describe the effective "flow" of the material. The calibration of each model class is difficult. Detailed frictional behaviour may depend on the velocity and velocity

history of the sliding interfaces. In assigning point properties to the volumetric elements, it may be necessary to assume that the outcome of a laboratory experiment, in which detailed localisation mechanisms occur, is representative of the average behaviour of a different sized zone.



## 6. Conclusions

The organic integration of seismic monitoring with numerical modelling is not a fashionable buzz-word, but the next logical stage in the development of reliable tools for intelligent mining design and production planning.

An integrated numerical model

- incorporates, explicitly or implicitly, all the experience accumulated from years of mining-oriented numerical modelling and rock-engineering practice, and
- combines it with state-of-the-art analysis of high-resolution data from a modern seismic monitoring system, and
- uses the real seismic events as a direct input and
- addresses the main issue of rockmass stability at a particular location, in a given interval of time and under specified conditions.

The modern seismic monitoring systems are capable of providing high quality data about the local seismicity in mines. The seismological analysis of the records about a particular seismic event could, in principle, reconstruct the seismic source mechanism and produce the values of the relevant source parameters. The statistical processing of long local seismicity records can throw light on the correlations between the character of the mining activity, the existing geological structures and could even highlight some general trends in the seismic activity. However, neither of these approaches would lead to a statement about how a certain sequence of real seismic events would affect the stability of a particular volume of rock, in a particular interval of time and under specified production conditions in the mine. It is precisely the answers to this type of question that is vital for planning and organising the mining process for maximum safety and efficiency.

The behaviour of the rockmass under specified loading conditions is governed by the laws of continuum mechanics, thermodynamics, material damage evolution and damage-driven rheology. In addition there are the very important and yet poorly understood processes of energy dissipation and friction on material discontinuities. The problem is of such complexity that even the formulation of it as a mathematical system of equations is not possible without massive simplifications. Even when such simplifications are made and a corresponding mathematical problem is correctly set, its solution is, as a rule, inaccessible by analytical means and has to be sought numerically. The formulation of a mathematical problem designed to correspond to a realistic situation of rockmass behaviour under loading, together with the numerical algorithm for finding an approximate solution to the problem defines a concrete numerical model applicable to the planning and conducting of the mining process.

The reliability of the conclusions drawn from the data generated by a numerical model strongly depends on the accuracy of the information the model takes as an input. Ideally this information should fully characterise the initial state of stress and deformation in the rockmass. In real life one has to settle for a very approximate estimation of the actual loading conditions and even less knowledge about the physical state and the structure of the rock. Under the circumstances every possibility has to be exploited for improvement in both directions. The concept of integrating seismic monitoring with numerical modelling is in response to the stated need. The observed local seismicity contains valuable information about the state of the rock mass and its environment. This information was either not included or inaccurately presented in the initial setting-up of the model. By taking real data as an input an integrated numerical model will continuously correct itself and perform as an adaptive system.



## **6.1. Requirements imposed by the integration on the numerical models**

A numerical model of the rockmass response to loading is suitable for a functional integration with observational seismic data when:

- it implements a reasonable approximation of the fundamental relationships between the relevant physical degrees of freedom.
- it is designed to solve a forward problem about the evolution of the physical state of the rock under the given initial and boundary conditions.
- it can convert the data about a real seismic event into a corresponding addition to the loading at the correct moment of time.
- it can itself emulate seismic events in a way which allows for calibration of the model to the observed local seismicity.
- it must have an adequate resolution in the size, location and time of modelled events.
- the computer code must run sufficiently fast so that the numerical clock does not lag behind the physical clock.

## **6.2. Numerical models that are suitable for seismic integration**

### **6.2.1. Existing models**

The “classic” tool for the analysis of stress distribution problems in tabular mining has been the displacement discontinuity method (DDM). It is possible to use this numerical framework for the integration of seismic activity by allocating slip patches to appropriate regions of defined fault planes, according to the observed record of seismic event sequences. Each slip area can be made to conform to the observed seismic moment and forward assessment of future seismic activity can be made at any stage of the integration cycle. This approach is constrained, at present, to the analysis of static deformation problems but is accessible to most of the current 3D-DDM software available in South Africa. Additional interface computer codes for automatic conversion of recorded event moments to slip plane positions may be required.

The static DDM models can be used to model fault creep by postulating laws that define the fault creep rate in terms of the shear loading stress. Regions of each fault surface can be assigned different material properties to designate asperities or creeping “gouge” material. As stress accumulates on the asperities, these will be broken at intermittent intervals. This process can be used to replicate some aspects of the statistical nature of seismic activity. Event frequency-magnitude statistics will be controlled by the asperity density and strength, as well as the characteristic relaxation time, of the fault creep law.

At present, the incorporation of an observed event may be incompatible with the existing stress state over the selected fault position. Future studies will have to be directed to devising strategies to treat these incompatibilities in a systematic manner.

## 6.2.2. Future model development

Future developments should explore the possibility of formulating a fully dynamic version of the DDM to allow dynamic fault slip and the accompanying wave propagation effects. This would have to be integrated with slow creep dominated deformations and would allow a much richer incorporation of waveform characteristics into the integration process. Difficulties relating to the numerical stability of 3D dynamic DDM models have to be resolved.

Hybrid methods, such as the Integrated Damage Rheology Model (IDRM) described in this report, hold promise for the detailed dynamic simulation of complex seismic source processes and their integration with mine planning. At the quasi-dynamic level damage rheology modelling is conceptually well-suited for integration with real seismic data by converting seismic events into corresponding additional loading on the rockmass.

Non-linear continuum models, such as the finite element method (FEM) or other forms of finite difference models, may also prove to be suitable tools for developing a hybrid seismic damage model. In these cases, numerical strategies have to be used to treat absorbing boundary problems for mining applications.

## 6.3. Recommendations for integration in practice

Integrated numerical models of rockmass response to loading have serious advantages compared to models which are not capable of assimilating seismic data in real time, and will inevitably become an industry standard for mining design and production planning. The methodologies for using integrated numerical models will eventually crystallise from the experience of employing such models for practical problem-solving but even at this very preliminary stage one can make some recommendations in this respect:

- the initial state of the modelled rockmass should be specified as accurately as possible.
- it must be ensured that high-quality seismic data exists, or will be provided, for the location and time-interval of interest.
- the numerical model has to be set up for the required resolution with respect to both the real and the modelled seismicity, while staying within the available computational resources (computer memory and CPU speed), and ensuring that the numerical time-stepping is faster than the pace of physical time.
- the loading on the studied rockmass, due to the existing and planned mining, has to be estimated as accurately as possible.
- The perturbations to the physical state of the modelled material, caused by the real seismic activity in the area, have to be quantified so that they can be introduced in the running model as an input at the appropriate time.

What can reasonably be expected from an integrated monitoring-modelling system? First and foremost, the integration of data with modelling will improve the reliability of the forecasts about the evolution of the physical state of a particular volume of rock, subjected to a variable loading due to specified mining activity, and the actual local seismicity. In particular, the data generated by an integrated monitoring-modelling system should, when analysed, allow definite statements to be made about:

- the elastic and plastic deformation within the modelled volume of rock at a particular moment of time.
- the distribution of static stress at a particular moment of time.

- the level of micro-seismic activity within the modelled volume of rock.
- the rockmass stability and, in particular, any expected loss of stability of the modelled rockmass.

A conceptual view of the integration of seismic monitoring with numerical modelling for the needs of the mining industry is the first step towards developing the new generation of mining design and planning tools. This development is not a matter for the distant future but has already started. Even at this very early stage it has become evident that a data-driven numerical model has considerable advantages over its non-integrated counterpart.



## 7. References

- Aki, K and Richards, P.G. 1980.** Quantitative Seismology, Theory and Methods. W.H. Freeman and Company, San Francisco.
- Andrews, D. J. 1986.** Objective determination of source parameters and similarity of earthquakes of different size. In: *Das, S., Boatwright, J. and Scholz, C.H. Earthquake source mechanics. American Geophysical Monograph 37*, p259-267.
- Archuleta, R. J, Cranswick, E., Mueller, C. and Spudich, P. 1982.** Source parameters of the 1980 Mammoth Lakes, California, earthquake sequence. *J. Geophys. Res.*, 87, 4595-4607.
- Bek, D.A. Brady, B.H.G, Grant, D.R. 1996.** Analysis of seismicity and rock deformation during open stoping of a deep orebody. (In: *Barla. Eurock '96. Balkema, Rotterdam. 1171-1177*).
- Ben-Zion, Y. 1998.** Criticality, Self-organized-criticality, Dynamic Complexity, Chaos, And Earthquakes. Meeting of the European Seismological Commission, 1998.
- Ben-Zion, Y. 2001.** On quantification of the earthquake source. *Seis. Res. Lett.*, vol. 72, 2, p151-152.
- Ben-Zion, Y. and Rice, J.R. 1993.** Earthquake failure sequences along a cellular fault zone in a three dimensional elastic solid containing asperity and non asperity regions. *J. Geophys. Res.* 14109-14131.
- Ben-Zion, Y. and Lyakhovsky, V. 1999.** Frequency-Size and Temporal Statistics of Earthquakes in a Regional Lithospheric Model for Coupled Evolution of Earthquakes and Faults, *EOS Trans. Amer. Geophys. Union*, 80, F923
- Chakrabarti, B. and Stinchcombe, R. 1999.** Stick-slip statistics for two fractal surfaces: A model for earthquakes.
- Cichowicz, A. 2001.** Quantification of complex source. Submitted to 5<sup>th</sup> Symposium on Rockbursts and Seismicity in Mines, South Africa, September 2001.
- Coates, R.T and Schoenbug, M. 1995.** Finite-difference modeling of faults and fractures. *Geophysics* 1514-1526.
- Cochard, A. and Madariaga, R. 1996.** Complexity of seismicity due to highly rate-dependent friction. *J. Geophys. Res.* pp 25321-25336.
- Crouch, S.L. and Starfield, A. M. 1983.** Boundary element methods in solid mechanics. George Allen & Unwin: London.
- Cundall, P.A. and Lemos, J.V. 1990.** Numerical simulations of fault instabilities with a continuously yielding joint model. (In: *Fairhurst C. 2<sup>nd</sup> Int Symp. Rockbursts and Seismicity in Mines. Balkema. Rotterdam, p 39-44*).
- Di Bona, M. and Rovelli, A. 1988.** Effects of the bandwidth limitation on stress drops estimated from integrals of the ground motion. *BSSA*, Vol. 78, 5, p1818-1825.
- Dragoni, M. 1990.** A model of interseismic fault slip in the presence of asperities. *Geophys. J. Int.*, Vol. 101: 147-156.
- Eneva, M. and Ben-Zion, Y. 1997.** Application of pattern recognition techniques to earthquake catalogs generated by model of segmented fault systems in three-dimensional elastic solids. *J. Geophys. Res.* p 24513-24528.
- Everitt, B.S. 1993.** Cluster Analysis, Edward Arnold.
- Evernden, J.F. 1969.** Precision of epicentres obtained by a small number of world wide stations. *Bull. Seism. Soc. Am.*, 59, 1365-1398.
- Finney, G.J. 1999.** Some statistical aspects of mining induced seismic events. (In: *Proceedings, SARES Symposium, Johannesburg, pp. 132-139.*)
- Flatcher, J., Harr, L., Hanks, T. and Baker, L. 1987.** The digital array at Anza, California: Processing and initial interpretation of source parameters. *J. Geophys. Res.*, 92, 369-382.
- Flinn, E.A. 1965.** Confidence regions and error determinations for seismic event location. *Rev. of Gophys.*, vol. 3, p157-185.
- Fukuyama, E. and Madariaga, R. 1998.** Rupture dynamics of a planar fault in a 3-D Elastic medium: Rate and slip weakening friction. *Bull. Seis. Soc. Am.* pp 1-17.

- Graves, R. W. 1996.** Simulating seismic wave propagation in 3D elastic media using staggered-grid finite differences. *Bull. Seis. Soc. Am.* pp 1091-1106.
- Gusev, A.A. 1989.** Multiasperity fault model and the nature of short-period subsources. *PAGEOPH*, Vol. 130, No. 4.
- Hanks, T. C. and Kanamori, H. 1979.** A moment magnitude scale. *J. Geophys. Res.* vol 84, pp 2348-2350.
- Hazzard, J. 1998.** Numerical modelling of acoustic emissions and dynamic rock behaviour. *Ph.D. Thesis.* Keele University.
- Hirata, T., Satoh, T., Ito, K. 1987.** fractal structure of special distribution of microfracturing in rock. *Geophys. J. R. Astr. Soc.* 369-374.
- Hoffmann, G. 1999.** Software code to randomly distribute asperities of different strengths across a surface, ISS International.
- Ilchev, A. and Lyakhovsky, V. 2001.** Practical aspects of the hybridisation of the boundary integral method with damage rheology modelling for the simulation of seismic data. (*In: van Aswegen, G., Durrheim, R. and Ortlepp, W.D. Proceedings of 5<sup>th</sup> Symposium on Rockbursts and Seismicity in Mines, September 2001, South Africa.* South African Institute of Mining and Metallurgy, Johannesburg, South Africa).
- Ito, K. and Matsuzaki, M. 1990.** Earthquakes as self-organised critical phenomena. *J. Geophys. Res.* pp 6853-6860.
- Jager A. J. and Ryder J. A. 1999.** A handbook on rock engineering practice for tabular hard rock mines. Safety in Mines Research Advisory Committee, Johannesburg. Cape Town: Creda Communications.
- Jordan, T. 1999.** Lecture notes. M.I.T.
- Jordan, T.H. and Sverdrup, K.A. 1981.** Teleseismic location techniques and their applications to earthquake clusters in the south-central Pacific. *Bull. Seism. Soc. Am.*, 71, p1105-1130.
- Kemeny, J. and Hagaman, R. 1992.** An asperity model to simulate rupture along heterogeneous fault surfaces. *PAGEOPH*, Vol. 138, No. 4: 549-567.
- Kostrov, B.V. 1974.** Seismic moment and energy of earthquakes and seismic flow of rock. *Izv. Phys. Solid Earth*, 13, p13-21.
- Kostrov, B.V. & Das, S. 1988.** Principles of earthquake source mechanics, Cambridge University Press.
- Lachenicht, R. 1999<sub>1</sub>.** Fundamental aspects of the integration of seismic monitoring with numerical modelling. *SIMRAC Progress Report, GAP603(a). June 1999.* Pretoria: Department of Minerals and Energy.
- Lachenicht, R. 1999<sub>2</sub>.** Fundamental aspects of the integration of seismic monitoring with numerical modelling. *SIMRAC Progress Report, GAP603(a). September 1999.* Pretoria: Department of Minerals and Energy.
- Lachenicht, R. in prep.** An analysis of the asperity model under viscoplastic displacement loading and its integration with quantitative seismology. *MSc Dissertation*, University of the Witwatersrand, Johannesburg.
- Lachenicht, R. and van Aswegen, G. 1999.** An engineering method to evaluate the seismic potential of geological structures as a function of mine layout. (*In: Hagan, T.O. SARES 99, pg 233-237*).
- Lawn, B.R. and Wilshaw, T.R. 1975.** Fracture of brittle solids. Cambridge University Press.
- Lyakhovsky, V., Ben- Zion Y. and Agnon, A. 1997a.** Distributed damage, faulting and friction. *J. Geophys Res.* pp 27635-27649.
- Lyakhovsky, V., Reches, Z. Weinberger, R. and Scott, T. 1997b.** Non linear elastic behaviour of damaged rocks. *Geophys. J. Int.* pp 157-166.
- Lyakhovsky, V., Ilchev, A. and Agnon, A. 2001.** Modelling of damage and instabilities in rock mass by means of a non-linear rheological model. (*In: van Aswegen, G., Durrheim, R. and Ortlepp, W.D. Proceedings of 5<sup>th</sup> Symposium on Rockbursts and Seismicity in Mines, September 2001, South Africa.* South African Institute of Mining and Metallurgy, Johannesburg, South Africa).
- Madariaga, R. 1979.** On the relation between seismic moment and stress drop in the presence of stress and strength heterogeneity, *Journal of Geophysical Research*, Vol. 84, No. B5, May10: 2243-2250.

- Madariaga, R., Olsen, K. and Archuleta, R. 1998.** Modeling of dynamic rupture in a 3D earthquake fault model. *Bull. Seis. Soc. Am.* pp 1182-1197.
- McCreary, R.G., Grant, D. and Falmagne, V. 1993.** Source mechanisms, three dimensional boundary element modelling and underground observations at Ansil Mine. (*In: Young, R.P. Rockbursts and seismicity in mines.* Rotterdam: Balkema. pp 227-232.)
- Mendecki, A.J. and Niewiadomski, J. 1997.** Spectral analysis and seismic source parameters. (*In: Mendecki, A.J. Seismic Monitoring in Mines.* Chapman and Hall, p 144-158).
- McGarr, A. 1976.** Seismic moment and volume changes. *J. Geophys. Res.* pp 1487-1494.
- Mendecki, A.J., van Aswegen, G. and Mountfort, P. 1999.** A Guide to Routine Seismic Monitoring in Mines. (*In: Ryder, J. and Jager, A. A Handbook on Rock Engineering Practice for Tabular Hard Rock Mines.* Safety in Mines Advisory Committee to the Department of Minerals and Energy of South Africa (SIMRAC), Johannesburg, South Africa. Printed by Creda Press, Cape Town.)
- Michael, A.J. 1987.** Use of focal mechanisms to determine stress: a control study. *J. Geophys. Res.*, 92, 357-368.
- Milev, A. and Spottiswoode S. 1997.** Integrated seismicity around deep-level stopes in South Africa. *Int. J. Rock Mech. Min Sci.* paper no 199.
- Minney D.S. and Naismith, W.A. 1993.** Quantitative analysis of seismic activity associated with the extraction of a remnant pillar in a moderately deep level gold mine. (*In: Young, R.P. Rockbursts and seismicity in mines.* Rotterdam: Balkema. pp 95-100.)
- Mora, P., Place, D. and Zeng, Y. 1997.** The effect of gouge on fault strength and dynamics. Localizations phenomena and dynamics of brittle and granular systems. Lamont Doherty Earth Observatory. Columbia University.
- Morrison, D. M. 1993.** Chaotic behaviour and mining induced seismicity. (*In: Young, R.P. Rockbursts and seismicity in mines.* Rotterdam: Balkema. pp 233-238.)
- Napier, J. A. L. 1990.** Modelling of fracturing near deep level mine excavations using a displacement discontinuity approach. (*In: Rossmanith, H. P. Mechanics of Jointed and Faulted Rock.* Rotterdam: Balkema, pp 709-715).
- Napier, J.A.L. and Malan. D.F. 1997.** A viscoplastic model of time-dependent fracture and seismicity effects in brittle rock. *Int. J. Rock Mech. Min Sci.* pp 1075-1089.
- Nelder, J.A. and Mead, R. 1965.** A simplex method for function minimisation. *Computer Journal.* Vol. 7, p308-313.
- Oden, J.T., Vemaganti, K. and Moes, N. 1999.** Hierarchical modeling of heterogeneous solids. *Comput. Meth. Appl. Mech. Engrg.* pp. 3-25.
- Oreskes, N., Shrader-Frechette, K. and Belitz, K. 1994.** Verification, validation and confirmation of numerical models in the earth sciences. *Science.* pp 641-645.
- Ozbay, M.U., Spottiswoode, S. and Ryder, J.A. 1993.** A quantitative analysis of pillar associated large seismic events in deep mines. (*In: Young, R.P. Rockbursts and seismicity in mines.* Rotterdam: Balkema. pp 107 - 110.)
- Pierce, A. P. and Napier, J. A. L. 1995.** A spectral multipole method for efficient solution of large-scale boundary element models in elastostatics. *Int. J. Num. Methods Eng.*, vol. 84, pp4009-4034.
- Potyondy, D. and Cundall P.A. 1998.** Modelling notch formation mechanisms in the URL mine-by test tunnel using bonded assemblies of circular particles. (*In: Proc 3<sup>rd</sup> North American Rock Mechanics Symposium NARMS 98.* Paper number USA-828.)
- Rice, J. R. 1993.** Spatio-temporal complexity of slip on a fault. *J. Geophys. Res.* 98, pp 9885-9907.
- Robinson, R. and Benites, R. 1995.** Synthetic seismicity models of multiple interacting faults. *J. Geophys. Res.* pp 18229-18238.
- Rundle, J.B. 1988.** A physical model for earthquakes. 1. Fluctuations and interactions. *J. Geophys. Res.* pp 6237-6254.
- Rundle, J.B. 1988.** A physical model for earthquakes. 2. Application to Southern California *J. Geophys. Res.* pp 6255-6274.
- Rundle, J.B. and Klein, W. 1993.** Scaling and critical phenomena in a cellular automaton slider-block model for earthquakes. *J. Statistical Physics.* pp 405-411.
- Ryder J. A. 1988.** Excess shear stress in the assessment of geologically hazardous situations. *J. S. Afr. Int. Min. Metall.* vol 88 pp. 27 - 39.

- Ryder, J. A. and Napier, J. A. L. 1985.** Error analysis and design of a large-scale tabular mining stress analyser. (*In: Fifth International Conference on Numerical Methods in Geomechanics*, Nagoya, 1985, pp1549-1555).
- Salamon, M.D.G. 1993.** Some applications of geomechanical modelling in rockburst and related research. (*In: Young, R.P. Rockbursts and seismicity in mines*. Rotterdam: Balkema. pp 297-309.)
- Sammis, C., G, Chen, Y. and Ben-Zion, Y. 1999.** An Asperity Model for Repeating Earthquakes, *EOS Trans. Amer. Geophys. Union*, 80, F705
- Scholtz, C. 1998.** A further note on earthquake size distributions, *Bulletin of the Seismological Society of America*, Vol. 88, No. 5: 1325-1326.
- Scholtz, C.H. 1990.** The mechanics of earthquakes and faulting. Cambridge: Cambridge University Press.
- Sellers, E. J. 1997.** A tessellation approach for the simulation of the fracture zone around a stope. (*In: 1st Southern African Rock Engineering Symposium*, Johannesburg, 1997, pp143-154).
- Shaw, B.E. 1995.** Frictional weakening and slip complexity in earthquake faults. *J. Geophys. Res.* pp 18239-18251.
- Sornette, D. Davy, P. and Sornette, A. 1990.** Structuration of the lithosphere in plate tectonics as a self organized critical phenomenon. *J. Geophys. Res.* pp 17353-17361.
- Spottiswoode, S. 1990.** Volume excess shear stress and cumulative seismic moments. (*In: Fairhurst, C. 2<sup>nd</sup> Int Symp. Rockbursts and Seismicity in Mines*. Rotterdam: Balkema. pp 39-45.)
- Spottiswoode, S. 1997.** Energy release rate with limits to on-reef stress. (*In: SARES 97. SANGORM*. pp 252-258.)
- Spottiswoode, S. 1999.** Modelling seismicity and creep on multiple stope-parallel layers. (*In: Hagan, T.O. SARES 99. SAIMM*.)
- Thurber, C.H. and Rabinowitz, N. 2000.** Advances in seismic event location. Kluwer Academic Publishers.
- Tse, S. T. and Rice, J. R. 1986.** Crustal Earthquake instability in relation to the depth variation of frictional slip properties. *J. Geophys. Res.* pp 9452-9472.
- Turcotte D.L. 1992.** Fractals and Chaos in geology and geophysics. Cambridge University Press.
- Vetterling, W. T., Press, W.H., Teukolsky, S. A. and Flannery, B. P. 1986.** Numerical Recipes. Cambridge University Press.
- Webber, S. J. 1990.** Numerical modelling of a repeated fault slip. *J.S. Afr. Inst. Min. Metall.* pp 133-140.
- Wiles, T. 2000.** Help manual in Map3D, standard version 42, build date 2001.
- Wilson, S. A., Henderson, J. R. and Main, I. G. 1996.** A cellular automaton fracture model: the influence of heterogeneity in the failure process. *J. Struc. Geol.* p 343 - 348.